ION BOMBARDMENT INDUCED COMPOSITIONAL CHANGES IN COMPOUND SEMICONDUCTOR SURFACES STUDIED BY XPS COMBINED WITH LEISS

YU WEI

Doctor of Philosophy

THE UNIVERSITY OF ASTON IN BIRMINGHAM

PHD

November, 95

THE UNIVERSITY OF ASTON IN BIRMINGHAM

Ion Bombardment Induced Compositional Changes in Compound Semiconductor Surfaces Studied by XPS Combined with LEISS

Yu Wei

Doctor of Philosophy

1995

SUMMARY

Surface compositional change of GaP, GaAs, GaSb, InP, InAs, InSb, GeSi and CdSe single crystals due to low keV noble gas ion beam bombardment has been investigated by combining X-ray Photoelectron Spectroscopy (XPS) and Low Energy Ion Scattering Spectroscopy (LEISS). The purpose of using this complementary analytical method is to obtain more complete experimental evidence of ion beam modification in surfaces of compound semiconductors and GeSi alloy to improve the understanding of the mechanisms responsible for these effects.

Before ion bombardment the sample surfaces were analysed nondestructively by Angular Resolved XPS (ARXPS) and LEISS to get the initial distribution of surface composition. Ion bombardment experiments were carried out using 3keV argon ions with beam current of 1μA for a period of 50 minutes, compositional changes in the surfaces of compound semiconductors and GeSi alloy were monitored with normal XPS. After ion bombardment the surfaces were re-examined with ARXPS and LEISS. Both XPS and LEISS results showed clearly that ion bombardment will change the compositional distribution in the compound semiconductor and GeSi surfaces.

In order to explain the observed experimental results, two major theories in this field, Sigmund linear collision cascade theory and the thermodynamic models based on bombardment induced Gibbsian surface segregation and diffusion, were investigated. Computer simulation using TRIM code was also carried out for assistance to the theoretical analysis. Combined the results obtained from XPS and LEISS analyses, ion bombardment induced compositional changes in compound semiconductor and GeSi surfaces are explained in terms of the bombardment induced Gibbsian surface segregation and diffusion.

KEYWORDS: XPS, LEISS, ion bombardment, nonstoichiometric sputtering, Gibbsian surface segregation, diffusion, compound semiconductor

ACKNOWLEDGEMENTS

It is a pleasure to thank

Dr John L Sullivan for his guidance and encouragement throughout this work.

Mr Andy M Abbott for his assistance in use of ESCA LAB at Aston

Mr R S Bassi and Mr E P Watson for their help in making standard samples

All at Surface Science Group for creating wonderful environment for research.

All from my family for their full support for my study abroad.

This work would not have been possible without financial support from Aston University

Table of Contents

Page

List of Tables

List of Figures

Figure **Page**

Chapter 1 Literature Review

1.1. Introduction

Low energy ion sputtering, i.e., the erosion of a solid due to ion bombardment of a few keV, has become an increasingly important technique in the modern sciences and high technologies of surface characterisation, processing and microfabrication. In surface science, it is employed as a convenient vehicle for cleaning of a sample surface and for depth profiling during analysis. Without it Secondary Ion Mass Spectroscopy (SIMS), one of the most useful surface analytical techniques would not exist. In the semiconductor industry, ion beam processing, lithography and ion implantation have been used successfully for developing various kinds of high quality electronic devices.

In these applications, it is hoped that sputtering will not change the physical and chemical properties of the treated surfaces, but it is found that for many materials ion bombardment always produces damage in the solid surface. This damage may be categorised as: (1) physical damage, i.e. energetic ions will eventually destroy the surface structure of a structured material and produce a large number of defects in the surface; (2) chemical damage, i.e. sputtering will alter surface concentrations and chemical states in the surfaces of many compound materials. The reasons for the physical damage may be relatively easily understood, but chemical damage is more difficult to explain, although a large number of theoretical and experimental studies have been made in last two or three decades. Many models have been proposed in order to explain these effects in various kinds of multicomponent system, but there is still no clear picture of the mechanisms responsible for these effects. The difficulties in this field are due to not only the complexity of the theoretical analysis, but also the fact that complete information on an ion bombarded compound surface is still not easily obtained from experiments.

This thesis is not concerned with a theoretical approach for establishing a universal model to explain every phenomenon occurred in the sputtering of all compound systems, but more with an experimental study of ion beam modification of surface composition in one type of multicomponent system, that is compound semiconductors, using complementary surface analytical techniques. It is hoped, however, that this study may provide general guidelines for application of sputtering techniques in the semiconductor industry to reduce chemical damage to semiconductor surfaces in fabrication, processing and characterisation and to take full advantage of ion bombardment effects to improve

electronic or optical properties of semiconductor devices. It is also hoped that this work provides more information on the ion bombardment induced compositional changes in compound semiconductor surfaces and that the results will improve the understanding of the mechanisms responsible for these phenomena.

In the first chapter, a background of the present knowledge on sputtering of compound systems is presented. After a short historical introduction, experimental work on multicomponent sputtering is reviewed, according to the categories of different effects occurring in sputtering of a compound. This is followed by an introduction to various theoretical models for the prediction of multicomponent sputtering. Two major explanations are considered in detail, these are Sigmund's linear collision cascade theory and the models based on bombardment induced Gibbsian segregation and diffusion. Computer simulation methods are also mentioned briefly. Although this approach is still very new and current models may be too simple to explain the ion bombardment effects, some advantages, however, of using this approach may be helpful for theoretical analyses. Following the literature review, comments on previous work are included together with an analysis of the problems of both theoretical and experimental studies in this field. This chapter concludes with a description of the research programme.

1.2. Phenomena of Sputtering

The phenomenon of sputtering was reported for the first time in 1852 by Grove who found that a small circular spot was rapidly formed on the plate, "quickly deepening in colour, and apparently eating into the plate" when he applied a DC voltage across a Pt needle electrode and a silver plate in a vacuum belljar and admitted a small amount of air into the belljar [Grove, 1852]. When he replaced air with hydrogen gas, he observed that whether the plate electrode was positive or negative, the oxide layer on the plate electrode was always "rapidly and beautifully cleaned off". He could not explain his results by the theory of discharge at that time and certainly did not realised that he had discovered a new phenomenon, which is called *sputtering*, or more accurately speaking, *plasma etching*, by his successors.

After about 77 years, Asada *et al.* [1929] conducted the first experiment of multi-component sputtering. They used Hg^+ ion bombardment on Cu which contained small amount of Au, and found the Au sputtering yield higher in the surface than that in bulk. They believed that this was due to Au diffusion from bulk to the surface creating a Au enriched surface layer.

The sputtering of compounds has become a much more attractive topic for scientific study since the 1950's. A change in surface composition of Cu-Au and Ag-Pd systems due to noble gas ion bombardment was first clearly observed by Gillam[1959]. He obtained evidence to show that an altered layer of about 40Å enriched in Au might exist in the bombarded Cu-Au surface. For Ag-Pd systems he did not observed enrichment for a lower Pd concentration alloy, but did for a higher Pd alloy.

Before 1967, however, no quantitative predictions on multicomponent sputtering could be derived from experiments, since surface-sensitive methods were not available at that time. It is in the last two to three decades since highly sensitive surface analysis methods and devices, such as Auger Electron Spectroscopy (AES), Secondary Ion Mass Spectroscopy (SIMS), Ion Scattering Spectroscopy (ISS), Rutherford Backscattering Spectroscopy (RBS), and Electron Spectroscopy for Chemical Analysis (ESCA), or X-ray Photoelectron Spectroscopy (XPS) *etc.* were available, that quantitative experimental analysis for multi-component sputtering has been possible. In that time, a large amount of very reliable experimental evidence have been obtained by employing one or more of these analytical techniques. The original work was confined to alloy systems[Betz and Wehner, 1983], but in recent years many multi-component systems, such as oxides[Malherbe *et al.*, 1986], halides and semiconductors [Liau *et al*, 1977], have been studied. The structure of the studied materials is also not limited to amorphous solids but also single crystals and polycrystalline solids. Betz and Wehner[1983] reviewed the progress of sputtering of multicomponent materials and collated almost all experimental data before 1982. Shimizu[1987] continued this work and compiled all available experimental results from 1982 to 1987. More recently, a newly established technique, Scanning Tunnelling Microscopy (STM) as well as its derivatives, such as Atom Force Microscopy *etc.*, has been used to investigate structure of an ion bombarded solid surface on an atomic scale. This provides invaluable additional evidence for the investigation of mechanisms of sputtering [Wilson, 1988].

In studying sputtering of compound systems, several major effects, including mass effects, surface binding energy, Gibbsian surface segregation and diffusion and chemical driving force were found crucial in the explanation of surface composition changes. In the following sections, the review of experiments was carried out according to these effects. Although the main interest of this project is on sputtering of compound semiconductors, an understanding of sputtering in general is essential as many similarities in sputtering between semiconductors and other systems are apparent. The review will, therefore, not be limited to semiconductors, but also extended to metallic alloys and oxides.

1.2.1. Mass effects

Mass difference of target components was the first factor to be considered important in determining surface compositional changes. This is very easily understood in the low keV regime. When a collision cascade process occurs in a solid, the momentum and energy of incoming ions or recoils will be distributed differently to each constituent. According to classic binary collision mechanics, this generally results in the lighter component having higher momentum and higher probability to escape from the target surface or to move deeper inside the bulk. This leads to surface enrichment of the heavier component. The former effect is so-called *nonstoichiometric sputtering* or *preferential sputtering*, the latter called *recoil implantation*.

Using the RBS technique, Liau *et al.* [1977] studied the surfaces of various alloys and compounds subject to 20 to 80 keV Ne^+, Ar^+, Kr^+ and Xe^+. The materials used included solid solutions (Ag-Au, Cu-Au), metallic compound phases (Au_2Al, $AuAl_2$), intermetallic silicides (PtSi, Pt_2Si, NiSi, GeSi), compound semiconductors (GaP, InP) and an oxide (Ta_2O_5). They found that the lighter components in all systems except semiconductors were preferentially sputtered in the projected range of ions in the surface. They concluded that the lighter components suffer less energy loss and can emerge from a greater depth in the bulk.

Ho *et al.* [1979] reported an AES investigation on surfaces of homogeneous Al-Pd, Si-Pd and Al-Si alloy films bombarded with a 1keV argon ion beam. Both Al and Si were observed to be preferentially sputtered relative to Pd, although pure Pd has a higher sputter yield. They explained these results using Sigmund linear collision cascade theory and concluded that the mass difference appears to dominate over binding energy in determination of the trend of preferential sputtering.

Winter's experiments [Winter, 1982] of sputtering of nitrogen chemisorbed W(100) and Mo(100) crystals using Ar^+ and Xe^+ ions in the energy range from 0.3 to 5keV showed that ion bombardment causes a depletion of nitrogen in the surface region, and the sputtering yield of nitrogen tends to increase with increase in the mass of the surrounding atoms, specially in the lower energy of bombardment or when heavier ions are used.

In sputtering of metallic oxides, preferred loss of oxygen, resulting in reduction of the oxides was found in a large number of experiments [Hofmann and Sanz, 1982/1983; Choudhury, *et al.*, 1989; Sullivan *et al.*, 1991, Bertóti *et al*, 1993]. Since the mass of oxygen is usually much lighter than metal cation, the mass effects seems always applicable in the prediction.

In the sputtering of some semiconductor materials the preferential loss of the lighter component was also observed. For example, sputtering of GaP [Liau and Mayer, 1978] and InP [Malherbe, 1993] will cause an apparent deficiency of phosphorus in the surface. Even for lighter ion beams at very low energy, ion bombardment may also induce significant modification to semiconductor surface. Gallet *et al.* [1993] characterised InP(100) surfaces bombarded by 20-200eV hydrogen ion beam using XPS and RHEED, they found H^+ bombardment will cause a phosphorus loss.

1.2.2. Surface binding energy

Bonding of surface atoms is also thought to be one of the critical factors influencing composition of ion bombarded compound surface. Differences in the surface binding energy of the constituents will result in a preferential emission of the component with the lower binding energy and therefore cause enrichment of the component with higher surface binding energy.

The importance of surface binding effects are clearly reflected by the variation of the sputtering yields of pure elements with atomic number under the same experimental conditions, which is illustrated in Figure 1.1. The fluctuations of the sputter yields are obviously due to the different bonding strengths of different element.

In many cases, the bonding effect seems more dominant than the mass effect in sputtering of a compound. Some examples could be found in Betz and Wehner [1983]'s review paper. In the systems, like Ag-Cu, Ag-Pd, Al-Si, Au-Ni, Au-Pd, Cu-Ni, In-Sn, Mg-Al, Pb-Sn, Pb-In, Pd-Fe, *etc.*, heavier species were observed preferentially removed.

Even for sputtering of oxides, surface binding energy effects are thought to be predominant in determining surface composition changes [Malherbe *et al*, 1986; Kelly, 1987a].

Both the mass effect and the surface binding energy have been considered in predictions of sputtering of compound semiconductors. Malherbe and Barnard [1991] studied the surface of InP bombarded with 0.5 to 5 keV Ar^+ ions using AES. Within the limit of experimental errors, they found good agreement between experimental results. Atomic ratio P/In in the bombarded InP surface changed from 0.68 to 0.78 for the incident angle of ion beam from 18 to 42°, which is close to theoretical calculation (P/In=0.72) using model combining the mass and surface binding effects. Another interesting materials is GaAs. Although element Ga and As are very close in atomic mass, it has been reported by many researchers that sputtering of GaAs will result in a

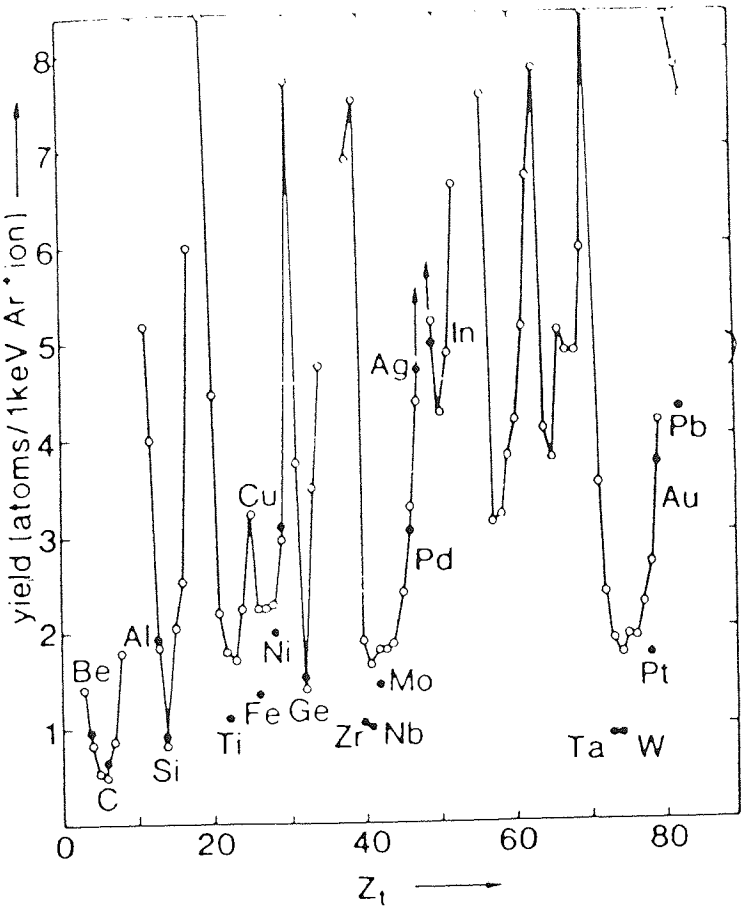

Figure 1.1 The variation of sputtering yield with target atomic number (after Zalm [1988])

significant loss of arsenic (heavier component)[Oostrom, 1976; Kang *et al.*, 1989; Valeri and Bona, 1991]. Malherbe *et al.* [1992] explained this by the fact that since the sublimation heat of As is about 29.0kJ/mol, which is much smaller than 64.8kJ/mol of Ga, a weaker bonding of As in GaAs matrix is expected, resulting in preferential removal of As atoms during ion bombardment.

1.2.3. Bombardment induced segregation and diffusion

In previous sections, the ion bombardment effects discussed are based on the different probabilities of each constituent escaping from the surfaces, so principally these effects only cause compositional changes within a depth corresponding to the origin of particle emission. However, many experimental results have shown that the changes may occur to much larger depth, which are generally comparable with the projected range of the incident ions. This layer of changed composition is called the *altered layer* [Betz and Wehner, 1983]. Although many processes may influence the altered layer, the two major effects, i.e., bombardment induced segregation and enhanced diffusion, are thought dominant. There have been a large number of experiments conducted in last two decades to show these effects.

Wilson [1973] used micro-analytical method to study ion bombarded InP and InSb surface and observed structural changes in both surfaces due to bombardment induced diffusion. SEM showed cone generation in the InP surface after 50keV Ar^+ bombardment. He suggested that ion bombardment causes the preferential loss of P and surface diffusion of In. In the case of InSb under similar conditions of bombardment, Wilson found that the excess indium diffuses to form tall filaments which grow above the original bombarded surface.

Shimizu *et al.* [1973, 1982] investigated the surface compositional changes in Cu-Ni systems during 3keV argon bombardment from room temperature up to 600°C using AES and X-ray microanalysis(XMA) and observed long range depletion of copper of the order of 1000Å in depth, depending on the sputtering time, target temperature and dose rate. Enhanced diffusion of copper was found in the damaged layer at low temperature, this suggests that an interstitial type diffusion mechanism may be predominant.

Swartzfager *et al.* [1981] reported their LEISS profiling analysis of ion bombarded Au-Pd at different elevated temperatures. The surfaces of $Au_{20}Pd_{80}$ alloys were pre-bombarded by 2keV Ne at 200 to 500°C, then the bombarded surfaces were quenched to -90°C, surface composition was finally profiled and probed with 2keV Ne ions. The results showed that Au concentration was increased to about 28% at the first atomic

layer and depleted in the subsurface. This is very good evidence that bombardment induced surface segregation enhanced by elevated temperature plays an important role in ion beam modification of compound surface.

Similar experiments were carried out by Li and Koshikawa [1985] on AuCu systems. They bombarded $Au_{56}Cu_{44}$ surfaces with 2keV argon beam with a current density of $40\mu A/cm^2$ at temperature of -120°C up to 25°C, then the surfaces were cooled to a temperature of -120°C. Surface compositions were obtained with low energy AES depth profiling with the same ion beam, but at a current density of $0.4\mu A/cm^2$. Figure 1.2 shows the compositional depth profile in AuCu surfaces bombarded by Ar beam at different sample temperature. Gold enrichment was found at the top layer, they were convinced that sputtering removal plus Gibbsian surface segregation assisted by ion bombardment enhanced diffusion might play a important role in determining surface compositional distribution of an alloy at or below room temperature. They compared the ion bombardment-enhanced diffusion coefficient estimated from their experiments with the normal inter diffusion coefficient at the same temperature (25°C) without ion radiation, and found that there is about 10^6 times enhancement.

Jiang *et al.* [1990] studied the surface concentration profiles in $Cu_{0.57}Ni_{0.43}$ system bombarded with 7 keV Ar^+ ion beams. They used the conventional depth profile method but with very low energy (0.7keV) and low current argon ion beam to minimise interference to the profile and employed low-energy Auger signals to achieve high surface sensitivity. The measurements indicated a bombardment-induced segregation of Cu in agreement with the results obtained by other spectroscopies. They also observed that Cu depletion in subsurface can be observed as the initial ion fluence increases.

The studies of bombardment induced segregation and diffusion phenomena on compound semiconductors using conventional surface analytical techniques started at the beginning of 1980's. Singer *et al.* [1981] conducted a series of experiments with AES on GaAs single crystal surfaces subject to 0.5 to 5keV Ar^+ ion bombardment at different temperatures. They employed both the low energy (MNN) Auger lines of Ga and As and the high energy (LMM) lines in monitoring surface compositional changes in sputtering, which allows simultaneous measurement of the surface composition with sampling depths of about 20Å and 60Å respectively. They found that although As depletion was observed within both sampling depths, the As/Ga ratio in deeper region was much lower than it in near surface. This implies that similar to metallic alloy bombardment induced segregation also plays a key role in surface compositional change of compound semiconductors.

Bussing *et al.* [1988] did similar work on GaAs surfaces bombarded by 1.5, 3.0

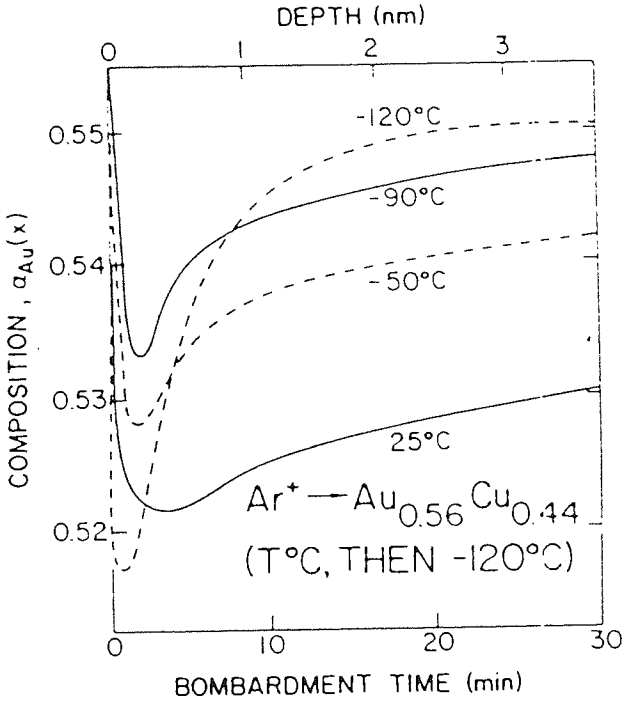

Figure 1.2 Compositional profiles for bombarded $Au_{0.56}Cu_{0.44}$

obtained by first bombarding to steady state with a 40μA/cm^2 beam of 2 keV Ar^+ at the indicated temperature, then cooling to -120°C and finally profiling with 0.4μA/cm^2 beam of 2 keV Ar^+. Compositions were obtained with low-energy AES. (after Kelly and Olive [1986] Li and Koshikawa [1985])

and 5.0 keV Ar^+ beams but using Angular Resolved XPS (ARXPS) technique. They suggested that ion bombardment induced As depletion in the subsurface is due to Gibbsian surface segregation. The As atoms on the surface were replenished by diffusion from the radiated surface region with a diffusion rate enhanced by the high defect density in the region.

Chemical and compositional changes in SiC system induced by ion bombardment have been observed and interpreted in terms of a number of radiation-induced transport processes. The work was reviewed by Miotello *et al.* [1994]. They concluded that for N^+ implantation at least five processes may affect surface composition of SiC system, including (a) Gibbsian segregation, (b) vaporisation, (c) long-range forces such as that provided by unbalanced charges, (d) defect-induced transport, and (e) preferential loss of C from the surface.

Using LEISS and LEIRS (low energy ion recoil spectroscopy), Evdokimov *et al.* [1994] observed the compositional changes in the outermost layer of InSb(100) surface due to 4.8keV Ar^+ beam bombardment. They found that Sb increased at the outermost layer and believed that this is due to the rapid diffusion of Sb to the surface from the Sb depleted lattice.

Complimentary technique of combining LEISS with AES has also been demonstrated by du Plessis and Taglauer [1994] in studying surface concentration modification of Pt_XPd_{1-X} alloys (x=0.3, 0.5 and 0.7) alloys by noble gas ion sputtering. The He, Ne, Ar and Xe ion beams with an energy range from 0.5 to 1.25keV were used. It was shown that Pd is preferentially sputtered from the PtPd surfaces and depleted in the near-surface region. This effect was found to be greater for lighter ion (He) and most pronounced for the lowest energies used. Only a very weak dependence on the surface concentration on the energy of the heaviest ion (Xe) was detected. They ascribed this to the radiation-enhanced diffusion and segregation. Here, it may be necessary to point out that the bombardment effects observed by du Plessis and Taglauer should be more adequately interpreted by the near threshold sputtering theory, which is one of the exceptions to the linear cascade theory [Zalm, 1988]. The near threshold sputtering effects occur normally when very low bombarding energy (0.1-1keV) and/or lighter bombarding ions (i.e. H^+, He^+) are employed. In this regime, the sputtering is predominantly due to primary recoils (see Section 1.3.1.3). Experiments show that, above the minimum threshold energy (a few tens of eV to 100eV), sputtering yield increases superlinearly with bombarding energy, but above ten times of the minimum threshold energy or for heavier ions sputtering yield approaches that expected in the collision cascade regime. A review on these effects has been given by Zalm [1988].

1.2.4. Structural damage

Although the structural modification by ion bombardment is generally not a topic of this research, it is still necessary to have certain basic knowledge of this since such effects may influence the measurement of composition in an ion bombarded surface, for example, in single crystal materials.

For heavy ions (mass >20 amu) incident on a target at the certain dose, either *amorphization* or *crystallisation* may occur, depending on the crystallisation temperature, T_C and the melting temperature of the target materials, T_m. A criteria is adopted for judging the structural changes, that is [Kelly, 1984]:

$$T_c / T_m \geq 0.3 \rightarrow amorphization \qquad T_c / T_m \leq 0.3 \rightarrow crystallization$$

Metals and alloys are normally found to resist amorphization. Surfaces of semiconductor single crystals, however, are generally amorphised by ion bombardment, so the crystallographic effects often seen on metal surfaces will not occur [Wilson, 1984]. For example, Si single crystal surface was observed amorphised after ion impact [Kelly, 1984], which may be predicted by the $T_C/T_m = 0.59$.

The amorphization of the (100) and (110) faces of InP single crystals due to argon ion bombardment was found by Malherbe and Barnard [1991] using SEM, their experimental results showed that the equilibrium surface composition in both faces are not dependent of the crystal orientation.

1.3. Theoretical Predictions

Although there are many models proposed for the prediction of compositional changes in ion bombarded compound surfaces, theoretical analysis on sputtering in low keV regime is generally based on two different approaches: (1) Sigmund linear collision cascade theory based on Boltzmann linear transport equation and classical binary collision approximation; (2) thermodynamic approach, considering the effects of bombardment induced surface segregation and/or diffusion. Both approaches have merits in particular circumstances.

1.3.1. Sigmund's theories

1.3.1.1. Boltzmann linear transport equation

In the low keV regime Sigmund's linear collision cascade theory is based on Boltzmann linear transport theory. For a gas kinetic system, f the particle distribution

function of the gas molecules in phase space (r, p) should satisfy Boltzmann linear transport equation:

$$\frac{\partial f}{\partial t} + \vec{v} \cdot \frac{\partial f}{\partial \vec{r}} + \vec{F} \cdot \frac{\partial f}{\partial \vec{p}} = C(f) \tag{1.1}$$

here r, p, v represent co-ordinate, momentum and velocity of gas molecules; $f=f(r, p)$ is the particle distribution function in phase space (r, p). The collision integral $C(f)$ represents the change of f due to collisions between particles. The third term on left-hand side shows the effect of external field F. In the absence of an external field and when the system is in equilibrium, $C(f)$ is identical to zero.

If we set f', $f_1'$and f, f_1 to be the distribution functions of two particles after and before a collision, then $C(f)$ may be written as:

$$C(f) = \int |\vec{v} - \vec{v}_1| (f' f_1' - f f_1) d\sigma \tag{1.2}$$

here v, v_1 are velocities of two particles before collision; $d\sigma$ is the differential cross section. Generally speaking, every kind of problem on particle collision may be described by the Boltzmann equation with appropriate assumptions.

1.3.1.2. Monoatomic material sputtering

When an ion bombards a solid surface, the schematic of possible collision processes which occur under ion bombardment can be illustrated by Figure 1.3. These processes are: (1) a surface atom receives energy and after several collisions is reflected away from the target. (2) the incoming ion creates a primary recoil which in turn produces a collision cascade that penetrates the surface. (3) a collision cascade which does not penetrate the surface. (4) reflected ion creates a cascade which creates a collision cascade that penetrates the surface. (5) reflected ion gives energy to a surface atom which is sputtered. (6) ion reflected into the vacuum with kinetic energy. (7) atom with momentum component directed away from the surface returns due to attractive forces.

In general the first collision does not lead directly to sputtering since the target atom has a momentum component into the target. Therefore, sputtering is a multi-collision process involving a cascade of moving target atoms, or a collision cascade governing the sputtering process. From this point of view and based on Boltzmann transport equation Sigmund developed a theory of physical sputtering for amorphous or polycrystal targets by low energy ion bombardment based on the following assumptions:

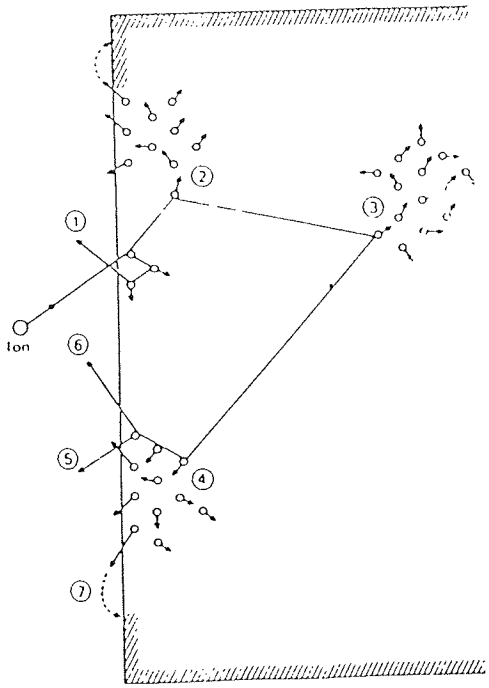

Figure 1.3 Schematic of possible collision processes (after Winter [1975])

Assumptions

1 Atoms are described as *point particles* associated with a cross section which determines the probability for the occurrence of collision.

2 The target is assumed structureless and characterised by a density N of randomly distributed atoms.

3 Collisions are assumed binary and elastic.

4 Particle motion is described by classical dynamics.

5 The density of atoms moving with energy in excess of U is small.

The steps for calculation of a sputtering yield are:

1 to determine the differential cross section, $d\sigma$, for the transfer of energy between T and $T+dT$ from the ion to the target atom and from one target atom to another (introducing the approximation of interaction potentials)

2 to determine the amount of energy deposited near the surface.

3 to convert this energy into the density of low energy recoil atoms.

4 to determine the number of recoil atoms which reach the very surface.

5 to select those atoms which are able to overcome surface binding force and thus be emitted into the gas phase.

Binary collision approximation

Based on the above assumptions, the two-particle collisions should be described by classical dynamics. A schematic of collision between two particles is shown in Figure 1.4.

If we let M_1 and $E=\frac{1}{2}M_1v_0^2$ be the mass and the initial energy of an incoming particle; $E_1=\frac{1}{2}M_1v_1^2$ the final energy of the primary particle after collision at the scattering angle θ, M_2 and $E_2=\frac{1}{2}M_2v_2^2$ the mass and the received energy of target particle moving at a recoil angle ϕ, according to the conservation laws of energy and momentum:

$$\frac{1}{2}M_1v_0^2=\frac{1}{2}M_1v_1^2+\frac{1}{2}M_2v_2^2 \tag{1.3a}$$

$$M_1v_0=M_1v_1\cos\theta+M_2v_2\cos\phi \tag{1.3b}$$

$$0=M_1v_1\sin\theta-M_2v_2\sin\phi \tag{1.3c}$$

Solving the above equations, after substitution $A=M_2/M_1$, we obtain:

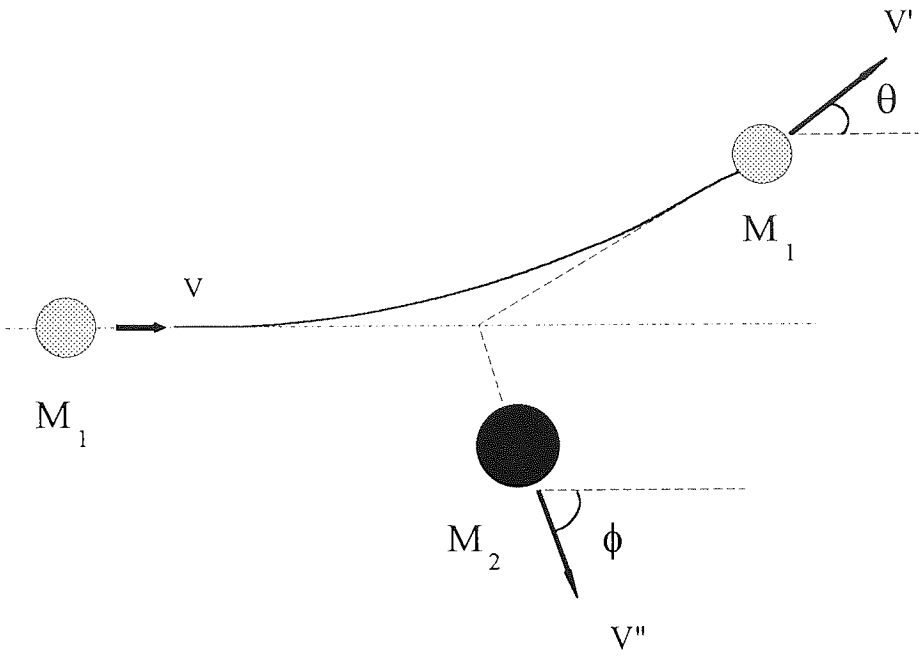

Figure 1.4 Schematic of binary collision approximation

$$\frac{E_2}{E} = \frac{4A\cos^2\phi}{1+A^2} \tag{1.4}$$

$$\varphi = \pi - 2P\int_0^{\infty} \frac{dR/R}{\left(1-\frac{U(R)}{E_R}-\frac{P^2}{R^2}\right)^{\frac{1}{2}}}; \qquad E_R = \frac{M_2}{M_1+M_2}E \tag{1.5}$$

$$d\sigma(\varphi) = -2\pi P dP \tag{1.6}$$

here φ the scattering angle from the centre of mass; ***P*** the impact parameter; ***U(R)*** the inter atomic potential; ***R*** the inter nuclear distance; R_0 the shortest distance between two particles, which is the root of the equation:

$$\left(1-\frac{U(R_0)}{E_R}\right)R_0^2 = P^2 \tag{1.7}$$

Nuclear stopping

From the above analysis, it may be seen that after a collision, a certain mount of energy will be transferred from the incoming particle to the target atoms, more accurately speaking, nuclei, and the incoming particle will slow done. This procedure of the slowing-done due to atomic collision is called *Nuclear Stopping*. The task to evaluate the nuclear stopping of an energetic particle in matter is to calculate the energy loss of the particle in the target.

Since electrons move randomly around the nucleus, the interaction between the nucleus of two particles within the interaction distance cannot be described by simple Coulomb potential. The Thomas-Fermi statistical approach, which assumes that the inter atomic potential varies slowly enough within an electron wavelength and the many electrons can be localised within a volume over which the potential changes by a fraction of itself, is commonly accepted:

$$U(R) = \frac{Z_1 Z_2 e^2}{R}\phi\left(\frac{R}{a}\right) \qquad \text{and} \qquad a \cong \frac{0.885a_0}{(Z_1^{2/3}+Z_2^{2/3})^{1/2}} \tag{1.8}$$

here $\phi(R/a)$ is called the screening function; a is the *screening radius*. a_0 is the Bohr radius, 0.59Å.

In Sigmund's model the T-F potential developed by Lindhard and co-workers is used. The screening function is:

$$\phi\left(\frac{R}{a}\right) = \frac{k_s}{a}\left(\frac{a}{R}\right)^{s-1} \tag{1.9}$$

where k_S and s are constants. Substituting $\phi(R/a)$ into $U(R)$ as well as previous equations, one can obtain:

$$d\sigma(E,T) = C_m E^{-m} T^{-1-m} dT; \qquad m = \frac{1}{s} \tag{1.10}$$

This is called *Power Scattering Cross Section*. here

$$C_m = \frac{1}{2}\pi\lambda_m a^2 \left(\frac{M_1}{M_2}\right)^m \left(\frac{2Z_1 Z_2 e^2}{a}\right)^{2m} \tag{1.11}$$

λ_m corresponds to the Rutherford scattering and depends on m; The *power scattering parameter* m is a very important parameter in the study of ion-atom interaction in a solid, it depends on the mass of ions and atoms and range of energy. With the above approximation, the *nuclear stopping cross section* can be expressed as:

$$S_n(E) \equiv \int_0^{T_m} T d\sigma = \frac{C}{1-m}\left[\frac{4M_1M_2}{(M_1+M_2)^2}\right]^{1-m} E^{1-2m} \tag{1.12}$$

Electronic stopping

Not only can the energy of an energetic particle be transferred to nuclei, but also to an electronic system. The latter is called *electronic stopping*, which may result in electronic excitation or ionisation. The total stopping power should include both the nuclear stopping and the electronic stopping.

Electronic stopping has also been studied by many researchers. In general, for high projectile velocities, electronic stopping dominates the slowing-down of ions, and the electronic stopping cross section is described as: [Sigmund, 1981]

$$S_e = \frac{4\pi q_1^2 Z_2 e^2}{mv^2}\left(\log\frac{2mv^2}{I} + cor.terms\right) \tag{1.13}$$

where q_1 is the projectile charge. I is the mean ionisation potential.

At lower velocities ($v<Z^{2/3}e^2/h$), it can be expressed as:

$$S_e \cong \frac{8\pi\zeta_e a_0 Z_1 Z_2 v}{(Z_1^{2/3}+Z_2^{2/3})^{1/2} h} \tag{1.14}$$

where ζ_e is a function of the atomic number Z_1.

Figure 1.5 systematically shows the nuclear stopping and electronic stopping as a function of energy [Sigmund, 1981]. It may be seen that in the high energy range or for

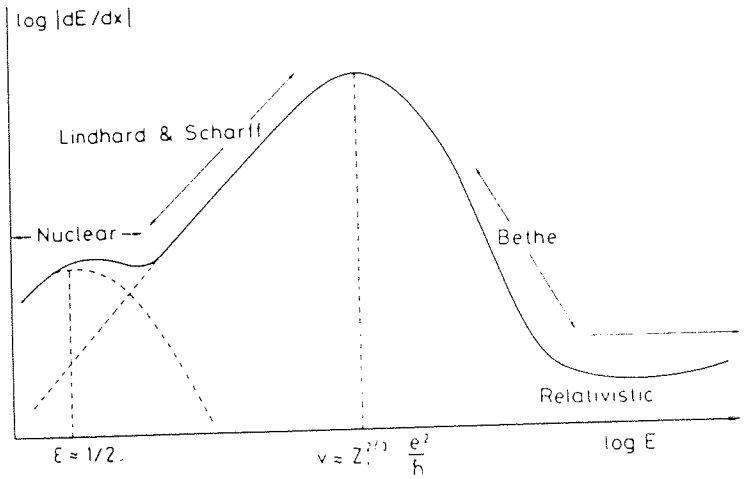

Figure 1.5 Nuclear and electronic stopping power as function of energy (after Sigmund [1981])

lighter ions, electronic stopping is generally dominant, but in the lower energy range or for heavier ions, nuclear stopping is the major contribution to the energy loss. Thus, in talking about low energy atomic collision, the electron stopping is often omitted.

Project range of ions in solids

According to the penetration theory, the energy loss of a particle moving through a random medium is given by:

$$\frac{dE}{dx} = -NS(E) \tag{1.15}$$

here N is the atomic density of the target. $S(E)$ represents the total stopping power which includes both the nuclear stopping and the electronic stopping.

One important penetration parameter, *the mean projected path length, R(E)*, can be defined from the above equation:

$$R(E) = \int_0^E \frac{dE'}{NS(E')} \tag{1.16}$$

Another parameter is *the mean projected range* $R_p(E)$, which is the projection of $R(E)$ in the initial direction of the projectiles. The relation between $R_p(E)$ and $R(E)$ may be illustrated more clearly by Figure 1.6 [Sigmund, 1981].

The accurate calculation of the mean projected range $R_p(E)$ is rather complicated, and one needs to know the angular probability distribution function of ion motion in both polar and azimuthal directions [Biersack, 1987b].

For heavy ions of low energy, nuclear stopping is dominant the slowing-down process, so $S(E) \approx S_n(E)$, Equation 1.16 then yields:

$$R(E) \cong \frac{1-m}{2m} \cdot \frac{E^{2m}}{NC_m} \cdot \left(\frac{4M_1M_2}{(M_1+M_2)^2} \right)^{1-m} \tag{1.17}$$

The mean projected range:

$$R_p = \int < \cos\theta > dR = \frac{R(E)}{1 + \frac{M_2 / M_1}{4m}} \tag{1.18}$$

Sputtering yield of monoatomic materials

With the first two assumptions in the above section it may be deduced that the configuration of particles in (r, p) space is randomised after every individual collision. This is determined only by statistical distribution function $f(r, p, t)$ in Boltzmann transport equation and not by any previous event.

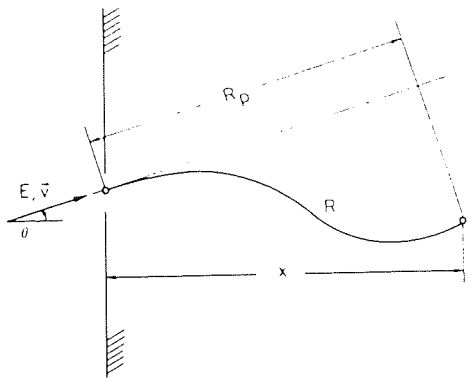

Figure 1.6 Mean projected path length *R(E)* and mean projected range $R_p(E)$ (after Sigmund [1981])

Taking an approach similar to neutron penetration theory and using the fifth assumption in Boltzmann equation, Sigmund obtained the equation for describing the motion of recoil atoms [Sigmund, 1981]:

$$-\left(\frac{\partial}{\partial t}+v\cdot\nabla_r\right)G(r,v,v_0,t)=Nv\int(G-G'-G'')d\sigma \tag{1.19}$$

This is the basic equation for the linear cascade theory. The physical meaning of the function G is the density of atoms moving with velocity v_0 at time t in space. v is the initial velocity of the particle initiating a cascade at $r = 0$, $t = 0$. For simplicity, here only a one dimensional problem (X-direction) is considered and the projectile ion is assumed to be the same species as the target. The following substitutions have been used by Sigmund to develop the analytical solution to sputtering yield [Sigmund, 1969b]:

$$G(x,\vec{v}_0,\vec{v})\rightarrow F(x,\vec{v}_0,\vec{v})=\int_0^\infty G(x,\vec{v}_0,\vec{v})dt\rightarrow H(x,\vec{v})=\int|v_{0x}|F(x,\vec{v}_0,\vec{v})d^3v_0 \tag{1.20}$$

The integration over v_0 obey the condition:

$$\eta_0=\frac{v_{0x}}{v}\le 0;\qquad E_0=\frac{1}{2}Mv_0^2\ge U(\eta_0)$$

here $U(\eta_0)$ is binding energy between target atoms. $H(x,v)$ can be expressed as $H(x, E,)$. $H(0,E,)$ represents the backward sputtering yield. By involving extension in Legendre polynomials, after sophisticated mathematical work, the expression of $H(x, E,)$ can be finally obtained for $m = 0$:

$$H(x,E,\eta)=\frac{3}{4\pi^2}\frac{D(x,E,\eta)}{NC_0U} \tag{1.21}$$

$D(x, E,)$ is defined as the deposited energy in layer (x, dx) by an ion of energy E starting at x=0 and by all recoil atoms. For power scattering it can be shown that at x=0:

$$D(0,E,\eta)=\alpha NS_n(E) \tag{1.22}$$

where α is a dimensionless parameter depends on the relative masses and incident angle.

The sputtering yield for single elemental target may be written as:

$$Y(E,\eta)=H(0,E,\eta)=0.042\alpha\frac{S_n(E)}{U} \tag{1.23}$$

This is the basic equation in yield calculation and has been widely used in computer simulation.

For theoretical analysis the distribution of the mean number of atoms displaced by ions or energetic atoms in energy space has been derived from Sigmund's linear cascade theory. For convenience $F(E, E_0)dE_0$ is defined as the *recoil density*, that is, the average number of atoms recoiling with an energy (E_0, dE_0) as a consequence of a primary ion slowing down from E to zero. $F(E, E_0)$ should satisfy the following integral equation according to Sigmund's theory[Sigmund, 1969a]:

$$\int_0^E K(E,T)dT[F(E,E_0)-F(E-T,E_0)-F(T-U,E_0)]-\delta(T-E_0)=0 \qquad (1.24)$$

here T and U are the kinetic energy and binding energy of displaced atoms, respectively. $K(E, T)$ is the differential cross section.

Using Thomas-Fermi power approximation the asymptotic solution to the above equation can be obtained:

$$F(E,E_0)=\frac{m}{\psi(1)-\psi(1-m)}\cdot\frac{E}{(E_0+U)^{1-m}E_0^{1+m}}\approx\Gamma_m\frac{E}{E_0^2};\quad E>>E_0>>U \qquad (1.25)$$

here $\psi(x)= d[\ln\Gamma(x)]/dx$. $\Gamma(x)$ is *Gamma* function.

If $D(E, \Omega, r)$ is defined as the deposited energy in solid angle Ω, then:

$$\int D(E,\Omega,r)d^3r = E \qquad (1.26)$$

here the electronic stopping can be easily considered by employing the Lindhard scheme, or the E in the above equations is replaced by E-$\eta(E)$. $\eta(E)$ stands for the energy loss due to electron excitation. In regime of low keV the electron stopping is very small part, so it is normally omitted. The distribution of the recoil atoms in space is:

$$F(E,E_0,\Omega_0,r)dE_0d\Omega_0d^3r\approx\Gamma_m\frac{D(E,\Omega,r)}{E_0^2}dE_0\frac{d\Omega_0}{4\pi}d^3r \qquad (1.27)$$

From Equation 1.25 for power scattering approximation, The backsputtering yield from surface of a monoatomic target can be finally expressed as:

$$Y=\frac{\Gamma_m}{8(1-2m)}\cdot\frac{1}{NC_mU_0^{1-2m}} \qquad (1.28)$$

In the above procedure it is assumed that implanted ions have the same mass as target atoms. For unequal masses of ion and target atoms the above conclusions are also valid [Sigmund, 1969b].

Depth range of sputtered atoms

After integration of Equation 1.27 over the hemisphere and insertion of Equation

1.12, the mean number of sputtered atoms per ion with an energy exceeding an arbitrary minimum energy E_0 (E_0>>U) may be calculated from:

$$Y(E_0) \cong \frac{\Gamma_m}{4} \frac{1-m}{1-2m} \frac{E_0^{2m}}{NC_m} \frac{D(E,\theta,0)}{E_0} \tag{1.29}$$

here θ is the incident angle of the ions.

By definition and Equation 1.25, the $Y(E_0)$ can also be written as:[Sigmund, 1981]

$$Y(E_0) \cong \frac{\Gamma_m}{4} \cdot \frac{D(E,\theta,0)\Delta x_0}{E_0} \tag{1.30}$$

here the second term represents the number of atoms per ion in motion, with an energy exceeding E_0 , in the depth interval (0, Δx_0), and 1/4 is a cosine factor averaged over the hemisphere (outside surface).

Obviously, the quantity Δx_0 should be:

$$\Delta x_0 \cong \frac{1-m}{1-2m} \frac{E_0^{2m}}{NC_m} \tag{1.31}$$

From the above equation, it can be concluded that the sputtered atoms with higher energy will come from deeply inside the target, and for low energy ions (m≤0.2), Δx_0 is rather insensitive to ion energy. Sigmund also proved that Δx_0 is generally less than 10Å [Sigmund, 1969b]. For E_0 approaching U, Equation 1.31 is modified slightly due to surface binding.

1.3.1.3. Multi-component material sputtering

For a compound material the sputtering is not necessarily stoichiometric, one of the obvious reasons is that for atoms with different atomic number, mass and binding energy the energy share between atoms is different. Generally, two kinds of topics, which are associated with multi-component sputtering, are discussed in the literature: the first, the physics of an individual sputtering event on a target with a given composition; the second, the changes in target composition caused by prolonged bombardment. The former is called by Sigmund the ***Primary effect*** and the later called the ***Secondary effect.***

Primary effect

For the primary effect the energy share in a binary system has been studied within the linear cascade regime by Andersen and Sigmund [1974]. Based on the theory of monoatomic sputtering the following integral-differential equations can be derived from the Boltzmann transport equation.:

$$\sum_k c_k \int d\sigma_{ik}\{F_{ik} - F'_{ik} - F''_{kj}\} = c_j \frac{d\sigma_{ik}(E, E_0)}{dE_0} \tag{1.32}$$

here $$\frac{d\sigma_{ik}(E, E_0)}{dE_0} = \int \delta(T - E_0) d\sigma_{ik}$$

$$\sum_k c_k \int d\sigma_{ik}\{G_{ik} - G'_{ik} - G''_{kj}\} = \frac{\psi}{N v_0} \delta_{ij} \delta(E - E_0) \tag{1.33}$$

here subscription ij stands for j-atoms recoiling in a collision cascade initiated by an i-ion bombardment. c_j is the concentration of j-atoms. $F'_{ij}=F_{ij}(E', E_0)$ and $F''=F_{kj}(E'', E_0)$, E' and E'' are the energies of a scattered i-atom and a recoiling k-atom, respectively. Therefore:

$$\frac{d\sigma_{ij}(E, E_0)}{dE_0} = \int_{E', E''} d\sigma_{ij}(E, E', E'') \delta(E'' - E_0) \tag{1.34}$$

By comparison between the two integral-differential equations and based on *the Green's function* theorem, F_{ij} has the following relation with G_{ij}:

$$F_{ij}(E, E_0) = c_j \sum_l \int dE_1 \frac{N v_1}{\psi} G_{ij}(E, E_1) \frac{d\sigma_{ij}(E_1, E_0)}{dE_0} \tag{1.35}$$

In order to obtain the solution to Equation 1.33, the following approximation is made that:

$$G_{ij}(E, E_0) \approx g_j(E_0) \cdot [E - \eta_i(E)] \tag{1.36}$$

here $\eta_i(E)$ is the electronic energy loss. When the electronic energy is ignored, the two important features can be easily seen, that is: (i) the linear dependence on energy deposition E; (ii) the independence on the type of bombarding atom. Using Thomas-Fermi interatomic potential in the calculation of cross section and Laplace transform, together with a mathematical approximation, the ratio of the fluxes of moving atoms in binary element target is:

$$\frac{G_{i1}(E)}{G_{i2}(E)} \approx \frac{c_1 S_{21}(E_0)}{c_2 S_{12}(E_0)} \qquad i=1, 2 \tag{1.37}$$

here $S_{ik}(E)$ is the nuclear stopping cross section of an i-atom colliding with a k-atom. The ratio of the recoil density can be derived according to Equation 1.35:

$$\frac{F_{i1}}{F_{i2}} \approx \frac{c_1 S_{21}(E_0) c_1 S_{11}(E_0) + c_2 S_{12}(E_0)}{c_2 S_{12}(E_0) c_2 S_{22}(E_0) + c_1 S_{21}(E_0)} \qquad i=1, 2 \tag{1.38}$$

The above equations show that: (1) the ratio of the fluxes of moving 1-atoms to 2-atoms is proportional to the ratio of the relative concentration, but not necessarily identical to it. (2) an even more pronounced deviation from stoichiometry is expected in the ratio of the number of recoiling 1-atoms and the recoiling 2-atoms, since the concentrations enter non linearly.

Following the procedure in derivation of monoatomic sputtering the partial sputtering yield Y_i of the i-atom is:

$$Y_i = c_i \Lambda'_i D(E,\varphi,0); \qquad \Lambda'_i = \frac{\Lambda_i}{c_i} \cdot \frac{G_i/(G)_i}{[U_i/(U)_i]^{1-2m_i}}; \qquad i=1,2 \tag{1.39}$$

In above equations the $D(E,\varphi,0)$ is the energy deposited (per unit depth) in the alloy; $G_i/(G)_i$ and $U_i/(U)_i$ stand for the ratio of the fluxes of i-atoms moving and the binding energy in the alloy to that in an i-elemental target, respectively.

According to Equation 1.37 and 1.39 and the previous calculation for the energy share in binary case the ratio of partial sputtering yield can be written as [Sigmund, 1981]:

$$\frac{Y_1}{Y_2} = \frac{G_1(E_0)(dE_0/dx)_1}{G_2(E_0)(dE_0/dx)_2} \cdot \frac{U_2^{1-2m_2}}{U_1^{1-2m_1}} \approx \frac{c_1}{c_2} \cdot \frac{S_{21}(U_2)}{S_{12}(U_1)} \tag{1.40}$$

here E_0 is an arbitrary energy $<<E$; S_{ij} is the stopping cross section for an i-atom colliding with a j-atom.

For $M_1 \cong M_2$, the power scattering parameter $m_1 = m_2$, so

$$\frac{Y_1}{Y_2} = \frac{c_1}{c_2} \cdot \left(\frac{M_2}{M_1}\right)^{2m} \cdot \left(\frac{U_2}{U_1}\right)^{1-2m} \tag{1.41}$$

Equation 1.41 predicts a tendency for the lighter component to be removed preferentially. However, since m is normally very small (especially in the low keV regime), $0 \le m \le 0.2$, this effect is less important than the effect of surface binding energy, assuming that no other effects are involved in the sputtering.

In 1987 Sigmund presented a theoretical model for sputtering of isotopic mixtures and near-neighbour elemental targets [Sigmund, 1987], which is based on the previous work and mathematical approximations to cross section for binary elastic collision. The main limitation is that the model is restricted to small relative differences in mass of isotopic atoms or the near-neighbour elements, that is:

$$\Delta M_i << M = \sum_i c_i M_i \qquad \text{and} \qquad \Delta Z_i << Z = \sum_i c_i Z_i \tag{1.42}$$

here M, Z is the mean mass and the mean atomic number of the target; c_i is the abundance of i-element or isotope. Although this effort did not give many useful results for practical work, the importance of atomic interaction in compound material sputtering has been extensively emphasised. As Sigmund said "*details of the interatomic potential governing collisions between target species are crucial for both magnitude and sign of the nonstoichiometry of the emitted particle flux in case of an alloy target.*"

Secondary effects

After prolonged bombardment the composition in the surface region will be changed by some mechanisms, including the non-stoichiometric sputtering due to the differences in mass and surface binding energy of target atoms. Therefore, the contribution of the enriched species (lower sputtering yield) will increase until the composition of the sputtered flux reflects the composition of the bulk target.

If Δx is the depth of atoms emerging from surface, the composition of a surface layer after sputtering should be [Sigmund, 1981]

$$\left(\frac{c_1}{c_2}\right)_{\Delta x} \approx \left(\frac{c_1}{c_2}\right)_{bulk} \cdot \left(\frac{c_1 Y_2}{c_2 Y_1}\right) \tag{1.43}$$

$(c_1/c_2)_{\Delta x}$ can be determined experimentally using various surface analytical tools, such as AES, XPS, ISS, RBS etc.

Since ion bombardment not only causes surface sputtering, but also bulk processes, in which the ion composition changes extend to the order of the ion projected range rather than a shallow layer of Δx, the topic on ion bombardment, in fact, is much more complicated.

At least four different bulk processes are active: (i) segregation (ii) recoil implantation (iii) cascade mixing (iv) diffusion. Recoil implantation projects *lighter* species into the bulk and causes the *heavier* ones to be enriched in the near surface region. Cascade mixing and radiation enhanced diffusion tend to reduce the concentration gradients generated by preferential sputtering or recoil implantation. Radiation induced surface segregation has been recognised to be significant in multi-component sputtering. These effects will be discussed in detail in the following subsections.

1.3.1.4. Nonstoichiometric sputtering model (Malherbe's model)

Based on Sigmund's theory, Malherbe *et al* [1986] derived a formula from

Equation 1.41 and 1.43 and applied it in the prediction of composition change in ion bombarded surfaces of metallic oxides. According this model, the atomic ratio of metallic atoms to oxygen in the ion bombarded surface is determined by:

$$\frac{(x_M / x_O)^s}{(x_M / x_O)^b} = \left(\frac{M_M}{M_O}\right)^{2m} \cdot \left(\frac{U_M}{U_O}\right)^{1-2m} \tag{1.44}$$

here subscripts *M, O* represent metal and oxygen; Superscripts *s, b* stand for surface and bulk. The power scattering parameter m=0.165 was chosen by Malherbe *et al* to give good agreement between theory and experiments. In this model, the role of surface binding energy was particularly emphasised.

They proposed a new approach to calculate the binding energies of metal oxides by modifying the Pauling formalism [1967] for the bond energies in a covalent bond. For molecule M_xO_y the average bond energy is given by:

$$D(M_xO_y) = \frac{x}{x+y}D(M-M) + \frac{y}{x+y}D(O-O) + \frac{x}{x+y}D(M-O) + \frac{1}{2}(\varepsilon_M - \varepsilon_O)^2 \tag{1.45}$$

where *D(M-M)*: metal-metal bond energy; *D(O-O)*: the dissociation energy of the oxygen molecule; *D(M-O)*: the metal-oxygen bond energy of diatomic metal oxides; ε_M and ε_O: the electronegativities of metal and oxygen. So the average energy required to remove only an oxygen atom given by [Malherbe *et al.*, 1986]:

$$U_o = \frac{y}{x+y}D(O-O) + \frac{x}{x+y}D(M-O) + \frac{1}{2}(\varepsilon_M - \varepsilon_O)^2 \tag{1.46}$$

For a metal atom in an oxide, the binding energy is assumed to be:

$$U_M \equiv H_s + \frac{1}{2}(\varepsilon_M - \varepsilon_O)^2 \tag{1.47}$$

here H_S is the sublimation energy of the (pure) metal.

These formalisms were also used by Malherbe and Barnard [1991] in a description of sputtering of InP, and agreement of the predictions of the model with the experimental results was very good. The model, however, was not applied in their study of sputtering of GaAs. The reasons become apparent from this author's work and are discussed in Chapter 5.

1.3.2. Kelly's models for nonstoichiometric sputtering

Kelly is one of the most important contributors to this field, and much significant work has been done by him and his co-workers in the last two decades. Unlike Sigmund

whose model on sputtering is generally based on theoretical analysis, namely direct derivations of Boltzmann linear transport theory, Kelly's theories are generally based on experimental observations.

An initial model was based on Sigmund's linear cascade sputtering theory [Kelly, 1978], but Kelly assumed that linear collision cascade sputtering does not take place in the top monolayer. He then arrived at the formulae for the partial sputtering yield ratio:

$$\frac{Y_1}{Y_2} = \frac{(x_1 + x_2\gamma)}{(x_2 + x_1\gamma)} \cdot \frac{U_2}{U_1} \tag{1.48}$$

here γ is the maximum energy transfer factor. For a random binary alloy the surface binding energies were expressed by Kelly [1980] as functions of the nearest-neighbour bond strengths U_{11}, U_{12}, U_{22}, thus the surface binding energy for U_1 is calculated from:

$$U_1 = -x_1^s Z_s U_{11} - x_2^s Z_s U_{12} \tag{1.49}$$

where Z_s is the surface co-ordination number; $x^s_{1,2}$ are surface atomic concentrations of two elements. Using the first-order approximation to replace U_{11}, U_{12}, U_{22} with the heat of atomisation H_1 and H_2, Kelly obtained the following equation:

$$\frac{Y_1}{Y_2} = \frac{x_1 + \gamma x_2(1 + x_2^s)H_2 + (1 - x_2^s)H_1}{x_2 + \gamma x_1(1 + x_1^s)H_1 + (1 - x_1^s)H_2} \tag{1.50}$$

From this model the enrichment of one component is predicted by surface binding energy, namely the component with higher surface binding energy will enrich the sputtered surface. This is in general agreement with experimental results for many alloys although the enrichment observed from experiments is much greater than that predicted by the above equation [Betz and Wehner, 1983].

By considering surface-vacancy formation during sputtering, Kelly [1987] proposed models based on chemical dynamics for calculating surface binding energies in Sigmund's theory. Normally, for metals and alloys the surface binding energy was thought to be identical to the cohesive energy, i.e. the heat of atomisation. This value has been proved experimentally to be too low. Kelly suggested that the process of a metal atom sputtering from a solid should take place in two steps: (1) the atom moves due to linear collision cascade from *an in-surface* to a *half-space* site, if the step is sufficiently slow (say 10^{-14} to 10^{-12} seconds), this step can be characterised by the surface-vacancy formation energy, E_f^s .(2) then the atom leaves the solid from a *half-space* site to vacuum, characterised by the heat of atomisation, H_a. The surface binding energy should include these two energy terms. If this is done, then the resultant surface binding energy is about 30% larger than the heat of atomisation of the atom. For an ionic oxide or

halide, the calculation in surface binding energy is based on the defect theory, the lattice energy for vacancies, ionisation potential, the formation energy of a hole inclusive of electronic and ionic relaxation, and that of lattice electron are considered in the model. A unique feature in this approach is that binding for a diatomic oxide can be easily taken into account, which is very useful in practical work since in experiments a large amount of molecular-type products are found in the sputtered particles. For example, using SNMS, Oechsner *et al.* [1978] found the MO yield in Ta_2O_5, MoO_3 and WO_3 systems is higher than pure metal *M* yield. Kelly calculated the binding energies of Al, AlO and O, and explained the fact observed in experiments that more AlO (over 50%) products are found in sputtering Al_2O_3 due to the fact that AlO has the lowest surface binding energy.

In his review papers on the sputtering of insulators Kelly [1984] classified the sputtering mechanisms into several processes according to time scale, which are shown in Table 1.1

Table 1.1 Kelly's classifications for sputtering processes

Process	Time Range (second)
Prompt collisional	10^{-15} - 10^{-14}
Slow collisional	10^{-14} - 10^{-12}
Prompt thermal	10^{-12}-10^{-10}
Slow thermal	10^{-10} - 10^{0}
Exfoliational	10^{0} - 10^{1}
Electronic Transition	10^{-13} - 10^{0}

He commented that the current theories on sputtering of metals (alloys) and oxides (and halides) are similar only in talking about total yields, when dealing with atom yields, diatomic yields, ion yields and preferential effects they are significantly different. He thought that the mass effect is predominant in preferential sputtering only in isotope sputtering or sputtering under near-threshold conditions. For non-stoichiometric sputtering of alloys, he pointed out that preferential effects are mainly dependent of bombardment induced Gibbsian segregation, but for oxides, the effects are "originally not due to segregation", since an oxide in the highest oxidation state, such as TiO_2, Ta_2O_5, Al_2O_3, etc., does not permit excess O at surface. He emphasised that for sputtering of oxides including covalent oxides surface binding energy is dominant. He also showed from experimental results that the presence of chemical reactive gas such as O_2 will substantially change binding energies of components in an ionic substances and then lead to a surprisingly different results.

In 1990, Kelly published a paper on thermal sputtering. Based on the assumption

of one-dimensional unsteady adiabatic expansion (UAE), he developed a gas-dynamic model for analysis of the phenomenon of thermal sputtering. Using this model he proved that within the given experimental uncertainties the energy flux appropriate to thermal sputtering generally has Maxwellian form and the sputtering yield greatly exceed those predicted for collisional sputtering. The most important conclusion obtained from Kelly's analysis was that it is physically possible for a system temperature greater than the thermodynamic critical temperature. This means that thermal sputtering is more likely to be a gas-dynamic process rather than true vaporisation [Kelly, 1990].

1.3.3. Radiation induced surface segregation and diffusion

Since the 1980's, the role of surface segregation and diffusion induced and/or enhanced by ion bombardment has been emphasised in explaining the sputtering effects of metallic alloys, especially in interpretation of the differences between the experimental results obtained by different surface analytical techniques. Segregation is generally classified into two different categories in literature: (1) equilibrium segregation, such as Gibbsian surface segregation (or Gibbsian adsorption), which is driven by a force minimising surface free energy (2) non-equilibrium segregation, such as radiation-induced segregation described by Wagner *et al.* [1983], which results from the preferential transport of certain alloying elements via persistent defect fluxes generated during radiation [Was, 1990]. Many models have been developed based on various theoretical approaches. Kirschner [1985] reviewed all experimental and theoretical work up to 1985 on surface segregation and its implication for sputtering and discussed various driving forces and kinetics in the segregation process. He classified the current models on surface segregation into three different theories: first principles theories, semiempirical and phenomenological models. Another comprehensive review was given by Lam and Wiedersich [1987].

1.3.3.1. Thermodynamic interpretation to equilibrium surface segregation

Consider a binary system AB. The numbers of element A and B in surface and in bulk are N_A^s, N_B^s, N_A^b and N_B^b, respectively. The total numbers in the surface and in the bulk are N^s and N^b. The change in the free energy ΔF that accompanies the exchange of a surface B atom with a bulk A atom [Zangwill, 1988]:

$$\Delta F = F\left(\frac{N_A^s+1}{N^s}, \frac{N_A^b-1}{N^b}, \frac{N_B^s-1}{N^s}, \frac{N_B^b+1}{N^b}\right) - F\left(\frac{N_A^s}{N^s}, \frac{N_B^b}{N^b}, \frac{N_B^s}{N^s}, \frac{N_B^b}{N^s}\right) \qquad (1.51)$$

Expand the first term to first order and replace N_A^s/N^s, N_B^s/N^s, N_A^b/N^b and

N_B^b/N^b with x_A^s, x_B^s, x_A^b and x_B^b, the concentrations of element A and B at the surface or in the bulk:

$$\Delta F = (\frac{\partial F}{\partial x_A^s} \cdot \frac{1}{N^s} - \frac{\partial F}{\partial x_B^b} \cdot \frac{1}{N^s}) + (\frac{\partial F}{\partial x_B^b} \cdot \frac{1}{N^b} - \frac{\partial F}{\partial x_B^s} \cdot \frac{1}{N^s}) \tag{1.52}$$

Assuming that the total number of A and B atoms is fixed, the conditions for the system having minimum free energy at equilibrium are:

$$N^b \frac{\partial F}{\partial x_A^s} = N^s \frac{\partial F}{\partial x_A^b} \qquad \text{and} \qquad N^b \frac{\partial F}{\partial x_B^s} = N^s \frac{\partial F}{\partial x_B^b} \tag{1.53}$$

Therefore, combining Equation 1.52 with 1.53, it may be found that the free energy of the interchange, $\Delta F=\Delta U-T\Delta S$, vanishes at the equilibrium. Since the change in entropy $\Delta S = -k\Delta\Sigma N_i \ln x_i + \Delta S_0$, ($k$ is Boltzmann constant; i represents A and B atom at the surface and in the bulk), the relation of the surface composition of the system in terms of the bulk composition:

$$\frac{x_A^s}{x_A^b} = \frac{x_B^s}{x_B^b} e^{-(\Delta U - \Delta S_0)/kT} \tag{1.54}$$

In surface region the internal energy of one element U is given by Gibbs equation:

$$U=TS-PV-\mu N+\gamma a \tag{1.55}$$

where P, V, N and μ stand for pressure, volume, total number of the system and chemical potential of one atom. γ and a represent surface tension and the area of the surface. The product of γ and a is the surface energy.

Supposing no changes in pressure, volume, temperature and chemical potential of the system during surface segregation, Equation 1.54 may be expressed as:

$$\frac{x_A^s}{x_A^b} = \frac{x_B^s}{x_B^b} e^{-Q/kT} \tag{1.56}$$

This is the well-known Langmuir-Mclean equation [Kirschner, 1985]. Q is called the heat of segregation, which is equal to the difference in surface energy between atoms A and B. From Equation 1.56, it may be expected that the surface is enriched in the component with the lower surface energy.

1.3.3.2. Miedema's model and the other models

Miedema's model [Miedema, 1978] is based on the phenomenological electronic theory. The model is derived generally from the Langmuir-Mclean equation, but

Miedema included the heat of solution term for dilute alloys to account for the modified environment of the exchanged atoms in the bulk and at the surface. He also demonstrated that the surface energy or surface tension is related to the electron density at the boundary of a bulk atomic cell, so some relaxation of the electron density distribution and the position of the atoms at the surface layer were taken into account in the model.

According to Miedema's model, the heat of segregation for a metal A diluted into metal B is expressed as:

$$Q = f\Delta H_{sol}(A,B) - \frac{g}{3}(\gamma_A - \gamma_B)V_A^{2/3} \tag{1.57}$$

where $\Delta H_{sol}(A, B)$ is the partial molar heat of solution of metal A in metal B; V_A represents the molar volume of A; the relaxation factor f is equal to 0.71; the constant g is equal to 4.0×10^8.

Miedema thought that due to the relaxation of electron density distribution and the position of atoms in the surface layer, the fraction of the surface area of a surface layer atom contact with vacuum should be smaller than one third of the total surface area. He assumed that this value was 24%. He also pointed out that in some cases the heat of evaporation could not be used to measure the strength of the cohesive bonds in a solid which are broken at a metal-vacuum surface. The heat just measures the difference of a atom in the solid and it to be a free atom in gas.

In Miedema's model not only the effect of surface energy but also that of mismatch between two kinds of elements in sizes have been considered in segregation. Miedema has also derived a table of values for the surface energies of B Group elements. Compared with experiments for many transition metal alloy systems Miedema's calculation gives a very good agreement.

Robbins and Falicov [1983] developed another methods by taking the results of first principles calculations for elemental solids as an input quantity to calculate heats of formation between 4d-metals to predict surface segregation. This model enables the roles of s-p electrons, band-width mismatch and band mixing to be examined, the latter two are found to be dominant for 4d-transition metal alloys.

The semiempirical theories [Kumar *et al.*, 1976] have been studied extensively in quantitative prediction. They have been used to describe segregation over whole range of temperatures including short-range order, long-range order and phase transitions. The effects of chemically induced segregation were tackled by this approach.

Beside above models there are a few of other models have been derived based on

electronic theories. The tight binding approximation [Kerker *et al.*, 1977] is widely used to predict surface segregation in d-band metals. A common agreement is that segregation should strongly depend on more open crystal surfaces and weakly on dense planes. An embedded cluster model of muffin-tin atoms has been considered by Muscat [1982], it was found that the presence of the surface potential plays the predominant role in surface segregation. Similar to Muscat's model Barnett *et al.* [1983] propose an electron theory by using local ionic pseudo potential and a linear response model.

Generally speaking, none of models claims to be universally applicable but within their range of validity the agreement with experiments is quite good.

1.3.3.3. Kelly's model for bombardment induced segregation

Recently the failure of models based on mass and binding energy for sputtering of alloys have been emphasised and the conclusion that radiation induced surface segregation, mainly ion bombardment induced Gibbsian segregation [Kelly and Oliva, 1986] plays a dominant role in preferential sputtering in a wide range of materials has been reached. This situation is manifested in the conflict of evidence between different techniques employed in the investigations. Many ISS experiments show contradictory results to those obtained from AES and XPS. Because ion scattering spectroscopy has a different sampling depth from standard AES and XPS, these "contradictions" give very good evidence that ion bombardment leads to the changes in component distribution in near surface regions.

Combining the mass and surface binding energy effects with the diffusion properties of target atoms, Kelly and Oliva [1986] developed a model for describing the bombardment induced segregation effect on the composition changes of an alloy system. Since the composition predicted by this model is controlled by three ill defined parameters, these are, the power-law parameter m, the subsurface sputtering fraction β and the segregation ratio K, it is impossible to use this model for quantitative analysis. But some conclusions were reached from their model: (1) bombardment-induced Gibbsian segregation in alloys will lead typically to composition profiles as shown in Figure 1.4. thence to preferential sputtering of the segregating species. (2) steady state outer-surface composition is determined by not only the effects of mass and surface binding energy, but also bombardment induced segregation and diffusion. It is measurable only with surface sensitive technique, such as ISS or SIMS. (3) steady-state sub-surface composition is only influenced by bombardment induced segregation, which is similar in form to Gibbsian equilibrium surface segregation.

In his paper published on 1989, Kelly emphasised the role of segregation in ion

bombardment-induced compositional change. He pointed out that although the sputtering of alloys is linked to differences in mass or binding energy, but these are generally much weaker driving forces than segregation [Kelly, 1989].

Recently, Kelly and co-worker published a serious of papers on ion beam mixing with chemical guidance [Kelly and Miotello, 1992] [Miotello and Kelly, 1994a&b]. They studied various aspects on this topic including the heat of positive heats of mixing in a binary system when motion is in partially ballistic and partially chemically driven, phase formation as a kinetic phenomenon and thermodynamic effects without invoking thermal spikes.

1.3.3.4. Wiedersich's model (non-equilibrium segregation)

Wiedersich's model of radiation-induced segregation was established on the concept of preferential coupling between defect fluxes and fluxes of certain alloying elements. A unique character of this model is that the defects created by ion bombardment are clearly considered in surface segregation and diffusion. This model was summarised by Wagner *et al.* [1983].

When an ion beam incidents on a solid surface, both the migration of vacancies and interstitials via atoms and the atom fluxes via the vacancies and the interstitials may occur. In a binary alloy AB, the defect fluxes and atom fluxes may be expressed in terms of partial diffusion coefficients of A and B components. For example, the partial diffusion coefficient of k (k=A or B) atoms via vacancies and that for vacancies via k atoms can be written as:

$$D_k^v = d_{kv} C_v \qquad \text{and} \qquad D_v^k = d_{kv} C_k \tag{1.58a \& b}$$

where C_V is the atomic fraction of vacancies; C_k is the concentration of k atoms; d_{kv} is the diffusivity coefficient of k atoms via vacancies.

Similarly, the partial diffusion coefficients of the elements via interstitials and interstitials via elements may be easily derived from Equation 1.58a&b with the subscripts and superscripts v replaced by i. That is:

$$D_k^i = d_{ki} C_i \qquad \text{and} \qquad D_i^k = d_{ki} C_k \tag{1.59a \& b}$$

The total diffusion coefficients for an A-B system may be calculated from the above equations, as follows:

$$D_v = d_{Av} C_A + d_{Bv} C_B \qquad D_i = d_{Ai} C_A + d_{Bi} C_B \tag{1.60a \& b}$$

$$D_A = d_{Av} C_v + d_{Av} C_i \qquad D_B = d_{Bv} C_v + d_{Bi} C_i \tag{1.60c \& d}$$

The coupled partial differential equations then can be written as:

$$\frac{\partial C_v}{\partial t} = \nabla[-(d_{Av} - d_{Bv})C_v \nabla C_A + D_v \nabla C_v] + pK_0 - K_{iv}C_i C_v - K_{sv}C_v C_s \quad (1.61a)$$

$$\frac{\partial C_i}{\partial t} = \nabla[(d_{Ai} - d_{Bi})C_i \nabla C_A + D_i \nabla C_i] + pK_0 - K_{iv}C_i C_v - K_{sv}C_v C_s \quad (1.61b)$$

$$\frac{\partial C_A}{\partial t} = \nabla[D_A \nabla C_A + C_A(d_{Ai} \nabla C_i - d_{Av} \nabla C_v)] \quad (1.61c)$$

here K_0 is the defect production rate and p is the efficiency factor which takes into account that only a fraction of the defects produced in a cascade will escape spontaneous recombination and clustering and contribute to the radiation induced segregation. The terms K_{iv} K_{sv} *and* K_{si} are the rate coefficients for mutual recombination and for the annihilation of vacancies and interstitials at the internal sinks.

At steady state, the following relation between ∇C_A and ∇C_v holds:

$$\nabla C_A = \frac{C_A C_B d_{Av} d_{Bv}}{C_B d_{Bi} D_A + C_A d_{Ai} D_B} \cdot \left(\frac{d_{Av}}{d_{Bv}} - \frac{d_{Ai}}{d_{Bi}} \right) \cdot \nabla C_v \quad (1.62)$$

It is shown that in the steady state the concentration gradient in a compound surface is determined by the ratios d_{Av}/d_{Bv} and d_{Ai}/d_{Bi} which reflect the preferential association of vacancies and/or interstitials with A and B atoms. During radiation, the defect concentrations always decrease towards a defect sink, so the above equation predicts that the element A becomes enriched at sink if $d_{Av}/d_{Bv} < d_{Ai}/d_{Bi}$.

Using this model, Wagner *et al.* [1983] successfully predicted the compositional changes in Ni-Cu alloy surfaces.

1.3.3.5. Bombardment induced/enhanced diffusion

Diffusion in solids is another dynamic process influenced by ion bombardment. Ordinary diffusion (Fickian diffusion) in alloys proceeds through defects interactions. Normal defects which are produced by thermodynamic lattice disorders decrease so strongly at room temperature that little or no diffusion occurs, particularly in a perfect semiconductor system. The diffusion coefficient is generally expressed by the relationship:

$$D = D_0 e^{-\frac{Q_a}{kT}} \quad (1.63)$$

where the pre-exponential factor D_0 is nearly independent of temperature; Q_a is the activation energy. For an atom jumping from a lattice site to a neighbouring one in a

perfect system, the activation energy should include two parts: (1) the formation energy H_f of the vacancy; (2) the motion or migration energy H_m of the atom; that is, $Q_a=H_f+H_m$. Figure 1.7 shows the potential energy diagram of an atom along a lattice row (the direction of atom motion) with barrier.

With ion beam radiation, vacancies will be generated by atomic collision, hence only H_m is required for the atom to jump from one vacancy to the next, that is, the activation energy $Q'_a \approx H_m$. Since H_f for diffusion in semiconductor materials is generally much greater than H_m, the difference in diffusion coefficient with and without ion radiation can be large. For example, H_f and H_m for Si self-diffusion in Si and for Ge in Ge are 3.9, 0.4eV and 2.4, 0.2eV respectively [Tu *et al*, 1987]. The ratios of diffusion coefficients in Si and Ge with and without ion beam radiation at room temperature may be calculated from Equation 1.63, and are as high as 5.6×10^{67} and 4.9×10^{41}, respectively.

Ion bombardment not only causes atomic displacement by elastic ion-atomic collisions, but also may induce inelastic ionisation processes which provide additional driving forces for diffusion [Appleton, 1984]. These latter effects are more important for semiconductor materials. During ion-atom interactions, recoils may be charged in two different ways: (1) electron transfer from target atoms to ions by Auger and/or resonant processes (2) energy transfer from ions (or energetic recoils) to the electrons of target atoms. The first mechanism is less important since one ion, for example, an Ar^+, only causes one atom to be charged. The second mechanism, however, is much more important, since it may excite electron systems of several target atoms.

Normal ionisation enhanced mechanism described by Bourgoin *et al.* [1973] is the process in which the potential energy traverse through the lattice varies with charge state so that a change of charge to the favourable charge state will lower the migration energy H_m and enhanced diffusion will result (see Figure 1.7).

To a compound system, composition may be changed by ion bombardment through the defect migration and/or ionisation processes if there are significant differences in the characteristics of diffusion and ionisation between components.

1.4. Computer Simulation

Computer simulation of atomic collisions in solids is another vigorous aspect in this field. It was performed for the first time by Harrison research group at Oak Ridge National Laboratory in Brookhaven at the end of the 1950s [Webb, 1992], and then became popular in the middle of the 1960s, at about the same time as Sigmund's

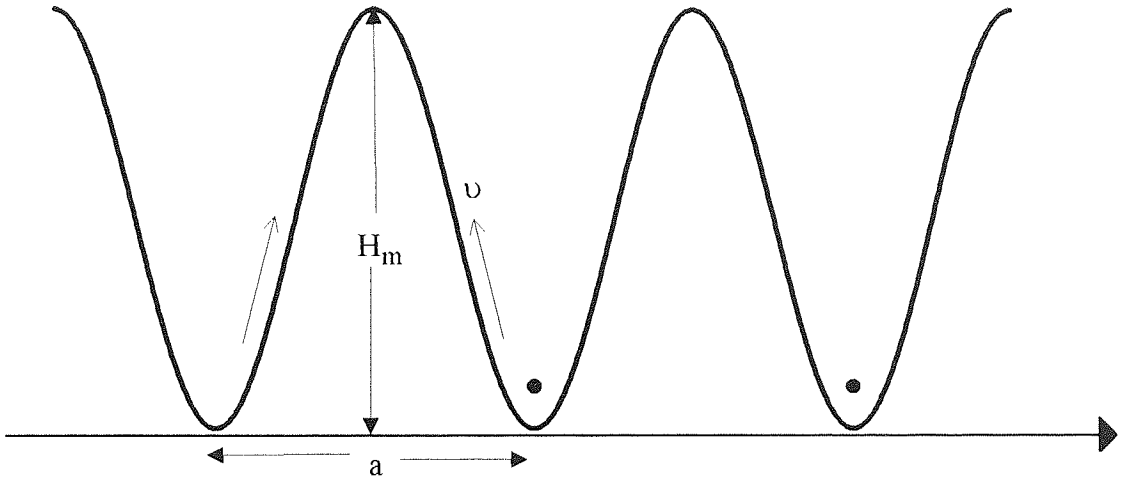

Figure 1.7 Energy potential diagram along a lattice row (moving direction)

analytical transport theory of sputtering was developed [Sigmund, 1969b]. But a greater progress in this area was made from the end of the 1979s, since sputter processes became increasingly interest in surface analysis, such as SIMS, and the high-speed, large-memory computers were developed.

One of the advantages using a simulation technique in the study of atomic collisions in solids is that the behaviour of incoming particles and bombarded target atoms in a solid may be clearly visualised on a screen, and some information, such as, projectile range, energy deposition, defect distribution in a solid and sputter yields could be obtained more easily with an accuracy. Now, even very complicated simulation can be performed, and expertise in simulation and special computer hardware are no longer necessary for the majority of calculations. More and more people have been attracted in this field, and many papers on development and application of this technique are published every year. All the aspects in the field have been reviewed extensively by Andersen [1987], Eckstein [1989] and Webb [1992].

As a very brief introduction to this field, two major approaches for the simulation, binary collision approximation (BCA) and molecular dynamics (MD), are mentioned in Section 1.4.1. This is followed by a description to TRIM, one of the most successful and popular codes for the simulation.

1.4.1. Binary collision approximation and molecular dynamics

In Webb's review paper [1992], about 12 computer programs for simulation of atomic collision phenomena were described, but many more codes have not been mentioned in the paper. All of these existing computer programs can be divided into two major groups:

(1) **BCA approach:** Programs based on the binary collision approximation. In this model, it is assumed that collision occurs only between two particles at a time, and one of them (usually, the target atom) is always considered to be initially stationary.

(2) **MD approach:** Programs based on molecular dynamics. This is a multiple interaction model, involving solving Newton's equations of motion for many particles as a function of time.

Both approaches have their advantages and disadvantages. In BCA programs, many body problems were avoided, so the calculations can be conducted very quickly, and a good statistics may be obtained within relatively short computing time. For the colliding particles with energies lower than a few hundreds eV, the interaction cross-

section of the particles is so large that the collisions with more than one other particles may take place simultaneously, that means the BCA breakdown at this point. And also the binding energies of target atoms have to be known for the calculation. In contrast to BCA, the many-body effects are automatically included in MD codes and the binding energies are not required. The major disadvantage of MD codes is the extremely large time consuming and therefore the low statistical relevance.

Although MD programs have greater potential [Eckstein, 1989], the BCA approach is still much more popular at the present time. Most comparative studies between experimental results and computer simulation have been done using BCA codes. Thus the following subsection will be focused only on BCA approach.

1.4.2. TRIM - A example of BCA

TRIM (**TR**ansport of **I**on in **M**atter) is probably one of the most popular computer codes for simulating interaction between energetic ions and solids under the basic assumption of binary collision approximation using Monte-Carlo technique. TRIM was originally written by Biersack and Haggmark in 1976, and recently improved by Ziegler [Webb, 1992]. Now, the PC-version TRIM codes are very popular in use, which make use of 3-dimension dynamic graphic display of the histories of incoming ions and recoils to provide a very pleasant working environment, but the most important point is that the time saving algorithms have been used to speed up the simulation.

As with many other binary collision codes, TRIM follows a large number of individual ion (or recoil) histories in a target. Each history begins with a given position, direction and energy of the ion (or recoil). The ion (or recoil) is then followed through a sequence of binary collision with the target atoms. The flight of ions (or recoils) is assumed to be in a straight line, and the flight distance is determined by so called *mean free-flight path*, L, determined by [Biersack, 1987]:

$$\pi P_{\max}^2 \cdot L = N^{-1} \tag{1.64}$$

where N is the atomic density of target materials; P_{max} is the maximum impact parameter .

For each collision in TRIM code, the impact parameter P and the scattering angle φ are obtained from a random number R_n ($0<R_n<1$) according to [Biersack, 1987b]:

$$P = \sqrt{R_n} \cdot P_{\max} \quad \text{and} \quad \varphi = R_{n+1} \cdot 2\pi \tag{1.65}$$

The particle's energy is reduced after each free flight path by the amount of electronic energy loss and then after each collision by nuclear energy loss. Each ion's

history is terminated either when ion energy drops below a pre-specified value or when the particle has move out of the front or rear surface of the target.

In the latest version of TRIM code, the calculation of the nuclear stopping has been improved by Ziegler, Biersack and Littmark [Ziegler, 1988]. They found that the screening radius defined in Equation 1.8 should be expressed more accurately as:

$$a_U = \frac{0.8854 a_0}{(Z_1^{0.23} + Z_2^{0.23})} \tag{1.66}$$

Secondly, from a large number of experimental results, it was found that the screening function can be fit by [Ziegler, 1988]:

$$\Phi_U = 0.1818\exp(-3.2x) + 0.5099\exp(-0.9423x) + 0.2802\exp(-0.4028x) + 0.02817\exp(-2.016x) \tag{1.67}$$

This is so called the *universal screening function*. Using Equations 1.66 and 1.67 and following the same procedure as described in Section 1.3.1.2, Ziegler [1988] rewrote the expression of the nuclear stopping power as:

$$S_n(\varepsilon) = \frac{\ln(1 + 1.1383\varepsilon)}{2(\varepsilon + 0.01321\varepsilon^{0.21226} + 0.19593\varepsilon^{0.5})} \qquad \text{for e< 30} \tag{1.68a}$$

$$S_n(\varepsilon) = \frac{\ln(\varepsilon)}{2\varepsilon} \qquad \text{for e>30} \tag{1.68b}$$

where ε is called *reduced energy*, which is defined as:

$$\varepsilon \equiv \frac{a_U M_2 E}{Z_1 Z_2 e^2 (M_1 + M_2)} \tag{1.69}$$

Equation 1.68 is the famous *universal nuclear stopping power*. It gives a more realistic description for the energy loss of ions in matter due to nuclear stopping with accuracy of a few percent[Ziegler, 1988].

1.5. Concluding Notes

Experimental work

Within the last two or three decades, substantial experimental evidence on ion bombardment induced compositional changes in various types of compound surfaces have been obtained by many surface analytical techniques. This has helped in the understanding the ion bombardment effects, however, some problems exist in previous experimental work:

(1) For different surface analytical techniques, surface sensitivity, detection limitations, experimental environment and conditions may be quite different. Thus the surface composition measured by the different techniques varied significantly, and

sometimes led to controversy results. This fact is not emphasised sufficiently in explaining the observed ion bombardment phenomena.

(2) Even for one surface analytical technique, such as XPS or AES, because the knowledge of this technique on both fundamental principles and practical application were limited in the early years, the experimental arrangement may not be optimised to show ion bombardment effects. Methods of quantification may also be inadequate, resulting in the published data being unreliable.

(3) Only recently complementary techniques, that is, two or more analytical techniques with different sampling depth used simultaneously, has attracted attention in studying ion bombarded compound surfaces. Some special surface analytical techniques, such as angular resolved XPS and energy resolved AES, have also been proved good vehicles to obtain a more complete and more reliable picture of the composition of bombarded surfaces. These techniques have, however, been utilised only for a few systems and need to be extend.

(4) Compared to oxides and metallic alloys, ion bombardment effects in compound semiconductors surfaces have not been studied systematically using proper surface analytical techniques. Only a few results on III-V compounds have been published. More experimental studies on compound semiconductors, not only III-V but also IV-IV and II-VI materials are necessary to obtain the complete spectrum of ion bombardment effects in compound semiconductor surfaces.

Since compound semiconductor materials have become increasingly important in hi-tech areas, specially in modern electronic industries, it is essential to gain a better understanding of ion bombardment effects on compositional changes in compound semiconductor surfaces. This is crucial for both fundamental research and industrial application of ion beam technology.

Theoretical work

All the theoretical models currently used for predicting the compositional changes in ion bombarded compound surfaces were generally developed through two theoretical approaches: (1) Sigmund's linear collision cascade theory derived from Boltzmann transport equation and binary collision approximation. (2) thermodynamic approach by considering segregation and diffusion induced/enhanced by ion beam radiation.

Sigmund linear cascade theory was established on several fundamental assumptions and approximations, it has been used quite successfully for describing low energy (e.g. 1-10keV) ion sputtering of monoatomic materials. For multicomponent systems, the effects of mass and surface binding energy were included in Sigmund's theory, the

nonstoichiometric stoichiometric sputtering model derived from Sigmund's theory gave correct prediction for some compound system, but for the other materials, the models failed. There are several possible reasons: (1) some basic assumptions used in Sigmund's theory may be no longer valid for some systems (2) some mathematical approximations may be inadequate (3) some variables, like surface binding energy in a compound system, were not evaluated in a correct manner. (4) other mechanisms rather than the nonstoichiometric sputtering effects dominate the compositional changes in the bombarded surfaces. The first three reasons are not vital, leading to the failure of the nonstoichiometric sputtering model. The model may still be valid as long as those three aspects can be improved. Therefore, to improve this model from these three aspects is a good starting point for a better understanding of the ion bombardment effects.

Several models established on the basis of both equilibrium surface segregation and non-equilibrium segregation and diffusion have been used successfully in the prediction of surface compositional changes in many metallic alloy systems, but few are applicable to semiconductor systems.

It was found that surface compositional changes caused by ion bombardment is governed by bombardment induced surface segregation and the segregation ratio is similar numerically to that observed in the Gibbsian equilibrium surface segregation [Kelly and Olive, 1986]. This leads to a questions that if the bombardment induced surface segregation is essentially the Gibbsian segregation and what the function of ion bombardment is.

Low energy ion bombardment usually creates defects in the near surface region, according to Wiedersich's model, the radiation induced segregation may cause redistribution of elements, depending on the distribution of vacancies and the diffusion properties of elements. In addition, the ionisation processes due to ion bombardment is also crucial factor determining elemental redistribution. All of these are particularly important to semiconductor materials.

1.6. Research Programme

This project aims to accomplish a series of experimental studies on ion bombardment induced compositional changes in compound semiconductor surfaces to gain a better understanding of the mechanisms responsible for the effects.

For obtaining more reliable and more complete experimental evidence, more than one surface analytical techniques were carefully chosen and effectively used. The experimental work was carried out on several different binary systems, including III-V, II-VI compound semiconductors and IV-IV alloys to generate a complete spectrum of

ion bombardment effects in compound semiconductor surfaces.

All 'as received' compound semiconductor surfaces were examined by the selected analytical techniques to gain initial information on compositional distribution in sample surfaces. Ion bombardment using low energy noble gas ion beam was conducted under the highly controlled conditions. The bombarded surfaces were re-examined. By comparison with the initial analyses, ion bombardment effects may be clearly observed. For quantitative analysis, pure elemental samples were well prepared and examined under the same conditions to be used as reference standards.

Using the obtained experimental results, the current theoretical models mainly from two different approaches, they are Sigmund linear collision cascade theory derived from Boltzmann linear transport equation and ion bombardment induced Gibbsian segregation and diffusion, can be tested. Efforts may be made to modify and improve the current models. Computer simulation using TRIM code may also be used for studying some aspects which cannot be dealt with current analytical models. Based on experimental observation and theoretical analysis, a possible theoretical hypothesis may be proposed, and ion bombardment effects on surface compositional changes of compound semiconductors can be explained.

Chapter 2 Surface Analytical Methods

2.1. Introduction

Obviously, studies of ion-surface interaction are not only a matter of theoretical studies, since the theoretical analysis depends basically on the experimental observations, it is crucial to select appropriate experimental methods to obtain more evidence on ion bombarded surfaces. At the beginning of this chapter, four common surface analytical techniques are compared. The comparison leads to the conclusion that XPS confined with LEISS may be the best choice for this study. The two techniques are discussed extensively, from fundamentals to practical use.

2.2. A comparison between different analytical techniques

Four types of techniques for surface analysis are available within the research group: Auger Electron spectroscopy (AES), X-ray Photoelectron Spectroscopy (XPS), Low Energy Ion Scattering Spectroscopy (LEISS) and Secondary Ion Mass Spectroscopy (SIMS). A general comparisons of the characteristics of the four analytical methods are given in Table 2.1 [Seah and Briggs, 1990].

SIMS is a technique using keV ion beams to bombard a sample surface and analysing the mass of sputtered ions of elements and clusters with a mass spectrometer to get elemental or chemical information on the surface. It has the highest sensitivity in surface analysis. There are two SIMS modes used in routine work: static SIMS, i. e. bombarding a sample surface with very low current density, say, 0.1nA/cm^2, so there is almost no change in the sample condition during analysis. The spectrum of elemental and cluster ions generated in this way contains a large amount of information regarding the

chemistry of the surface layer. Since a very low ion dose ($<10^{13}$ions/cm^2) is used in this working mode, rather large fluctuations of sputtering yields introduce much greater errors in experimental data, making static SIMS nearly impossible to be used for quantitative analysis [Wittmaack, 1992]. In contrast, dynamic SIMS is performed at a very high dose (typical value $>10^{17}$ions/cm^2) to establish a steady-state sputter rate which reflects surface concentration of elements in the surface [Dowsett and Clark, 1992]. Dynamic SIMS is quite often used for elemental analysis, especially for depth profile generation. Two fundamental properties of this technique limit the use of dynamic SIMS in this project: (1) heavy bombardment will seriously modify the surface chemistry of the sample surface during the measurements; (2) the strong interaction between ions and samples leads to complex mass transport effects (atomic mixing, radiation-enhanced diffusion and segregation, *etc.*) which take place in a region deeper than the projected range of primary ions (dynamic SIMS usually has a quite large sampling depth of over 10 monolayers). In addition, mass interference, matrix dependence, chemical conditions, and strong influence of charging effects on sputter yields, make reliable quantitative analysis by SIMS techniques very difficult.

AES is a surface analytical method in which the sample is bombarded by a beam of low energy electrons. The principle of this technique may be illustrated in Figure 2.1. When the electron beam hits a sample, core electrons may be ejected, the core holes are then filled by an internal process in the atoms where electrons from higher energy levels fall into the core holes and release the extra energy to the third core electrons. The third electrons (so called *Auger electron*), obtain kinetic energies unique to each type of atoms and were ejected from sample surface. If the Auger electrons are collected and analysed by an electron energy analyser, an AES spectrum can be obtained, which provides information on surface composition and chemistry. In AES, a sampling depth of a few atomic monolayer may be achieved if the Auger electrons have very small kinetic energies. Such a high surface sensitivity is based on the limited escaped depth of electrons in a solid [see the following sections]. AES is commonly used in elemental analysis and is particularly useful in micro-area studies since it is much easier to reduce the spot size of an electron beam into a few hundreds Å by an electrostatic or magnetic focusing lens. Since electrons can be deflected by applying a rastered electric or magnetic field, the electron beam may be used in the scan mode, just like a SEM, to generate chemical image to show the spatial distribution of elements in 2D, or 3D space if it is conjunct with ion sputtering. However, the recent research showed that a low energy electron beam deposits its energy in semiconductor surfaces, this is enough to stimulate volatile products (if any) dissociated [Oostra and Vries, 1987], hence AES may be not easy to provide true information on a sample surface without any modification. For insulating or semiconducting samples, the

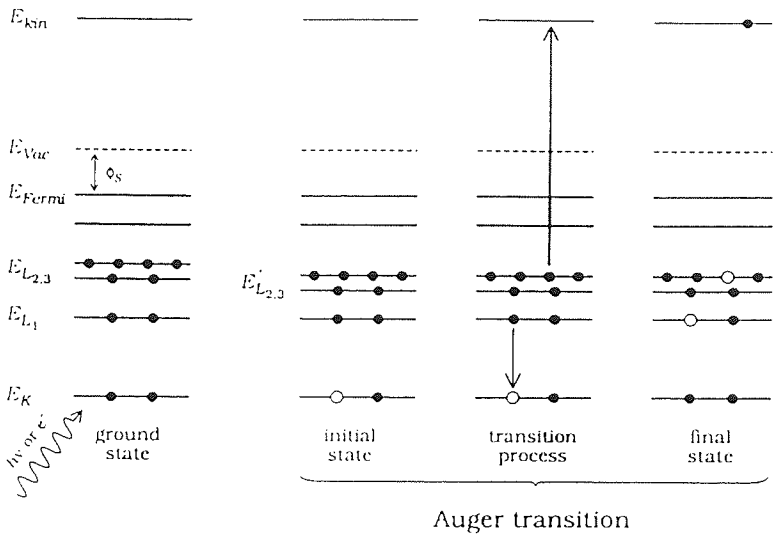

Figure 2.1 Schematic of Auger process
(after [Linsmeier, 1994])

surface charging effects may cause more serious problem in AES measurements. The strong surface electric field may steer primary electrons away, resulting in much less chemical information available. Quantification of AES results is complicated by back-scattering of primary electron beam [Seah, 1990]. In addition, AES is rarely used in study of the chemical states of elements, specially with high spatial resolution, due to electron stimulated desorption effects [Seah and Briggs, 1990]. It is clear that AES is not an ideal vehicle for this project.

Many of the above drawbacks of AES may be overcome by using XPS. In XPS, soft X-ray source, commonly Al K_α ($h\nu$=1486.6eV) or Mg K_α ($h\nu$=1253.6eV), is used to radiate a sample surface and to excite core electrons in atoms, the energy of the core electrons contain information about the elements and their chemical states. Similar to AES, these core level electrons can be collected and analysed to obtain an energy spectrum of the photoelectrons. Elemental and chemical analyses may be carried out with the aid of data processing procedures. Compared to AES, the main advantages of using XPS to study effects of ion bombardment on solid surfaces are:

(1) Surface chemical states of most of materials are not changed by X-rays illumination.

(2) Surface chemical states can be more easily identified using chemical shift theory.

(3) Quantitative study using XPS is more convincible than using AES since no additional effects, such as back-scattering in AES, needs to be considered. Also background subtraction is more reliable.

(4) The beam steerage effect in AES due to surface charging does not occur in XPS.

(5) Using special XPS techniques, such as Angular Resolved XPS or Energy Resolved methods, depth profile information may be generated non-destructively, this gives a better chance in studying some specific effects, such as ion bombardment induced surface segregation and diffusion, *etc.*.

From the above points, it is obvious that XPS is the most favourable technique in this project. A more detailed discussion about this technique will be given in the following sections.

LEISS is a special technique in which a low flux of low mass ions of the energy range from 0.5 to 5KeV is employed to impact on a solid surface. The energy of the scattered ions depends on the mass of target atoms. By analysing the energies of the scattered ions, similar to that for electrons in XPS and AES, information on surface composition may be extracted from the energy spectrum of the scattered ions. Although both SIMS and LEISS analyses are carried out by identifying the mass of target

elements, since the interaction between ions and target atoms in LEISS is described adequately by the classical binary collision approximation, in principle, no mass interference occurs in LEISS. This makes this technique more suitable than SIMS in quantitative study. An unique character of LEISS technique is that it is the only technique having a surface sensitivity of the first monolayer. Because of that, ISS has been successfully used in studying phenomenon of surface segregation [Niehus, 1992]. Combined with XPS, LEISS may provide important and complimentary information on ion bombarded surfaces.

2.3. X-ray Photoelectron Spectroscopy

Photo-electron emission was discovered as early as the end of last century. Although theoretical studies had taken place, the pioneer work on XPS was not carried out until the early 1950's, and it is not until the late 1960's did XPS became a practical vehicle for chemical analysis of atomic, molecular and solid states. The breakthroughs in both theory and technology are due to the pioneering work by Siegbahn and his co-workers. [Siegbahn *et al*, 1967].

In 1967, Siegbahn and his group completed a series of systematic researches on the XPS technique and found for the first time the phenomenon of binding energy shift of electrons in the innermost shell (core level electrons) due to changes in chemical state and environment and solved many technical problems on the analysis of electron energy. They measured the electron binding energies of every core levels of almost all elements (except hydrogen) and successfully applied XPS in studies of many chemical systems. Because of the importance of this technique in chemical analysis, this analytical technique firstly appeared in Siegbahn's works with the acronym ESCA (Electron Spectroscopy for Chemical Analysis), but now the term, XPS is more commonly used since it clearly shows the principle of this technique.

2.3.1. Fundamentals

2.3.1.1. Basic principles

Schematic of the process of X-ray induced photoelectron emission is shown in Figure 2.2.

When an X-ray with sufficient energy, $h\nu$, strikes a solid, some electrons within atoms may be excited and receive sufficient energy to overcome the core level binding

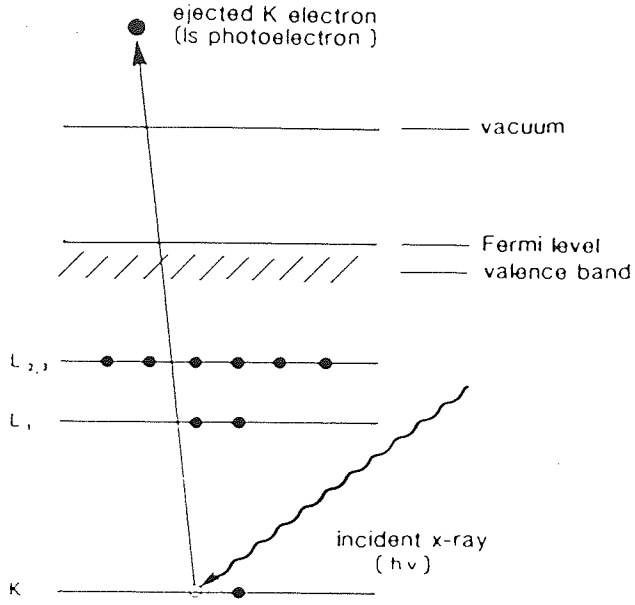

Figure 2.2 Principle of X-ray photoelectron spectroscopy (after [Watts, 1994])

energy and escape from the surface of the solid. The kinetic energy of the emitted photoelectrons can be measured by an electrostatic energy analyser, so the binding energy of electrons can be simply calculated from Einstein photo-emission equation:

$$E_k = h\nu - E_b - W \tag{2.1}$$

here E_b represents the binding energy of a core electron in the certain energy level and E_k is the kinetic energy of the electron emitted from this core level. W is called the instrument work function for a solid sample, that is, the minimum energy required for an electron to escape from the sample surface and to be measured by the analyser, it includes contributions from both sample and instrument.

Since E_b values of core level electrons are associated with specific species of elements, the electron energy spectrum is a fingerprint of the type of the target atoms. By measuring the intensity and energy of electrons one can calculate the concentration of an element in the solid. A typical XPS spectrum taken from Cu surface is shown in Figure 2.3.

2.3.1.2. Chemical shift theory

For the same atom in different chemical environment and chemical states, the binding energies of core level electrons vary. A good example of this effect is the C 1s XPS spectrum in Figure 2.4 obtained from carbon in ethyl trifluoroacetate by Siegbahn *et al.* [1967]. The four peaks from right to left are clearly distinguished, showing the differences in C 1s electron binding energy in C-H, C-O, C=O and C-F bonds.

The binding energy shift can be briefly explained by the redistribution of electric charge which occurs in the peripheral orbital when a chemical bond is formed. This so-called charge potential approach was proposed by Siegbahn *et al.* [1967]. If the atomic valence electron orbital are assumed as a spherical shell of electric charge, and core electrons reside inside this charged shell, the valence electrons may shield the core electrons. When the atom is bound to other atoms in a molecule or a crystal, the charge density of valence electrons in the atom vary due to valence electron transfer (in ionic molecule) or redistribution (in covalent molecule), resulting in change of binding energy of core level electrons. The charge potential model may be simply expressed as:

$$E_i = E_i^0 + kq_i + \sum_{i \neq j} \frac{q_i}{r_{ij}} \tag{2.2}$$

where E_i is the BE of particular core level on atom i, E_i^0 is an energy reference, q_i is the charge on atom i. The final term is the potential at atom i contributed from the

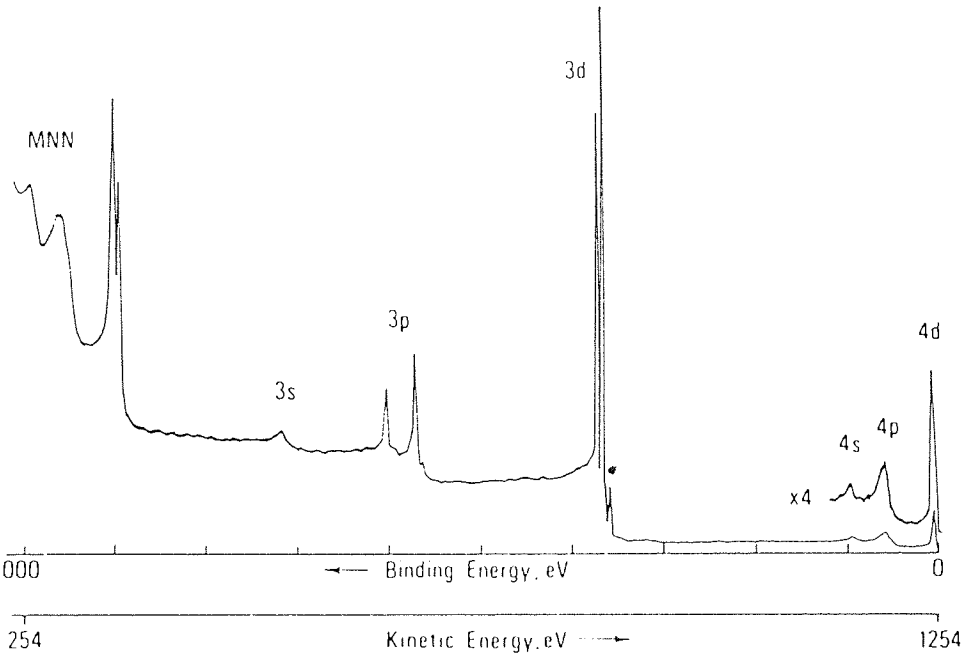

Figure 2.3 A typical XPS spectrum taken from Ag surface (after Smith [1990])

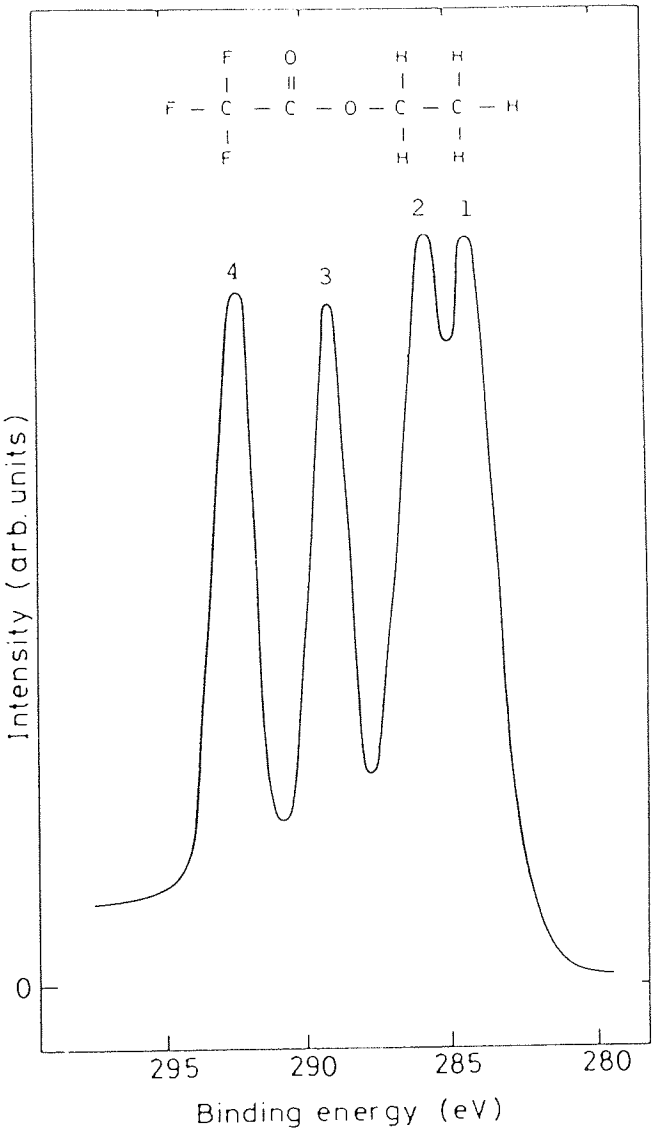

Figure 2.4 XPS spectrum of C 1s line from ethyl trifluoroacetate.

Peaks 1-4 correspond to C in C-H, C-O, C=O and C-F bonds (after Siegbahn *et al.* [1967])

surrounding atoms j. For simplicity, the final term is abbreviated to V_i, which is related to the Madelung energy of a solid. For a given core level of atom i in two different environments, the BE shift is:

$$E_i^{(1)} - E_i^{(2)} = k(q_i^{(1)} - q_i^{(2)}) + (V_i^{(1)} - V_i^{(1)}) \tag{2.3}$$

So it is clear that changes in both the charge on the atom and distribution and the type of the surrounding atoms may cause a BE shift. A accurate description should be made by considering the final state effects, for example, the relaxation effect, that is, the polarisation of the core hole on the surrounding electron on both intra-atom i and extra-atom j [Briggs and Rivière, 1990].

2.3.1.3. Basic Considerations

The intensity of photoelectrons from a solid sample surface excited by X-ray may be expressed generally as:

$$I = J\sigma(h\nu)L(\gamma)D(E_k)T(E_k)\int_0^\infty n(z)\exp[-\frac{z}{\lambda(E_k)\cdot\cos\theta}]\cdot dz \tag{2.4}$$

here J is the flux of the X-ray; $\sigma(h\nu)$ is the cross-section for emission of a photoelectron from a core level of an atom excited by a photon of energy $h\nu$; $L(\gamma)$ is the angular asymmetry of the intensity of the photo-emission of the core level electron of the atom, which is a function of the angle between the direction of X-ray incidence and the direction of electrons emission. $D(E_k)$ is the detection efficiency for an electron with a kinetic energy of E_k transmitted by the electron spectrometer; $T(E_k)$ is the analyser transmission function; $n(z)$ is the atomic density of the atom at a depth of z; $\lambda(E_k)$ is the attenuation length and θ is the electron take-off angle, that is the angle of electron emission to the surface normal. In the above equation, it is assumed that the sample surface is illuminated homogeneously by X-rays and elemental distribution in the surface region is also constant in horizontal directions.

The surface sensitivity of XPS is based on the fact that the number of electrons is reduced exponentially by a factor of $e^{-z/\lambda\cos\theta}$ after travelling a distance of z in a solid. That means 95% of photoelectrons emerge from a depth of $z=3\cdot\lambda\cos\theta$, so the maximum sampling depth of XPS (when θ=0°) for a specific core level on an atom is approximately $3\cdot\lambda$. Values of λ for almost all core levels are in the range of 2 to 10 atomic layers, as shown in the compilation of experimental data (see Figure 2.5) by Seah and Dench [1979], so the sampling depth of XPS technique is generally from 20 to 100Å, depending

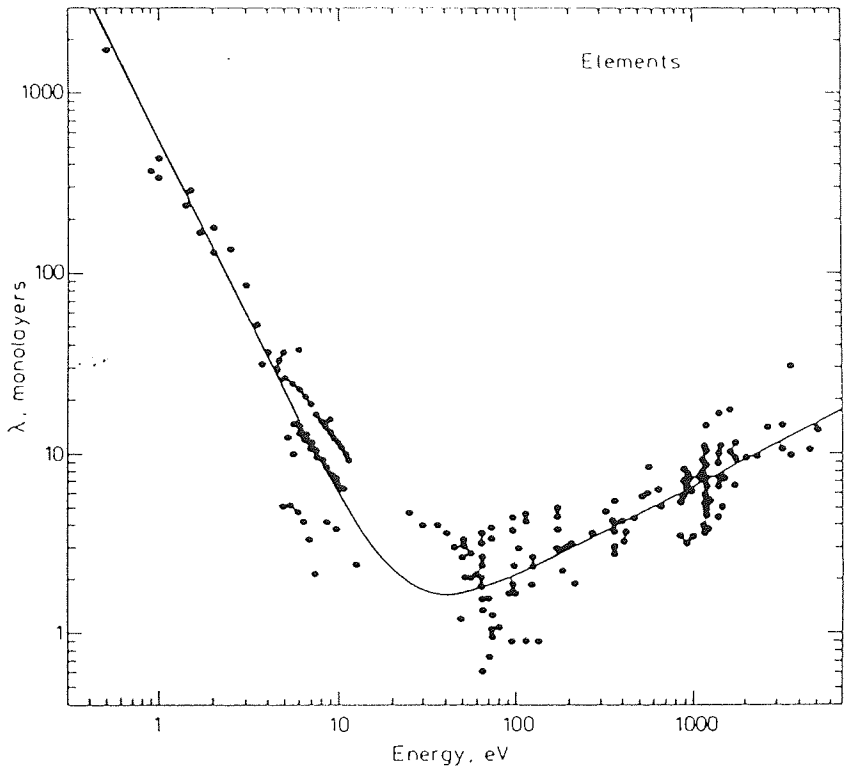

Figure 2.5 Attenuation length as a function of electron kinetic energy. (after Seah and Dench [1979])

on the electron kinetic energy, sample materials and electron take-off angle. It is this important phenomenon that makes XPS surface sensitive.

The calculation of the attenuation length is obviously important in analysing experimental results. Many formalisms have been proposed to describe the relation of λ with electron energy, characteristics of materials, *etc.*. The models derived from the systematic studies of a series of experimental results by Seah and Dench [1979] are universally accepted. For different types of materials over the energy range of 1eV to 6keV, λ may be calculated by one of the following equations:

For elements: $\lambda = 538E_k^{-2} + 0.41(aE_k)^{0.5}$ monolayers (2.5a)

Inorganic compounds: $\lambda = 2170E_k^{-2} + 0.72(aE_k)^{0.5}$ monolayers (2.5b)

Organic compounds: $\lambda = 49E_k^{-2} + 0.11(aE_k)^{0.5}$ mg/m^2 (2.5c)

Where a is the thickness of one monolayer, which may be simply estimated from the relation: $\rho Na^3=A$ [Seah, 1990]. A, ρ and N are the mean atomic weight of the matrix atoms, density and Avogadro's number, respectively.

Accurate calculation of the intensity of photoelectrons using Equation 2.4 is rather difficult, since the theoretical calculations for photoelectron cross-section, angular asymmetry coefficient, electron detection efficiency and transmission function are impossible without any assumptions. First, the interaction between photons and solids are very complicated processes so that it is impossible to describe it with a simple model. The current methods of calculation for the photoelectron cross section is based on the assumption of single-atom model, which is somewhat uncertain for a molecule or a solid. Second, the angular asymmetry coefficient formulated by Scofield [1975] is actually reduced due to the effect of elastic scattering of electrons moving through solids [Ward and Wood, 1992], but this effect is difficult to quantify. Third, the electron detection efficiency and the transmission function vary from one instrument to another, depending on the type of the analyser and the geometry of the instrument used. Hence, the absolute measurement of surface concentration using Equation 2.4 is impossible for accurately quantitative analysis.

Instead, relative measurement using pure reference sample is more practical. For a homogeneous materials with components A and B, the integral over z in Equation 2.4 becomes $N\lambda cos\theta$, so if the spectra of the reference sample are collected on the same instrument, Equation 2.4 can be expressed in a very simply form of:

$$\frac{I_A / I_A^\infty}{I_B / I_B^\infty} = \left[\frac{\lambda_{AB}(E_A)\lambda_B(E_B)}{\lambda_{AB}(E_B)\lambda_A(E_A)}\right]\left(\frac{R_B^\infty}{R_A^\infty}\right)\left(\frac{N_A / N_A^\infty}{N_B / N_B^\infty}\right) \qquad (2.6)$$

where λ_{AB} represents the attenuation length in the AB system. R represent the factors of the effect of surface roughness and N are the atom densities of element A or B in AB compound and pure reference sample. Since

$$N_A^{\infty} = a_A^{-3} \qquad \text{and} \qquad N_A = a_{AB}^{-3} X_A \quad \rightarrow \quad \frac{N_A / N_A^{\infty}}{N_B / N_B^{\infty}} = \frac{X_A}{X_B}\left(\frac{a_A}{a_B}\right)^3 \tag{2.7}$$

where X is the molar fractional composition of the solid. If R factor is ignored, Equation 2.6 may be further simplified by:

$$\frac{X_A}{X_B} = F_{AB}\frac{I_A / I_A^{\infty}}{I_B / I_B^{\infty}} \tag{2.8}$$

Here F_{AB} is called matrix factor, which is defined as:

$$F_{AB} = \frac{\lambda_{AB}(E_B)\lambda_A(E_A)}{\lambda_{AB}(E_A)\lambda_B(E_B)} \cdot \left(\frac{a_B}{a_A}\right)^3 \tag{2.9}$$

If the first terms in Equation 2.5a, b and c are omitted, which are usually a few percent of contribution to the attenuation length, the matrix factor may be simply calculated by:

$$F_{AB} = \left(\frac{a_B}{a_A}\right)^{3/2} \tag{2.10}$$

This factor varies little across the composition range from A to B and may usually be considered as a constant for the AB system [Seah, 1990].

2.3.2. Spectrum analysis

When an original XPS spectrum is obtained from an experiment, the following steps in the data processing are essential in order to extract the maximum amount of information from the spectrum. The steps include: smoothing, energy scale calibration, background removal, peak synthesis and quantification. A comprehensive introduction to these processing techniques has been given by Seah [1990] and Smith [1990] and Sherwood [1990].

2.3.2.1. Smoothing

In practice, a certain statistical noise always exists in original data, it is sometimes so large that it is impossible to get any reliable information from the data. One method to reduce the noise is to increase acquisition time in the experiment to get higher signal-to-noise ratio, but this is very time-consuming, and it is sometimes still very difficult to obtain data with sufficiently good signal-to-noise ratio. Hence smoothing, which is a

mathematic process to increase the correlation between data points and suppress uncorrelated noise, can be very useful.

The extend smooth is a method using either a quadratic/cubic or quadratic/quitic function following the algorithm of Proctor and Sherwood [Sherwood, 1990].

2.3.2.2. Energy calibration

In an original XPS spectrum, core level peaks of photoelectrons may not be at the expected positions mainly due to surface charging, variation of sample work function or sometimes the inappropriate calibration of spectrometer energy scale, so the accurate energy calibration in XPS is essential in order to interpret chemical shift and to determine the chemical states of elements.

Absolute energy calibration of photoelectrons is rather complicated, the relative calibration method, e.g. using a reference peak line, is more acceptable in routine work. A number of core level peaks, for example, C 1s, Au $4f_{7/2}$, Ar $2p_{3/2}$, *etc.*, have been used as references for the calibration. Among them, C 1s peak line at 284.6 for C-C or C-H bond is the favourite and more convenient for use since adventitious carbon is almost always present on sample surfaces.

2.3.2.3. Background removal

When looking at a typical XPS spectra (Figure 2.3), one finds that the XPS peaks (and Auger peaks) are always superimposed on a background. This background arises from photoelectrons produced within the target materials that have been subject to one or more inelastic scattering processes before emission from the surface. Furthermore, the background is seen to rise on the high binding energy side of each peak, as a result of each individual photo-emission line acting as a source of additional electrons to undergo scattering events [Smith, 1990]. Hence background removal is an important step for quantitative analysis.

Obviously, the crucial thing for background removal is how to determine the background. A simple way is to draw a straight line between two suitably chosen points, so called *linear background*. This process can be effective when little change in background occurs. But in the case of the step background (like the spectra in Figure 2.3), especially when there are a mixture of more than one chemical states, the end points (see Figure 2.6) are difficult to choose for linear background, and this method will

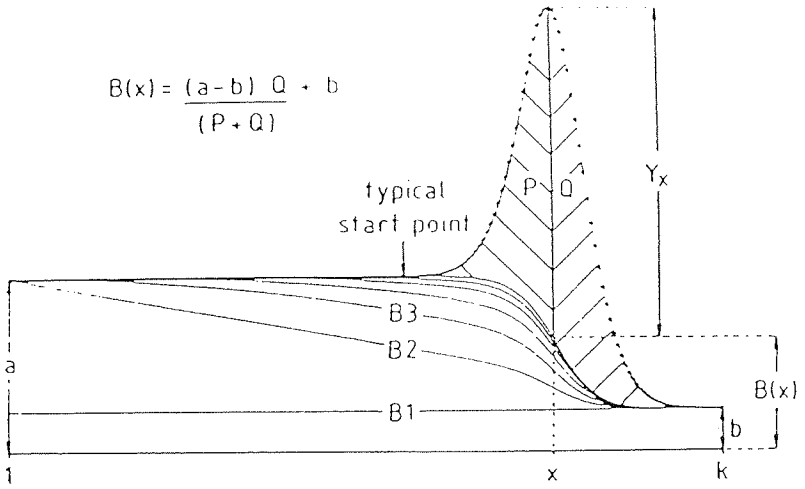

Figure 2.6 Determination of background in an photoelectron peak (after Sherwood [1990])

introduce significant errors. An alternative method for dealing with this kind of problem is due to Shirley [1972], in which the background intensity at a point is determined by an iterative analysis, it is proportional to the intensity of the total peak area above the background and to higher energy. This method merely assumes that each unscattered electron is associated with a flat background of losses. The background is calculated as:

$$B(x) = \frac{(a-b) \times Q(x)}{P(x)+Q(x)} + b \qquad (2.11)$$

Where a, b are the average start and end counts, respectively; $P+Q$ the total background subtracted and Q the peak are from point x. The subtraction of background is repeated until $P=Q$ remains essentially unchanged.

Shirley's method gives the curved background, the choice of the precise position of end points is not so critical, hence in the case of the step background this method give a more realistic estimation. Currently, researches in this field are still seeking better methods for determination of background by understanding the scattering processes of photoelectron in solid, some of models, for example, Tougart background, have been proposed to give much better consideration.

2.3.2.4. Curve synthesis and curve fitting

A spectrum, especially in which there is a mixture of more than one chemical state may not be resolved by the electron energy analyser. It is necessary to synthesise peaks using digital or analogue methods to sum a series of functions representing individual peaks in order to produce a final function that represents the experimental spectrum closely. The fitting can be carried out as a simple addition of guessed component peaks (curve synthesis) or after a least squares refinement (curve fitting) of the component peaks based on an initial curve synthesis [Sherwood, 1990]. Successful fitting depends on the choice of an appropriate fitting function and a proper background subtraction.

The basic shape of XPS peaks is Lorentzian-type function, modified by some instrumental and other factors to give a Gaussian contribution [Sherwood, 1990]. Usually, a mixed Gaussian -Lorentzian product functions suggested by Ansell *et al.* [1979] is used and has been proved to give good quality fitting. The function has the form of :

$$f(x) = \frac{1}{[1+M\cdot(x-x_0)^2/\beta^2]\exp[(1-M)[\ln 2\cdot(x-x_0)^2/\beta^2]} \qquad (2.12)$$

where x_0 is the peak centre; β is approximately 0.5FWHM; M is the mixing ratio of

Lorentzian and Gaussian functions, M=1 for pure Lorentzian peak and M=0 for pure Gaussian peak. XPS peaks often appear asymmetric due to extrinsic loss processes (including intrinsic processes), such as plasmons, satellites and conduction band interaction and inelastic scattering. A tail function may, therefore, be included in the fitting as:

$$T = TM \cdot CT + (1 - TM)e^{-D \cdot ET} \tag{2.13}$$

where D is the separation from x_0 in channels; ET exponential tail ratio; TM tail mixing ratio and CT constant tail ratio. So the peak function $Y(x)$ may be represented as

$$Y(x) = H[f(x) + (1 - f(x)) \cdot T] \tag{2.14}$$

where H is peak height. Peak synthesis is carried out after background removal.

After the initial curve fitting generated by a peak synthesis, curve fitting can be refined iteratively using *least squares method.* An chi-squared value is used to evaluate the goodness of the fitting, which is defined as:

$$\chi^2 = \sum_{i=1}^{n} w_i [y_i - F(x_i|q)]^2 \tag{2.15}$$

where y_i is the experimental data; $F(x_i|q)$ the fitting function depending on a series of parameters q. w_i is a weighting function which is chosen as y_i^{-1} to make χ^2 equal to the statistical chi-square. The objective is to choose q parameters to minimise the chi-square value, that is:

$$\frac{\partial \chi^2}{\partial q_j} = -2 \sum_i w_i [y_i - F(x_i|q)] \left(\frac{\partial F}{\partial q_j} \right)_{x = x_i} = 0 \tag{2.16}$$

This will give a set of equations with variable q. By solving this equation group, the optimised q parameters, that is, peak centre, peak height, peak width, G-L mixing ratio, and parameters for tail function may be found.

2.3.2.5. Quantification

One objective of XPS analysis is to give a quantitative description of the composition of the surface region in question. Quantification is the final step of data processing in normal XPS after smoothing, energy calibration, background removal and/or curve synthesis and fitting.

A common way of doing quantification is to compare intensities of photoelectron peaks for each element in the obtained spectrum, I_i, with intensities in standard spectra

of the elements, I_i^{∞}, or with so-called sensitivity factors for the elements, S_i, which is the relevant value of the intensity in standard spectrum for an element to that of a specific photoelectron peak, usually, C 1s or F 1s. So the concentration of element i in a compound containing n elements measured by means of XPS may be calculated from:

$$c_i = \frac{I_i / I_i^{\infty}}{\sum_{j=1}^{n} I_j / I_j^{\infty}} = \frac{I_i / S_i}{\sum_{j=1}^{n} I_j / S_j} \tag{2.17}$$

In the equation, the intensity is taken using the peak area (normalised by time and step size), that is, the area under the envelop of the photoelectron peak after removing background. The intensities in standard spectrum or sensitivity factors for the elements may be refereed to either systematically experimental measurements (e.g. Wagner scheme) or based on theoretical calculation (e. g. Scofield scheme) [Seah, 1990].

It is obvious that the above equation contains a number of approximations and may lead to certain errors in quantification. First, measurements for the standard intensities or the sensitivity factors may be done using different type of equipment under the different experimental conditions, so these values should be carefully refereed. It is preferable to repeat the calibration on the same experimental equipment. Second, it was found that there are variations in relative signal intensities which are sample-dependent [Smith, 1990], this is usually called matrix effect. It has been shown that for homogeneous samples this may be improved by including the matrix factor F in quantification, which has been defined in the previous section. Equation 2.17 may be written such that:

$$c_i = \frac{F_{iM} I_i / I_i^{\infty}}{\sum_{j=1}^{n} F_{jM} I_j / I_j^{\infty}} = \frac{F_{iM} I_i / S_i}{\sum_{j=1}^{n} F_{jM} I_j / S_j} \tag{2.18}$$

where the subscript M refers to the matrix containing all n types of atoms. For a binary system AB, the matrix factor can be simply estimated using Equation 2.10, and atomic ratio (or concentrations) may be calculated by Equation 2.8.

Generally speaking, to achieve the greatest accuracy in quantitative analysis in a specific XPS equipment, it is essential to calibrate every core level lines to be studied using standard samples, it is one of the major tasks of experimental work in this project.

2.3.3. Angular resolved XPS

In Equation 2.4 it can be found that intensities of photoelectrons depend on their take-off angle, θ, so Equation 2.4 may be rewritten as:

$$I(\theta) = I^0 \int_0^\infty n(z) \exp\left(-\frac{z}{\lambda \cdot \cos\theta}\right) dz \qquad (2.19)$$

When the take-off angle θ is varied in a series of XPS measurements, the function $I(\theta)$ can be obtained which contains the information about the in-depth distribution of element, $n(z)$. In principle, $n(z)$ can be resolved if a proper mathematics transformation can be found. This is the basis of Angular Resolved XPS (ARXPS).

ARXPS has been well demonstrated in study of a thin overlayer on a solid surface. In the case of a (homogenous) substrate with a uniform thin overlayer with a thickness t, the intensity of photoelectron signals coming from both substrate and overlayer can be simply calculated from Equation 2.19:

from substrate: $$I_s = I_s^0 e^{-\frac{t}{\lambda_s \cdot \cos\theta}} \qquad (2.20)$$

from overlayer: $$I_o = I_o^0 [1 - e^{-\frac{t}{\lambda_o \cdot \cos\theta}}] \qquad (2.21)$$

where subscript s and o mean *substrate* and *overlayer*, respectively. From the above equations, it may be understood clearly that increasing electron take-off angle will enhance the signal from the overlayer and reduce the signal from the substrate. On contrary, if a core level signal coming from an element increases with TOA, it means that this element is distributed more concentrated in the top layers of the surface.

By using regularization method with non-negativity constraints, Tyler *et al.* [1989] successfully developed an algorithm for generating depth profile from ARXPS data. This algorithm was demonstrated in studying a pure silicon substrate covered by a thin oxide layer and a little carbon contamination. The normalised XPS signal intensities of C 1s, O 1s, Si^0 (2p) and Si^{4+} (2p) at different TOAs measured by Tyler *et al* [1989] are listed in Table 2.2, and the depth profiles calculated from the data by Tyler's algorithm are shown in Figure 2.7. The figure gives a reasonable estimate of surface structure of the Si surface.

Table 2.2 Normalised XPS C, O and Si signals from thin oxide layer on silicon [Tyler *et al*, 1989]

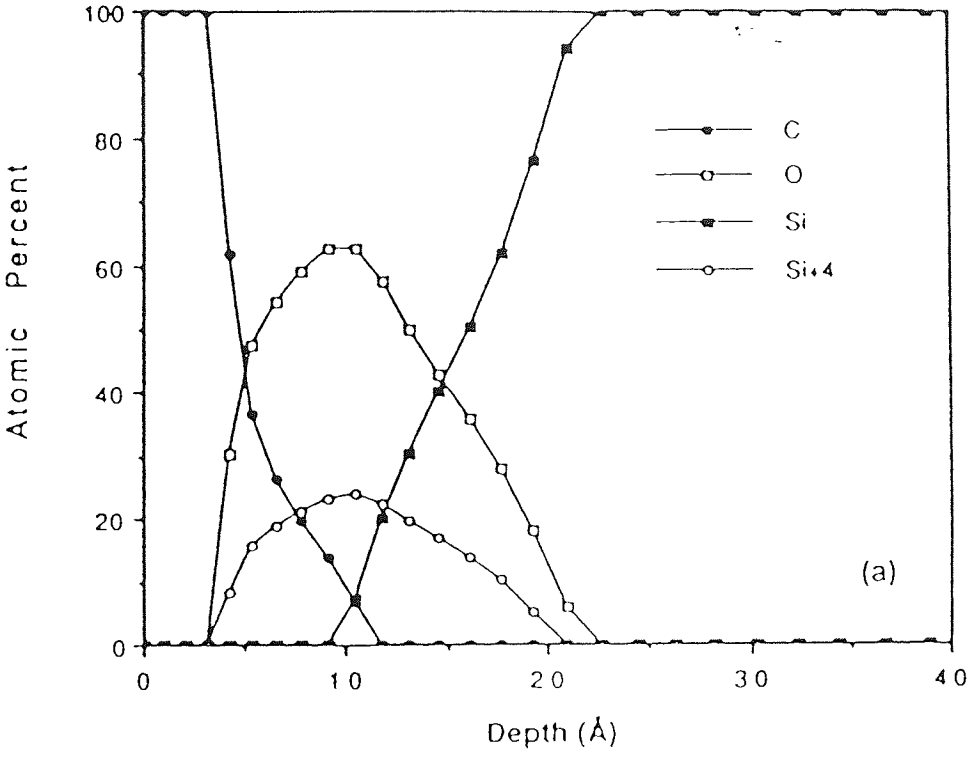

Figure 2.7 Angular resolved XPS analysis of SiO_2 overlayer on Si surface (after Tyler *et al* [1989])

2.3.4. Kinetic resolved XPS

Similar to ARXPS, Kinetic Resolved XPS (KRXPS) is based on the dependence of sampling depth on the kinetic energy of electrons travelling in solids. To consider the effect of electron kinetic energy, Equation 2.4 may be re-expressed as:

$$I(E_k) = I^0(E_k)\int_0^\infty n(z)\exp\left(-\frac{z}{\lambda(E_k)\cdot\cos\theta}\right)dz \qquad (2.22)$$

Using different core level electrons or collecting core electrons excited by X-rays with different energy, a spectrum of the intensity of photoelectrons against electron kinetic energy may be obtained, similarly, the elemental distribution in the surface may be obtained using a proper algorithm.

Both ARXPS and KRXPS can be used for non-destructive analysis of surface structure, both of them have many practical advantages and disadvantages, this is discussed further in Chapter 4 by comparing experimental investigation.

2.4. Low Energy Ion Scattering Spectroscopy

In XPS, elemental concentration is determined from the intensities of photoelectrons emitted from a solid surface. Low energy ion scattering spectroscopy (LEISS), however, is a surface analytical technique, by which the target atom mass is determined directly from energy or momentum losses of scattered primary ions.

Low energy ion scattering spectroscopy was first proposed by D. P. Smith in 1967 for elemental analysis[Niehus *et al.*, 1993] and is an ideal method for composition determination of the very surface layer if a few difficulties can be overcome. LEISS using noble-gas ions as the primary beam has two major characteristics:(1) high cross section for the ion-atom interaction; (2) high neutralisation rate. These effects lead to LEISS being very surface-sensitive, but the latter effect is matrix dependent and makes quantification difficult.

2.4.1. Classical scattering theory

2.4.1.1. Single collision theory

In the low energy range of 0.1eV to 10keV, ion scattering can be reasonably described by sequences of elastic two-body scattering events based on the single collision

model, since the interaction time for the collision is small compared with the period of phonon frequencies in the solid [Niehus, 1992]. Schematic of a hard-sphere collision is shown in Figure 1.3 in Chapter 1. The energy of primary particles after a collision may be obtained from Equations 1.3a to 1.3c, that is:

$$\frac{E_1}{E} = \frac{(\cos\vartheta \pm \sqrt{A^2 - \sin^2\vartheta})^2}{(1+A)^2} \qquad (A=M_2/M_1) \qquad (2.23)$$

For $A>1$, the above equation in the centre-of-mass co-ordinate system may be written:

$$\frac{E_2}{E} = \frac{4A\sin^2\frac{\varphi}{2}}{1+A^2} \qquad (2.24)$$

It may be seen in the above equations that the energy spectrum of the scattered ions directly reflects types of elements existing in the investigated surface area since the energy of the scattered particles for a fixed angle depends only on the mass ratio. The intensity of the scattered ions, however, depends on many factors, including scattering cross section, areal density of elements, neutralisation probability, *etc.*, which are discussed in the following subsections. A typical LEISS spectrum of 1keV He ion scattered at scattering angle of about 129° from a copper surface, in the centre area of which a silver dot is placed, is shown in Figure 2.8. The Cu (mass=63.5) and Ag (mass=107.9) scattering peaks appeared at the energies of about 810eV and 885eV.

2.4.1.2. Basic considerations

The intensity of ions scattered at atom i in a solid surface is generally expressed as:

$$I_i = I_0 \cdot \sigma_i(E_0, \varphi) \cdot N_i \cdot S_i \cdot P^+_i \cdot T \cdot \Delta\Omega \qquad (2.25)$$

where I_0 is flux of primary ions; $\sigma_i(E_0, \varphi)$ is the differential cross section of the ions with energy E_0 scattering at an atom i; N_i is the number density of atom i; S_i is the shadowing factor expressing the possibility of atom i being hit by the primary beam; P_i^+ is the ion survival probability accounting for possible charge exchanges during scattering; T is the transmission factor of the analyser, which is similar to that in XPS and $\Delta\Omega$ is the solid angle of acceptance.

The scattering cross section $\sigma_i(E_0, \varphi)$ may be calculated from a series of equations discussed in Chapter 1. (Equation 1.5 and 1.6). The factors of the shadowing S_i and ion survival P_i^+, however, are poorly known. The former influences ISS measurements by focusing the trajectory of the scattered ions near the edge of the shadow cone, which leads to a significant modulation of primary ion intensity for the elements being hit after a

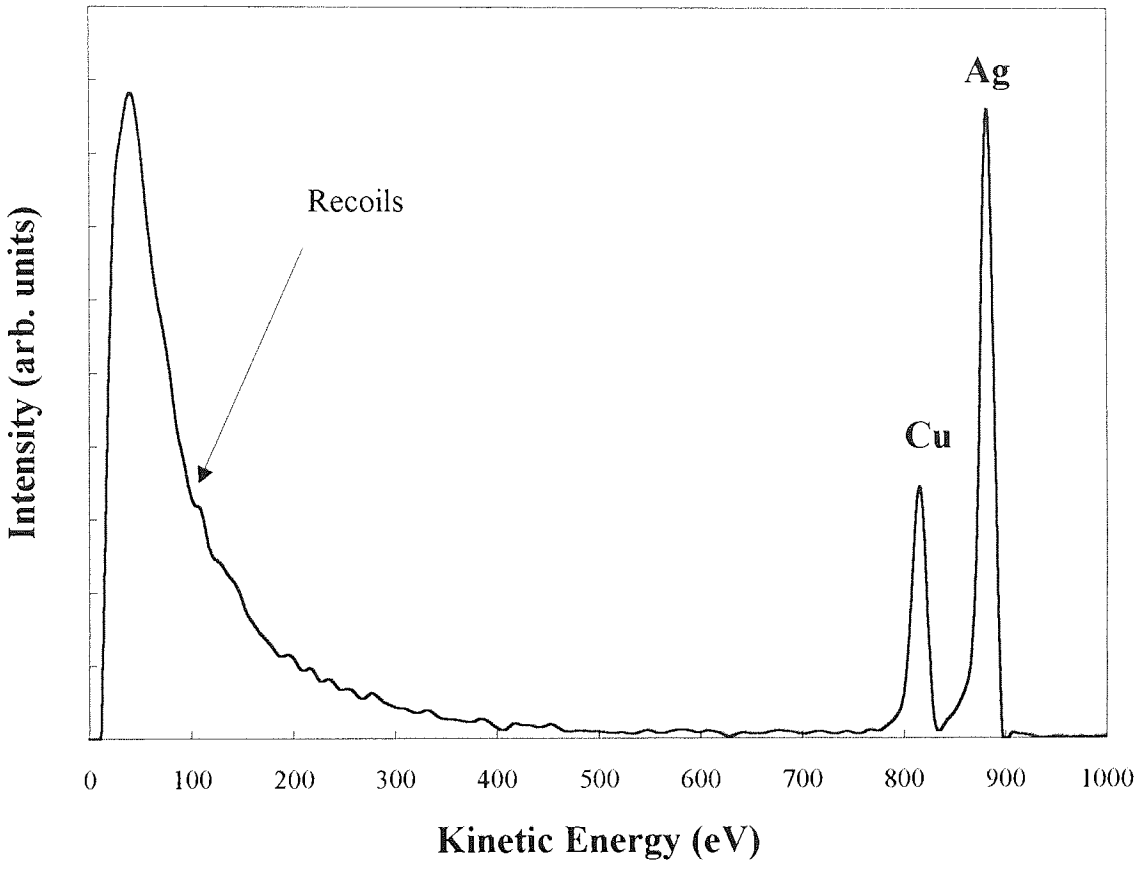

Figure 2.8 1keV He ISS spectrum from a Cu surface with an Ag dot at centre

small angle deflection. The latter causes dramatic changes of the scattered ion intensity due to several charge exchange processes, so most of the scattered ions are neutralised and not collected by the electrostatic energy analyser. More discussion on these two effects are given in the following sections.

2.4.1.3. Shadowing and blocking

Repulsive deflection of a primary particle at a scattering centre leads to the formation of the classical shadow behind the scattering centre. The shadowing effect may be understood by referencing to Figure 2.9a, in which the trajectories of the scattered ions are calculated based the classical scattering model [Niehus *et al.*, 1993].

It can be seen that the trajectories of the ions are focused near the shadow-cone edges. This is the focusing effect. The explanation of this focusing effect is that: the constant density of incoming particles is transformed by scattering and leads to a depletion of their trajectories behind the substrate atoms. Since most of the incoming particles are forward deflected and no particles are lost, the trajectories must accumulate near the shadow-cone edges. The flux distribution function $f(R_S)$ can be analytically described for two different regions as [Niehus *et al.*, 1993]:

$$f(R_s) = 0 \qquad R_S<R_C \text{ (inside the shadow cone)} \qquad (2.26a)$$

$$f(R_s) = \frac{1}{2}\left(\frac{1}{\sqrt{1 - R_c / R_s}} + \sqrt{1 - R_c / R_s}\right) \quad R_S>R_C \text{ (outside the shadow cone)} \quad (2.26a)$$

$$\text{where } R_c \equiv 2\sqrt{\frac{Z_1 Z_2 e^2 d}{E}} \quad \text{and} \quad R_s \approx p + \varphi d = p + \frac{Z_1 Z_2 e^2 d}{Ep} \qquad (2.27)$$

R_C is the Coulomb shadow-cone radius, which actually represents the closest approach of the scattered particle to the second atom. Z_1 and Z_2 are the charges on the primary particle and the target atom. E is the energy of a particle approaching the first atom. d and p are defined in Figure 2.10. At the edge of shadow cone $R_S=R_C$, $f(R_S)$ approaches a strong δ-like function and the flux intensity is dramatically enhanced.

When a flux of particles approaches a solid surface, some of them which penetrate the first atom layer might eventually be focused onto the atoms in deeper layers and backscattered out of the surface. On their way to the surface, these particles may be blocked by the atoms in the first layer, leading to the formation of blocking-cones (see Figure 2.9b). All discussion and calculations for the shadowing effect are also applicable to blocking effects.

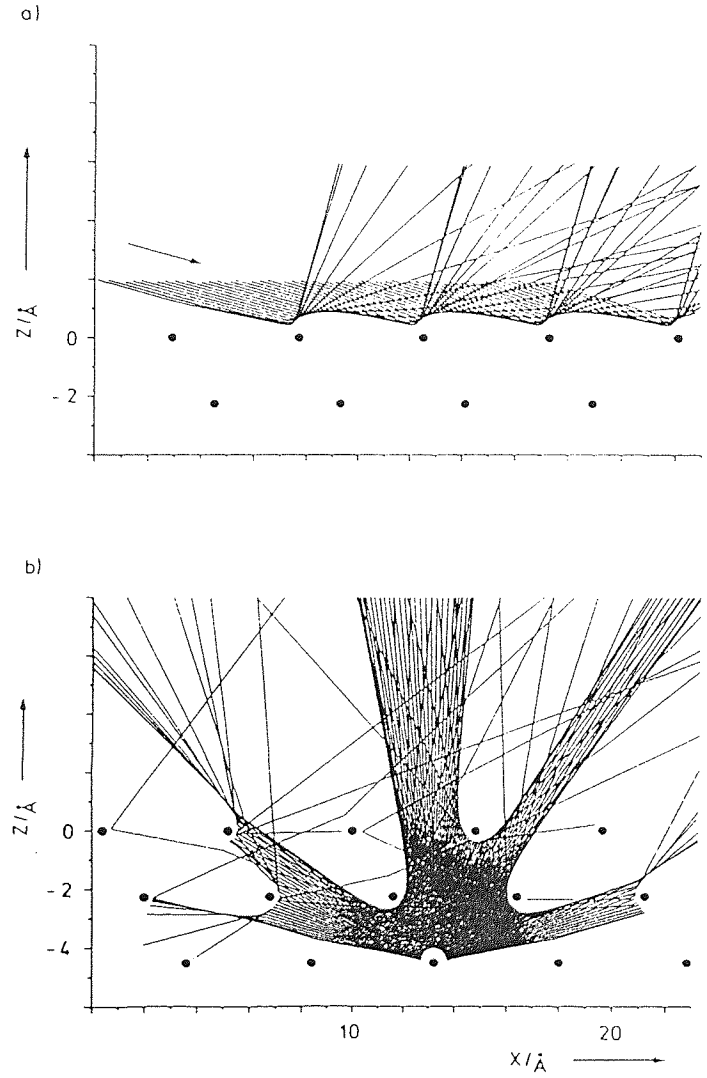

Figure 2.9 Shadowing & blocking effects of ion scattering at solid surfaces (after Niehus *et al*, [1993])

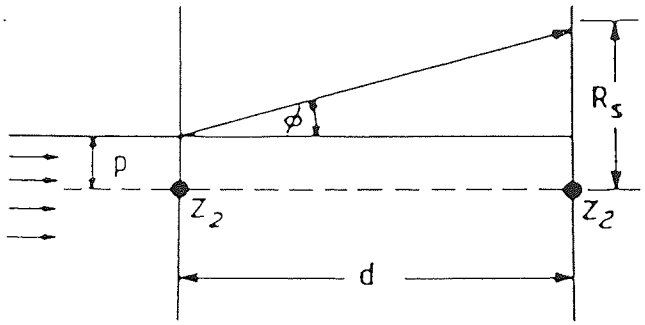

Figure 2.10 Scattering geometry for the calculation of the flux distribution (after Niehus *et al.* [1993])

2.4.1.4. Neutralisation

When particles, especially charged particles approach a surface, the interaction of the moving particles with the electronic system of the surface via electrons leads to charge exchange and energy loss. As a result of charge exchange, a large fraction of charged particles may be neutralised and are not able to be collected by electrostatic energy analysers.

Four types of charge exchange processes can occur in the interaction of charged particles with a surface. They are illustrated in Figure 2.11[Niehus *et al*, 1993]:

(1) **Resonant Neutralisation** involves tunnelling of electrons from the valence band in the solid surface into the unoccupied state of the incident charged particles.

(2) **Resonant Ionisation** is electrons tunnelling from the occupied state of incident particle back to the valence band in the solid.

(3) **Auger Neutralisation** involves two electrons in the solid which are exited by the Coulomb field of a charged particle so that one electron neutralises the charged particle and the other electron is emitted.

(4) **quasi-Resonant Neutralisation** is similar to RN but charge exchange occurs between relatively localised core levels.

The different neutralisation processes depend on the projectile-target combination, their relative energies, actual scattering trajectory near the surface and also on the chemical state at surface[Niehus, 1992]. In Hagstrum's adiabatic approximation, the ion survival probability depends exponentially on the perpendicular component of the partial velocity, $v_{\perp}$, i.e.

$$P^{+} = e^{-v_0/v} \tag{2.28}$$

where v_o is a characteristic velocity for a given projectile-surface combination. This model has a certain validity for resonant neutralisation and Auger neutralisation. In the case of noble gas ion scattering at metal surfaces, P^{+} is of the order of a few percent. A quantitative description of the neutralisation processes is rather difficult and needs knowledge of ion path and the behaviour of the transition matrix for electron exchange. A description for the later quantity still eludes researches[Niehus, 1992].

2.4.1.5. Multiple scattering

Multiple scattering is often found to occur in LEISS experiments. This means that

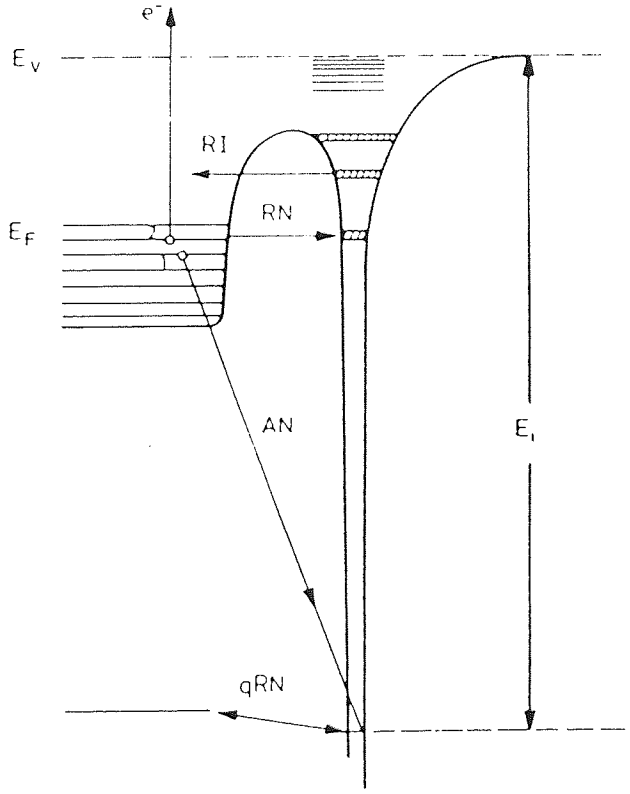

Figure 2.11 Charge-exchange processes between a ion and solid surface.

E_f is the Fermi energy of the solid; E_V is the vacuum level; E_i the ionisation energy; RI, RN and qRN stand for resonant ionisation, resonant neutralisation and quasi-RN. AN is Auger neutralisation (after Niehus *et al.* [1993])

the primary particles are scattered at the surface atoms more than once before being collected, resulting in peak shift (in the case of glancing angle scattering) or additional peaks appearing at higher energy positions in the scattering spectrum. Schematic of double scattering is shown in Figure 2.12. The occurrence of multiple scattering depends on the energy and incident angle of primary particles, scattering angles, impact parameters, inter atomic distance and atomic sizes of target atoms. This may be avoided in elemental analysis by using lower energy noble gas ions (less than 2keV) since the velocity of the particles may be reduced significantly and the trajectories of the particles of multiple scattering are usually longer. And also noble gas ions have a higher neutralisation probability. All of these lead to reduce probability of survival for the multiple scattered ions. For structural analysis, multiple scattering is important.

2.4.2. Spectrum analysis

Analysis of LEIS spectra is much more difficult than XPS spectra. This is not only because of the complexity of interaction mechanisms between ions and surface atoms, but also due to the fact that acquisition of useful LEISS spectra needs more strict experimental conditions, for example, much higher vacuum (~10^{-6} Pa), atomically clean and flat sample surface, high purity primary beam, *etc.*. Any insufficiency of these conditions may seriously affect the quality of LEISS spectra and may lead to totally false results. Two important aspects for LEISS spectrum analysis are shape (area) and position of a scattering peak.

2.4.2.1. Peak shape

A typical ion scattering spectrum has been shown in Figure 2.8. It may be seen that scattering of ions at target atoms may generate quite sharp peaks, but with a low-energy tail.

For most elements in an ideal sample surface, background noise is negligible, although a recoil peak always appears at very low energy. For contaminated or oxidised surfaces, ion bombardment may cause hydrogen, carbon and oxygen, *etc.* emission, since these light atoms obtain quite larger momentum from the primary ions, the recoil peak may stretch to higher energy, resulting in scattering peaks superimposed on a significant background (see Figure 2.8). In these cases, (linear) background removal is an essential step for the spectrum analysis. The background noise, sometimes, can be very large so that all scattering signals may be merged, this should be avoided in LEISS experiments.

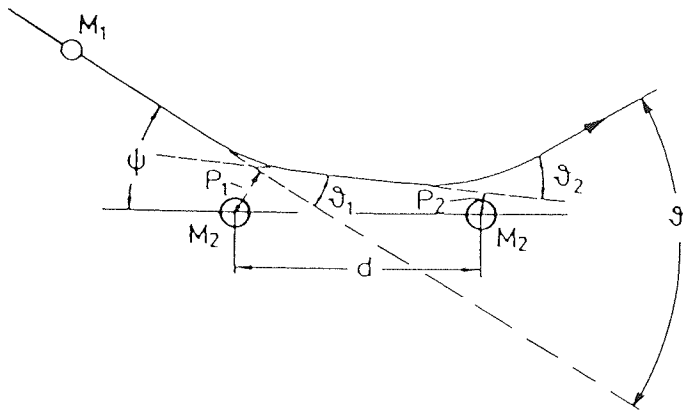

Figure 2.12 Schematic scattering trajoctory for a double collision (after Niehus *et al.* [1993])

The shape of a scattering peak is influenced mainly by the abundance of isotopes of both primary ions and target elements, purity and energy spread of ions. The first two effects are easily understood from the basic scattering equations. The purity of primary beam and the isotopic effect of ions should be particularly emphasised here,. Figure 2.13 is an LEISS spectrum taken from a clean indium surface using He ions mixed with air. The N_2^+ and $H2O^+$ scattering peaks definitely give a misleading spectral interpretation, if one does not realise the helium gas being contaminated. The isotopic effect of primary ions has been systematically studied by Melendez *et al.*[1991]. Figure 2.14 is a series of LEISS spectra using 2keV Ne ions with different abundance of ^{22}Ne and ^{20}Ne scattering at copper surface. The ratios of $^{22}Ne^+/^{20}Ne^+$ are about 1/99, 10/90, 76/24, 99/1.

Besides the above effects, the peak width, or FWHM, may be increased due to surface roughness and thermal vibrations of surface atoms (sample temperature) [Niehus, 1992]. The low-energy tail also extend when the energy of primary ions is increased.

2.4.2.2. Peak position

Although the classical model of two-body elastic collision is generally adequate for describing low energy ion scattering at surface atoms of a solid, and the energy of the scattered ions can be estimated from Equation 2.23. The actual position of the scattered peak may not be varied due to many reasons. One reason is the existence of the inelastic effects, for example, the charge-exchange processes described in Section 2.4.1.4. Experimental results [Niehus *et al.*, 1993] showed that in general this kind of inelastic losses depend linearly on the energy of primary ions for large scattering angles, but accurate calculation of the inelastic losses is very difficult. The inelastic effects generally result in the scattering peak shift to the low energy end.

Another factor affecting the peak position is the surface charging. The strong surface electric field due to the charging effect at poorly conductive sample surfaces may accelerate the scattered ions, the peak may move to high energy end by a few tens to about several hundreds eV, hence the proper earthing the sample is very important in ISS experiments to avoid the surface charging effects.

2.4.2.3. Mass Resolution

The mass resolution in ISS analysis is not just the matter of the energy spectrometer used, it also depends on the fundamental theory of the classical mechanics.

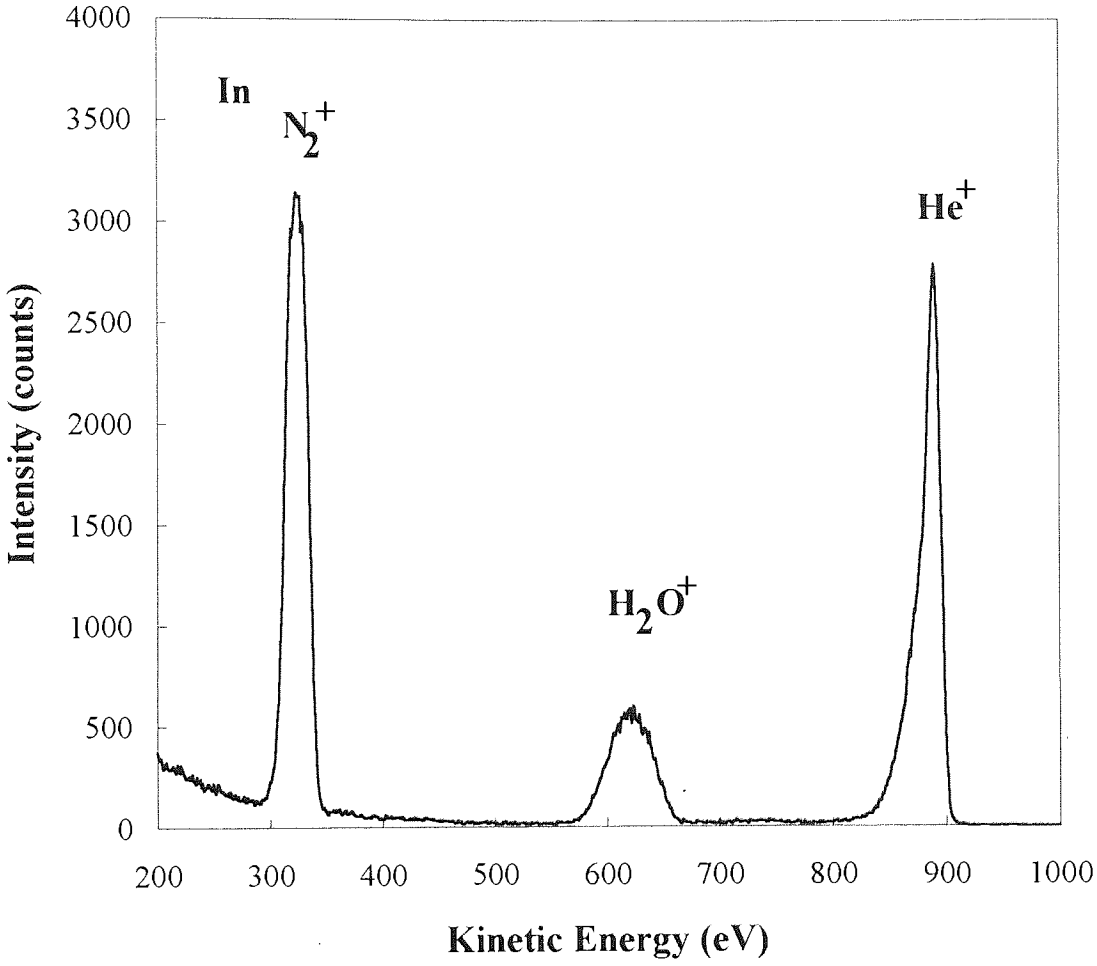

Figure 2.13 ISS spectrum from In surface using He beam mixed with air

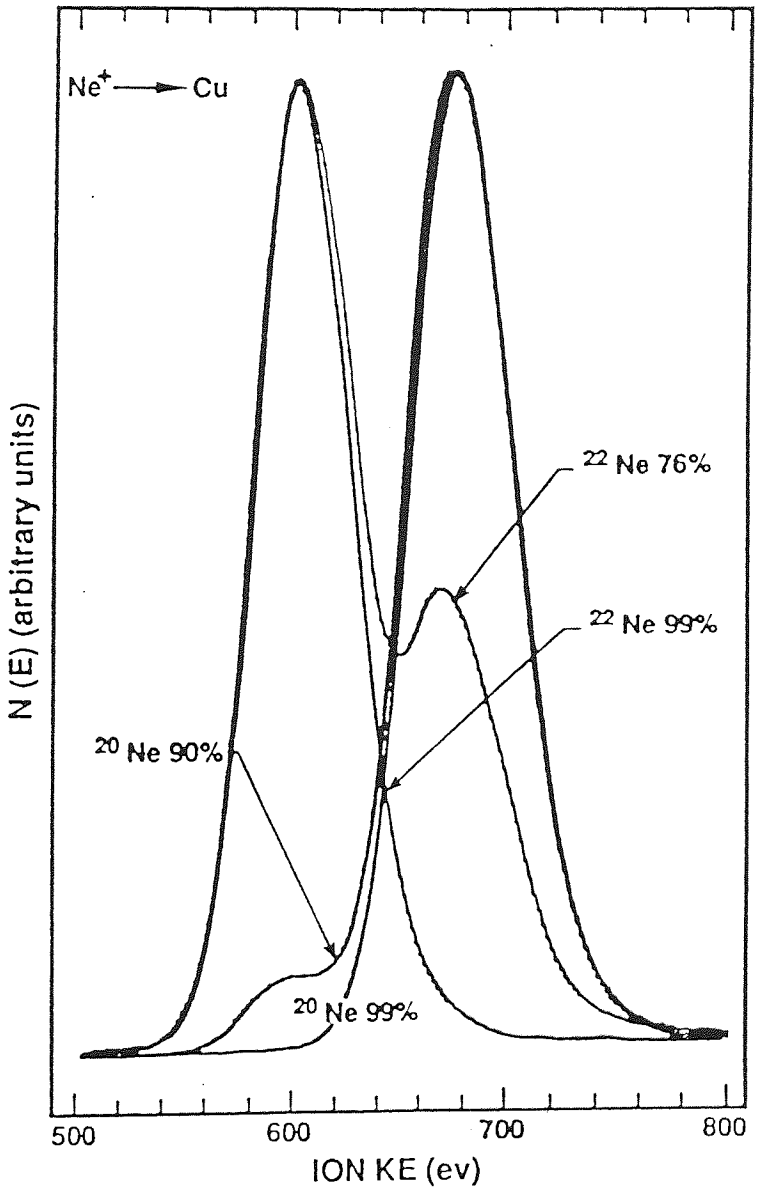

Figure 2.14 ISS spectra obtained by scattering 2keV $^{20}Ne^{+}$ with difference abundance of $^{22}Ne^{+}$ off polycrystalline Cu

(after Melandez *et al.* [1991])

The exact expression for the mass resolution can be deduced from Equation 2.23:

$$\frac{M_2}{\Delta M_2} = \frac{E}{\Delta E} \cdot \frac{2A}{A+1} \cdot \frac{(A + \sin^2\vartheta - \cos\vartheta\sqrt{A^2 - \sin^2\vartheta})}{(A^2 - \sin^2\vartheta + \cos\vartheta\sqrt{A^2 - \sin^2\vartheta})} \tag{2.29}$$

It may be seen from the equation that with a fixed energy resolution $E/\Delta E$, the mass resolution of LEISS is not identical for light elements and heavy ones, and the maximum mass resolution is obtained for about $A \rightarrow 1$. In order to distinguish between two heavy and closer mass elements, heavier ions should be employed as primary beam.

2.4.3. Quantitative study

In LEISS experiments, the surface composition in a compound surface may not be estimated directly from the Equation 2.25 since some mechanisms involved in the scattering, such as neutralisation, are still not well understood. However, a large number of experimental results showed that quantification is possible for many alloys by using pure elements as standards [Niehus *et al.*, 1993].

In a binary system with components A and B, the atomic ratio of element A to B is simply derived from Equation 2.25:

$$\frac{x_A}{x_B} = \frac{I_A}{I_B} \cdot \frac{I_B^0}{I_A^0} \cdot \frac{N_A^0}{N_B^0} \tag{2.30}$$

where I_A and I_B are the area intensities of A and B scattering peaks measured from AB surface; $I^0{}_A$ and $I^0{}_B$ are those from the pure A and B standards, respectively. N_A and N_B are the areal density of pure A and B standards, respectively. Equation 2.30 has already been used successfully by many researchers for quantitative analysis of many alloys, especially in studying the phenomenon of surface segregation [Niehus *et al.* 1993].

Chapter 3 Experimental Procedures

3.1. Introduction

The experimental procedure and details are described in this chapter. Eight binary systems of compound semiconductors and GeSi alloy were studied. Reference samples of pure semiconducting elements were also prepared by means of vacuum evaporation, and examined by LEISS and XPS as standards for accurately quantitative analysis.

The experimental work was conducted according to the following procedure: (1) Before ion bombardment, all of the eight compound semiconductors and GeSi alloy were analysed by LEISS and ARXPS to obtain initial information on surface composition. (2) After the initial analyses, samples were bombarded with an Ar^+ beam for up to 50 minutes, whilst the surface compositional changes were monitored with XPS. (3) The bombarded surfaces were re-examined by LEISS and ARXPS. Many technical details and considerations, including experimental parameter settings used in order to obtain more complete and reliable experimental evidences of ion bombardment effects are discussed in this chapter.

3.2. Selections of experimental materials

The experimental materials were selected not only due to their importance in modern electronics industry, but also based on the consideration of theoretical studies for this project. The eight binary systems employed in this project come from the different combinations of elements from Group IIb to VIb and from Period 3 to 5 in the Periodic Chart of the Elements (Figure 3.1). All the eight compounds were in the form of single crystals, including one IV-IV system: GeSi(100); six III-V systems: GaP(111), GaAs(100), GaSb(111), InP(100), InAs(100) and InSb(100); and one II-VI system: CdSe.

These eight samples represent most of the common compound semiconductors and GeSi alloy with a range of energy bandgaps from about 0.2 to 2.2eV. The lattice constant and energy bandgap for different group IV, III-V and II-VI compound semiconductors and GeSi alloy are shown in Figure 3.2. [Gunshor *et al.* 1992]

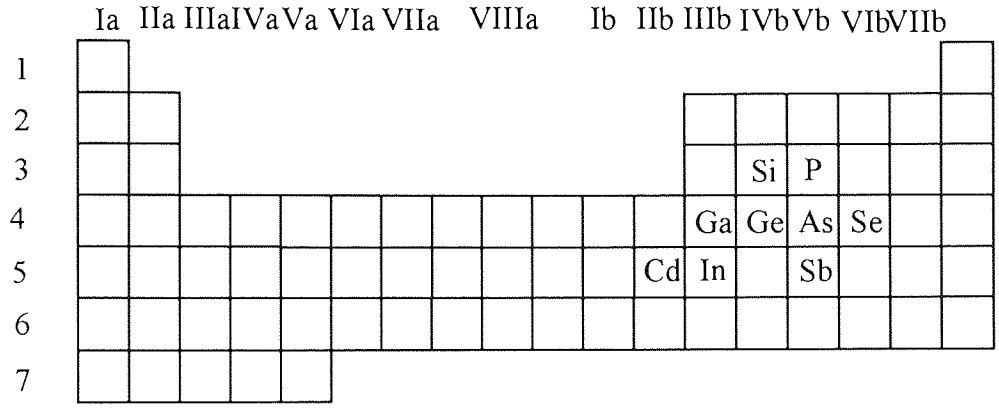

Figure 3.1 Periodic chart of the elements

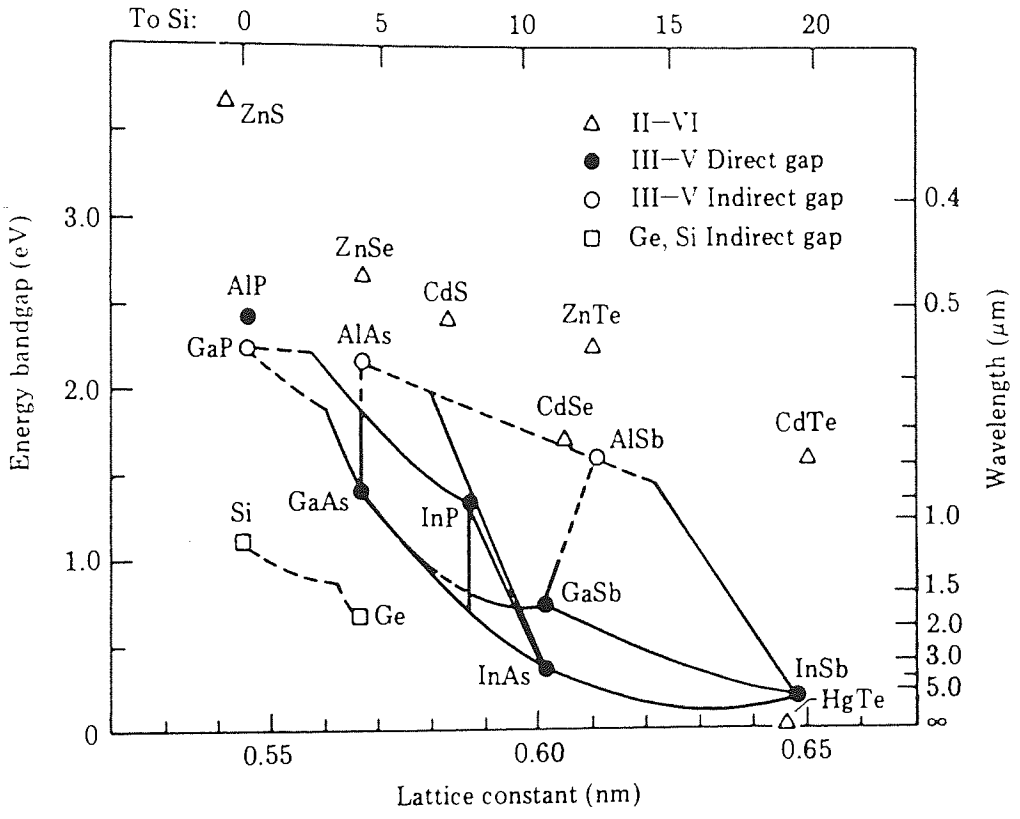

Figure 3.2 The lattice constant and energy bandgap for different group IV, III-V and II-VI compound semiconductors

(after Tu *et al.* [1987])

3.2.1. IV-IV System

GeSi is the only IV-IV system studied in this project. Ge and Si were the first two materials widely used in the semiconductor industry for making various electronic devices, but GeSi alloy has not attracted much attention in past four decades. It is only recently that Si-based Ge-Si heterostructures and superlattice have proved of great potential in band structure engineering [Abstreiter, 1992]. Since elemental silicon is available in large quantities and has a very stable native oxide, it has been proposed that such kinds of structures will be widely used in future of microelectronics and optoelectronic applications in competition with III-V compounds for fabrication of advanced electronic devices.

The GeSi sample used in the project was a GeSi(100) thin film of thickness greater than 5000 Angstrom, which was grown on a Si(100) substrate by molecular beam epitaxy. Between GeSi and Si substrate, there is a Si buffer layer with thickness of 100 angstrom. The atomic ratio of Ge to Si in the GeSi layer is 1:1.

The GeSi system is particularly interesting in this project. First, since it is a new material, and few result about of bombardment effects on this material has been reported. Second, according to Pauling's formalism [Pauling, 1967], Si and Ge are of the same electronegativity (ε_n=1.8eV), the electron structures of both Ge and Si atoms are not changed in the formation of GeSi system. It may be expected therefore that the ion bombardment effects on this material are similar to those on metallic alloys.

3.2.2. III-V Systems

The six III-V compounds were chosen to give a chance for systematically studying ion bombardment effects. With exception of GaAs, all five III-V other compounds were purchased from MCP Wafer Technology Ltd (UK). They were undoped and etched to remove damage from cutting and then the front surfaces chemically/mechanically polished to mirror finish.

GaP is generally used in making visible light-emitting devices. Since the GaP provided by MCP is still in the experimental stage, no technical information about the manufacturing procedure is available.

GaAs is one of the most important compound semiconductors in the modern semiconductor industry. Because of the success in the production of infrared and visible semiconductor lasers, this material has opened up potentially huge markets in optical communications, compact disc and related optical data storage, lighting and display

technologies. The GaAs samples used were n-type GaAs(100) crystalline surfaces doped with low dose Si.

Ga and As atoms have very small difference in mass, the mass effects should not be dominant in ion beam effects, and the other effects may be seen more clearly in the experiments.

GaSb has received increased attention as a material for preparing multilayer structures for a variety of device applications, including diode lasers, photo detectors and heterojunction transistors.

The GaSb single crystal used was grown by the liquid encapsulated Czochralski process modified to operate at the low melting point (712°C) of the gallium antimonide. The growth direction is (111). Undoped crystal is P type.

This materials is of particular interest in this project. The mass effects and binding energy effects may be investigated by comparing the experimental results of ion bombardment in GaP, GaAs and GaSb surfaces.

InP is a direct-bandgap and high mobility material, which is commonly used as a substrate for epitaxially grown III-V compounds in the fabrication of optoelectronic and high-speed electronic devices.

The InP sample used in the project was manufactured in three steps: (1) polycrystalline bar formed in a high pressure synthesis is used as charge material for an initial liquid encapsulated Czochralski (LEC) growth (2) a further high pressure LEC growth produces single crystal (100) InP which is subsequently wafered with orientation flat. (3) the wafer is precision edge rounded and individually laser scribed with ingot and slide identity to ensure perfect traceability.

Since In and P atoms have large differences in mass and electronegativity, it may be expected that mechanisms of ion beam interaction with InP surfaces will be similar to that with some ionic oxides, such as transition metal oxides [Malherbe *et al*, 1986; Hofmann and Sanz 1982/1983, Choudhury *et al.*, 1989].

InAs has been found great potential in fabrication of the double-barrier resonant tunnelling diodes. Like GaAs/AlAs, InAs/AlSb-based double barrier structures have recently demonstrated high peak-valley current ratios and large current densities [Chiang, 1994]. InAs is also a important component in InAlAs, InGaAs and InGaAsP compounds for making various MQW structures or semiconductor lasers.

The InAs single crystal is grown in (100) orientation under high pressure using pure indium and arsenic pure fused silica crucible. This material, together with InP and

InSb, is very helpful for investigation of the mass and surface binding effects due to ion bombardment.

InSb, due to its high electron mobility, is an excellent material for Hall effect devices. It is also used as IR detectors for 3-5μm atmospheric transition windows.

The InSb single crystal sample used in this project is grown in a pure fused silica system by the Czochralski method. The staring material is highly purified polycrystalline ingot.

Like Ga and As, In and Sb are nearly equal in mass, the mass effects presumably are not important factors to be considered in ion bombardment effects of InSb surfaces. Furthermore, since both In and Sb are of more metallic properties, it may be expected that this material is more like a metallic alloy in experiments of ion bombardment.

3.2.3. II-VI System

CdSe has been employed in this project. Although III-V compounds are the most popular materials for making semiconductor lasers, these lasers can only emit wavelengths in the visible and the infrared regions. However, II-VI materials, due to the larger bandgap energies (over about 2.5eV (see Figure 3.2)), have found special areas of application for compact lasers and LEDs at blue and green wavelengths. No research work in studies of ion bombardment on II-VI materials have been reported so far, hence the work on studying ion bombardment effects in CdSe may be very valuable.

3.3. Preparation of reference samples

3.3.1. Ge and Si

Ge and Si standard reference samples were prepared using high-purity Ge(100) and Si(100) single crystals cleaned by prolonged sputter cleaning in UHV using Ar^+ beam until C and O concentrations detected by XPS were reduced to less than 1%.

3.3.2. Ga, In, Cd and Se

Ga, In, Cd and Se standard samples were prepared by means of vacuum evaporation. The reason of using this methods to prepare the standard samples is that pure Ga, In, Cd and Se have very low melting points (30, 157, 322 and 220°C,

respectively), they are too soft to form ideal surfaces for analysis. The arrangement of the evaporation system is shown in Figure 3.3.

The evaporator was constructed in two parts: (1) evaporation chamber (2) vacuum pumping system. The evaporation chamber was made of a glass bell jar which was connected to vacuum system by an piece of circular viton rubber. In the chamber, the substrates (facing down) were fixed on a metal plate (mask) and located in the upper section of the chamber by three metal rods (see Figure 3.3). A Mo boat containing the materials to be evaporated was placed at the bottom. Two metal terminals are used to support the Mo boat. They also acted as two electrodes letting a high current pass through the boat so that the material in the boat was heated to vaporisation temperature. A shutter was paced between the substrate and the Mo boat to avoid the contaminants on the surface of materials reaching the substrates. The pumping system was composed of a diffusion pump to maintain a high vacuum in the evaporation chamber and a rotary pump to provide initial pumping for the chamber as well as pumping lines and backing to the diffusion pump.

The evaporation experiments were carried out according to the following steps:

(1) The Mo boat containing no materials was connected to the terminals and close the chamber.

(2) All valves were closed. The chamber was pumped down to high vacuum of pressure of about 1Pa.

(3) The boat was powered gradually by increasing electric current up to about 60amps. The colour of the boat changed from metallic blue to red and finally turned into very bright. After a few seconds, all contaminants on the boat were removed leaving the boat very clean. Then the power was switched off.

(4) All valves were closed. The air inlet was opened letting air into the chamber, then the chamber was opened.

(5) Substrate was put on the mask and the materials were loaded into the cleaned Mo boat. The chamber was closed.

(6) The chamber was pumped down to get vacuum of about $0.4 \sim 0.5$Pa.

(7) Shutter was closed. Electric power was switched on. Current was arised very gently.

(8) When materials started melting, current was stopped increasing. After the materials were completely liquid for 5 to 10 seconds, the shutter was opened, the evaporation started. The time used for evaporation was about 60 seconds,

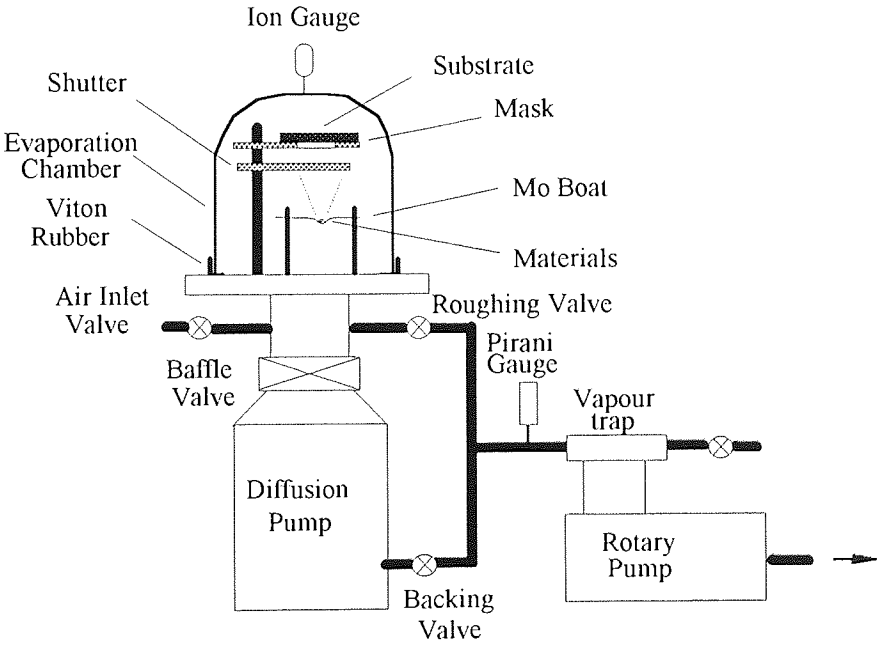

Figure 3.3 Layout of the vacuum evaporator

depending on the materials. The thickness of the thin films obtained on titanium substrate was about a few microns.

(9) After evaporation, the system was cooled down for about 30 minutes. the chamber was opened to the air. The standard samples now were ready for analysis.

High-purity gallium (bought from The Drug Houses Ltd, UK), indium, cadmium and selenium (bought from Johnson Mathey Materials Technology Ltd, UK) were used for making high quality Ga, In, Cd and Se films by evaporation. The titanium discs cut from a Ti bar (ϕ12mm) with a thickness of 2mm were employed as substrates. One side of substrates were polished mechanically until mirror-like surfaces were obtained. The Ti substrates were washed with iso-propl alcohol, rinsed in de-ionised water and baked out before the experiments of evaporation.

Following the above procedure, high purity Ga, In, Cd and Se standards were made successfully. The thickness of the films were several microns. After the evaporation, the samples were immediately transferred in air into the UHV chamber. After a short time of sputter cleaning to remove the contamination overlayer the samples were examined by XPS and LEISS for quantitative analysis.

3.3.3. P

Since there is no way to obtain a high purity P surface, the P element was calibrated indirectly using pure AlP powder sample (purity about 99.9999%). For this purpose, pure Al surface was also examined by XPS after prolonged sputtering.

3.3.4. As and Sb

Arsenic and antimony surfaces were prepared using pure As and Sb lumps. Since the lumps were of irregular shapes, it was impossible to find a base plane for the polishing. The lumps were first hold by conductive bakelite powder, an organic compound material special for mounting, using an automatic mounting press facility. The working principle of the mounting press is given in Figure 3.4.

The procedure of mounting lump samples was as follow:

(1) Sample was placed on the ram plug and lower ram using control level.

(2) Sufficient powder was added and head assembly was screwed down fully, then back one half turn.

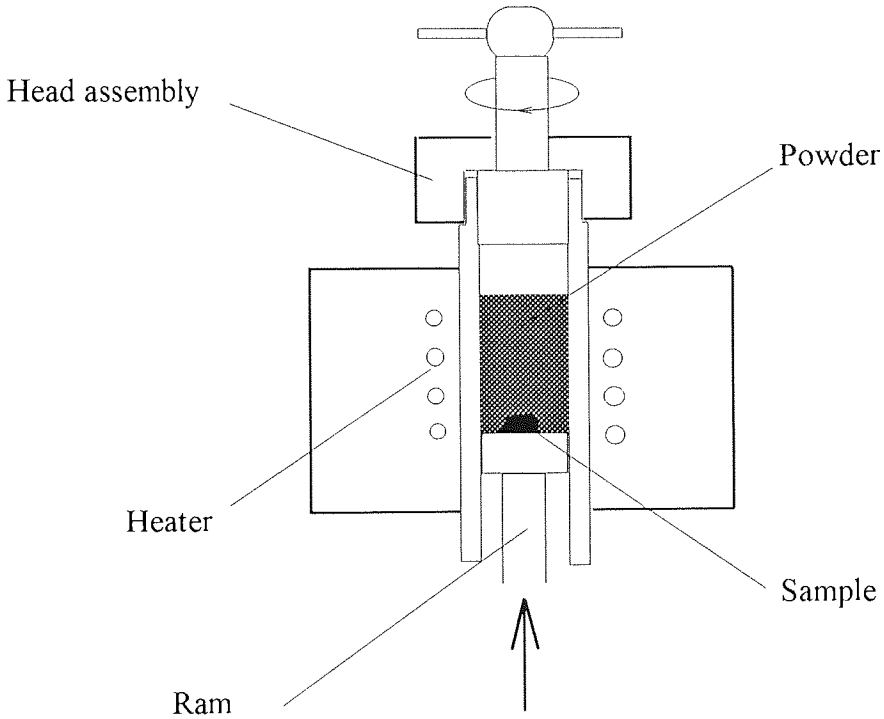

Figure 3.4 Schematic of automatic mounting press facility

(3) Ram control lever was raised to upper position to apply pneumatic pressure.

(4) The heating/cooling switches were set to AUTO and that the two timers were set to 8 minutes (heating) and 2 minutes (cooling).

(5) Mains was switched on. Heating and cooling cycles were indicated by red and green lights.

(6) When the white light came on and the buzzer sounded, power was switched off. Mounting was completed.

(7) The ram with control lever was lowered, the head assembly was removed.

The temperatures and pressure used for the mount were 150°C and 3×10^7 Pa, respectively. The size of the mounts was about $\phi25\times3$ mm. After the thermal treatment, the bakelite became very hard, and provided very good conditions for polishing.

The As and Sb lumps after the mounting press were polished mechanically on a series of different grade abrasive paper from P240 to 1U until mirror like surfaces were obtained. The polished samples were then washed ultrasonically in acetone. Since both As oxide and Sb powder are extremely toxic, special precaution was taken, gloves were put on all the time during the preparation.

3.4. VGS ESCALAB 200D Spectrometer

The spectrometer used in the project was a VGS ESCALAB 200D system. The layout of main components is shown in Figure 3.5.

All components for surface analysis are located on a spherical analysis chamber with an inner diameter about 600mm and the whole spectrometer is housing on four air feet for vibration damping during experiments. The directional relations of main components are tabulated in Table 3.1.

Table 3.1 Arrangement of main components in VGS ESCALAB 200D

Components	θ (°)	ϕ (°)
X-ray Source	60	40
Spectrometer	15	0
Ion Gun (EX05)	50	102
Sample Manipulator	90	90
CCD Camera	46	0
S. E. Detector	60	225
Viewport	75	5

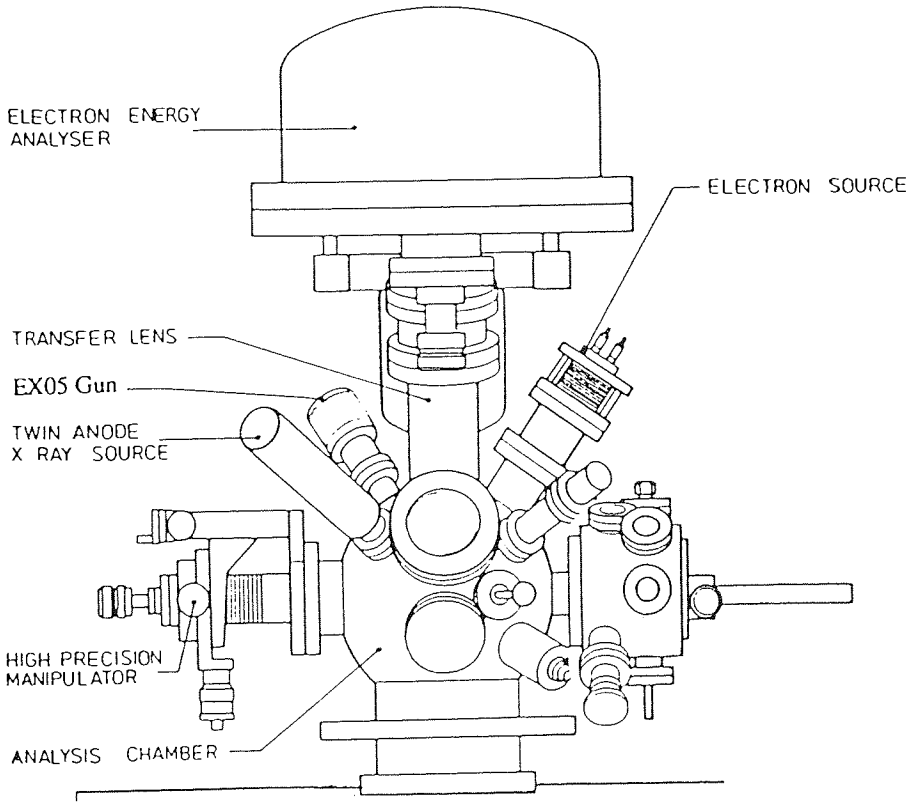

Figure 3.5 Layout of VGS ESCALAB 200D spectrometer

3.4.1. Vacuum system

The system is divided into two sections: a fast entry airlock and an analysis chamber. Two chambers have different working vacuum. In the fast entry airlock vacuum is from atmosphere to 10^{-3} Pa which is obtained by a turbo-molecular pump, in the analysis chamber it is from 10^{-3} to 10^{-6} Pa which is maintained by a diffusion pump. A liquid nitrogen cooling trap is located in the pumping line of diffusion pump to restrict oil molecule ingress into the analysis chamber for UHV. The fast entry airlock is used to transport samples quickly into the analysis chamber without breaking high vacuum in the analysis chamber.

3.4.2. Sample transfer mechanism

Samples to be analysed are fixed on stubs, usually by means of double-side adhesive tape, and put on a carousal, on which up to six samples can be accommodated at any time. There is a rail mounted in the fast entry airlock, the carousal is then located at the end of the rail and transported from the fast entry airlock into the analyser chamber. In the chamber there is a housing site for locating the carousal. Samples are placed on the sample holder at the end of a manipulator using a wobble stick.

The sample manipulator gives high-precision, 3-dimensional linear movement and a angular adjustment with a mechanical accuracy of 2.5°. A electrical heater, and a liquid nitrogen cooling system, together with a thermocouple temperature monitor, are also provided at the sample holder.

A CCD camera on the spectrometer is well aligned to the X-ray source using a standard sample for selecting the analysed area in XPS experiments. A secondary electron detector (not shown in Figure 3.5), consisting of a scintillator and a photo multiplier, is also employed for collecting secondary electrons, so that a physical image can be obtained and displayed on a TV monitor. This is very useful for aligning the ion beam and for choosing area to be analised in LEISS experiments.

3.4.3. X-ray source

The structure of twin anode X-ray source used in this study is shown in Figure 3.6. The X-ray source has Mg and Al anodes and is operated with the filament near earth potential and the anode at a positive potential of up to 15KV. X-rays generated in the

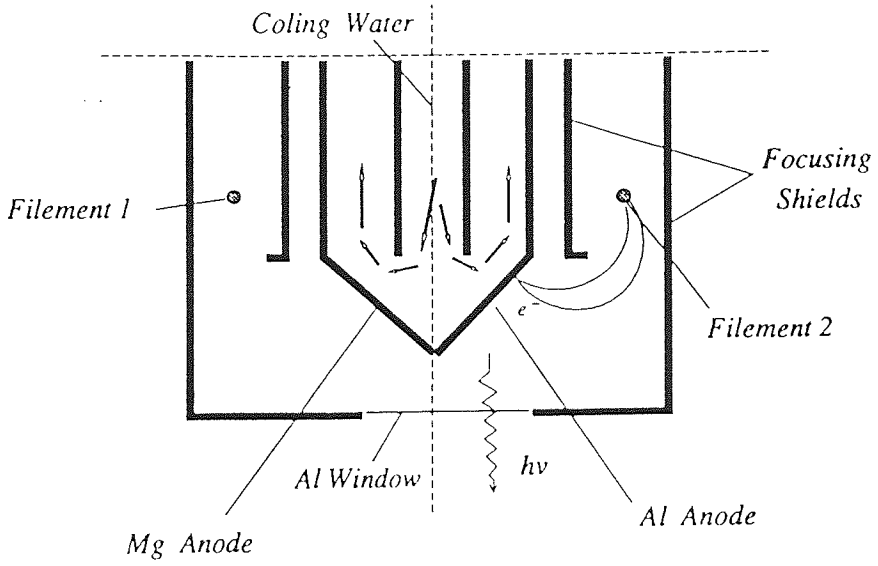

Figure 3.6 Structure of twin anode X-ray source in VGS ESCA 200D

anode face by hot-electron bombardment pass out through an aperture in the surrounding cylindrical shield, covered with a thin aluminium foil window which acts as a X-ray filter to prevent sample from stray electrons, heat effects and contamination originating in the source. The foil also removes other additional X-ray lines, such as, K_β, L, M, *etc.*. The distance between X-ray source and sample can be changed to improve the detecting sensitivity. For Mg and Al anodes the main X-rays are the K_α peak lines which come from the transit from $2p_{3/2}$ and $2p_{1/2}$ to 1s. The energies of Mg K_α and Al K_α are 1253.6eV and 1486.6eV, respectively; The Full Width Half Maximum (FWHM) for Mg K_α and Al K_α are 0.7 and 0.8 eV, respectively.

3.4.4. Ion gun

A VG-EX05 noble gas ion gun was employed in experiments of ion bombardment and in LEISS analysis. The specifications of the gun are given in Table 3.2:

Table 3.2 Specifications of EX05

Ion Energy (eV)	100 to 5000
Maximum Current (μA)	10
Minimum Spot (μm)	<120
Maximum Current Density (mA/mm^2)	>5
Maximum Scanned Area(mm^2)	5 × 5

The high purity ions are produced by an electron impact source equipped with two filaments. Electrons from a hot filament pass through a grid in the ionisation cell and suffer inelastic collisions with inert gas atoms or molecules. The anode and an electron repeller are designed so that electrons can oscillate in the ionisation cell to increase the ionisation probability. The atoms are thus ionised and the ions are extracted by electric field between anode and extractor. The ion energy is adjusted by the potential applied on anode. The ion emission current can be varied from 2μA to 10 mA continuously by adjusting the extraction voltage (0 to 10V). (which is normally done by a coarse control to select fixed values in the range 2μA to 10 mA and a fine control to get 30% to 100% emission).

Inert gas is supplied to the source region via the gas inlet valve from a high pressure ($>1\times10^5$ Pa) volume. Differential pumping of the source permits an analysis chamber vacuum partial pressure of better than 5×10^{-4} Pa during operation.

The conceptual schematic of the ion optics of EX05 is illustrated in Figure 3.7. When ions are extracted they are focused by the first triplet lens to get required ion

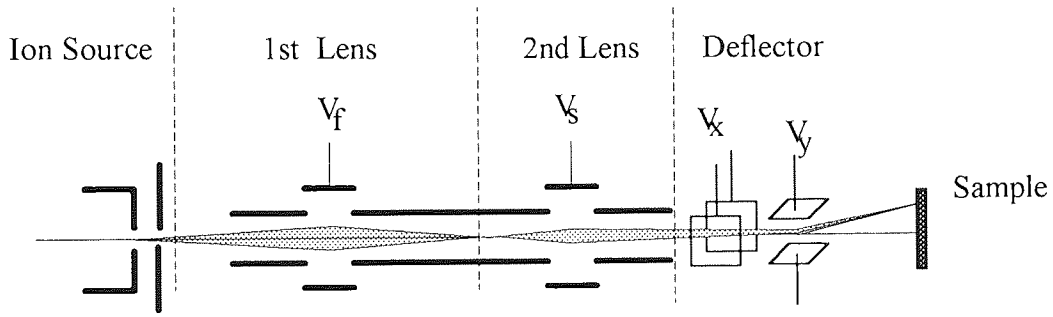

Figure 3.7 Ion optics of EX05 ion gun in VGS ESCA 200D

current and to form a cross over point at the aperture between two sets of lenses. The ions are further focused by the second triplet to obtain the expected beam spot at a certain distance.

The focused ion beam is deflected by two pairs of deflecting plates and rastered over sample surface at TV rates to give a homogeneous sputtering. A pair of bias (DC voltages) applied to the deflecting plates allow the ion beam to be shifted so the specific area can be selected.

3.4.5. Energy analyser

A 150° Hemispherical Sector Analyser (HSA) is used as a multifunction energy analyser in the system. The schematic of this analyser is shown in Figure 3.8. The analyser acts as narrow pass filter to allow electrons with an energy $E+\Delta E$ to pass. The energy resolution of the analyser is determined by ΔE. $\Delta E = HV$, where V is the potential difference between inner and outer hemispheres and H is a constant determined by the physical measurements of the analyser, i.e. the inner and the outer radius of the two hemispherical electrodes and the slits, *etc.*.

The sample is normally at earth potential and electrons are transmitted from the sample to the analyser by the electrostatic lens and retarded in energy by an amount R (eV) immediately before entering the analyser. The kinetic energy of electrons leaving the sample with respect to the Fermi level can be expressed as:

$$E_k = R + HV + W \tag{3.1}$$

where W is the work function of the spectrometer. The binding energy can be calculated from Einstein photoelectric equation, or Equation 3.1. The energy level schematic is shown in Figure 3.9.

Two working modes are normally used in analyser operation. In CAE mode the HV is kept constant during a spectrum, so the resolution of electrons with different kinetic energy is fixed, this mode is generally preferred in XPS. In CRR mode the ratio of kinetic to pass energy is constant during a spectrum, at low kinetic energy this mode produces a flatter background.

The electrostatic lens in front of input entrance of analyser is used for improving the transmission characteristics of the analyser. The inlet and exit apertures are used for control of the sample area and can be changed by a rotary drive mechanism. The dimensions of apertures may be changed from 3000 to 150μm. These also determine the resolution through the geometric parameter H.

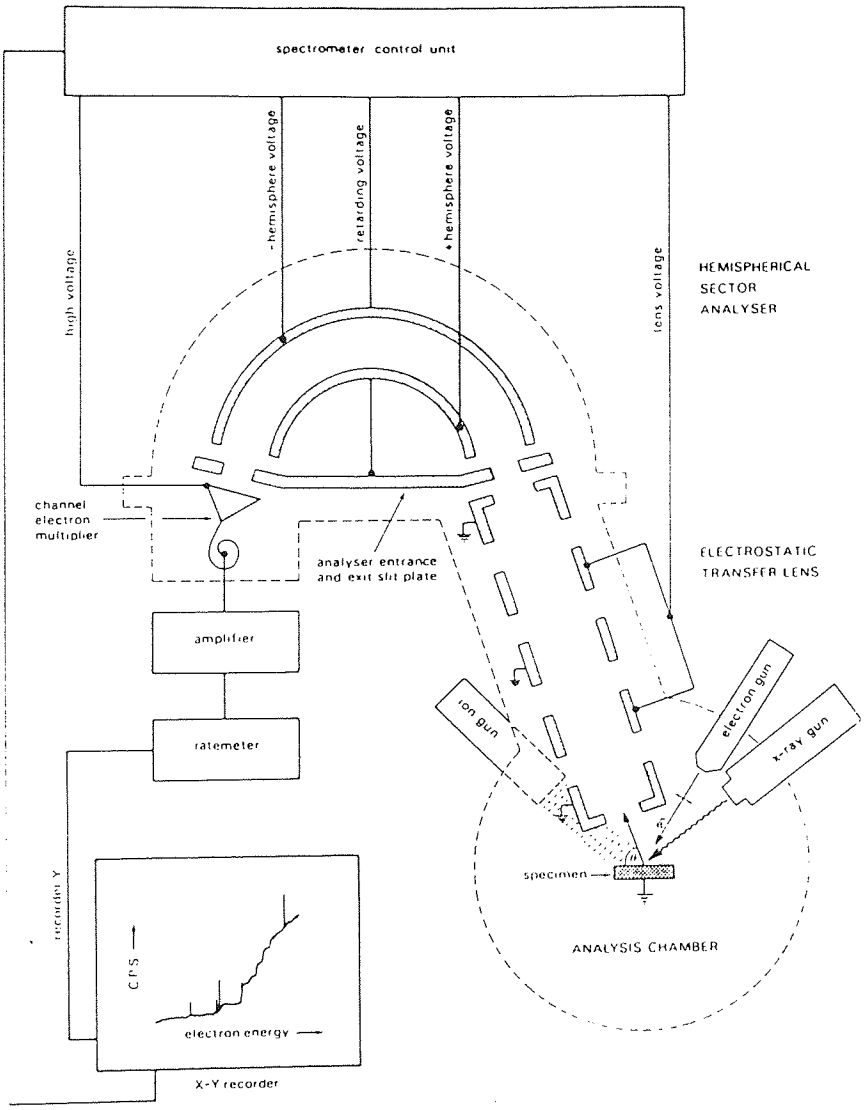

Figure 3.8 Schematic of a 150° Hemispherical Sector Analyser (after Watts [1994])

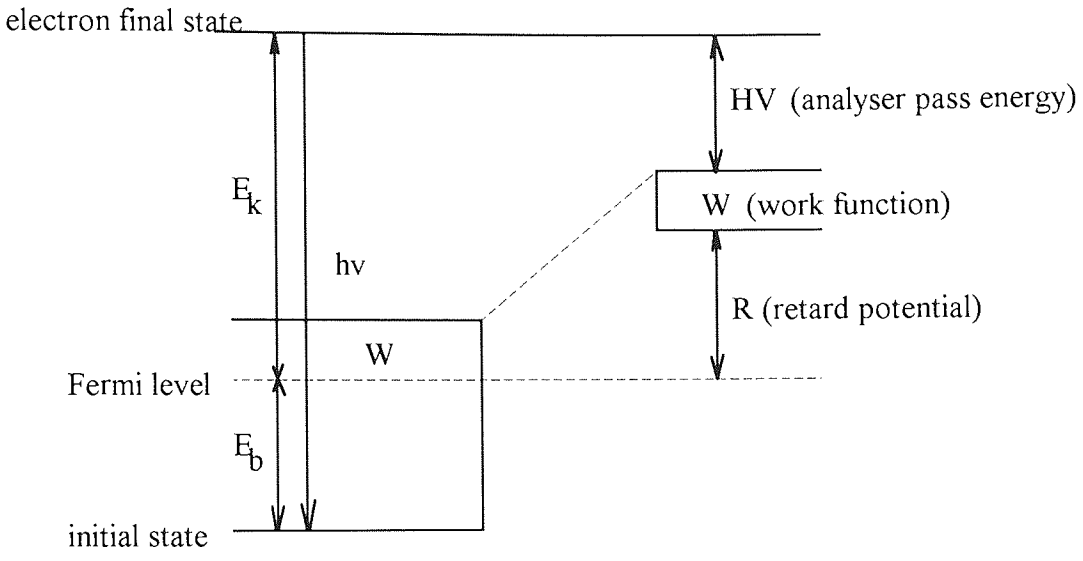

Figure 3.9 Energy level schematic of a hemispherical sector analyser

3.4.6. Computer system

The computer system used is PDP11/53 microcomputer. Two terminals are connected to the computer, so two users can use the system at the same time. The data acquisition and processing were carried out by VGS 5250 DATA SYSTEM (Version Jan.1992) which containes all functions for XPS spectrum analysis such as smoothing, satellite subtraction, charge correction, peak synthesis, quantification, profile, etc.. Data is stored on the 160 Mbit hard disk and can also be backed up on tapes for permanent storage. Analytical results can be output on an Epson printer or on a HP plotter.

3.5. Details of XPS and LEISS experiments

3.5.1. Before XPS and LEISS experiments

3.5.1.1. Alignments for CCD camera, X-ray source and the ion gun EX05

Since both XPS and LEISS techniques were employed in this study, it is obviously important to align the X-rays used in XPS and the ion beam used in LEISS to ensure the two probes detecting the same area on the sample surface. The alignment was carried out in two step: (1) to align CCD camera to x-rays; (2) to align the ion beam to the CCD camera. The sample used for the alignment is a copper stub, at the centre of its surface, a silver dot of diameter about 500 microns was mechanically inserted, the surface was flatted and then well polished.

The method for the alignment of the camera to the x-ray source is illustrated in Figure 3.10. The procedure for the alignment is as follows:

(1) The copper sample was positioned roughly at the centre of the analysis chamber using the manipulator. The sample tilled at a angle of about 300° to let the axis of the lens in the front input of the energy analyser perpendicular to the surface. The CCD camera was switched on, the silver dot may be seen on the TV screen, but may not at the centre.

(2) Under the UHV condition of better than 1×10^{-4} Pa, the x-ray source was operate at voltage of 15kV and a filament current of 20mA (using Mg anode). The spectrometer was run at medium resolution and the aperture of 3000μm on the spectrometer was selected to find both Ag 3d and Cu 2p signals.

(3) The aperture was reduced to 300μm and the accept angle of photoelectrons was

about 7°. The sample was moved in X dimension using the manipulator until the Ag 3d signal disappeared. Then the sample was moved in the opposite direction in steps of 50μm, at each step, XPS spectra of Ag 3d and Cu 2p were taken until the silver signal disappeared after it reached a maximum, the position at which the Ag 3d signal increased to the maximum and Cu 2p decreased spontaneously to the minimum value, were found.

(4) The sample was located at the above X position. Step 3 was repeated but in Y dimension to find the optimum Y position for Ag 3d signal.

(5) The silver dot was located at the optimum position, then CCD camera was fixed to locate the image of the silver at the centre of the TV screen.

The alignment of ion beam can be done using the secondary electron detector. The procedure is described as follows:

(1) After the CCD camera was aligned to the X-ray source, CCD camera was used to locate the silver dot at the centre of the TV screen. TV was switched to receive S. E. signal from the S. E detector.

(2) EX05 ion gun was operated at the desired energy and magnification. The S. E detector was switched on and the voltages were applied on the focusing lens to find the clear image of the silver dot.

(3) 'X shift' and 'Y shift' functions on the controller of the ion gun were used to vary the bias allowing the silver dot at the centre of the screen.

For the ion beam with very low energy, the spot size of the beam may become too blur and large, due to the dramatic increase in spherical and chromatic aberrations, to see the image of the silver dot. In this case, the silver sample may be replaced by a well polished metal disc, at the centre of its surface, a circle with a diameter of 2-3 mm acting as the silver dot is marked mechanically for the alignment.

3.5.1.2. Chemical cleaning of compound semiconductor surfaces

When semiconductor material is exposed to air, native oxide layers are always unavoidably formed at the surface, this makes the surface analysis much more complicated. In this project, an attempt was made to remove these oxide layers using the procedure of wet chemical cleaning described by Epp *et al.* [1989]. GaAs sample was employed for this purpose.

The procedure are: (1) the GaAs sample was cleaned in 1:1 HCl(conc.)/H_2O at

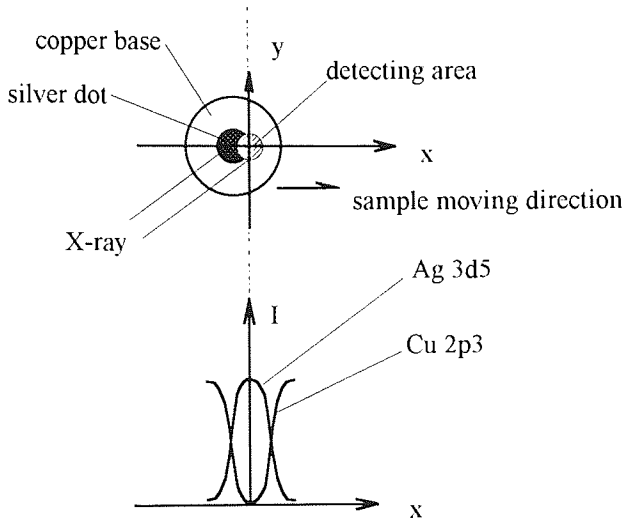

Figure 3.10 Procedure of aligning CCD camera to X-ray source

room temperature for about 10 minutes; (2) the sample was then rinsed in deionized water, then ultrasonically cleaned in methanol for about 2-3 minutes; (3) the sample was finally rinsed again in deionized water. The cleaned GaAs sample was quickly transferred in air to the analysis chamber and analysed by means of XPS.

3.5.1.3. Sample mounting

Reference samples Ga, In, Cd, As, Sb, Se and Al were fixed on stainless steel or nickel stubs by means of double-side adhesive tapes. A small piece of pure aluminium foil was wrapped around both sides of the tapes to shorten samples electrically to the stubs. The AlP powder was mounted on the stubs by spraying and pressing the powder on double-side tapes. The thickness of the AlP on the tape was about 0.5mm.

Since most of semiconductor materials have quite poor electric conductivity, the compound semiconductors and GeSi alloy and pure Si and Ge single crystal samples were mounted on special stubs to improve electric conductivity and to reduce the effects of surface charging. The facility used for mounting the semiconductor samples is illustrated in Figure 3.11.

It consists of two parts: (1) a stub with a spiral thread at the edge; (2) a metal cap with an opening hole of diameter 10mm at the top. The stub and the cap is matched by the thread. The sample can be placed between the metal cap and the stubs and fixed by tightening the cap on the stub. By the cap, the electrons from the earth may reach the analysed surface to compensate the electron loss due to ion beam or X-ray radiation and to minimise the charging effects.

3.5.2. Details of XPS measurements

XPS investigation consists of three parts: (1) a wide scan XPS analysis to find out all elements existing in the initial surfaces; (2) angle resolved XPS analysis before and after ion bombardment to get information on surface structure of the compound semiconductors and GeSi alloy; (3) normal narrow scan XPS measurements to monitor surface compositional changes during the ion bombardment.

In the XPS experiments, Al K_α X-ray radiation ($h\nu$=1486.6eV, FWHM=0.8eV) was used at anode voltage of 15 kV and a filament current of 20mA. The X-ray luminated area on the sample surfaces was about 500μm in diameter.

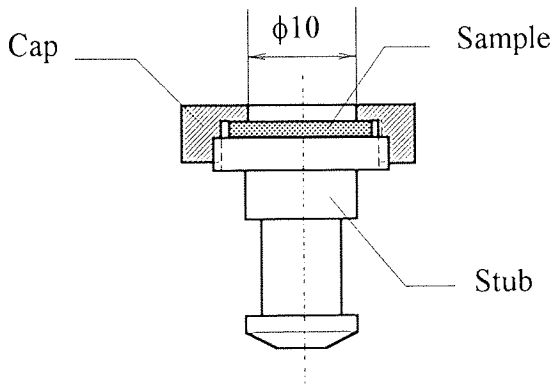

Figure 3.11 A diagram of sample mounting

The energy analyser was operated in the CAE mode. In the wide scan, the pass energy of 50eV, the step size of 0.3eV and the dwell time of 50ms were selected. In narrow scan analyses, the above parameters were 20eV, 0.1eV and 200ms, respectively. An aperture of 600μm and the acceptance angle of 9° were selected. The voltage applied to the lens in the front of the entry to the analyser was about 4.1eV, which was set using Ag 3d5/2 (at BE of 368.2eV) peak to gain the maximum counts.

In ARXPS, the electron take-off angles(TOA) were varied from 0 to 80° to the surface normal in steps of 10°. At each TOA, the samples were re-aligned using marks on the surfaces to correct the slight movement of the analysed areas due to the sample rotation. In normal XPS analysis, the TOA was fixed at 0°. During the XPS experiments, the base vacuum was always better than 1×10^{-5} Pa.

3.5.3. Details of LEISS measurements

Low energy ion scattering spectroscopy was employed to study compositional changes in the top layers of the ion bombarded compound semiconductor surfaces.

In LEISS experiments, He or Ne ion beams generated by the EX05 ion gun were used as primary beams. The ion energy and current were 1keV and 10nA respectively. In order to reduce damage to the analysed sample surface due to the primary beams, the beams were defocused to a spot size of about 1mm in diameter, which gave a dose rate of about 2×10^{13}ions/cm^2 sec. The beams were incident on the sample surfaces at 51° to the surface normal (at 0° TOA). The scattering angle in the system was about 129°.

The energies of the scattered ions were analysed by the HSA working at CRR mode to give an equally relative energy resolution. The retarding ratio was 4. An aperture of 1mm and acceptance angle of 9° were used. In all experiments, the LEISS spectra were taken from an energy range from 200 to 1000eV in steps of 1eV.

The base pressure during LEISS was kept less than 3×10^{-6} Pa, and the working pressure was maintained at 5×10^{-4} Pa by differential pumping.

All major parameters in XPS and LEISS are listed in Table 3.3 for comparison.

3.5.4. Experimental conditions of ion bombardments

Ion bombardment was conducted using the same EX05 ion gun , but using Ar^+

beams. The Ar ion energy and the beam current used were 3keV and 1μA, respectively. The Ar ions was incident at an angle of 51° and rastered in an area of 8×6mm^2 on the sample surface. The total bombarding time was 50 minutes, which gave a dose of 1×10^{17}ions/cm^2. The working pressure was maintained at about 1×10^{-3} Pa.

Table 3.3 A comparison between XPS and LEISS experiments

Experiment		XPS	LEISS
Source	probe	Al K_α X-rays	He^+ or Ne^+
	power	15kV, 20mA	1keV, 10nA
	radiation area	500μm	1000μm
Detected signal		photoelectrons	scattered ions
HSA	working mode	CAE=20eV	CRR=4
	scan step	0.1eV	1eV
	Aperture	600μm	1000μm
Base vacuum		1×10^{-5} Pa	3×10^{-6} Pa

Chapter 4 Results and Analysis

4.1. Introduction

The results obtained from the all experiments undertaken in this project are included in this chapter. Some discussion of the results from preliminary studies are given, but the complete analysis for the ion bombardment effects is presented in Chapter 5.

This chapter first describes the results of XPS and LEISS analyses of pure elemental samples, Si, Ge, Ga, In, Cd, Se, P, As, Sb and Al. This is followed by the demonstrations of non-destructive analytical techniques, that is, ARXPS and KRXPS, in studies of surface structures, using overlayers on Cu and Ge(100) surfaces as examples. ARXPS analysis on the GaAs surfaces cleaned by chemically wet etching is given in Section 4.4, and these show why this process may be inappropriate to obtain an ideal initial surface for studying ion bombardment effects. The results from the experiments of ion bombardment effects on GeSi, GaP, GaAs, GaSb, InP, InAs, InSb and CdSe single crystal surfaces are presented in the final part of this chapter. For each material, the experimental results are divided into three parts: (1) ARXPS and LEISS analyses on the surfaces prior to ion bombardment; (2) XPS measurements on surface compositional changes during 50-minute Ar^+ beam bombardment. (3) ARXPS and LEISS re-examinations on the bombarded surfaces of the semiconductors.

4.2. XPS and LEISS analyses on the reference samples

4.2.1. Sputter cleaning

Table 4.1 gives the surface compositions of the reference samples after prolonged sputter cleaning using an argon ion beam of energy 3keV and beam current of 2-3μA. The values in the table were determined from XPS measurements using Scofield sensitivity factors stored in the VGS 5250 data system.

The contaminants on the cleaned reference samples were composed of carbon and oxygen. These two elements originated mainly from the adsorption of residual organic gas molecules and also probably from the occasional ingress of oil and water vapour, this

is normally unavoidable in a system using an oil pump in the analysis chamber to maintain UHV, although a liquid nitrogen trap was always used to reduce the level of this kind of contamination.

Table 4.1 XPS measurement of surface composition of reference samples

Sample	Purity (%)	Carbon (%)	Oxygen (%)
Al	98.7	0.41	0.92
Si	98.2	0.88	0.95
Ga	95.0	<0.1	5.0
Ge	99.5	0.50	<0.1
As	97.9	1.66	0.40
Se	98.6	0.71	0.65
Cd	98.6	0.96	0.44
In	98.1	0.26	1.68
Sb	99.1	0.86	<0.1

In addition to the above, contamination of the samples may be due to the procedure of sample preparation or the physical properties of these surfaces. For example, the carbon level measured from As surface was slightly higher than that from the others, this is partly because of the impurities in the arsenic lumps and partly due to a little contamination from the conductive bakelite powders used during the mounting and polishing processes. For low melting point, soft materials, such as, Ga, In and Al, the energetic ions may drive the elements of the contamination overlayer into the substrates more easily by recoil implantation, this may be the reason for more oxygen being found in these sample surfaces, particularly in the gallium standard. In addition, it will be seen in the section 4.2.3 that silicon has a very high affinity for oxygen, resulting in oxygen adsorption, even in UHV environment. Considering all of these problem, contaminant level were acceptably low.

4.2.2. XPS analysis

The core level spectra taken from the sputter-cleaned pure Al, Si, Ga, Ge, As, Se, Cd, In, Sb surfaces and P 2p spectrum from standard AlP powder are shown in Figures 4.1 and 4.2. For most of the elements (with the exception of P and Si), two core level signals which have a large difference in binding energy were collected for each element.

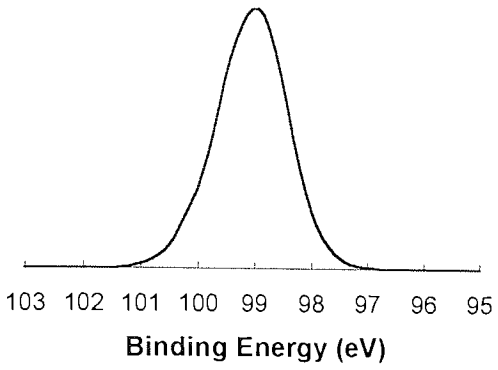

(a) Si 2p

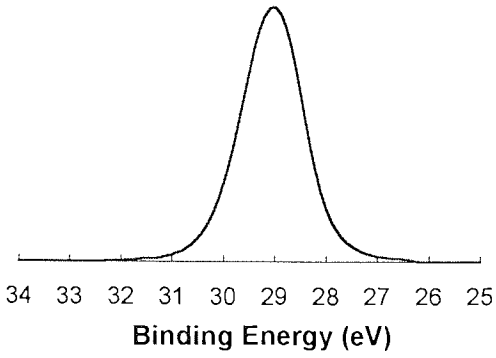

(b) Ge 3d

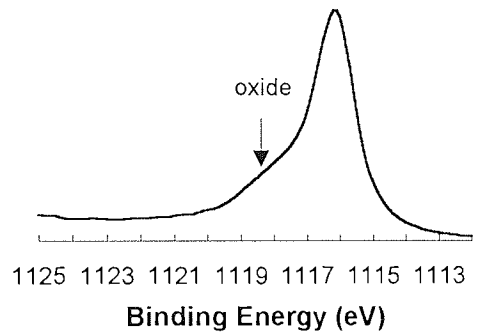

(c) Ga $2p_{3/2}$

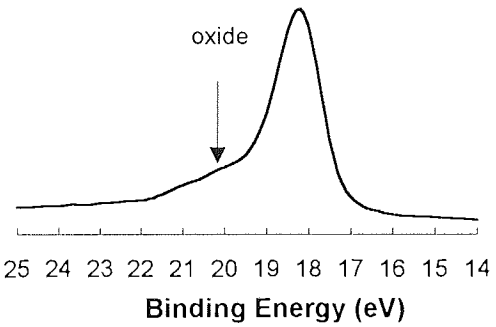

(d) Ga 3d

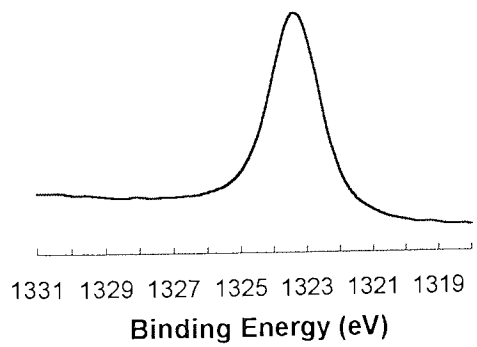

(e) As $2p_{3/2}$

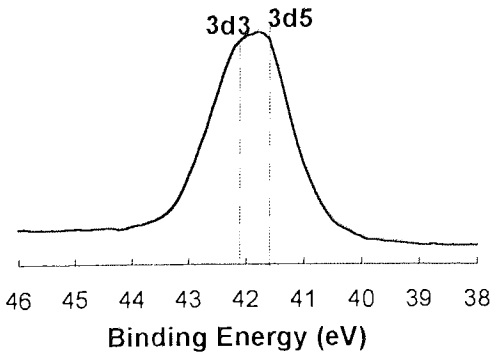

(f) As 3d

Figure 4.1 XPS spectra from sputter-cleaned Si, Ge, Ga and As surfaces

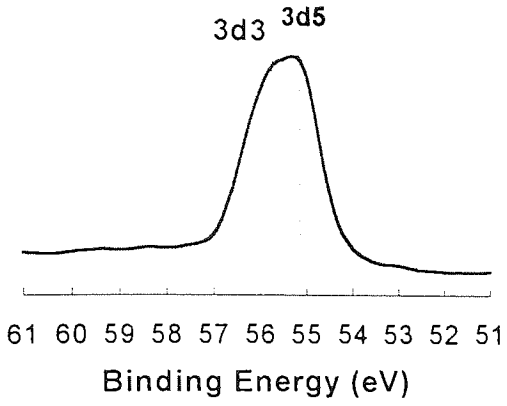

(a) Se 3d

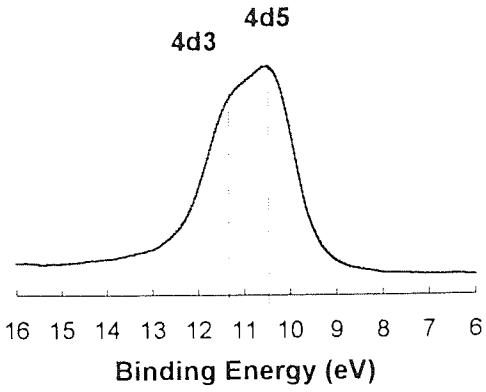

(b) Cd 4d

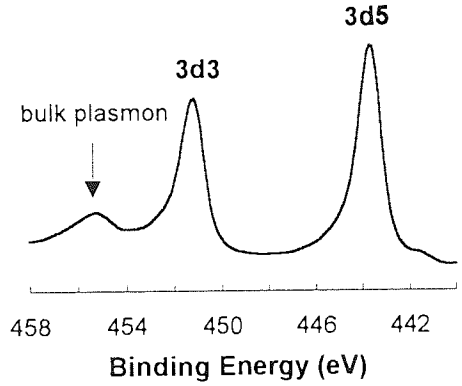

(c) In 3d

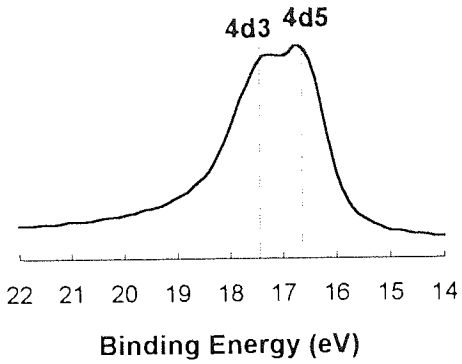

(d) In 4d

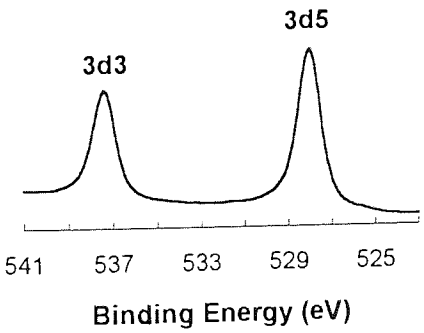

(e) Sb 3d

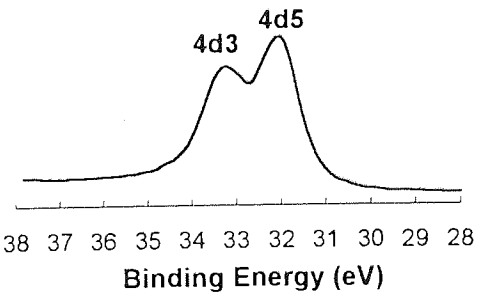

(f) Sb 4d

Figure 4.2 XPS spectra from the sputtered cleaned pure Se, Cd, In and Sb surfaces

The lower BE peaks, which are in energy range of 10 to 60eV, were chosen for quantification since they have nearly the same sampling depth, this is very important in XPS analysis of a compound system, particularly one in which elements are not distributed homogeneously in depth. The higher BE peaks were also very useful in the analysis of compound samples, since they have a quite small sampling depth compared to the lower BE peaks, and also the combination of these with the lower BE peaks give a good chance to use the KRXPS method in structural analysis (see Section 2.3.4). Sometimes, this technique is more efficient than ARXPS. For example, under the radiation of Al K_α X-rays ($h\nu$=1486.6eV), the sampling depth calculated from Equation 2.5a using Ga 3d (BE=18.8eV) and As 3d (BE=41.8eV) core electrons in GaAs at take-off angle of 0° are 67.2Å and 66.7Å, respectively, but those using Ga $2p_{3/2}$ (BE=1116.8eV) and As $2p_{3/2}$ (BE=1323.4eV) are only 33.7Å and 22.4Å. Similar results may be found in InSb using In and Sb 3d (sampling depth of about 60Å) and their 4d electrons (sampling depth about 80Å).

Additionally, since all the lower BE peaks listed in the table are doublets, peak synthesis may be difficult using these peaks when several chemical states are present. The higher BE peaks are single peaks and hence different chemical states are much more easily identified by chemical shift theory. These are illustrated by the Sb 3d and 4d peaks. Figure 4.3 shows the Sb 3d and 4d spectra taken from the partially oxidised Sb thin film evaporated on a Si substrate. It can been seen that the peak shape of Sb 4d core electrons was complicated by oxidation, the two peaks at 31.9 and 33.1eV are Sb $4d_{5/2}$ and Sb $4d_{3/2}$ core electron corresponding to antimony in the metallic state. The other two peaks in the Sb 4d spectrum at BE of 34.0 and 35.2 represent Sb $4d_{5/2}$ and $4d_{3/2}$ core electrons for the Sb oxidation state. Although some parameters, such as the BE separation, area ratios of $4d_{5/2}$ and $4d_{3/2}$ peaks, are easily found out, more uncertainties involved in quantifying Sb 4d may result in much bigger errors and hence the quantification becomes much easier using Sb $3d_{3/2}$ peaks. The two states of antimony are clearly distinguished by the two Sb $3d_{3/2}$ peaks at about 537.4 (element) and 539.6.eV (oxidation). It should be noted that the presence of oxidation Sb $3d_{5/2}$ peak cannot be directly used for peak synthesis due to the mixture of the oxide Sb $3d_{5/2}$ peak (BE=530.2eV) with the O 1s peak (BE≈530.6eV).

In the Ga 3d and $2p_{3/2}$ spectra shown in Figure 4.1, the shoulder peaks on the higher energy side of the peaks may be easily seen. This is apparently due to the existence of O in the surface, these oxygen atoms were chemically bounded to Ga atoms, resulting in about 2eV shift in the binding energies of 3d and $2p_{3/2}$ core electrons of these Ga atoms. In the In 3d (Figure 4.2) spectrum, satellites appear at higher binding energy sides of the $3d_{3/2}$ peaks due to the bulk plasmon loss of the 3d core electrons in

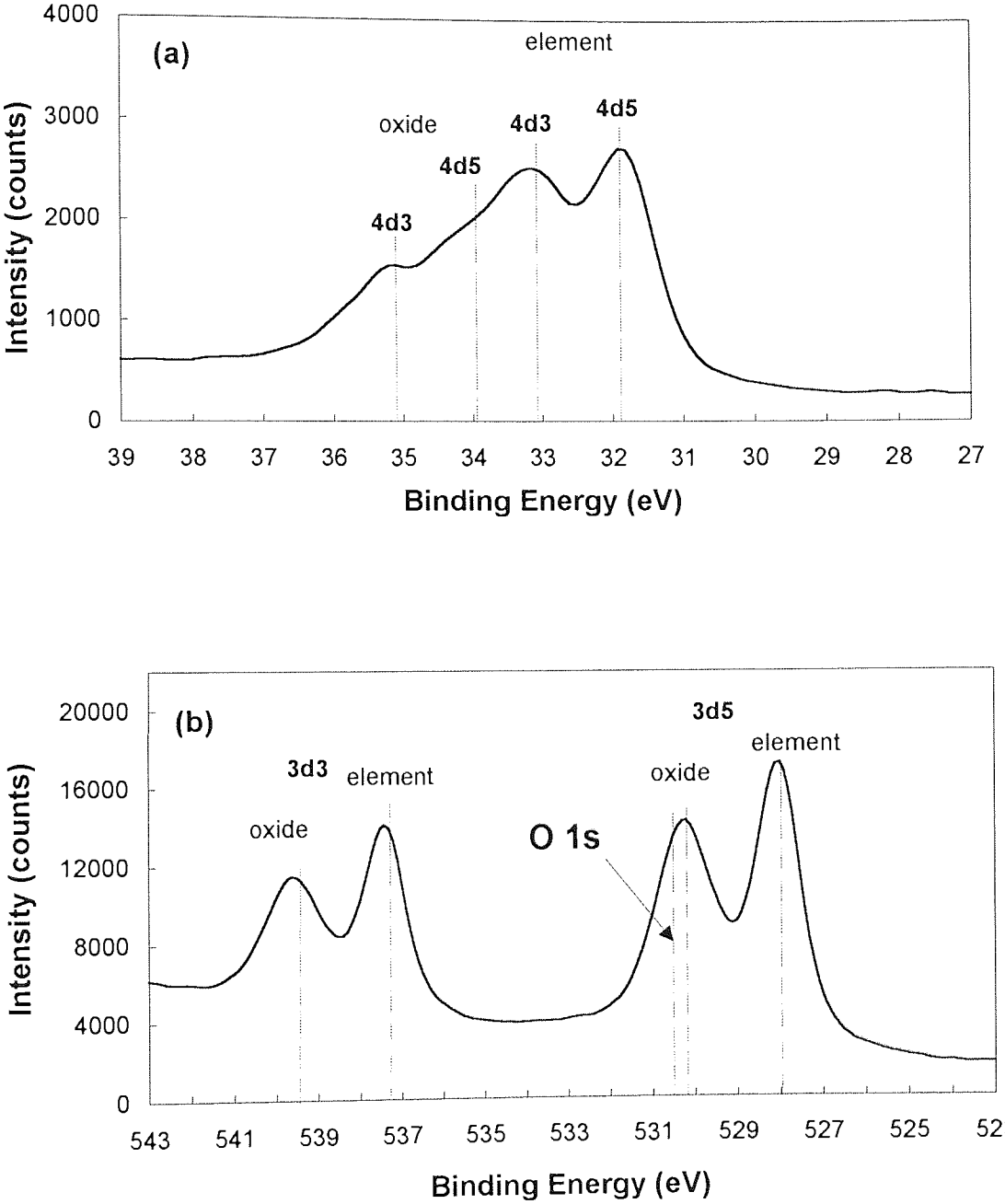

Figure 4.3 XPS spectra from the oxidised Sb surfaces: (a) Sb 4d; (b) Sb 3d

the pure In sample [Barr *et al*, 1979].

The results of the quantitative analysis of these core level spectra are listed in Table 4.2. The main peaks (lower BE) in the table (except P) appear very narrow in FWHM, this shows the success of the sample preparation and the reliability of the XPS calibration. The energy windows for each peak are given as references for quantitative analysis, but these values sometimes needs to be adjusted, specially when more than one chemical state exist. Using these windows, the peak area for each core level signal was calculated and used with the sensitivity factors for quantification.

Table 4.2 XPS analysis of reference samples

Sample	Peak	Peak position	FWHM	Window	Peak area
Al	2p	72.5	1.2	75-70	1.48
Si	2p	98.8/99.4	1.21/1.38	102-96	3.72
P*	2p	-	-	-	4.2
Ga	3d	18.2	1.35	24-16	4.2
	2p3	1116.8	1.48	1123-1113	87.4
Ge	3d	29.1	1.41	32-26	6.71
As	3d	41.6/42.2	1.11/1.23	45-39	5.44
	2p3	1323.4	1.81	1328-1319	57.3
Se	3d	55.6/56.4	0.98/0.94	59-53	5.74
Cd	4d	10.4/11.3	1.11/1.46	15-7	5.16
In	4d	16.8/17.7	1.04/1.17	21-15	8.95
	3d5	443.9	1.16	448-441	49.6
Sb	4d	32.1/33.3	1.01/1.28	37-29	10.8
	3d5	528.2	1.20	533-524	55.1

The sensitivity for P in this spectrometer was measured indirectly from XPS analysis of AlP powder sample and pure Al sample. If the compound was assumed to be still stoichiometric after air exposure, that is, P/Al =1, the peak-area of P may be calculated from the XPS analysis for pure Al using Equation 2.8. The matrix factor of AlP was taken into account in the calculation, which is about 0.734.

4.2.3. ISS analysis

The He ISS spectra from pure Si, Ga, Ge and In surfaces are presented in Figure

4.4. The Ne ISS spectra from Ga, As, Se, Cd, In and Sb surfaces are shown in Figure 4.5. With the exception of the Si sample, all He ISS spectra indicate very clean surfaces of the reference samples with almost no C (the scattering peak should be at KE of about 330eV) and O (KE at about 434eV), or other species found at the surfaces.

For the Si surface, a significant oxygen peak was always found at KE of 432.0 eV although the surface was cleaned for a very long period (over 3 hours) in UHV of base pressure less than 5×10^{-6} Pa. This may be due to the very strong affinity of Si to O atoms existing as residual gas molecules in the analysis chamber. This makes direct calibration difficult. A shoulder at higher energy side of the Si scattering peak may be due to contributions from ^{29}Si (4.7%) and ^{30}Si(3.1%) isotopes.

Broadening of ISS spectra for the lighter elements, such as He spectrum for Si in Figure 4.4, Ne spectra for Ga and As in Figure 4.5, were observed, and can probably be understood from the classical scattering model. From Equation 2.29, it may be seen that with a fixed energy resolution (CRR mode), the mass resolution will increase as the mass of ion is close to that of target atom.

For the pure Ga sample, because of weaker bonding between Ga-Ga atoms (about 1.43eV) and the larger momentum transfer from energetic Ne ions to Ga atoms, Ne ion impact may induce a larger fraction of target Ga atoms with high kinetic energy being sputtered, resulting in a wider range of energy distribution of Ga recoils existing in the Ne ISS spectrum. This, however, is not the case for He ISS spectrum due to much smaller momentum transfer from He ions to Ga atoms. Although a certain amount of oxygen was found in XPS analysis of sputter-cleaned Ga surface, it was hardly seen in the corresponding He ISS spectrum, this implies that most of oxygen exists in the deeper regions, driven by recoil implantation.

The peak shapes generally depend on the abundance of isotopes of target atoms and also those of incident ions. The effect of isotopes of incident ions could be seen clearly in Ne ISS spectrum from As surface. Since elemental As has no isotopes in nature, the shoulder peak at KE of about 400eV is clearly due to ^{22}Ne (9.2% in nature) ion scattering. This effect could also be seen in the Ne ISS spectrum from Ga by comparison with the corresponding He ISS spectrum. In some Ne ISS spectra, the shoulder peaks on the higher energy side always appeared, these may come from the isotope effects, but are more likely due to the occurrence of multiple scattering of a small fraction of the ions (see Chapter 2).

The results of the analysis of these spectra are given in Table 4.3. The measured peak positions, compared with theoretical calculation, are listed in the table. It may be seen that the experimental values are generally 1~2% less than the calculated ones using

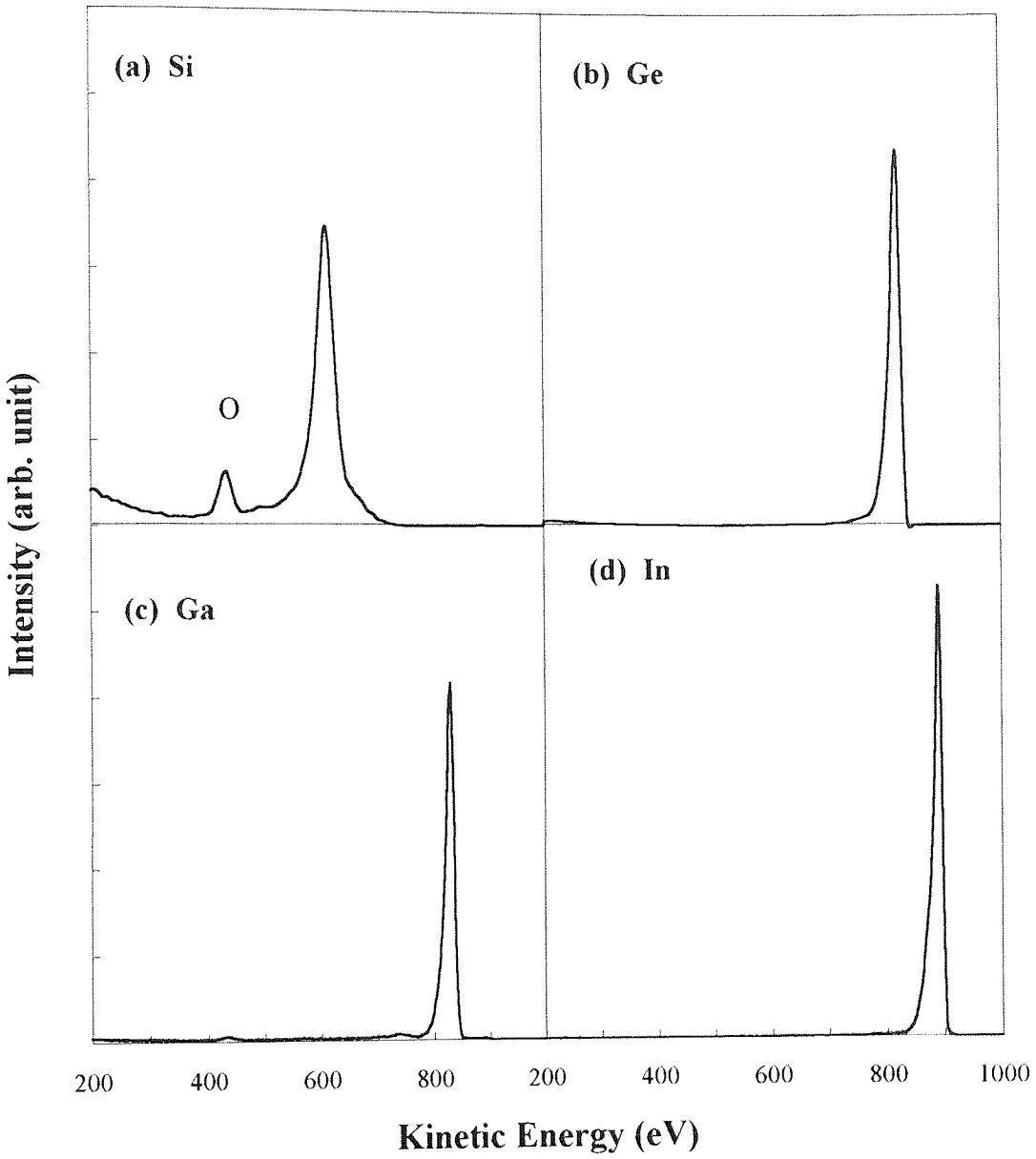

Figure 4.4 1keV He ISS spectra taken from pure Si, Ge, Ga and In surfaces

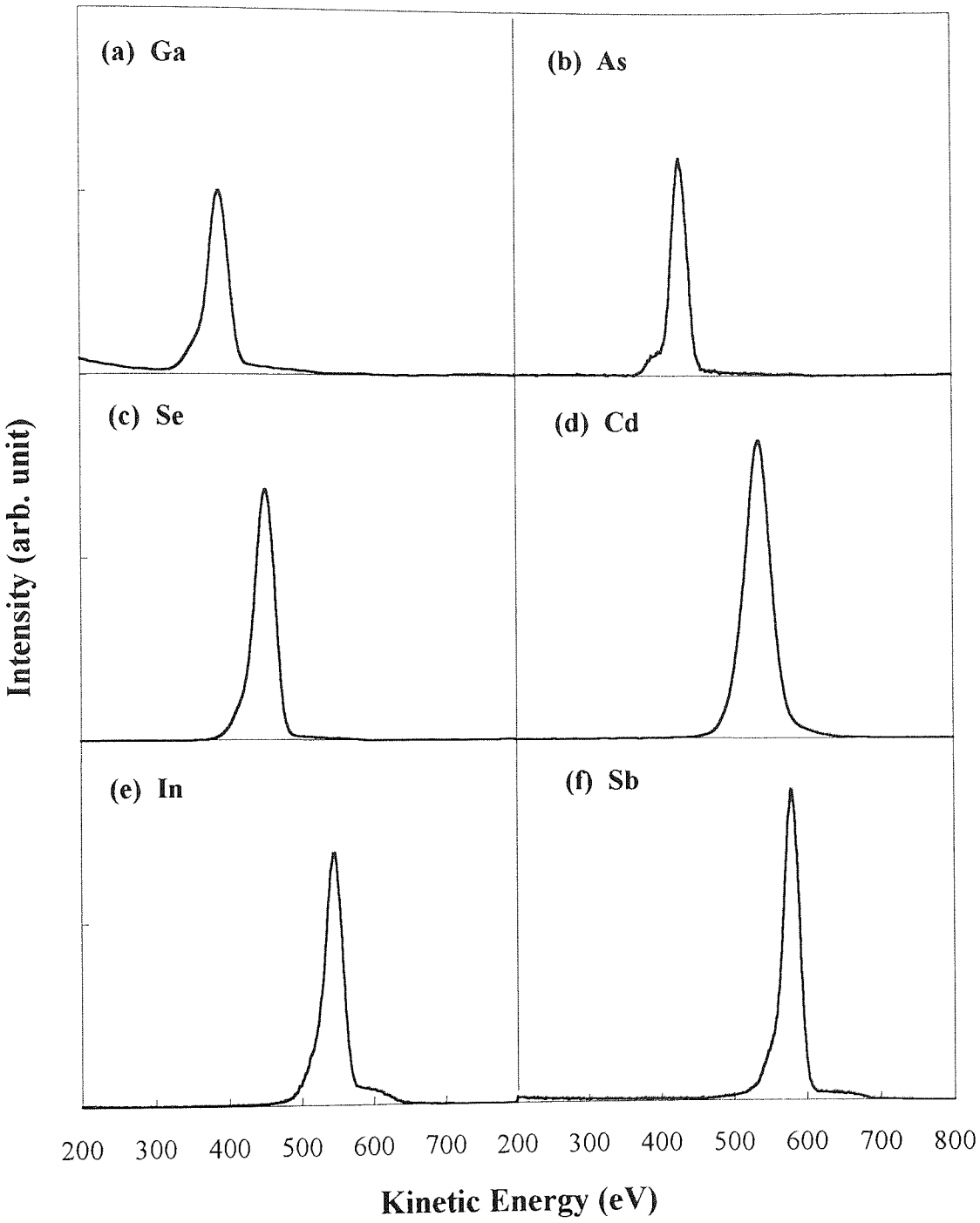

Figure 4.5 1keV Ne ISS spectra from pure Ga, As, Se, Cd, In and Sb surfaces

Equation 2.23, indicating very good agreements between the experiments and the classical scattering theory. This confirmed that for 1keV He and Ne ions, elastic collisions between the ions and the atoms in solid surfaces are predominant. It may be noticed that the measured energy of Ne ions scattered on an As surface is slightly higher than the predicted value, this was partly because of the difficulties in sample mounting, and partly due to the poorer electric conductivity of arsenic lump sample, resulting in a small charging field built up at the surface during Ar ion sputter cleaning.

Table 4.3 ISS analysis of reference samples

Sample	primary ions	Peak position(eV)		Window	Peak area
		measured	calculated	(eV)	(kCeV/sec)**
Si***	He	612 (97.8)	626	480-700	45.8
P***	He	-	650	-	19.6
Ga	He	827 (99.5)	831	765-875	168.8
	Ne	374 (98.2)	381	320-480	73.0
Ge	He	829 (99.4)	834	765-846	42.5
As	Ne	414 (100.1)	410	360-560	70.2
Se	Ne	428 (99.5)	430	350-600	102.4
Cd	Ne	537 (96.8)	556	450-650	123.7
In	He	891 (99.8)	893	815-915	201.6
	Ne	545 (97.0)	562	450-460	201.7
Sb	Ne	580 (99.5)	583	510-620	218.0

* figures in parentheses are the percentage of the measured values to the calculated ones.
**peak-area intensity is given in unit of kilo counts•electron volt per second (kCeV/sec)
*** calculated value (see text).

The table also shows two important features of the classical scattering model, that is, the lighter the ions and the heavier the target atoms, the less the inelastic energy loss. The intensities of He and Ne ions scattering at the surfaces generally increase with the mass of the target atoms because of the larger scattering cross sections, but the quantitative calculations are rather difficult, strongly depending not only on ion scattering cross section, ion survival probability and areal density of surfaces, but also on the experimental environment and sample conditions.

Since the information on He ions scattering from oxygen atoms is not available,

direct measurement of the intensity of He^+ scattering at a pure Si surface is impossible. Davidson *et al.* [1991] proposed a simple model to estimate the relative sensitivity of oxygen which is adsorbed on silver surface atoms. In this model, the total areal atom density is assumed not to be changed with O coverage, so the elemental sensitivity factor of oxygen to that of silver can be immediately derived from Equation. 2.25:

$$\frac{S_O}{S_{Ag}} = \frac{I_{O1} - I_{O2}}{I_{Ag1} - I_{Ag2}} \tag{4.1}$$

here S_i (i = O or Ag) represents the sensitivity factor for element i, which includes scattering cross section, ion survival probability, geometrical factors, *etc.*. I_{ij} (j=1, 2) is the intensities of scattering in the jth measurement.

In the case of Si oxide, the above assumption will be not valid due to significant O shielding effects. These effects have been studied systematically by Leerdam and Brongersma [1991]. To consider the shielding effects, the size of Si cation and O anion should be included in Equation 4.1, so Equation 4.1 can be modified into:

$$\frac{S_O}{S_{Si}} = \frac{I_{O1} - I_{O2}}{I_{Si1} - I_{Si2}} \cdot \frac{r_O^2}{r_{Si}^2} \tag{4.2}$$

where the (ionic) radius of O anion and Si cation, r_O and r_{Si}, are equal to 1.32Å and 0.42Å [Weast *et al.*, 1992], respectively. LEISS measurements under the exact same experimental conditions were carried out at two different areas, the peak area of O and Si scatter peaks are:

Peak area		Area 1	Area 2
Peak Area	O	3.87	3.32
(kCeV/Sec.)	Si	38.1	42.9

Based on the above experimental results, the S_O/S_{Si} ratio calculated from Equation 4.2 is 1.13. Compared to Leerdam and Brongersma's experiments [1991] of 1keV He^+ scattering at SiO_2 surface, this estimation is generally reliable. The peak-area intensity of He^+ scattering from pure a Si surface was estimated about 45.8kCeV/sec. The estimated O composition at these two local areas were 17% and 6.3%, respectively.

Since an ideal pure phosphorus sample was not available for LEISS calibration, the intensity of He^+ scattered at P atoms from pure P surface was calculated from Equation 2.25 and the data from the pure In surface. According to Equation 2.25, the intensity ratio of P to In under the same experimental conditions can be expressed as:

$$\frac{I_P}{I_{In}} = \frac{\sigma_P}{\sigma_{In}} \cdot \frac{P_P^+}{P_{In}^+} \cdot \frac{T_P}{T_{In}} \cdot \frac{N_P}{N_{In}} \tag{4.3}$$

here the difference of the shadowing effects on both sample surfaces was ignored.

For the scattering angle of 129°, the crossections for 1keV He^+ ions scattering at In and P atoms calculated from Equations 1.4-1.6 are 96.3×10^{-20} (cm^2) and 30.3×10^{-20} (cm^2), respectively [Giles, 1995]. In CRR mode (see Section 3.4.5), the transmission factor T of VGS EACALAB spectrometer is proportional to the kinetic energy of the detected particles [Seah, 1990]. The kinetic energies of 1keV He^+ scattered at In and P atoms are 650 and 893eV respectively (see Table 4.3). The ratio of ion survival probability can be derived from Equation 2.28:

$$P_P^+ = (P_{In}^+)^{\sqrt{\frac{KE_{In}}{KE_P}}} \qquad (KE_{In}=893;\ KE_P=650\ \text{eV}) \tag{4.4}$$

For noble gas ions scattering from the solid surfaces, the ion survival probability is normally less than 5% [Niehus, 1992]. Assuming P^+_{In}=5%; P^+_p calculated from Equation 4.4 is 0.027. Bringing all these data into Equation 4.3, the estimated intensity for He^+ scattering at P sample surface was 19.6kCeV/sec.

4.3. Experimental investigation of ARXPS and KRXPS techniques

Any "as received" sample will contain contamination overlayers on their surfaces due to native oxidation and/or carbonaceous adsorption in air. Removing these contaminants by, for example, chemical wet etching, sputter cleaning, *etc.*, may cause substantial chemical changes to the sample surface (see next section). In these cases, the nondestructive analytical techniques, that is, ARXPS or KRXPS, become very important vehicle to obtain structural and chemical information on these surfaces without any modification. Although the angle and energy dependence of the sampling depth of XPS are well understood, it is still necessary to investigate these effects experimentally to testify efficiencies and to gain the experience in use of these techniques in a specific system.

4.3.1. ARXPS

The angular effect in XPS was systematically investigated by studying the surface structure of contamination layers on the surface of polycrystal copper. XPS analysis showed that the contaminant layer is mainly composed of carbon with a little oxygen and the oxidised copper. If C 1s and Cu $2p_{3/2}$ are chosen as the signals from the overlayer and the substrate, respectively, according to Equation 2.20 and 2.21, ratios of Cu to C intensities normalised to the ratio at 0° TOA should be in the form of :

$$\frac{I_c^t(\theta)/I_{Cu}^t(\theta)}{I_c^t(0°)/I_{Cu}^t(0°)} = \frac{\dfrac{\exp(-t/\lambda_{Cu}\cos\theta)}{1-\exp(-t/\lambda_c\cos\theta)}}{\dfrac{\exp(-t/\lambda_{Cu})}{1-\exp(-t/\lambda_c)}} \cong f(\frac{t}{\lambda_{Cu}}, \cos\theta) \qquad (4.5)$$

where $\lambda_C \approx 1.73\lambda_{Cu}$, according to Equation 2.5b.

Figure 4.6 shows the angular variation of the ratios against electron take-off angle. Very good agreement was achieved between experimental results (star) and theoretical calculation(solid line) at t/λ_{Cu}=2.9. Since $\lambda_{Cu}\approx$16Å calculated from Equation 2.5b (*KE*(Cu 2p3)=323eV) , the thickness of the contaminant layer was estimated, 47Å. It can also be seen in the Figure that the angular distribution of the ratios is highly symmetric at 0° TOA, this feature can be deduced from Equation 4.1. This good agreement gives evidence that the angular effects described by Equation 2.20 and 2.21 are correct. It may be expected that for a compound surface covered by an overlayer the elemental distributions in the surface will be revealed by the angular resolved analysis.

4.3.2. KRXPS

The kinetic energy resolved XPS technique has been employed in studying the contaminant overlayer on a Ge(100) single crystal surface after long exposure to the atmosphere and after 4keV Ar ion sputter etching for up to 60 minutes.

The XPS analysis, in terms of C 1s, O 1s and Ge 3d lines, indicate that the contamination overlayer is generally composed of adventitious carbon, hydrocarbon, CO, water and oxidised Ge. The atomic concentrations of C, O and Ge after 0, 2, 8 and 60 minutes sputtering are given in Table 4.4. The corresponding XPS spectra of Ge $2p_{3/2}$ and 3d core level electrons after 0, 2 and 8 minute sputtering are shown in Figure 4.7. The peaks at 1217eV in the Ge $2p_{3/2}$ and at 29.1eV in the Ge 3d spectra represent elemental Ge originating from pure Ge substrate; The peaks at 1219-1220eV in the Ge $2p_{3/2}$ and 31.0-32.5eV represent Ge oxidation states in the overlayer.

Table 4.4 Atomic concentrations of carbon, oxygen and germanium with XPS

Sputter time (minutes)	Carbon (%)	Oxygen (%)	Germanium (%)	
			Oxide	Elemental
0	51.2	25.7	8.6	14.6
2	30.0	19.6	16.1	34.3
8	13.8	12.5	2.2	71.5
60	0.0	0.0	0.0	100.0

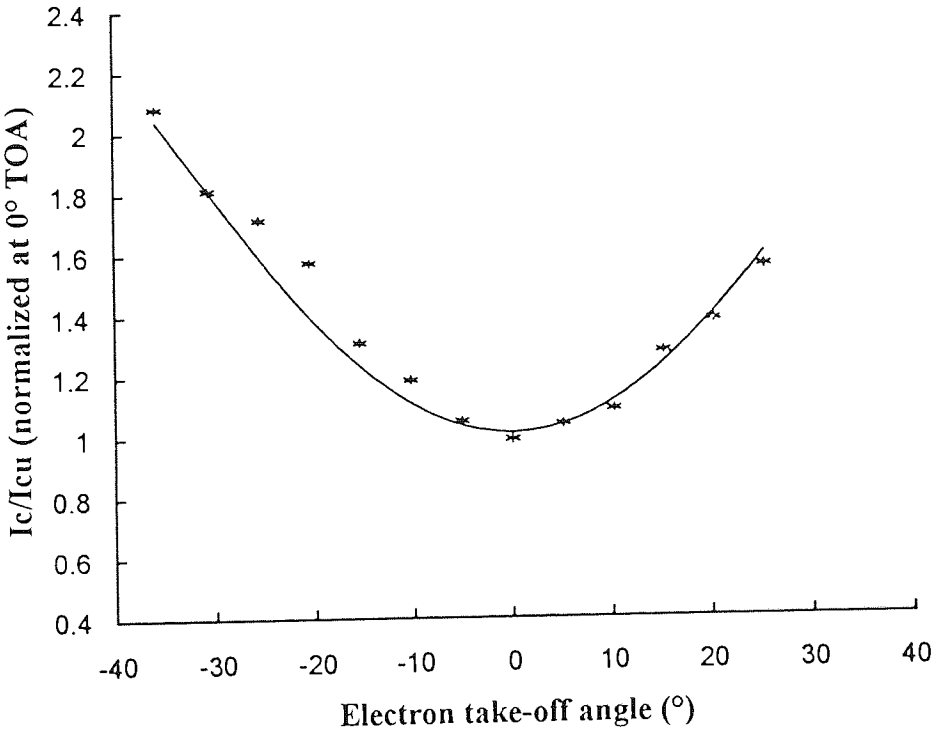

Figure 4.6 Variation of intensity ratios of C 1s to Cu $2p_{3/2}$ with TOAs

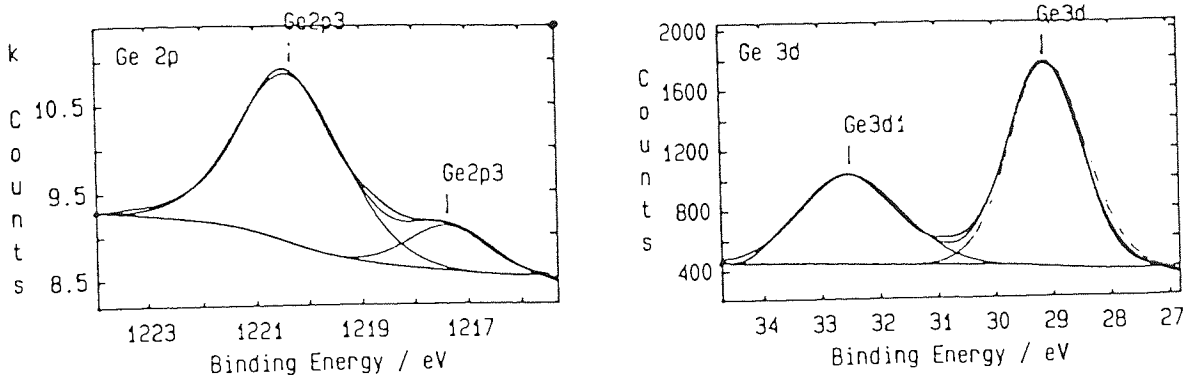

(a) t = 47.7 Å

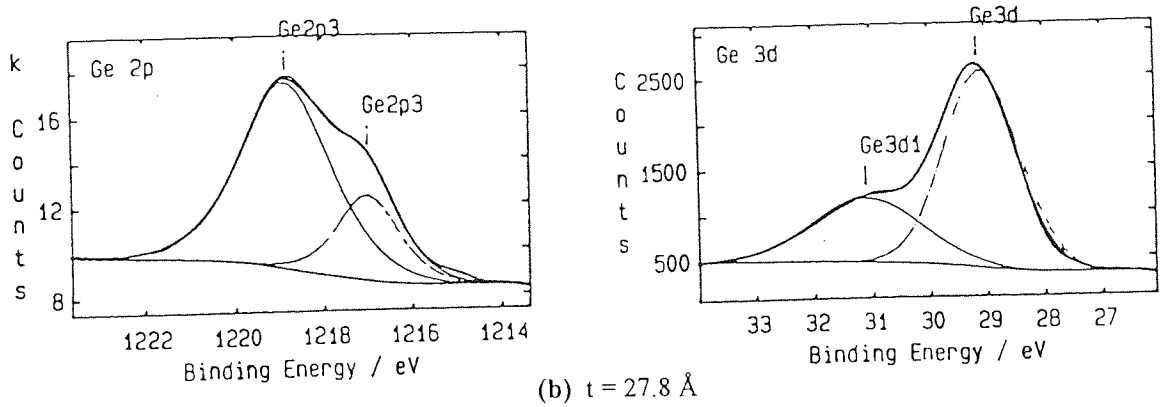

(b) t = 27.8 Å

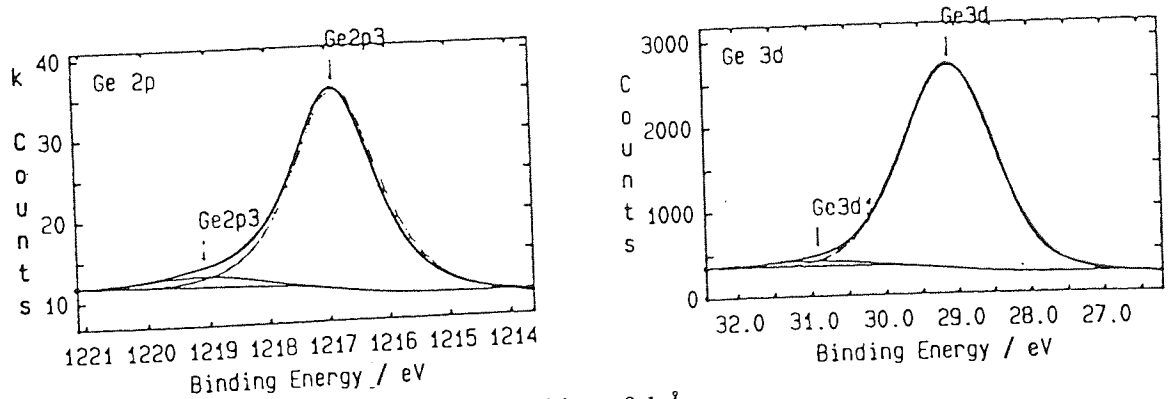

(c) t = 2.1 Å

Figure 4.7 Variations in Ge $2p_{3/2}$ and 3d peak shape from pure Ge surface with the different overlayer thickness

Table 4.5 Ge^+/Ge^0 ratios calculated from Ge $2p_{3/2}$ and 3d spectra

sputter time (min.)	0	2	8	60
Ge $2p_{3/2}$	5.7	3.2	0.064	0.0
Ge 3d	0.59	0.47	0.031	0.0

It is very interesting that the Ge $2p_{3/2}$ and Ge 3d spectra give totally different results. Ge $2p_{3/2}$ peak always shows a larger fraction of the oxidised Ge (Ge^+) than Ge 3d peak. The atomic ratios of the oxidised Ge to the elemental Ge resolved by peak fitting are give in Table 4.5.

The differences in the results is obviously due to the different sampling depth using Ge $2p_{3/2}$ and Ge 3d core level electrons. Since Ge $2p_{3/2}$ core electrons generated by Al K_α have kinetic energy of 270eV and Ge 3d electrons have kinetic energy of 1458eV, the sample depth using Ge $2p_{3/2}$ signal is only about 40% of that using Ge 3d, which can be estimated directly from Equation 2.5. In other words, Ge $2p_{3/2}$ signal is more sensitive to the surface than Ge 3d signal. Therefore, when elements are inhomogeneously distributed in the surface, (a particular example is a surface covered by an overlayer), XPS analysis using the photoelectrons on different core levels will give different results (such as, the top and middle spectra in the figure), but the difference will diminish when the elemental distribution approaches homogeneity (see the bottom spectra in the figure).

Using the energy dependence, the thickness of the overlayer on the surface may be estimated from Equation 2.21. For the contaminant overlayers on a Ge(100) surface, the estimated thickness of the overlayer after different sputter time are listed in Table 4.6. It may be seen that KRXPS is able to be used for investigating an overlayer or an inhomogeneous region with a thickness as thin as one monolayer !

Table 4.6 The estimated thickness of the overlayer after different sputter period

Sputter Time (min.)	0	2	8
Thickness (Å)	47.7	27.8	2.12

4.3.3. Concluding notes: A comparison between ARXPS and KRXPS

Compared to ARXPS, KRXPS has many practical advantages. First of all, it is independent of the geometrical arrangement of experiments. ARXPS using large area X-ray illumination will result in an inhomogenous angular response[Bussing *et al.*, 1988].

The sample surface should be positioned very close to the axis of tilt (this is not easily achieved in practice) to avoid a large movement of the detected area during sample rotation. Second, KRXPS relies much less on the sample conditions. A fundamental assumption in current models for ARXPS is that the sample surface should be atomically flat, rough surfaces average the angular effects [Fadley, 1976], and photoelectrons originating from a concave point on a surface may be shadowed or attenuated at low take-off angles by adjacent asperities. For crystal samples, ARXPS analysis will be influenced by crystallographic orientation. In KRXPS, this effect is reduced if relative signal intensities are considered. Third, KRXPS seems more applicable than ARXPS in measurement of very thin, say, one or two atomic monolayer films. In ARXPS, this may be achieved by using very high TOA where measurements are limited by electron refraction, reflection, and surface roughness [Fadley, 1976]. Fourth, KRXPS provides very high accuracy and reliability in measurements without the requirement for a high precision sample manipulator. This is essential in ARXPS to reduce experimental errors. The only drawback of KRXPS compared to ARXPS is that in current XPS devices a series of suitably spaced core level peaks are required to perform this technique, this may be overcome if variable-energy X-ray sources are available.

4.4. Effects of chemical cleaning on GaAs surface

To investigate the effects of chemical wet etching on semiconductor surfaces, a GaAs (100) single crystal surface cleaned by etching in diluted hydrochloric acid was analysed by means of ARXPS. The procedure used for cleaning is described in Section 3.5.1.2. A comparison of the Ga 3d and As 3d spectra from the GaAs surface taken at 0° and 80°, together with those taken from the "as received" GaAs surface, are shown in Figure 4.8. The sampling depths at the two TOAs are about 60 to 10Å estimated from Equation 2.5.

The binding energies and the widths of 3d core electron peaks of Ga and As taken from both the as received and the chemically etched GaAs(100) are given in Table 4.7 compared with the Ga and As reference samples. In both Ga 3d and As 3d spectra from the as received GaAs surface, the oxidation states of Ga and As are clearly distinguished (see Figure 4.8a). The binding energies of Ga 3d and As 3d peaks in GaAs corresponding to Ga_2O_3 and As_2O_3 components are shifted 1.3eV and 3.6eV respectively to higher binding energy. Referred to the Ga and As references, the BE shifts of the Ga and As 3d lines from the GaAs surface indicate that partial electron transfer from Ga to As atoms occurred during the formation of GaAs compound. This

may be predicted from the electronegativities of element Ga (ε_{Ga}=1.6eV) and element As (ε_{As}=2.0eV) defined by Pauling [1967].

Table 4.7 Binding energies and FWHM of Ga and As 3d peaks from the GaAs surfaces before and after chemical cleaning

		As received		Chem. cleaned	Element
		GaAs	Oxide	GaAs	
Ga	BE (eV)	19.1	20.4	19.0	18.2
	FWHM (eV)	1.38	1.60	1.58	1.35
As	BE (eV)	41.1	44.7	41.2	41.8
	FWHM (eV)	1.56	1.99	1.77	1.59

Quantitative analyses of both the as-received and the chemically cleaned GaAs surfaces at TOAs of 0° and 80° are listed in Table 4.8. The As/Ga ratios in the table were calculated from Equation 2.8 using the Ga and As reference standards given Table 4.2. From Figure 4.8 and Table 4.8, it may be seen that the concentration of Ga oxide is slightly greater than that of As oxide resulting in Ga enrichment in the air exposed GaAs surface. The formation of such an oxide overlayer may be due to the greater chemical driving force between O (ε_O=3.5eV) and Ga atoms than that between O and As, and also because As_2O_3 is volatile, resulting in the loss of the oxide in nature [Spicer *et al.*, 1979].

Table 4.8 As/Ga ratios in GaAs surface before and after the chemical etching

TOA (°)	As received			Chemical etched
	Ga^+/Ga^0	As^+/Ga^0	As^0/Ga^0	As^0/Ga^0
0	0.33	0.24	1.02	1.04
80	1.38	1.06	0.83	2.04

* Superscript 0 and + represent As or Ga in GaAs and their oxide state, respectively.

The spectra in Figure 4.8 show that chemical cleaning effectively removed the oxide overlayer on the GaAs(100) surfaces. But this pre-treatment caused certain modifications to the GaAs surfaces, resulting in significant Ga depletion (see Figure 4.8) and the broadening in both Ga and As 3d peaks.

The broadening may be understood by the fact that the etching process increased the defects in the GaAs surface and caused more Ga-Ga and As-As bond formation. The reasons for the Ga depletion are not very clear. It is thought that this is due to removal of the Ga-rich oxide overlayer [Brown, *et al*, 1986]. This explanation is not quite right. Since the etching rate of an acidic etchant is generally very high (0.1-1μm/min.), the thin As rich layers beneath the oxide overlayer formed by preferential oxidation of Ga would

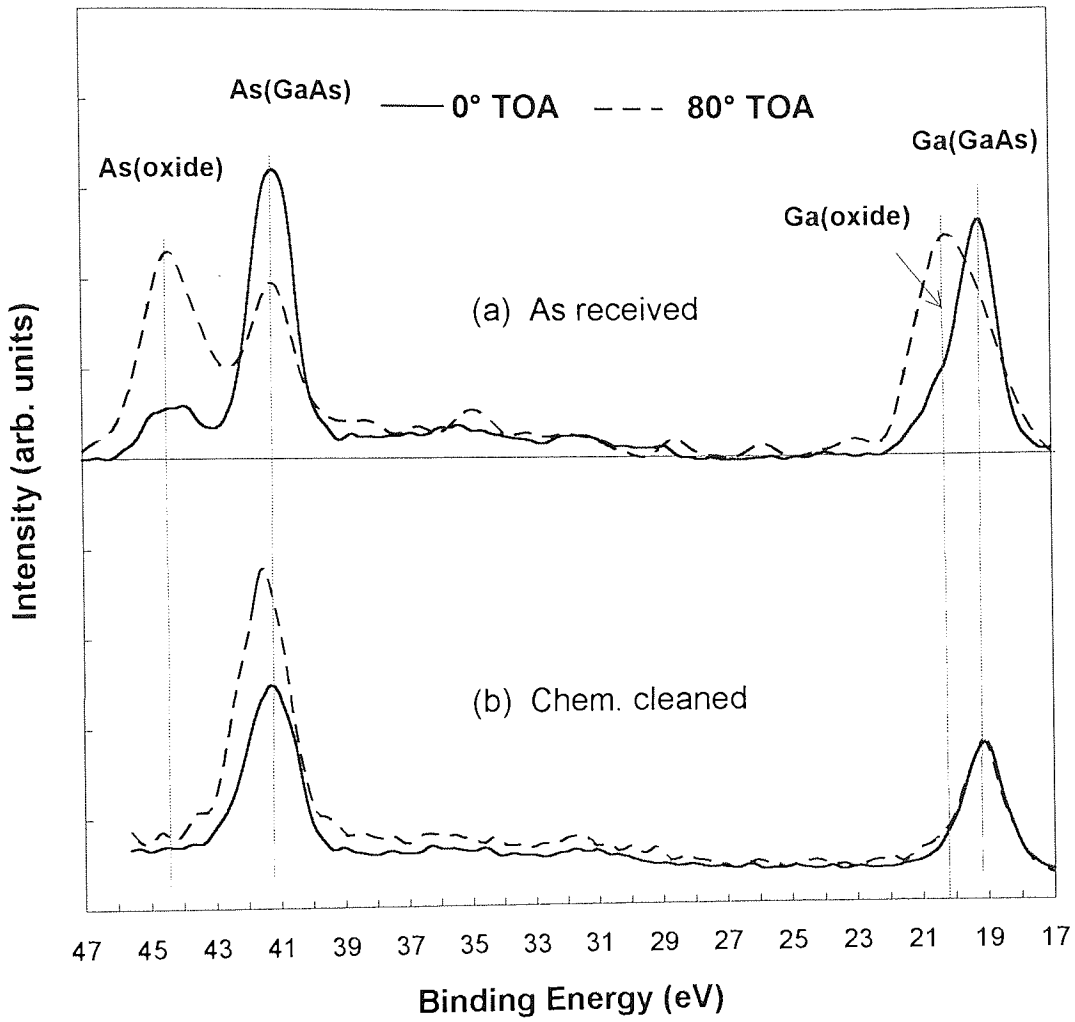

Figure 4.8 Acomparison of Ga and As 3d spectra taken from "as received" and "chemical cleaned" GaAs surfaces

be completely removed during the wet etching process. This Ga depletion may be more reasonably explained by the greater reactivity of Ga towards chlorine anions (ε_{Cl}=3.0eV) in the dilute acid, resulting in more Ga chloride formation, which is soluble in water and consequently washed away by rinsing.

From this study, it is clear that this chemical cleaning process will alter the surface conditions of GaAs single crystals and is not suitable in this project for pre-treatment. In fact, since the difference in electronegativity of the elements in a compound system, it may be impossible to find a chemical wet etching procedure for cleaning the surface without any chemical damage to the surface.

4.5. XPS and LEISS analyses of the bombarded compound semiconductors

The results of XPS and LEISS measurements from the compound semiconductor and GeSi surfaces before and after 3keV Ar^+ bombardment are described in this section.

Since the chemical cleaning process described in the above section is impossible to use for obtaining ideal surfaces for this project, the surfaces structures in the semiconductor surfaces prior to ion bombardment were analysed using the nondestructive method, ARXPS, to get information on the compositional distributions in the unbombarded surfaces and to show the ion bombardment effects clearly. After initial ARXPS analysis, the surfaces were bombarded by 1μA, 3keV argon ion beam, the surface composition was monitored with XPS at TOA of 0° for up to 50 minutes. After the ion bombardment, the surfaces were re-examined by ARXPS and KRXPS in order to show the changes of composition in the bombarded surfaces.

In XPS analysis, smoothing, energy calibration using C 1s line at binding energy of 284.6eV and linear background subtraction were applied in processing each core electron peak. Peak fitting was also used for distinguishing different chemical states. quantification was carried out using Equation 2.8. In the calculation, the intensities taken from the surfaces of the reference standards listed in Table 4.2 were used. The matrix effects were also considered in the quantification. For the eight binary systems, the matrix factors calculated from Equation 2.10 are listed in Table 4.9.

Table 4.9 Matrix factors for binary semiconductor compounds

A-B	AlP	GeSi	GaP	GaAs	GaSb	InP	InAs	InSb	CdSe
F_{AB}	0.76	1.05	0.83	0.96	0.81	0.96	1.10	0.93	0.91

LEISS has also been employed in studying the ion bombarded compound semiconductor surfaces. For some materials, including, GeSi, GaP, and InP, a He^+ beam was employed, for the others with smaller differences in mass, such as, GaAs, GaSb, InAs, InSb and CdSe, a Ne^+ beam was used in order to separate the two scattering peaks. Although LEISS was extremely difficult to use in analysis of the surfaces prior to the ion bombardment, due to the existence of contaminants on these surfaces, attempts were still made to use it to measure the atomic concentration at the top layers. The main purpose of using this technique, however, is to measure the atomic concentration at the first atomic layer of the compound semiconductor surfaces after ion bombardment. With a combination of XPS and LEISS results, the mechanisms of ion bombardment effects in the semiconductor systems may become clearer.

In LEISS analysis, atomic ratios of the first one or two atomic layers were calculated from Equation 2.30 using the intensities measured from the surfaces of reference standards, the results of which are given in Table 4.3. In the calculation, the areal densities of the element i, n_i, are assumed to be proportional to $(d/M)^{2/3}$. Here, d and M represents the density and the atomic mass of the elements, respectively. The ratios of the areal densities of the elements in the compound semiconductors and GeSi alloy are given in Table 4.10.

Table 4.10 Ratios of the areal densities of the elements in A-B systems

A-B	GeSi	GaP	GaAs	GaSb	InP	InAs	InSb	CdSe
n_A/n_B	0.92	1.29	1.06	1.33	1.06	0.91	1.10	1.17

4.5.1. GeSi

XPS

The surface structure of the as received GeSi single crystal was examined by systematical ARXPS. The surface was initially covered with carbonasous contaminants over an oxide layer over the GeSi substrate. Si 2p and Ge 3d spectra taken at 0° and 80° TOA from the as received GeSi(100) are shown in Figure 4.9a. The sampling depths at these angles are about 60Å and 10Å, respectively. In the figure, the Ge 3d peaks at BE of 29.1eV and Si 2p peaks at BE of 99.1eV indicate Ge and Si atoms respectively in GeSi matrix. The Ge 3d peaks at BE about 32.4eV and Si 2p 102.8eV represent Ge in GeO_x ($x<2$) and Si in SiO_2, respectively. Neglecting contaminant films of hydrocarbon, adsorbed water vapour and other oxygenated species, the figure shows that the dominant oxide on the surface was SiO_2. The amount of Ge oxide is so small that it can be seen

only at very large TOAs. The oxide layer is due to preferential Si oxidation, similar to that reported by Zhang *et al.* [1991]. A more systematic analysis on the surface structure of the initial GeSi surface is shown in Figure 4.9b, in which the atomic ratios of Si^0/Ge^0, Si^+/Ge^0 and Ge^+/Ge^0 are plotted against the electron take-off angles. It can be seen that because of the preferential oxidation, Si depletion occurs beneath the oxide overlayer, indicated by the Si^0/Ge^0 ratio of 0.64 at 80° TOA. But this ratio increases to 0.91 at 0° TOA with sampling depth, indicating that the bulk material was stoichiometric prior to bombardment.

After the initial analysis, the GeSi(100) surface was bombarded by a 3keV Ar^+ beam for up to 50 minutes. Changes in Si/Ge, C/Ge and O/Ge ratios monitored with XPS at 0° TOA are shown in Figure 4.10a. The carbon signal disappeared after 2-3 minutes bombardment. The oxide layer was completely removed within about 6 minutes. Figure 4.10a confirms a layered structure in the as-received GeSi surface revealed by previous ARXPS analysis. It also shows that the surface was Si-rich due to the preferential oxidation of surface silicon atoms mentioned above and that Si depletion exists beneath the Si-enriched layer. The Si/Ge ratio decreased from 1.6 prior to sputtering to a minimum of 0.96 after about 5 minute. After this it increased until after 13-14 minutes the ratio reached a steady state value of about 1.23. The latter increase in Si/Ge ratio after removal of the oxide overlayer is obviously due to ion bombardment effects.

The results of ARXPS re-examination of the GeSi surface after 50 minute Ar^+ bombardment are given in Figure 4.10b. It may be seen that Si/Ge ratios fluctuate around the average value of 1.23, but at higher TOAs the ratio drops slightly to about 1.18, indicating a possible increase in Ge concentration in the outermost surface region.

LEISS

The LEISS analysis of the GeSi surface was carried out after about 1-2 minute Ar ion sputtering to remove the carbonaceous layer on the GeSi(100) single crystal surface. The LEISS spectrum is shown in Figure 4.11a. The peaks at KE of 421eV and 626eV are the He^+ scattering peaks from O and Si surface atoms, respectively. A small sodium peak at KE of 540eV may be seen in the spectrum, which was not found by XPS investigation. This illustrates the surface sensitivity of LEISS to the first one or two layers. No Ge peak appears in the spectrum. This, again, confirms the ARXPS results, that is, silicon oxide was predominant in the outer layers of the air-exposed GeSi surface.

The LEISS spectrum from the GeSi surface after 50 minute argon ion bombardment is given in Figure 4.11b. An oxygen peak also appears in this spectrum. The areal intensities of Ge, Si and O scattered peaks measured from the spectrum are

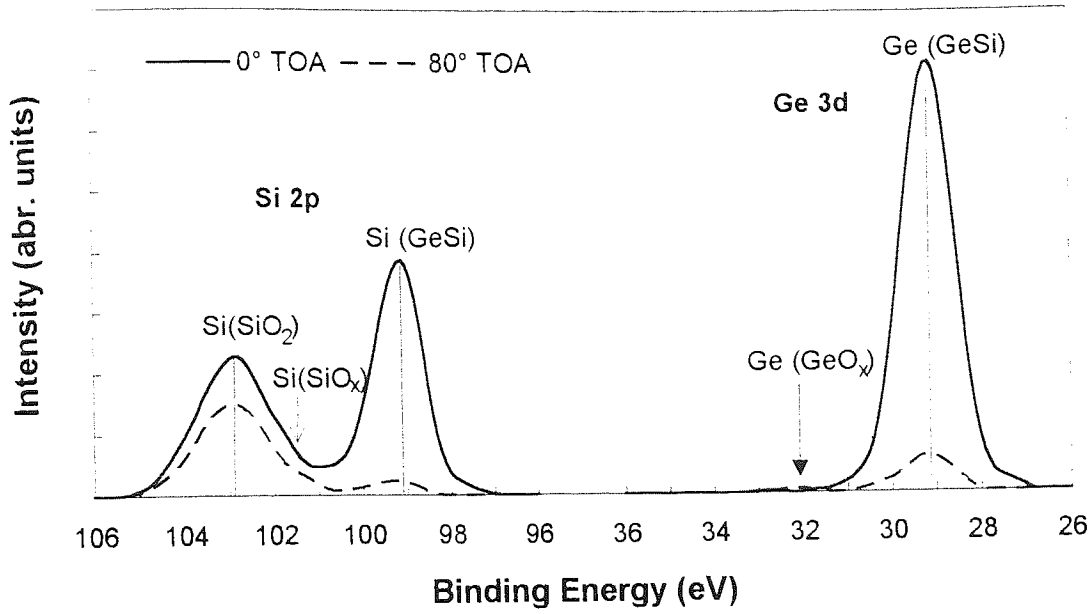

(a) Si 2p and Ge 3d spectra

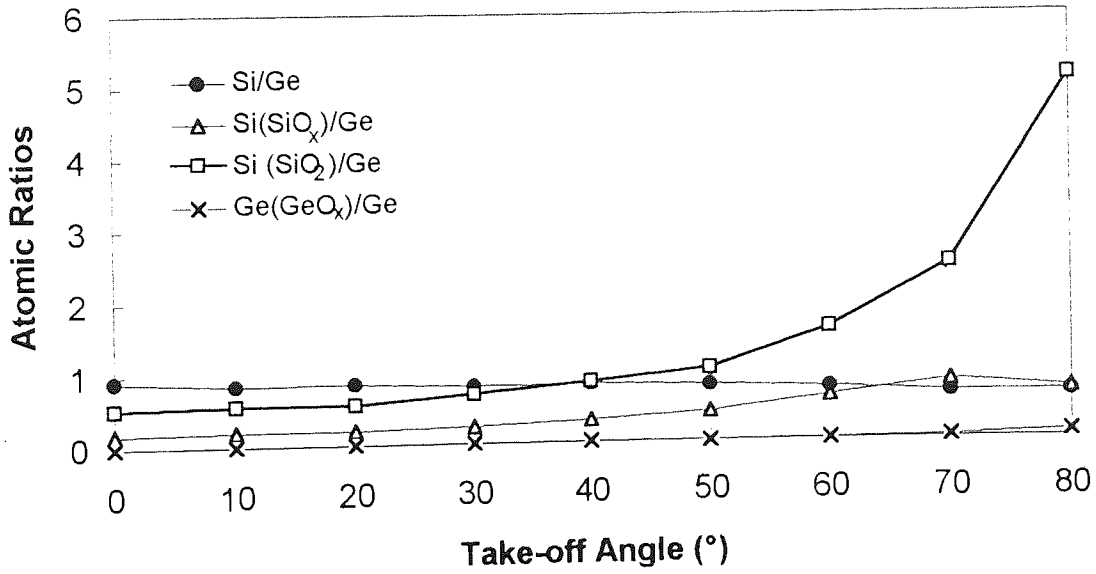

(b) Si/Ge, $Si(SiO_x)/Ge$, $Si(SiO_2)/Ge$ and $Ge(GeO_x)/Ge$ variations versus take-off angles

Figure 4.9 ARXPS analysis of as received GeSi(100) surface

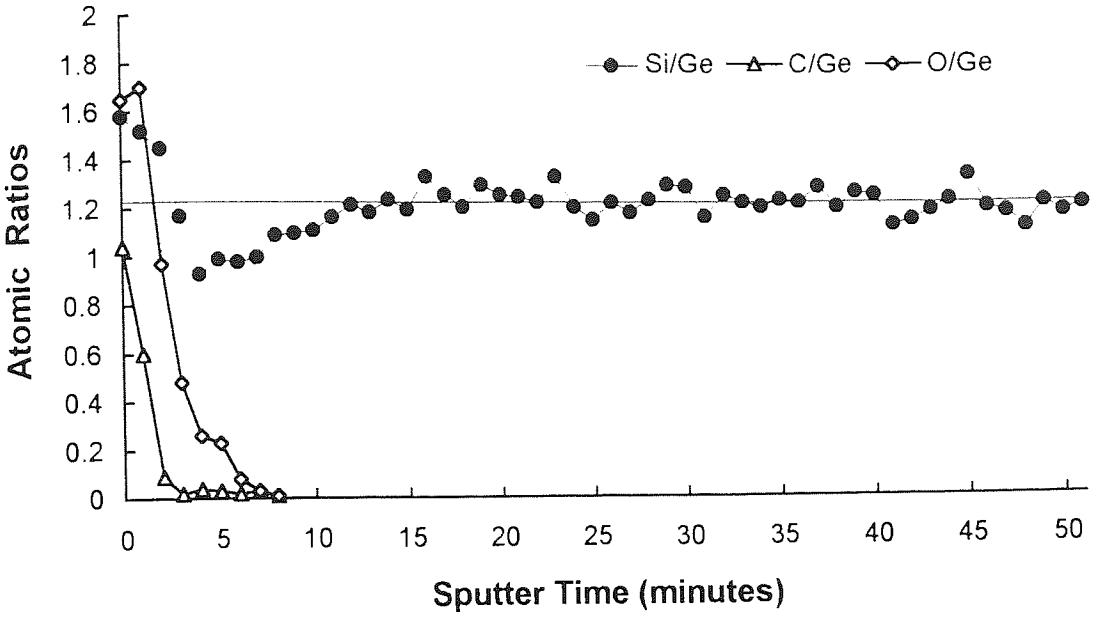

(a) Compositional changes in GeSi surface during Ar^+ beam bombardment

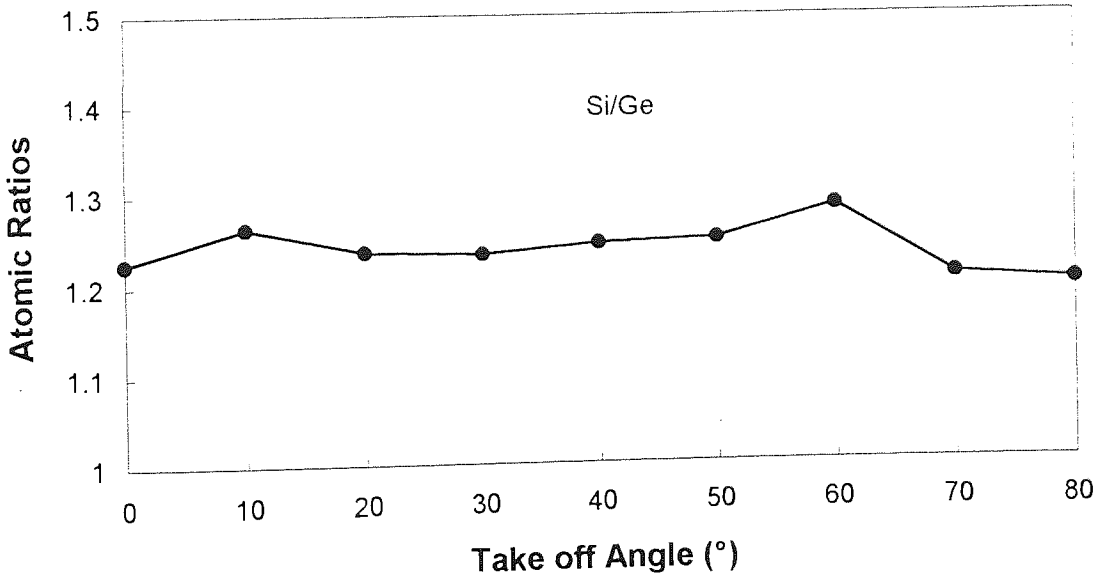

(b) ARXPS analysis of ion bombarded GeSi surfaces

Figure 4.10 Ion bombardment effects observed by XPS

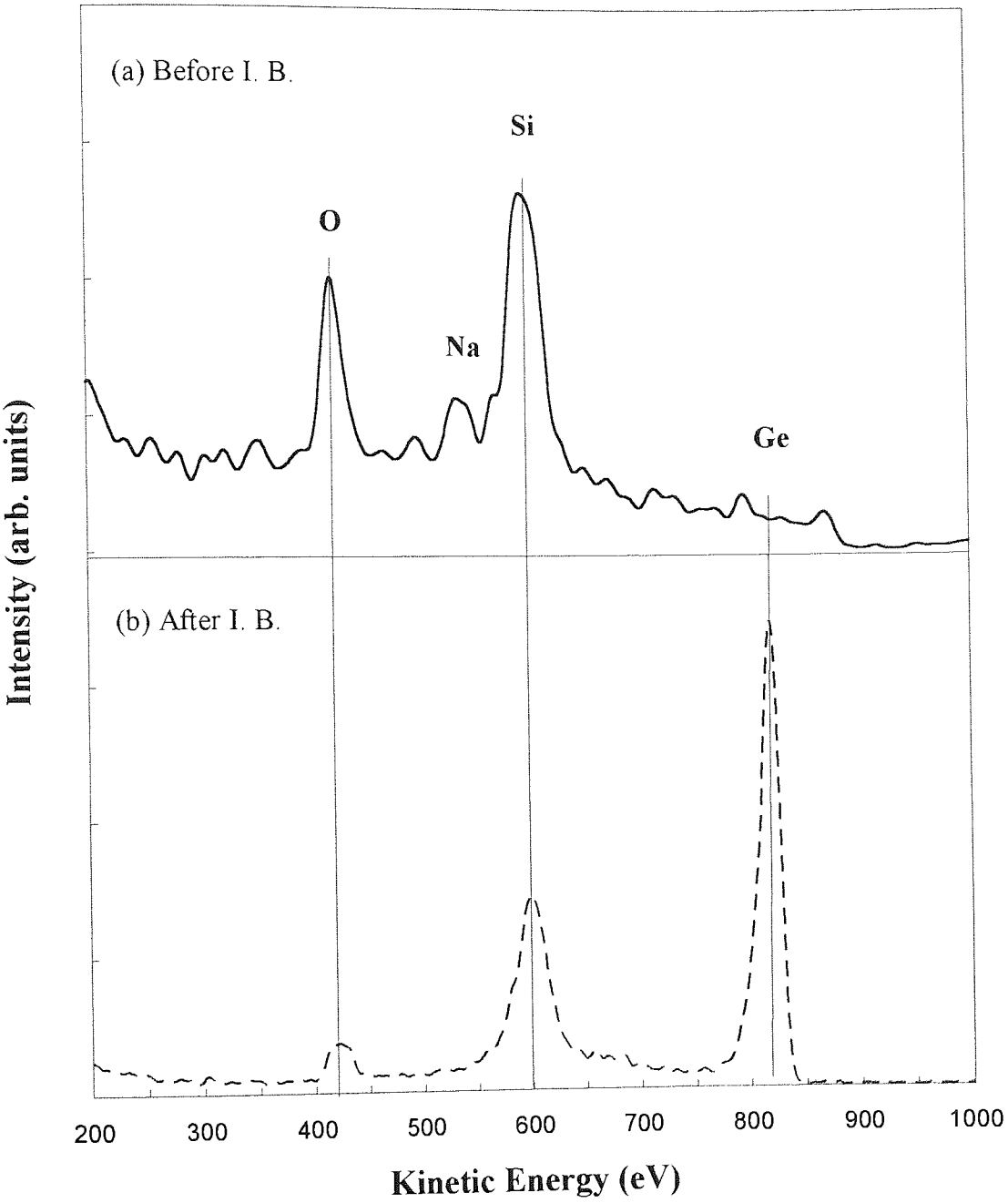

Figure 4.11 He ISS analysis of GeSi surfaces before and after ion bombardment

3.98, 2.65, 0.34kCeV/sec., respectively.

From the results of the analyses to the Si and Ge standard samples under the same experimental conditions, it is reasonable to assume that all the oxygen atoms on the surface are associated only with the surface Si atoms. Based on this assumption and the analysis in Section 4.2.3, the intensity of He^+ scattering from Si atoms would be equal to 2.95CkeV/Sec if no O adsorption occurs. Using the results listed in Table 4.3, the surface concentration may be estimated from Equation 2.30, this gives a Si/Ge ratio of 0.75 at the top layer of the bombarded GeSi surface. It is clear, therefore, that ion bombardment causes Ge enrichment in the outermost layer.

4.5.2. GaP

XPS

The initial XPS analysis showed an oxide overlayer existing on the top of the as-received GaP(111) surface. The oxide layer was covered by a carbonaceous overlayer as the same as that in GeSi. A small amount of Co was also found in the surface, which indicated by Co $2p_{3/2}$ peak at BE of 780.4eV. This element may come from the contamination from plastic thin film which protected the GaP original surface.

Ga 3d and P 2p spectra taken from the air exposed GaP surface at 0° and 80° TOA are given in Figure 4.12a. In each spectrum, two peaks were clearly distinguished. According to published results [Wagner, 1989], the P 2p peak at 128.7eV and that at 133.4eV in the P 2p spectrum correspond to P in GaP and in phosphate states, respectively. At TOA of 80°, a small peak emerges at BE of 135.0eV in P 2p spectrum, indicating that a thin layer of P_2O_5 may be formed at the top of the phosphate layer. A comprehensive theoretical description of such a native oxide layer has been given by Lucovsky and Bauer [1980]. They explained this structure using a Valence Shell Electron Pair Repulsion (VSEPR) model that at the top of the phosphide oxides a donor-acceptor pair bond, P=O, exists, which increases the stability of the oxides. This P=O bond makes the local order at the P-atoms identical to that of α-P_2O_5, which was observed in this XPS study. In the Ga 3d spectrum, the peak at 19.0eV represents Ga in GaP. Based on the analysis of P peaks, Ga at 20.4eV may be due to Ga in $GaPO_4$. This was further confirmed by the systematic ARXPS analysis. Figure 4.12b showed the change of each component with take-off angle. It may be seen that in the overlayer, P compositional distribution is the same as that of Ga. But at the higher TOA (80°), P in the overlayer was greater than Ga. This is probably one of reasons that P depleted at the interface between GaP substrate and the oxide layer. This was confirmed by the

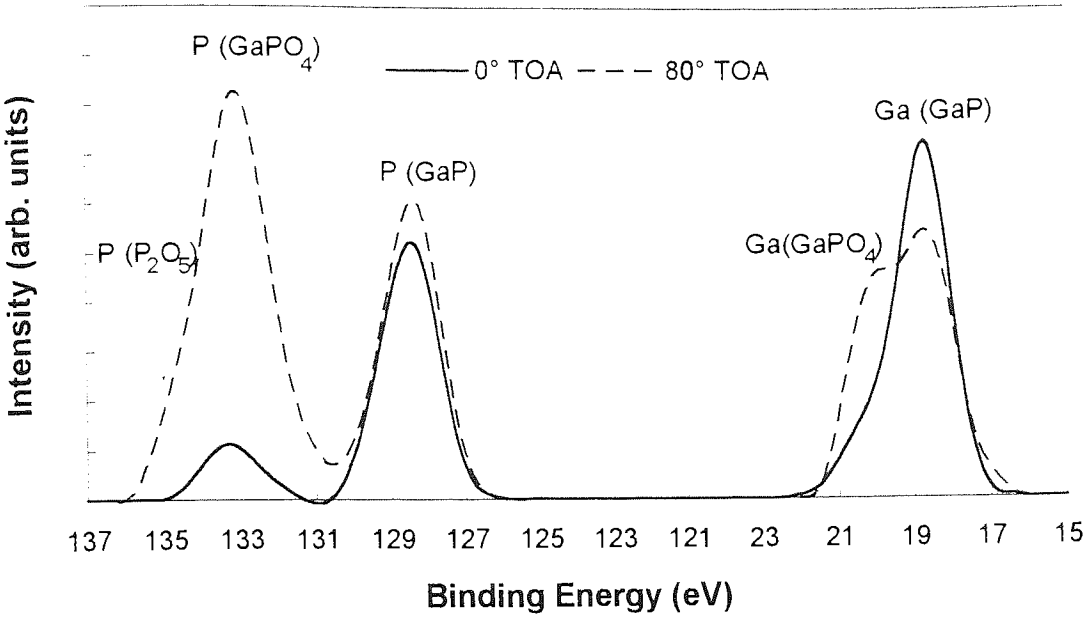

(a) P 2p and Ga 3d spectra

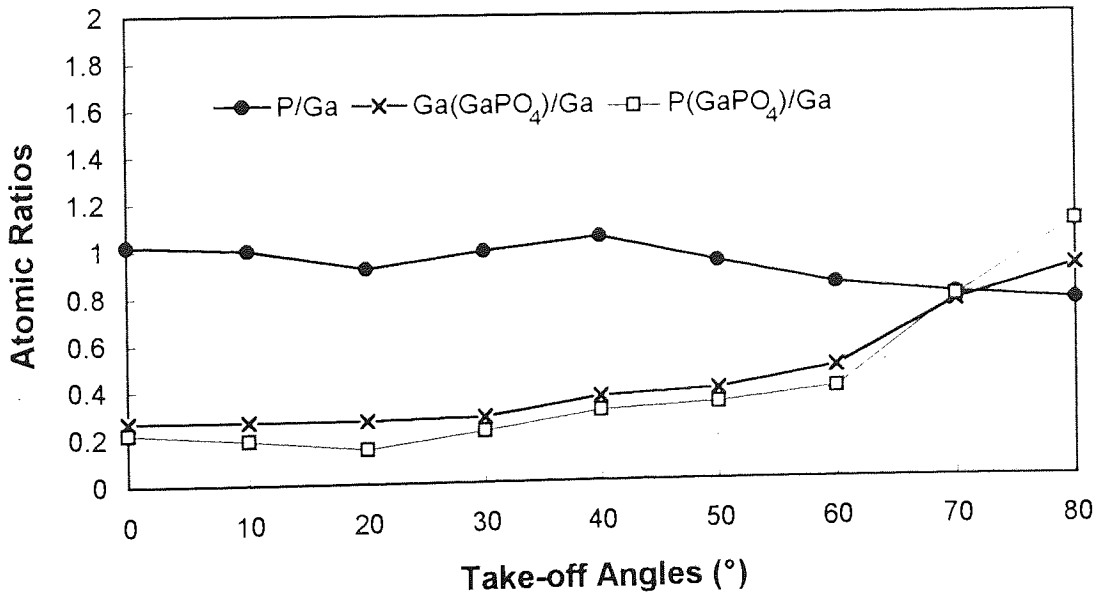

(b) P/Ga, $P(GaPO_4)/Ga$ and $Ga(GaPO_4)/Ga$ variations versus electron take-off angles

Figure 4.12 ARXPS analysis of as received GaP (111) surface

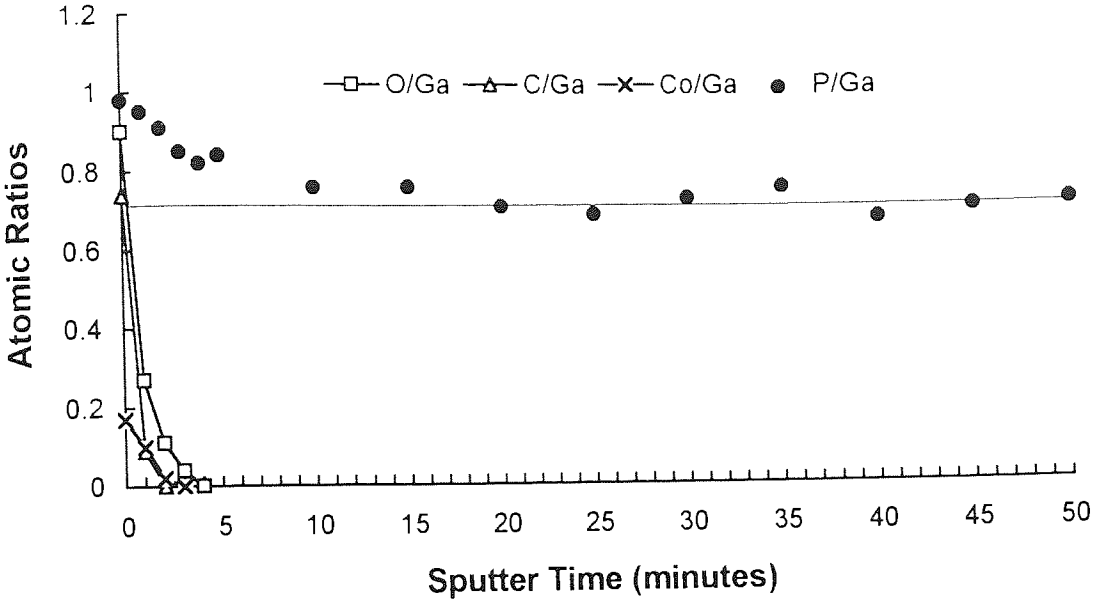

(a) Compositional changes in GaP surface during Ar^+ beam bombardment

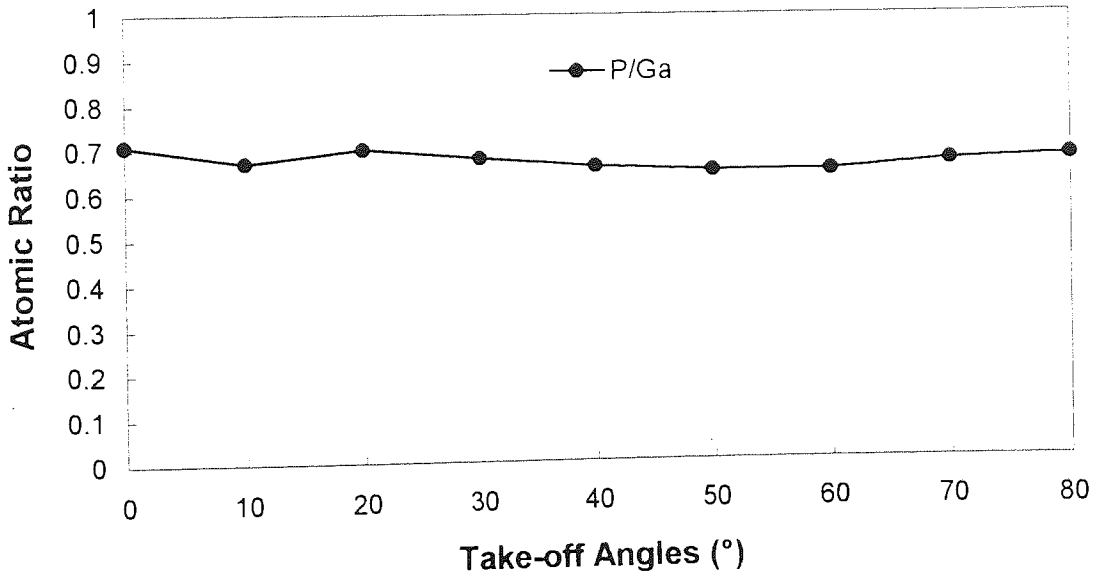

(b) ARXPS analysis of ion bombarded GaP surfaces

Figure 4.13 Ion bombardment effects in GaP surface observed by XPS

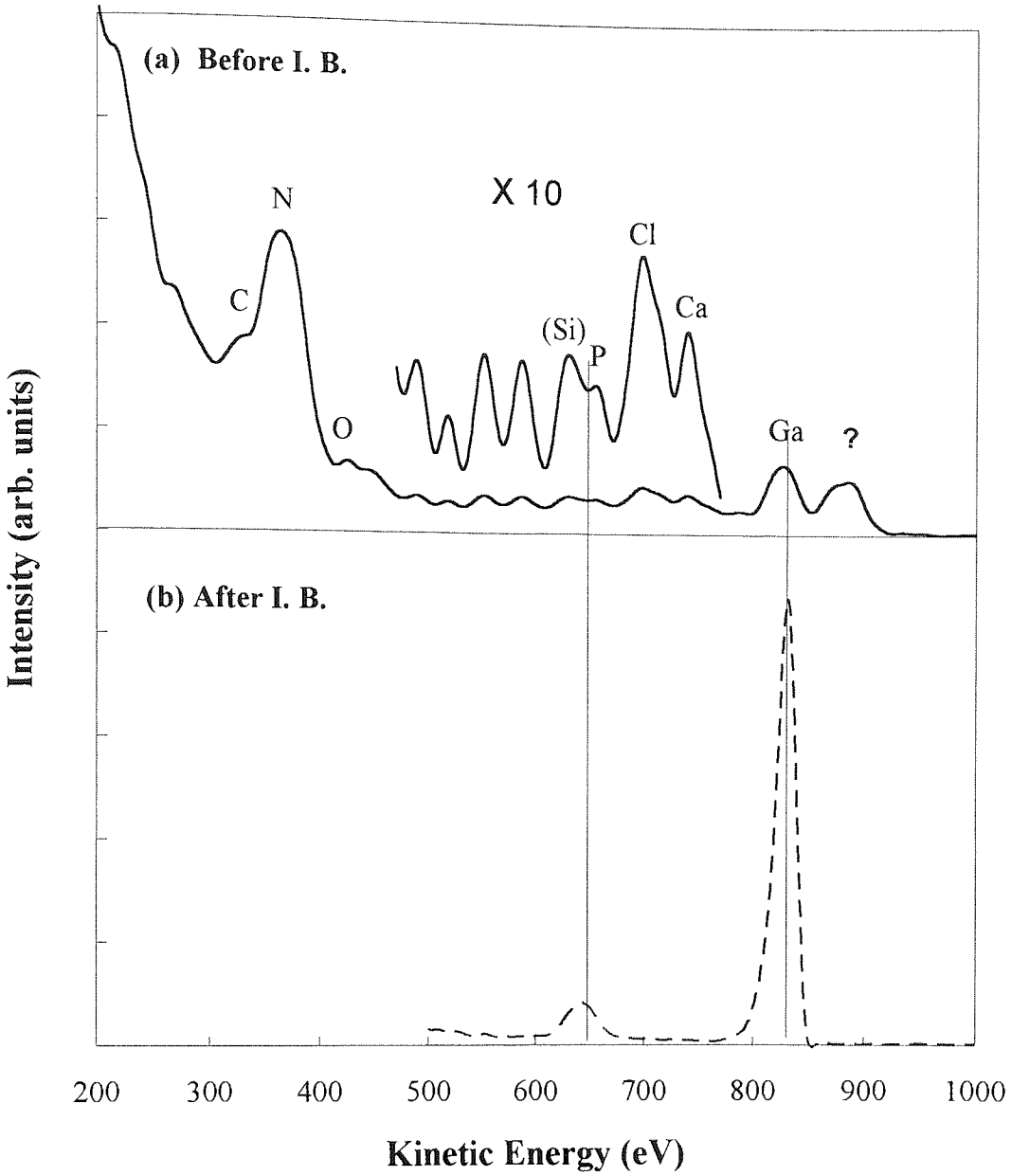

Figure 4.14 He ISS analysis of GaP surfaces before and after ionbombardment

fact that the P/Ga ratio at 80° TOA was about 0.76 (see Figure 4.12b) , but in the bulk of GaP, the P/Ga approached 1:1.

XPS observations of the composition changes in GaP surfaces during 50 minutes Ar ion bombardment is shown in Figure 4.13a. The O, C and Co signals disappeared after about 4 minutes sputtering. During the bombardment, the P/Ga ratio decreased from the stoichoimetric value of 1.0 until after about 10 minutes, the ratio reached a value of about 0.71, but with a little fluctuation.

The bombarded GaP surface was examined with ARXPS. The variation of the P/Ga ratios with the take-off angles are shown in Figure 4.13b. This shows a trend that the P/Ga ratios may increase slightly at very surface compared to those in the deeper surface region, but this is very unclear and needs to be confirmed by LEISS.

LEISS

Since most of contaminants are insulating materials, the intensity of the scattering ions is reduced substantially due to much larger probability of neutralisation, LEISS technique is very difficult to use for studying contaminated surfaces. However, an attempt was made to investigate the as-received GaP surface by LEISS. The He ISS spectrum from the surface is illustrated in Figure 4.14a. It is shown in the spectrum that the as-received GaP surface was heavily contaminated and contained many species, including C(at 323eV), N(373eV), O(429eV), Cl(697eV), Ca(741eV), Ga(826eV), *etc.*. Most of these elements were not found in XPS measurements, this, again, shows the unique features of LEISS technique. Significant nitrogen and carbon species found in the spectrum are obviously due to fragments of polymer molecules from the protective plastic film which covered the sample when received. Other elements, like Cl and Ca, may come from the surface processing, including mechanical polishing and chemical cleaning. According to Gallet *et al.* anlaysis [1992], the HF treatment can result in a significant P loss in a phosphide surface, thus, this may be another reason for P depletion at the surface of GaP observed in the above ARXPS analysis. A peak on the higher energy side of the Ga peak indicates that some higher mass species, such as Mo or Sn, may exist on the as-received GaP surface, but because of the lack of the information on the preparation and storage of the sample, the reasons of the existence of these elements cannot be discussed here. P signal is very low and may be mixed with Si, accurate calculation of the P/Ga atomic ratio from this spectrum is impossible.

LEISS spectrum from the GaP surface after ion bombardment is given in Figure 4.14b. Ga and P peaks appear at KEs of 832 and 645eV, respectively. The peak-area ratio of P/Ga in the surface is about 0.105. Using Equation 2.30 and the data given in

Tables 4.3 and 4.10, the estimated P/Ga ratio at the first atomic layer of the bombarded GaP surface is about 0.91. This confirms ARXPS observations and indicates that P concentration in the outermost layer of the bombarded GaP surface is higher than those in the deeper surface region.

4.5.3. GaAs

XPS

Ga and As 3d spectra taken from the as-received GaAs surface are given in Figure 4.15a. Analysis of the surface has been reported briefly in Section 4.3, further discussion on the surface structure is given here. In the GaP surface, a surface structure of the P_2O_5-like layer, due to the existence of P=O bonds, was found at the top layer of the phosphate. These structures are also possible in arsenic-oxygen chemistry, but they are not as stable as their phosphorus counterparts and occur much less frequently [Lucovsky and Bauer, 1980]. This is why no As_2O_5 component was seen in XPS analysis. In principle, the $(GaAs)O_4$ structures should be formed on GaAs surface, where each Ga is bonded to each As through a single O, but this species appear to be unstable and to break down into As_2O_3 and Ga_2O_3. When in contact with excess Ga or a GaAs substrate, Ga atoms may "steal" O from As_2O_3 (due to the difference in electronegativities), leaving metallic As [Spicer *et al.*, 1979]. That is why the concentration of oxidised Ga is slightly higher than that of As. Figure 4.15b shows the angular variations of the atomic ratios of each component to Ga(GaAs). The As/Ga ratio in the bulk of the "as received" GaAs sample is approximately equal to its stoichiometric value, but at the interface between GaAs substrate and oxide layer, the ratio decreased to about 0.82. The reasons have been given in Section 4.3.

Figure 4.16a shows the changes of As/Ga, O/Ga and C/Ga ratios against sputtering time observed with XPS. Both the 3d and $2p_{3/2}$ core level electrons of Ga and As atoms were monitored in XPS. This gives a good chance to apply KRXPS technique to study changes in As/Ga compositional distributions during ion bombardment. The figure shows that the contaminant overlayer was removed after about 1-2 minutes, both 3d and 2p ratios of As to Ga decreased starting from about 2 minute sputtering until after 15 minutes, the 3d ratio reached a steady value of 0.77; and the $2p_{3/2}$ ratio reached 0.82. The changes in both core level signal of Ga and As clearly illustrates that ion bombardment generally causes As depletion in GaAs surface. The difference in atomic ratios measured from 3d and 2p signals, however, indicates that the As concentration at the outermost surface may be higher than that in the deeper region (see Section 4.3.2).

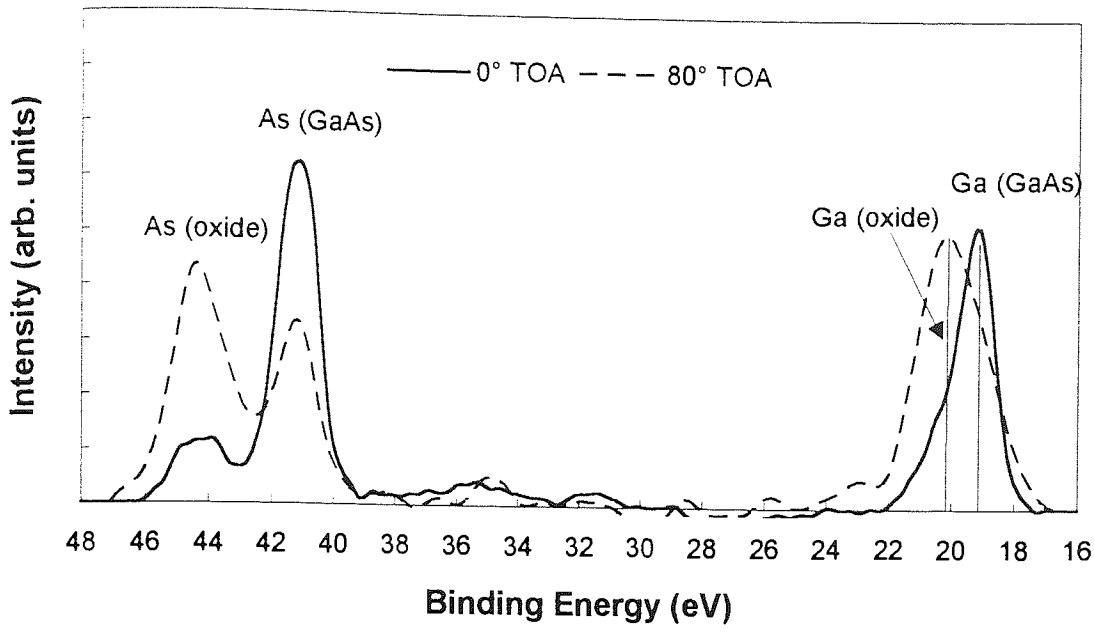

(a) Ga and As 3d spectra

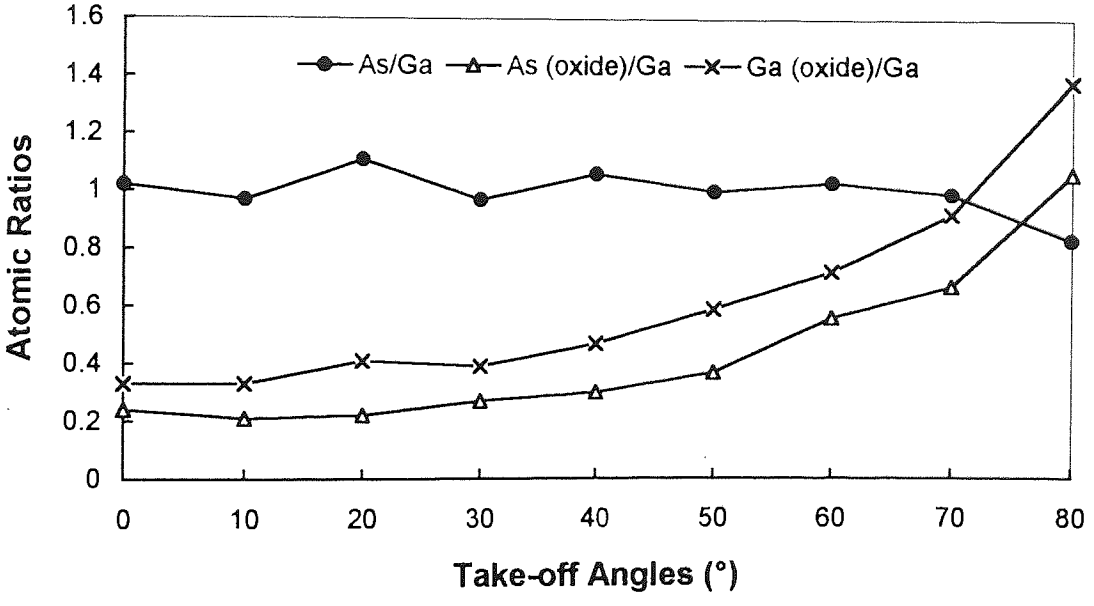

(b) As/Ga, As(oxide)/Ga and Ga(oxide)/Ga variations versus electron take-off angles

Figure 4.15 ARXPS analysis of as received GaAs (100) surface

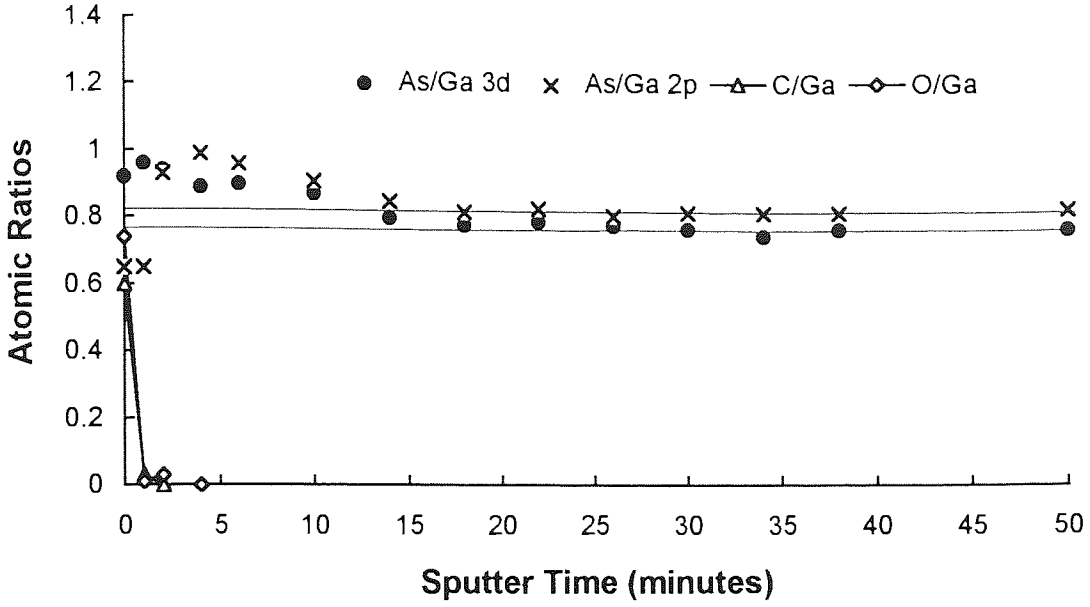

(a) Compositional changes in GaAs surface during Ar^+ beam bombardment

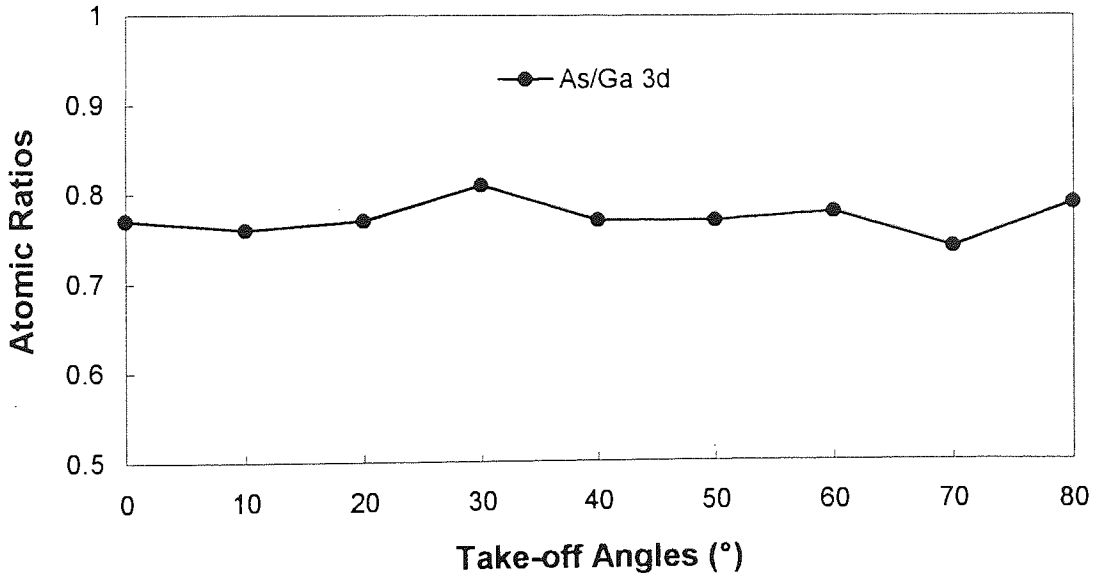

(b) ARXPS analysis of ion bombarded GaAs surfaces

Figure 4.16 Ion bombardment effects in GaAs surface observed by XPS

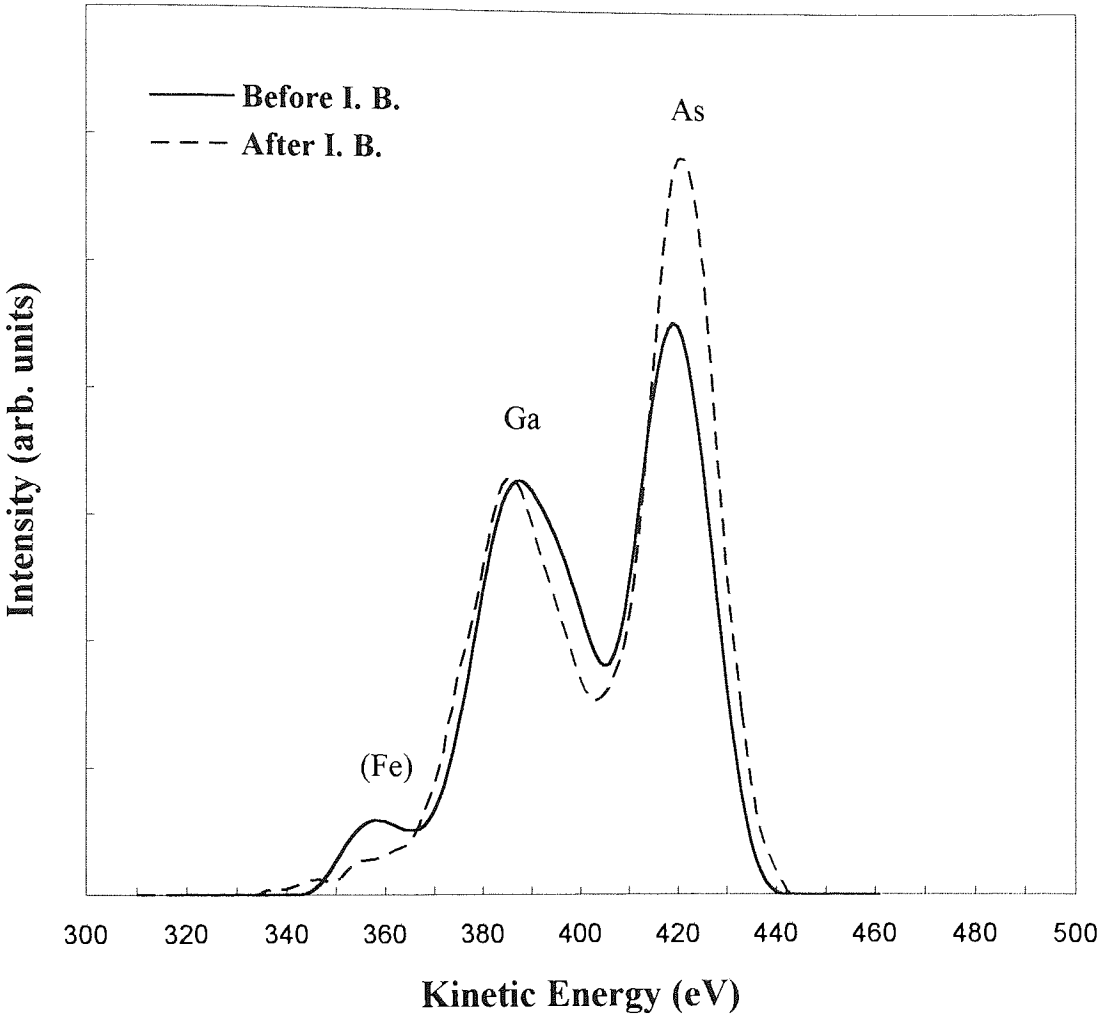

Figure 4.17 Ne ISS analysis of GaAs surfaces before and after ion bombardment

ARXPS analysis was repeated on the bombarded surface to gain more evidence, the results are shown in Figure 4.16b. Although there were quite large errors, this result showed the same trend as KRXPS analysis, that is, As concentration may increase in the outermost layer of the ion bombarded GaAs surface.

LEISS

Ne^+ LEISS spectra of the GaAs surface before ion bombardment are shown by the solid curve in Figure 4.17. Since the oxide layer was present on the as-received sample surface, LEISS analysis for GaAs surface prior to ion bombardment was carried out after heating the sample to 180°C for about 10 hours. A small Fe peak at KE of 359eV was found in the initial surface which may come from the contamination from the sample holder which is made of stainless steel. Quantification was performed by peak fitting. Three peaks, including $^{75}As(100\%)$, $^{69}Ga(60\%)$ and $^{71}Ga(40\%)$, were used for the fitting, which give a quite satisfactory synthesis. Results showed that the As/Ga ratio was about 1.02, within the experimental errors, LEISS results indicate that composition in the outermost atomic layer of GaAs surface before ion bombardment is close to stoichiometric.

The LEISS spectrum taken from the GaAs surface after 50 minutes of Ar^+ bombardment is represented by the dashed curve in Figure 4.17. The Ga and As peaks were normalised to the Ga peak from the surface prior to the ion bombardment. A significant increase in As is clearly seen in the spectrum. Quantitative analysis of the results shows the As/Ga ratio reach a value of 1.42. By comparison with the As/Ga ratio from the initial surface, this indicates that ion bombardment causes As enrichment at the outermost layer.

4.5.4. GaSb

XPS

The Ga 3d and Sb 4d spectra taken at TOAs of 0° and 80° from the GaSb sample surface prior to ion bombardment are illustrated in Figure 4.18a. For the Ga 3d peak, two well defined components at BE of 18.9eV and 20.2eV represent Ga atoms in two chemical states of GaSb and Ga oxide , respectively. As described previously in Section 4.2.2, Sb 4d peaks are quite complicated, and four components were identified by peak fitting. The two peaks at BEs of 31.7eV and 33.0eV are the $4d_{5/2}$ and $4d_{3/2}$ of Sb atoms in GaSb; the other two at 34.2 and 35.5eV are Sb $4d_{5/2}$ and $4d_{3/2}$ in Sb oxide. In order to study the surface composition, the Sb $3d_{5/2}$ and $3d_{3/2}$ have also been analysed. The

two chemical states of antimony were easily distinguished in the Sb $3d_{3/2}$ line, the peak positions corresponding to the Sb atoms in GaSb and in Sb oxide are at BE of 537.3 and 539.8eV, respectively. The Sb $3d_{3/2}$ peak was synthesised, the percentages of Sb atoms in the two chemical states were then used in peak synthesis of Sb $3d_{5/2}$ to resolve O 1s peaks (see Section 4.2.2). The surface chemistry of the native GaSb oxide is very similar to GaAs. According to Lucovsky and Bauer's analysis [1989], the oxides existing in GaSb surface are Ga_2O_3 and Sb_2O_3. The figure, however, implies that the GaSb surface was covered by a very thick overlayer so that the signals of Ga 4d and Sb 4d core levels from the GaSb substrate decrease dramatically at 80° TOA. Indeed, quantitative analysis showed that the atomic concentration of oxygen and carbon in this surface are about 5 and 10 times more than the others. The formation of such a thick overlayer on the GaSb surface may be due to two factors. First, since the sample was cleaned by the 1,1,1-trichloroethane and followed by the methanol washing to remove the packing wax, this procedure may result in heavy carbonaceous contamination. It is also possible that the wax was not completely removed. Second, since GaSb has very low heat of formation (41.8kJ/mol) compared to GaAs (71.1kJ/mol), bulk oxidation may occur in air when GaSb surface is subject to (unexcited) oxygen sorption, whereas GaAs needs excited oxygen to form bulk oxides [Spicer *et al*, 1979]. Indeed, the detailed ARXPS analysis shown in Figure 4.18b does give a clear indication that a thicker oxide overlayer is formed at the GaSb surface. The figure also showed that the oxide layer was dominated by the Ga_2O_3 component, this may be predicted from the electronegativities of Ga(ε_{Ga}=1.6eV) and Sb(ε_{Sb}=1.9eV). Again, ARXPS analysis indicates stoichiometric GaSb in bulk.

After the initial analysis, the GaSb surface was bombarded by a 3keV argon ion beam for up to 50 minutes. Changes in the atomic ratios of Ga^+/Ga^0, Sb^+/Ga^0 and Sb^0/Ga^0 measured with XPS are shown in Figure 4.19a. The figure confirms the previous ARXPS analysis and shows that a thick oxide layer exists on the GaSb single crystal surface and the major component in the oxide layer was Ga_2O_3 since the measured atomic ratio of Sb^0/Ga^0 ratio greater than 1.0. This oxide layer was completely removed after about 8 minute sputtering. The Sb/Ga ratios then decreased from 1.0, until after about 25 minutes the ratio reached the steady state value of 0.71.

ARXPS analysis of the bombarded GaSb surface is given in Figure 4.19b. The Sb/Ga ratios generally vary around the value of 0.71. It may be seen that a slight increase in the Sb/Ga ratio at TOA of 80°, but due to large errors in the measurement, the result needs the further confirmation.

LEISS

Since the as received GaSb surface was covered by a very thick oxide contaminant

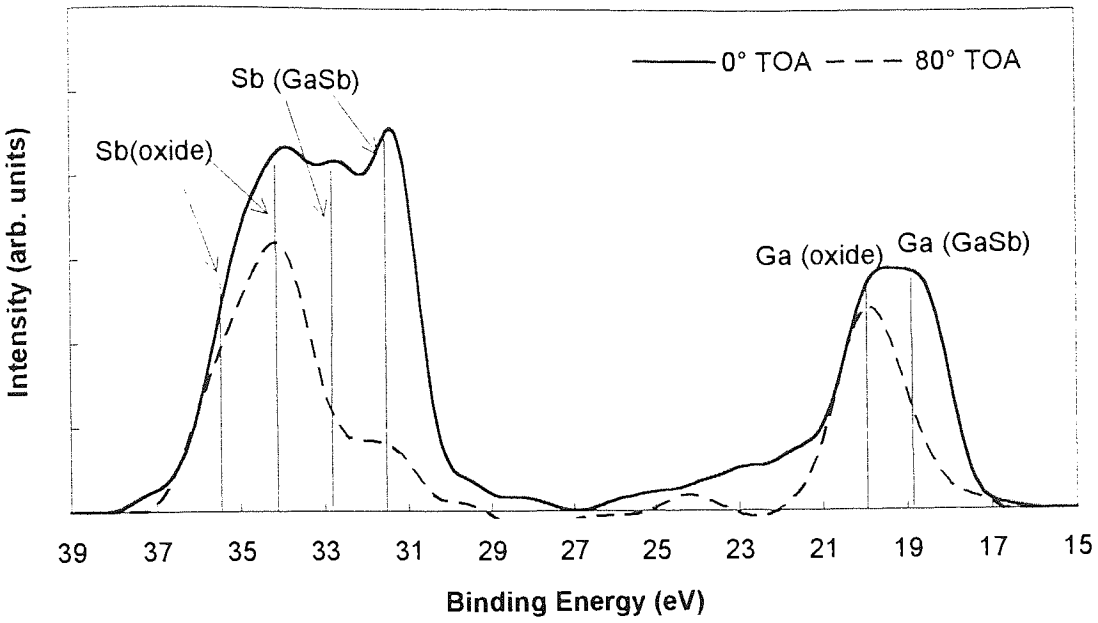

(a) Sb 4d and Ga 3d spectra

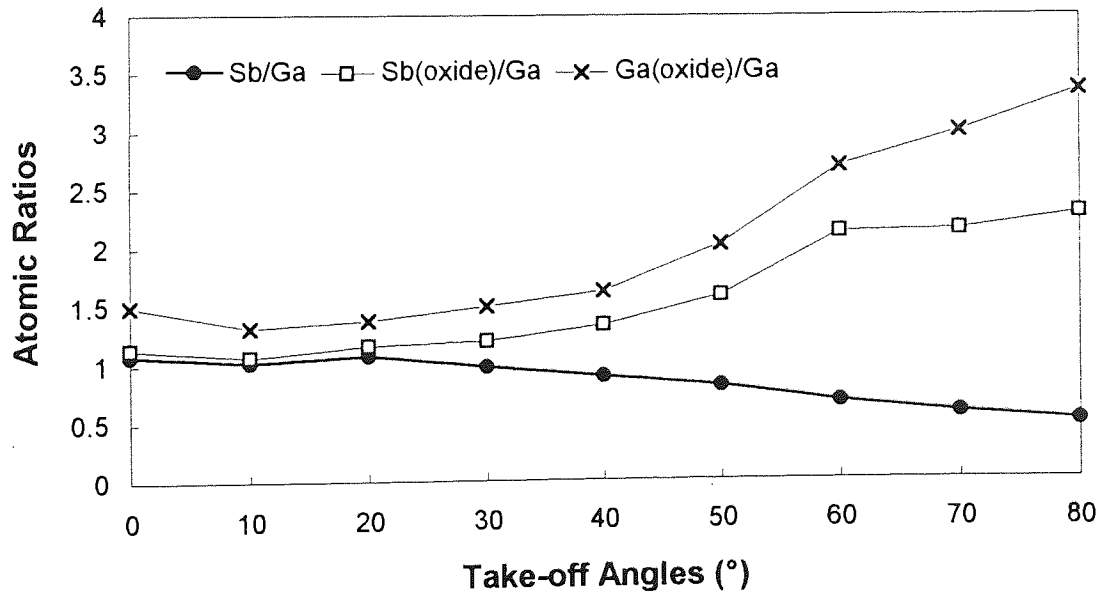

(b) Sb/Ga, Sb(oxide)/Ga and Ga(oxide)/Ga variations versus electron take-off angles

Figure 4.18 ARXPS analysis of as received GaSb (111) surface

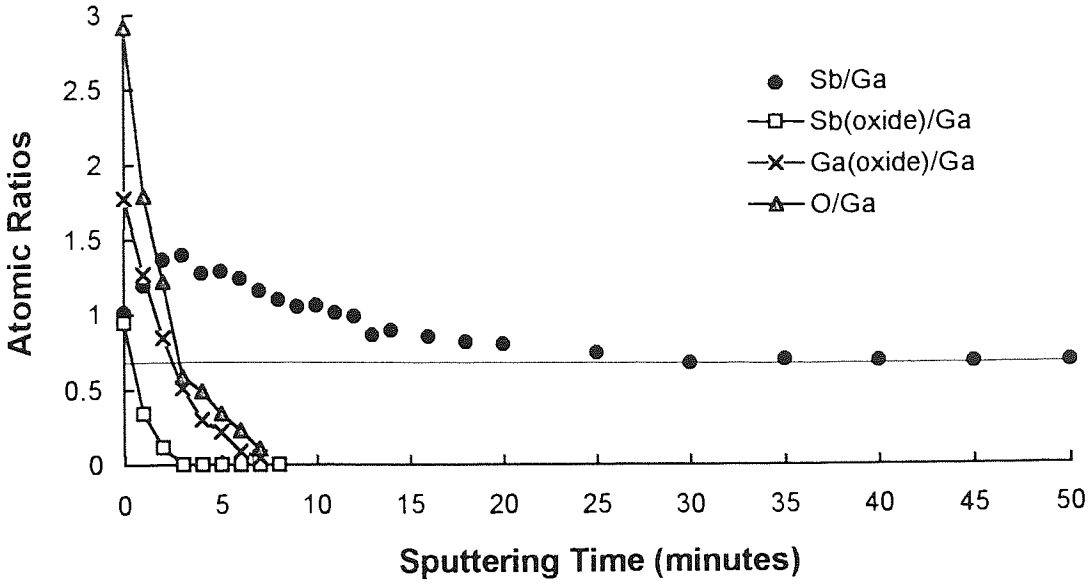

(a) Compositional changes in GaSb surface during Ar^+ beam bombardment

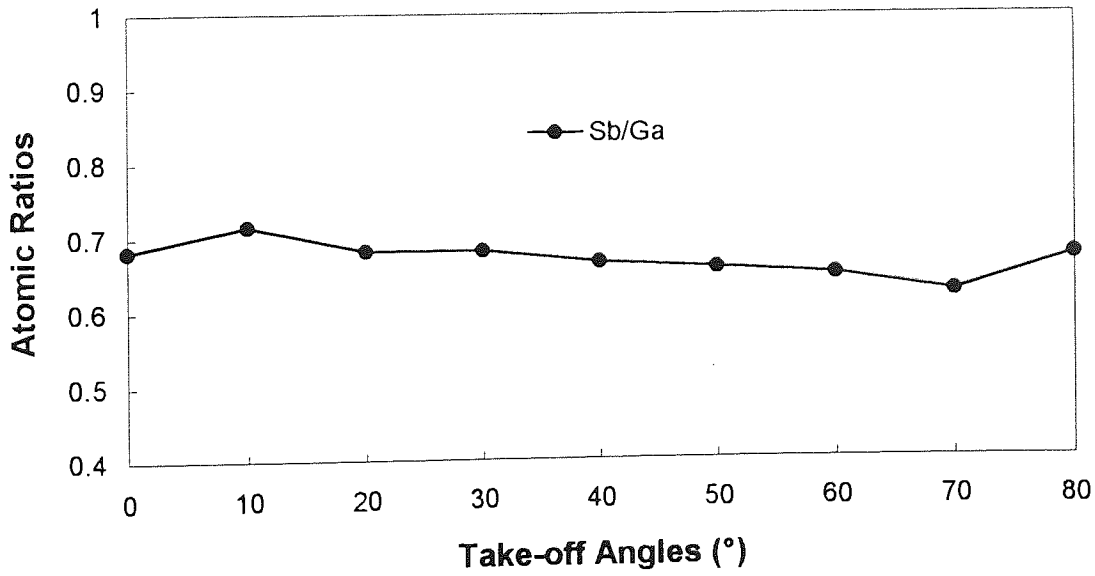

(b) ARXPS analysis of ion bombarded GaSb surfaces

Figure 4.19 Ion bombardment effects in GaSb surface observed by XPS

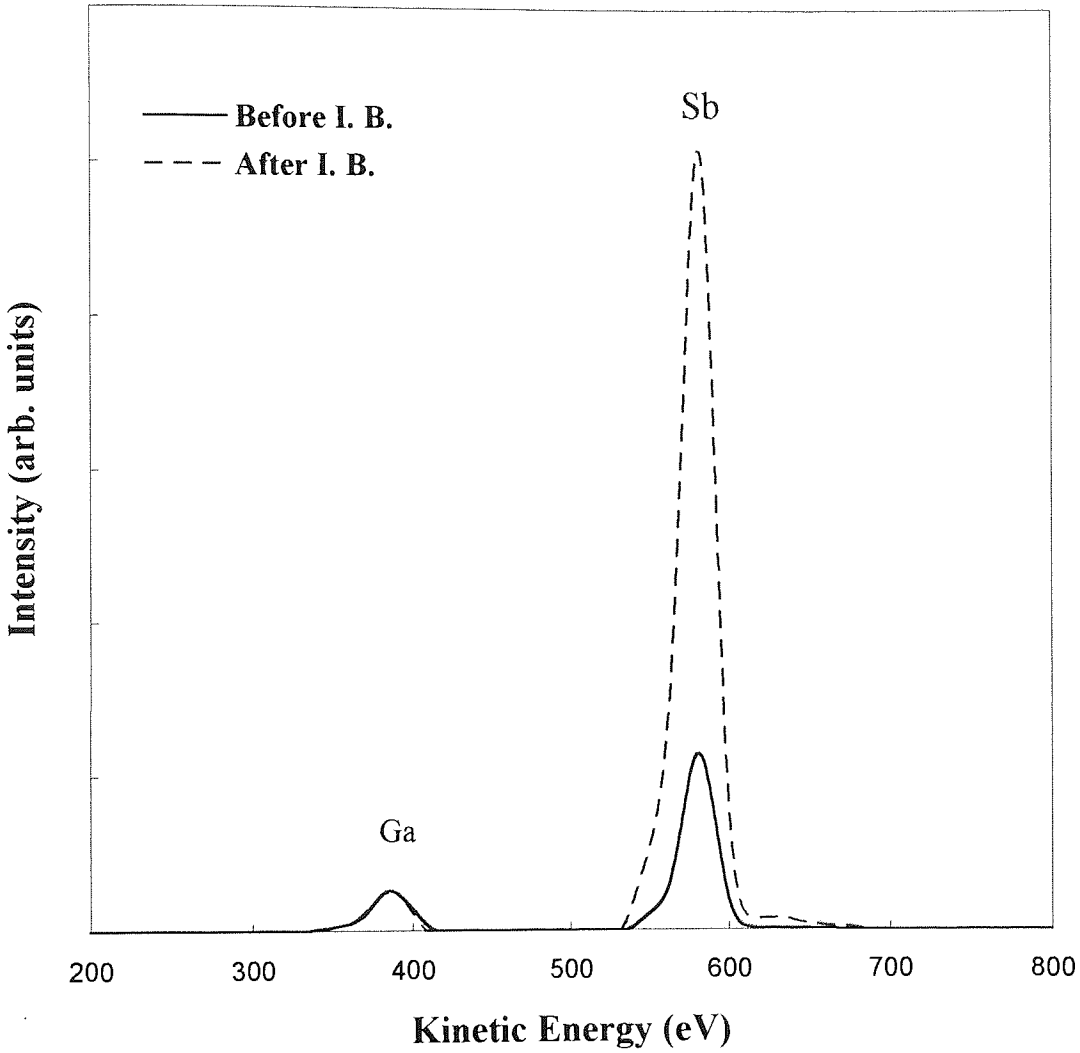

Figure 4.20 Ne ISS analysis of GaSb surfaces before and after ion bombardment

layer, the surface was first cleaned using 2keV Ne ion beam with a beam current of about 0.5μA for about 10 minutes. It was hoped that this would remove the oxide layer without producing the damage of Ar ion bombardment. The surface then was examined using Ne ISS. The results are shown in Figure 4.20. The solid curve in the figure represents the Ne ISS spectrum taken from the GaSb surface prior to Ar ion bombardment. The peaks at KE of 373eV and 581eV are the Ne^+ scattering peak from Ga and Sb surface atoms, respectively. The peak-areas of these two peaks are about 5.0 and 17.1kCeV/Sec., respectively. According to Equation 2.30, the Sb/Ga atomic ratio at the surface was estimated about 0.87, so the first atomic layer is nearly stoichiometric but with slight Ga enrichment. Apart from the experimental errors, this ratio may indicate more Ga oxide left on the surface.

The Ne ISS spectra from the GaSb surface after 50 minute Ar^+ bombardment was also plotted in Figure 4.20, represented by the dashed curve and normalised to the Ga peak from the unbombarded GaSb surface for comparison. It is seen clearly from Figure 4.20 that the Sb signal at the surface increases significantly. Quantitative analysis indicates that the peak-area of Ga peak in the spectrum is about 3.41kCeV/Sec., and that of Sb peak is 44.6kCeV/Sec., showing that the Sb/Ga ratio at the outermost atomic layer of the bombarded GaSb surface reaches 3.33. It is clear that the ion bombardment causes significant enrichment of Sb in the outermost atomic layer of the GaSb surface.

4.5.5. InP

XPS

The P 2p and In $3d_{5/2}$ core level spectra taken from the as-received InP surface are given in Figure 4.21a. The surface chemistry of the air-exposed InP surface is similar to that of the GaP sample. Two peaks at BE of 128.5eV and 133.1eV were clearly seen in P 2p spectrum, which can be attributed to bulk InP and phosphate in the overlayer. The synthetic analysis of the P 2p peak shows that another component exists at BE of 135.1eV, indicating a P_2O_5-like layer formed at the top of the oxide layer, similar to that in GaP. The chemical states of indium may be more easily identified in In $3d_{5/2}$ spectrum, the peaks at BE of 444.3eV and 445.3eV represent In in InP and in oxidation states. According to the analysis of the GaP sample, the main component in the oxide layer is probably $InPO_4$. Compared to the GaSb and the GaP, much less oxidation occurred on the InP. Apart from the fact that the InP sample was well packed to avoid the long time exposure to air, this could be explained in terms of the heat of formation of InP, which is about 91.9kJ/mol and much greater than that of GaSb (see above).

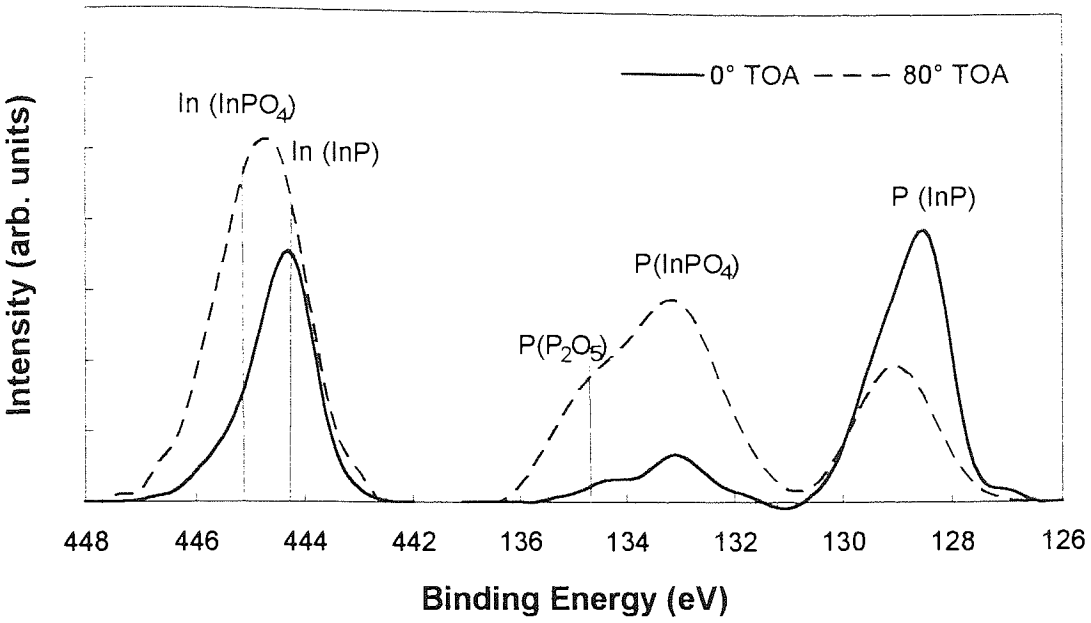

(a) P 2p and In $3d_{5/2}$ spectra

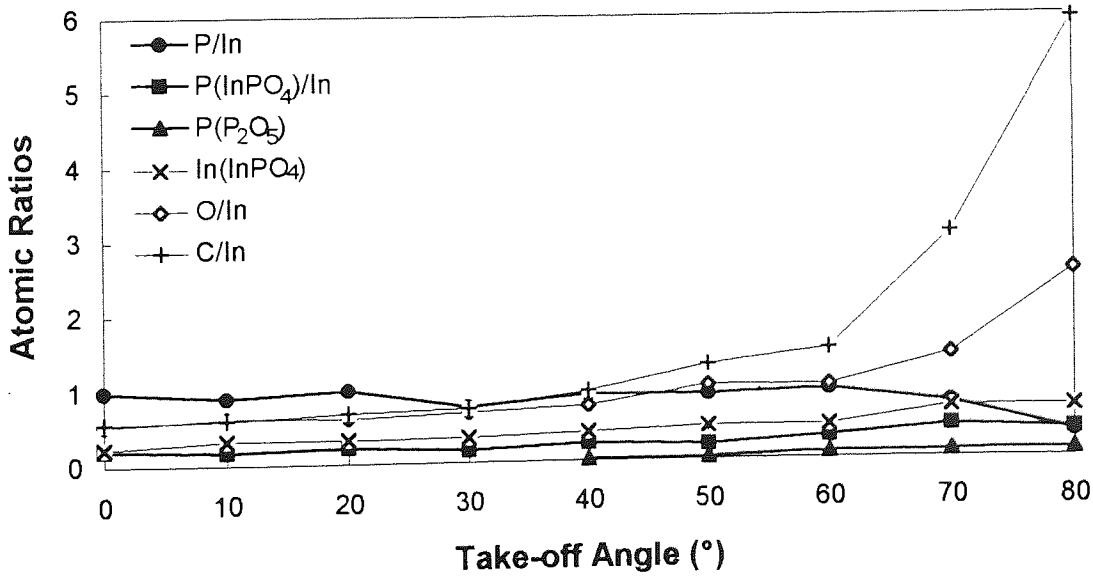

(b) P/In, $P(InPO_4)/In$, $In(InPO_4)/In$, O/Ga and C/Ga variations versus take-off angles

Figure 4.21 ARXPS analysis of as received InP (100) surface

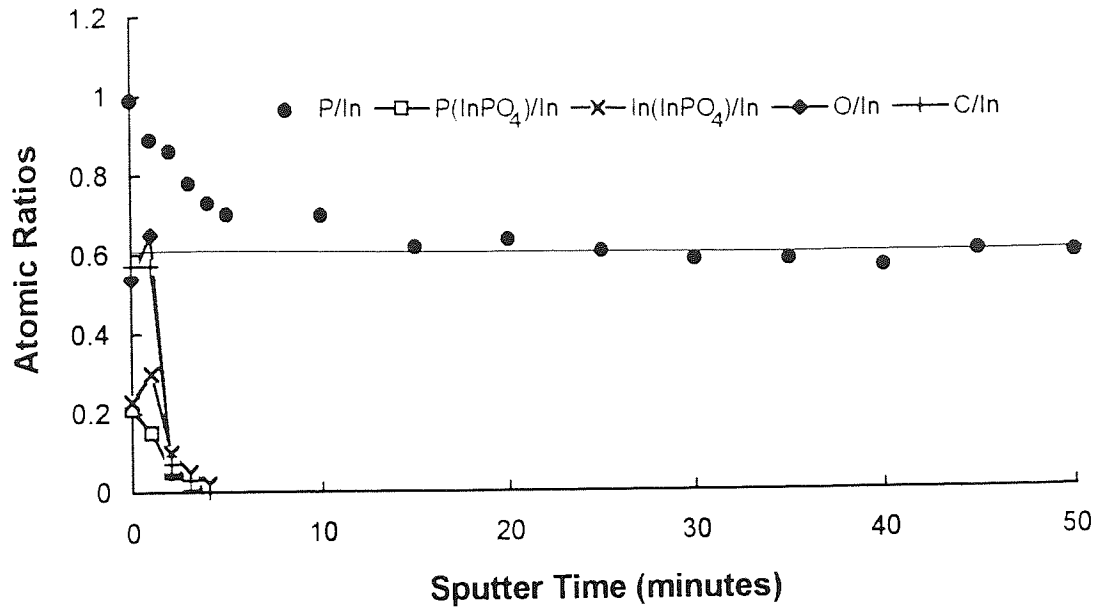

(a) Compositional changes in InP surface during Ar^+ beam bombardment

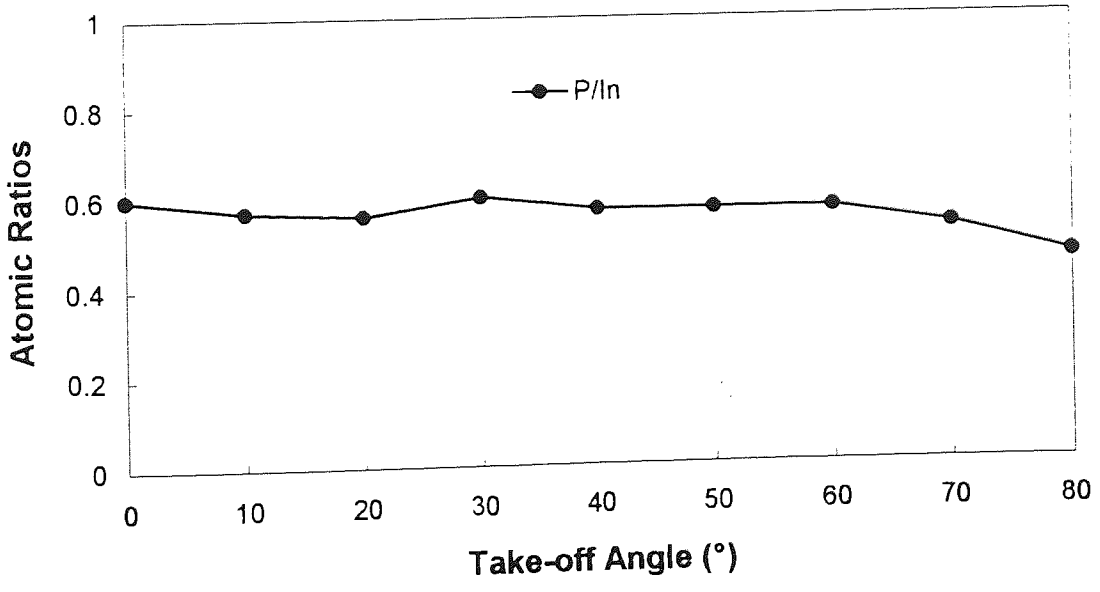

(b) ARXPS analysis of ion bombarded InP surfaces

Figure 4.22 Ion bombardment effects in InP surface observed by XPS

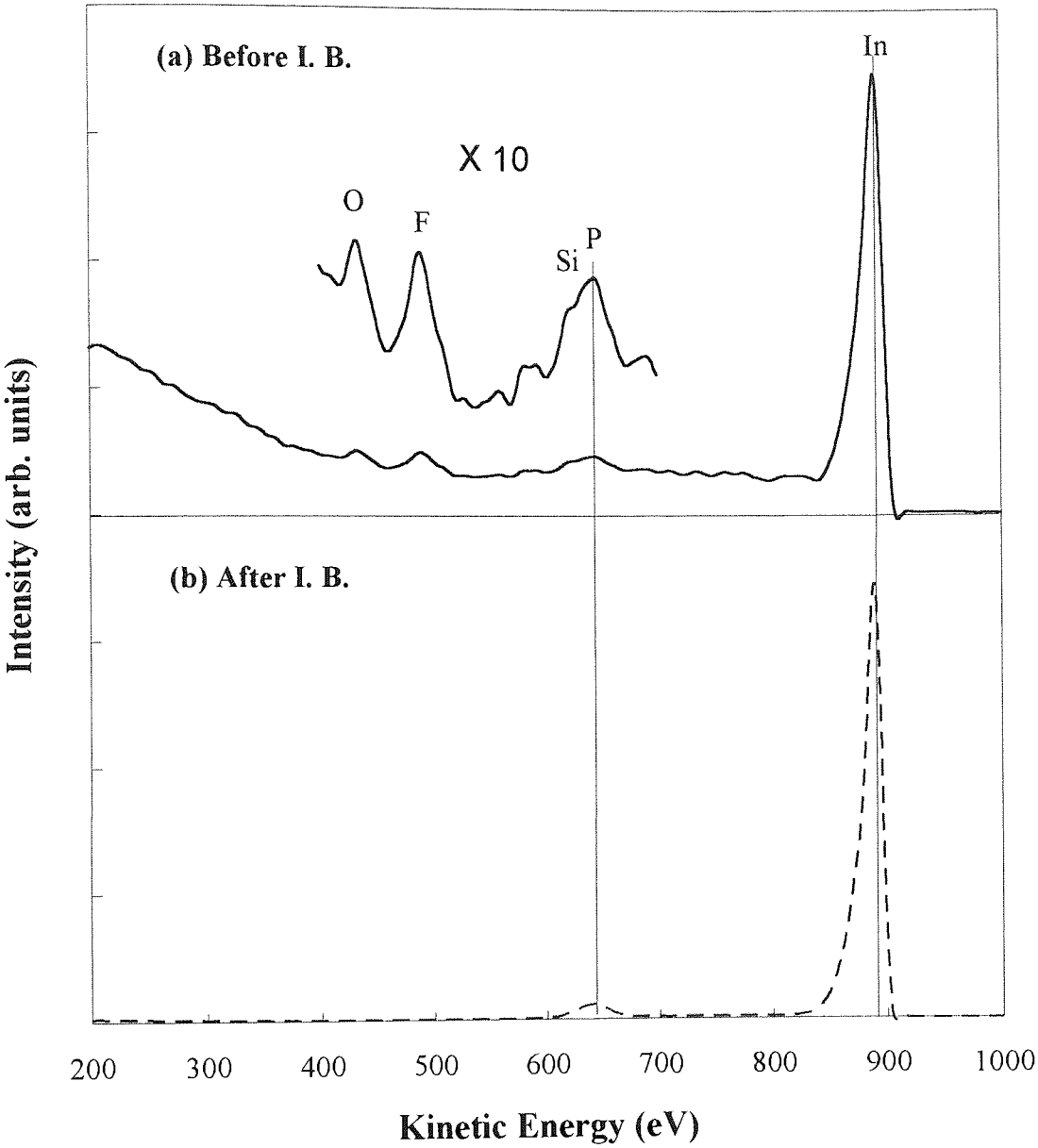

Figure 4.23 He ISS analysis of InP surfaces before and after ion bombardment

Hence surface InP molecules are not easily broken by oxygen molecules to form bulk oxides or even surface oxides during O sorption [Spicker *et al.*, 1979]. The surface structure of InP is more clearly revealed by the systematic ARXPS analysis, which is presented in Figure 4.21b. The atomic ratios of each component relate to the In in InP matrix and are plotted against the electron take-off angles. The results show much lower level of O and C contaminants in the surface than in those previously examined. It may also be seen in the figure that in InP substrate the P/In ratio is low at about 0.34, which is presumably due to surface cleaning procedures. For example, the P depletion in the HF treated InP surface has been reported by Gallet *et al.* [1992]. The composition in the bulk of InP, however, was close to its stoichiometric value, the measured P/In atomic ratio was about 0.99.

Figure 4.22a shows the surface compositional changes of InP monitored by XPS during a period of 50 minute Ar ion beam bombardment. The contamination layer was completely removed after about 5 minute of sputtering. The P/In ratio decreased at the beginning until after about 15 minutes, then reached a steady value of 0.6, indicating a significant P loss from the bombarded InP surface.

The results of ARXPS re-examination on the InP surface after ion bombardment are presented in Figure 4.22b. It may be seen that the P/In ratios decreased at higher take-off angles, from 0.6 at 0° TOA to 0.46 at 80°, clearly showing that depletion of P occurred at the surface.

LEISS

The He^+ ISS spectrum from the as-received InP surface is shown in Figure 4.23a. As analysed in ARXPS, the InP surface was much less contaminated than GaP surface. Besides In and P, the contamination species found in the surface were O (at 433eV), F (493eV), Na (559eV), Mg (581eV) and Si (621eV). The P intensity was estimated by peak synthesis after removal of the Si component from the P peak. The intensities of P and In estimated from the spectrum are 1.12 and 21.3 kCeV/Sec., respectively. The P/In ratio at the outermost atomic layer of the as received InP surface is about 0.54, which means that In atomic concentration was nearly two times as that of phosphorus atoms in the top layer. This results are coincident with the ARXPS observations (see Figure 2.22b). Since relatively large amount of F has been found at the surface, LEISS study gave clear evidence that the InP was treated by HF cleaning procedure, resulting in In enrichment at the surface.

The He^+ ISS spectrum taken from the ion bombarded InP surface is presented in Figure 4.23b. The surface appeared to be very clean, the P and In peaks are clearly

identified in the spectrum. Quantitative analysis indicates that the intensities of P and In scattered peaks are 9.61 and 129.5 kCeV/Sec. This results in the atomic ratio of P/In of 0.81. Similar to GaP, although LEISS showed the P loss at the outermost layer of the ion bombarded InP surface, but the P/In ratio in this layer was higher than those measured by XPS.

4.5.6. InAs

XPS

Figure 4.24a shows As 3d and In 4d core level spectra taken from the as received InAs surface. The surface chemistry of InAs is very similar to that of GaAs. In the As 3d spectrum, peaks at BE of 40.6eV and 44.1eV indicates As in InAs and As_2O_3 states, respectively. As for InP sample, the chemical states were analysed by inspecting the In $3d_{5/2}$ core level line. Similar to the InP surface, the oxide layer on InAs sample surface was very thin. This could be seen more easily not only from the variations of the atomic ratios of In and As components against the electron take-off angle, but also from that of carbon and oxygen, which are illustrated in Figure 4.24b. The concentration of the In oxide was slightly higher than As oxide, similar to that observed on the GaAs surface. The As/In ratio was about 0.68, which is obviously lower than the expected, this is probably due to some surface cleaning procedure (see Section 4.4), similar to the GaP and InP surfaces. But the As/In ratio in the bulk was about 0.91, which is close to the expected stoichiometric value.

Figure 4.25a shows that the compositional changes in the InAs surface during the 50 minute Ar ion bombardment. The carbonaceous and oxide overlayers were removed after 1 and 2 minutes sputtering, respectively. The As/In atomic ratio decreased gradually from 0.9 within 15-20 minutes. After that, the ratio approached a stable value of 0.77 with a small variations.

The bombarded InAs surface was re-examined by ARXPS. The variations of InAs ratios with the electron take-off angles are shown in Figure 4.25b. The As/In ratio at 80° TOA was clearly dropped to about 0.68, showing that the As may decrease further at the bombarded InAs surface. LEISS analysis is needed to confirm this result.

LEISS

The as received InAs surface was investigated with Ne^+ ISS, the ISS spectrum is represented by the solid line in Figure 4.26. The As and In scattered peaks appear at kinetic energies of 412 and 541eV, respectively. The quantitative analysis indicated that the areal ratio of As to In peak is about 0.12, so the As/In atomic ratio at the outermost

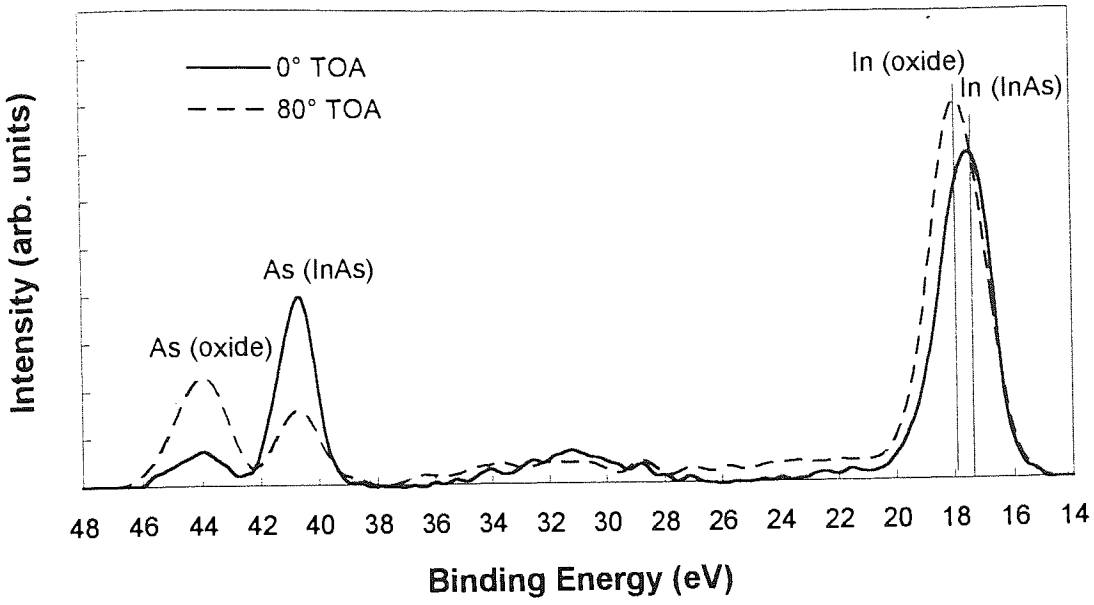

(a) As 3d and In 4d spectra

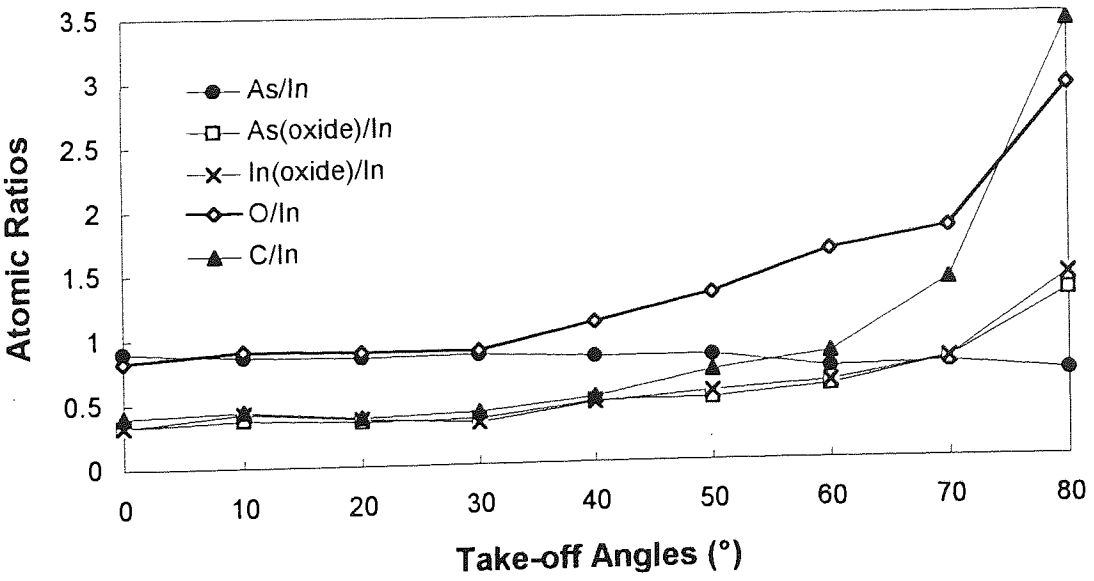

(b) As/In, As(oxide)/In, In(oxide)/In, O/In and C/In variations versus take-off angles

Figure 4.24 ARXPS analysis of as received InAs (100) surface

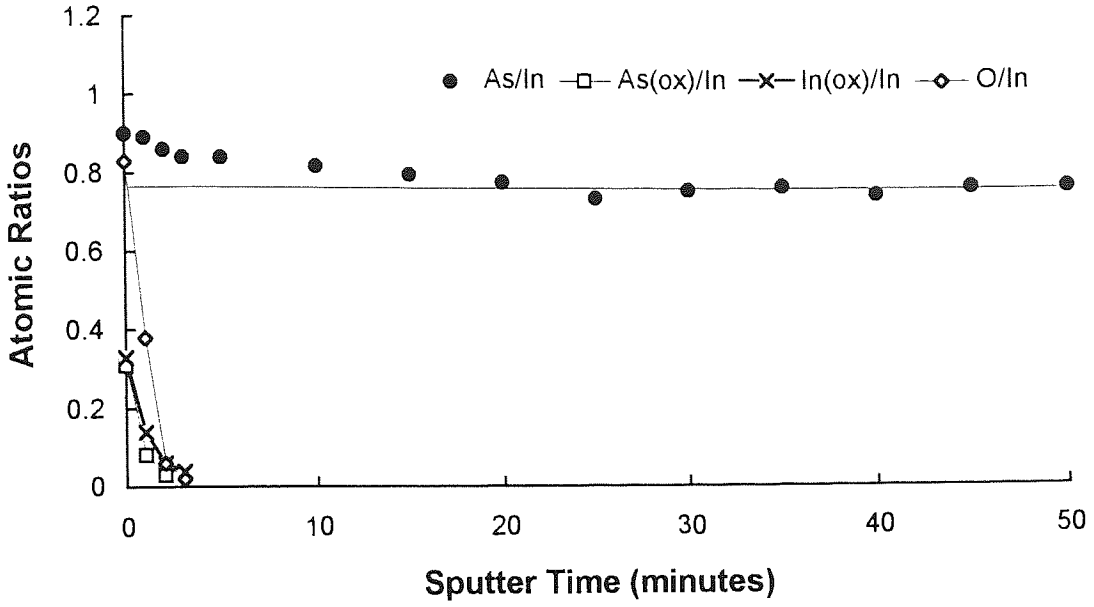

(a) Compositional changes in InAs surface during Ar^+ beam bombardment

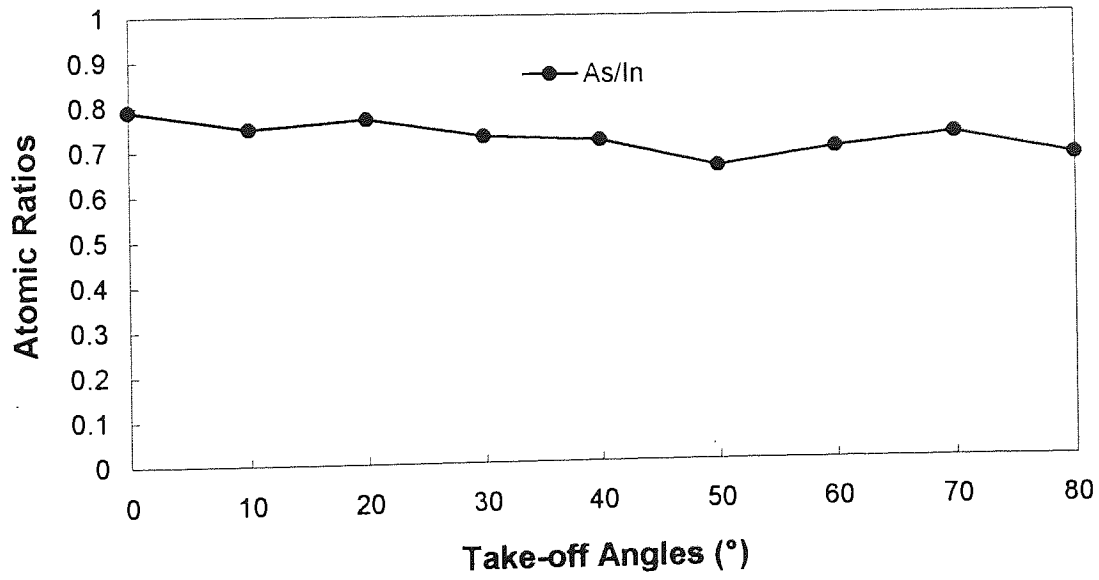

(b) ARXPS analysis of ion bombarded InAs surfaces

Figure 4.25 Ion bombardment effects in InAs surface observed by XPS

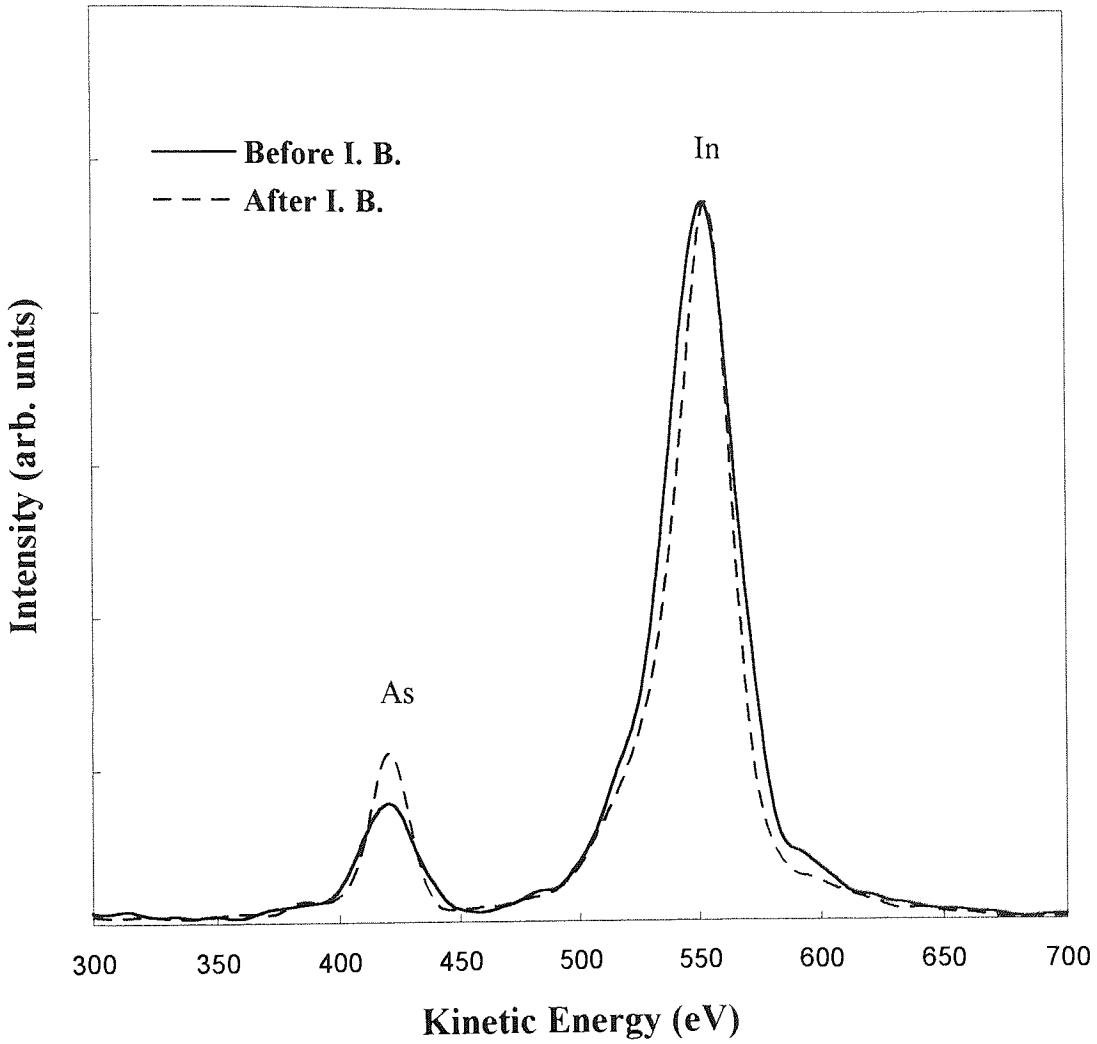

Figure 4.26 Ne ISS analysis of InAs surfaces before and after ion bombardment

layer of the as-received InAs surface calculated from Equation 2.30 is about 0.38, which is in agreement with ARXPS analysis.

The Ne^+ ISS spectrum from the InAs surface after ion bombardment is indicated by the dashed curve in Figure 4.26. It is clearly seen that ion bombardment caused an increase in As concentration at the outermost layer. The calculation using Equation 2.30, however, showed that the As/In ratio is about 0.47, which means that concentration of As at the outermost atomic layer concentration was less than that in the intermediate subsurface.

4.5.7. InSb

XPS

Both 4d and 3d core lines of In and Sb atoms were employed in the XPS analysis of InSb surfaces, this provide a good opportunity to use KRXPS technique in study surface structure. The In 4d, Sb 4d, In 3d and Sb 3d spectra taken from the as received InSb surface are shown in Figure 4.27a&b. In In $3d_{5/2}$ spectrum, two components of In have been resolved by peak fitting. According to the published results [Wagner, 1989], the peak at BE of 444.0eV represents In in InSb matrix, and the other peak at BE of 445.1eV corresponds to In in In_2O_3 state. In Sb $3d_{3/2}$ spectrum, the two chemical states are clearly distinguished, the two peaks at BE of 536.9 and 539.6eV are Sb in InSb and Sb_2O_3 states, respectively. As discussed in Section 4.2.2, the ratio of Sb in InSb to that in Sb_2O_3 state obtained from analysis of Sb $3d_{3/2}$ was used for synthesis of Sb $3d_{5/2}$ peak to resolve O 1s peak for quantification. The analyses of In and Sb 4d spectra from the as-received InSb surface are similar to those from the as-received InAs and GaSb surface. Two components at BE of 16.8 and 17.9eV resolved from In 4d peak represent In in InSb and In_2O_3 states. In Sb 4d spectrum, two components at about 31.0 and 32.2 eV correspond to Sb $4d_{5/2}$ and Sb $4d_{3/2}$ for Sb in InSb matrix, and the other two at BE of 33.9 and 35.1 eV are Sb $4d_{5/2}$ and Sb $4d_{3/2}$ for the oxidised Sb.

In both 3d and 4d spectra at TOA of 80°, the peaks responsible for In and Sb in InSb matrix were reduced significantly, indicating a thick oxide layer existing at the as-received InSb surface. This is obviously due to the stronger metallicity of In and Sb elements, which results in serious oxidation when the sample surface exposed to air. Systematic ARXPS analysis showed that the concentration of Sb_2O_3 is slight higher than that of In_2O_3 in the contamination layer, presumably, this is due to the chemical cleaning procedure used in sample preparation, but in the InSb substrate, ARXPS indicated a stoichiometric InSb surface, the Sb/In atomic ratio was about 0.99.

XPS measurements on surface compositional changes in InSb surface during a

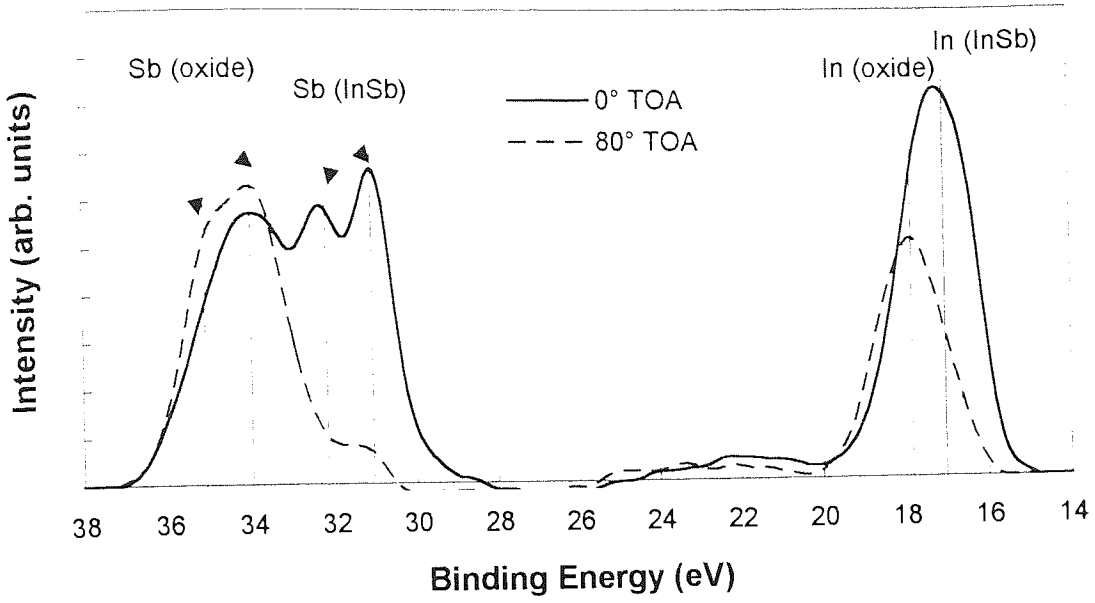

(a) Sb 4d and In 4d spectra

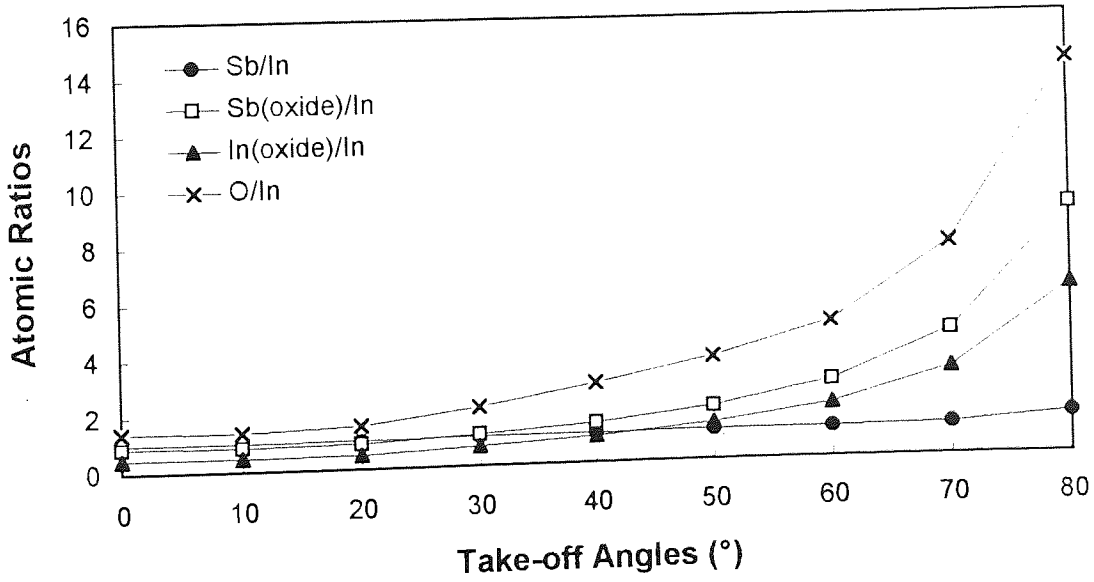

(b) Sb/In, Sb(oxide)/In, In(oxide)/In and O/In variations versus electron take-off angles

Figure 4.27 ARXPS analysis of as received InSb (100) surface

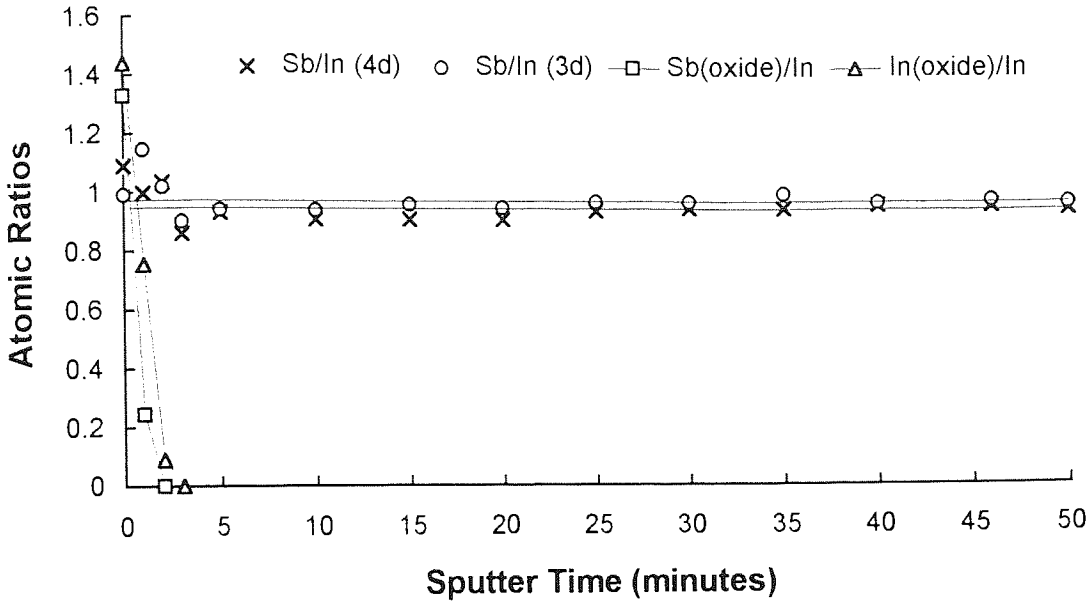

(a) Compositional changes in InSb surface during Ar^+ beam bombardment

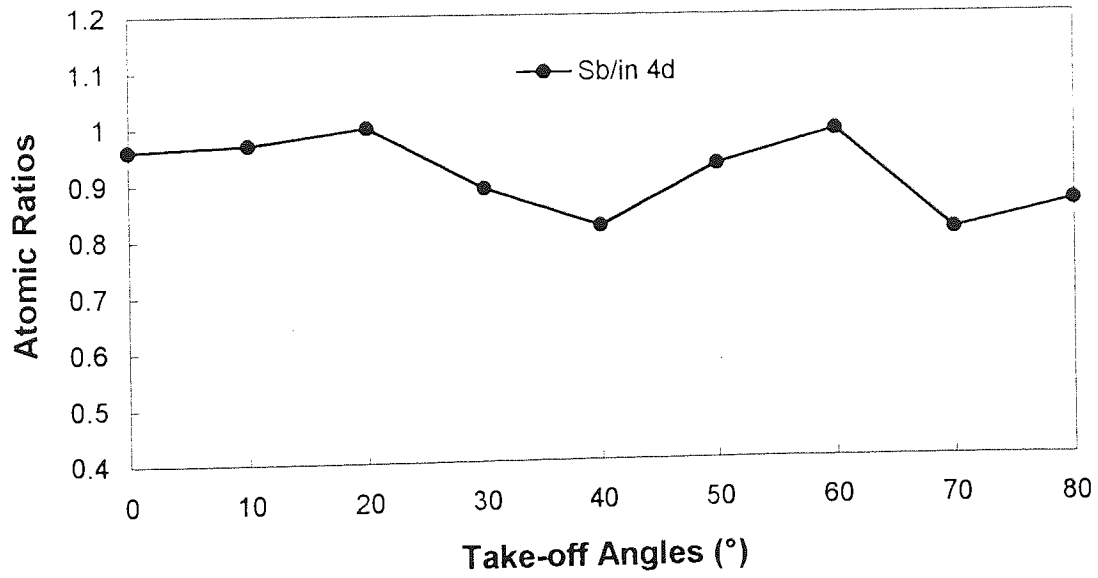

(b) ARXPS analysis of ion bombarded InSb surfaces

Figure 4.28 Ion bombardment effects in InSb surface observed by XPS

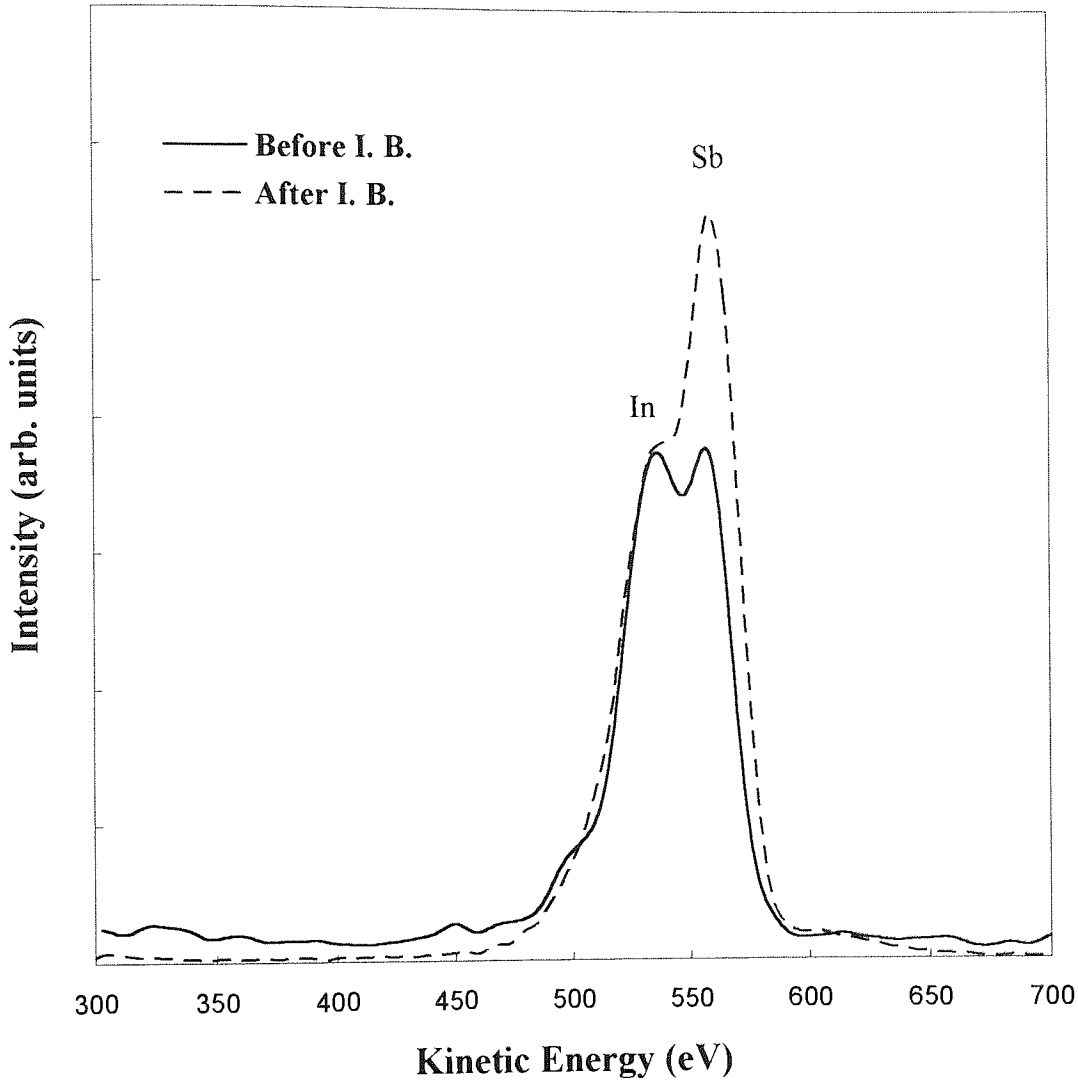

Figure 4.29 Ne ISS analysis of InSb surfaces before and after ion bombardment

period of 50 minute Ar ion beam bombardment is given in Figure 4.28a. The Sb/In atomic ratio measured from In and Sb $3d_{5/2}$ signals showed a slight increase after about 1 minute sputtering, but that measured from In and Sb 4d signals shows a decrease in Sb/In ratio, this variance is obviously due to the difference in the sampling depth between the 3d and 4d core electrons, indicating a slightly Sb-rich thin layer existing between the oxide layer and InSb crystal surface. The formation of such layer is probably because of preferential oxidation of In in air. When the contamination layer (mainly oxide) was completely removed after about 3 minutes of sputtering, the Sb/In atomic ratio indicated by both core electrons are about identical to 1. The ratios then decrease slightly as the sputter time. After about 10 minutes sputtering, the Sb/In ratio indicated by both 3d and 4d signals reached to steady state, the ratio presented by 4d electrons is about 0.92, and that presented by $3d_{5/2}$ signal is about 0.95. Based on the principle of KRXPS described in Section 2.4.3, this difference may imply a Sb enrichment at the outermost layer of the ion bombarded InSb surface.

ARXPS was also performed in analysis of ion bombarded InSb surfaces, the results are shown in Figure 4.28b. It is probably because of the roughing effects, the ARXPS investigation did not provide meaningful evidence showing the compositional distribution.

LEISS

The as received InSb surface was analysed by Ne^+ ISS technique after a few minute sputtering using 2keV Ne^+ beam with a beam current of about 0.5μA to remove the oxide layer. The corresponding spectrum is shown by the solid curve in Figure 4.29. Although In and Sb have very small difference in mass, the In and Sb scattered peaks were identified clearly by using Ne ion as a probe and are seen clearly at KE of 532 and 556eV synthesis, respectively. Quantitative analysis by peak synthesis indicated that the atomic ratio of Sb/In is 1.02, that is, the outermost layer of InSb sample surface prior to Ar ion bombardment was highly stoichiometric.

The Ne^+ ISS spectrum taken from the InSb surface after Ar ion bombardment is presented by the dashed curve in Figure 4.29. A dramatic increase in Sb peak can be clearly seen. The areal ratio of Sb to In component obtained from peak synthesis is about 1.6, so the Sb/In atomic ratio may be calculated from Equation 2.30, which is about 1.63. This is clear that Sb enrichment in the InSb surface took place during the ion bombardment.

4.5.9. CdSe

XPS

XPS analysis of the as received CdSe surface was conducted. Since the surface has been exposed in atmosphere for a very long time (probably over 10 years), it was heavily contaminated mainly by carbonaceous species, the C/Cd ratio measured with XPS at TOA of 80° is as high as 33.2. Figure 4.30a shows the Cd 4d and Se 3d spectra taken at 0 and 80° from the as received CdSe surface.

In the Cd 4d spectrum, the primary peak at BE of 10.4eV is attributed by the Cd atoms in the CdSe matrix, the small peak at BE of 9.3eV is due to the Cd in Cd oxide, more likely, CdO, which means that the binding energy of the core level electrons of an atom in oxidation state or ionic charge is lower than that in a free atom or metallic atom. This extraordinary feature has been explained by Gaarenstroom and Winograd's theoretical calculation [1977], in which the effects of extra-atomic relaxation are considered. In fact, similar phenomena have also been found in many systems, such as ionic compounds of IIa Group elements.

The Se 3d spectrum implies a more complicated surface chemistry in the CdSe surface. The Se 3d at 80° TOA shows that the Se atoms were found in three different chemical states. The major peak at BE of 53.4eV represents Se atoms in CdSe matrix. According to the analysis for pure Se surface (see Section 4.2.2), the should peak at BE of 55.1 is corresponding to the elemental selenium. A small peak at BE about 57.9eV may be due to Se atoms in oxidation states. Because the histories of the sample preparation and storage were unknown, the theoretical investigation of the as received CdSe surface was impossible. The sample surface was also very dirty and not flat (sample was cleaved from the lump CdSe), which makes the systematically angular analysis difficult. For this reason, the sample surface was polished using the procedure described in Chapter 3, and then washed by ultrasonic bath in methanol, finally, rinsed in the deionised water and dried in air within a very short time.

The polished CdSe surface was very clean with almost no chemical adsorption found in either Cd 4d or Se 3d spectra. The results of ARXPS analysis of the polished CdSe surface are given in Figure 4.30b. In the figure, the atomic ratios of Se/Cd, O/Cd and C/Cd are plotted versus the electron take-off angles. The C and O contamination levels were significantly reduced, but still found in the surface. These are mainly due to the physical adsorption of the molecules of the organic solvent and also may come from the slight oxidation in air (even this can not be identified in XPS analysis). The Se/Cd ratio at 0 TOA was 0.98. The elemental distribution was homogeneous but may

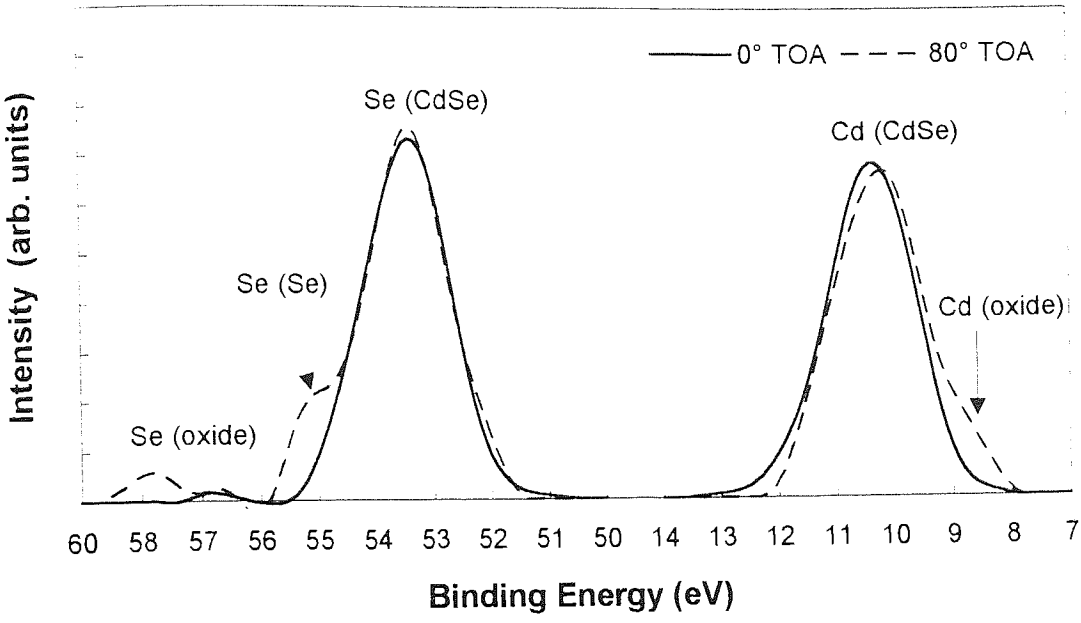

(a) Se 3d and Cd 4d spectra

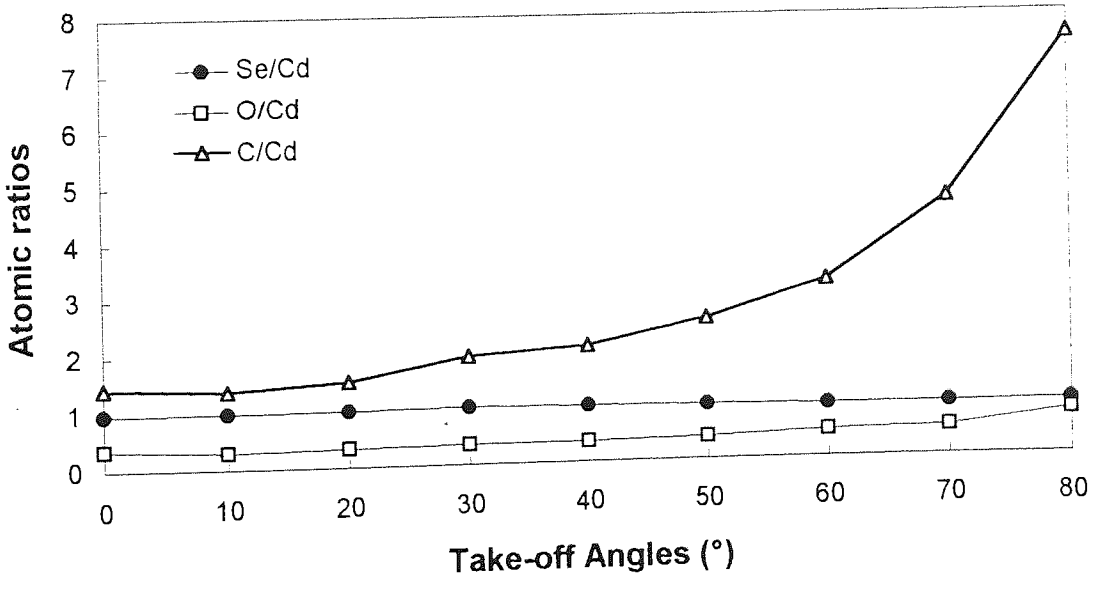

(b) Se/Cd, O/Cd and C/Cd variations versus electron take-off angles

Figure 4.30 ARXPS analysis of as received CdSe surface

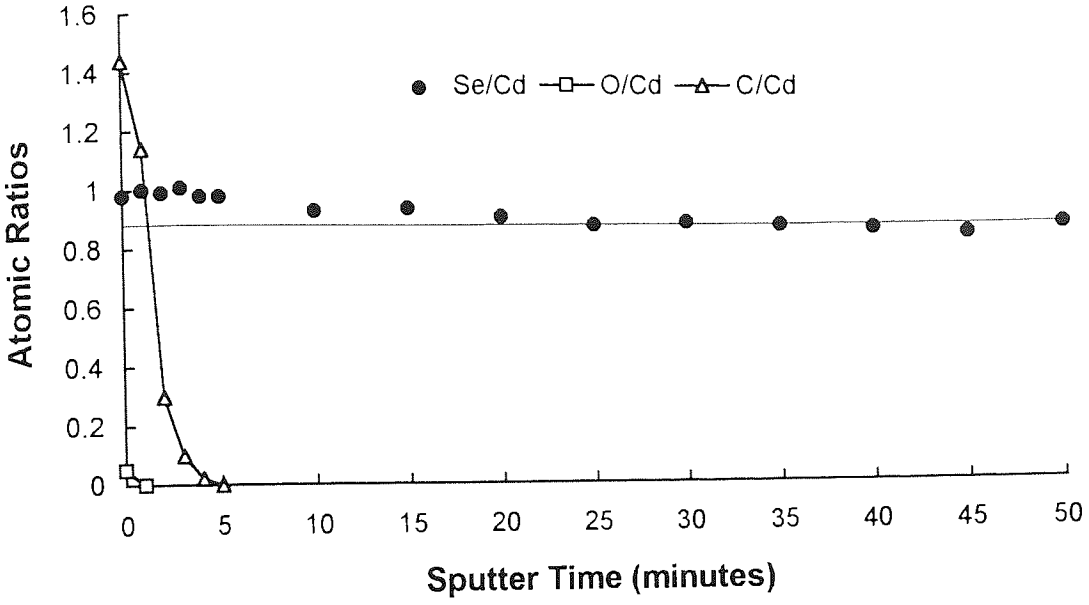

(a) Compositional changes in CdSe surface during Ar^+ beam bombardment

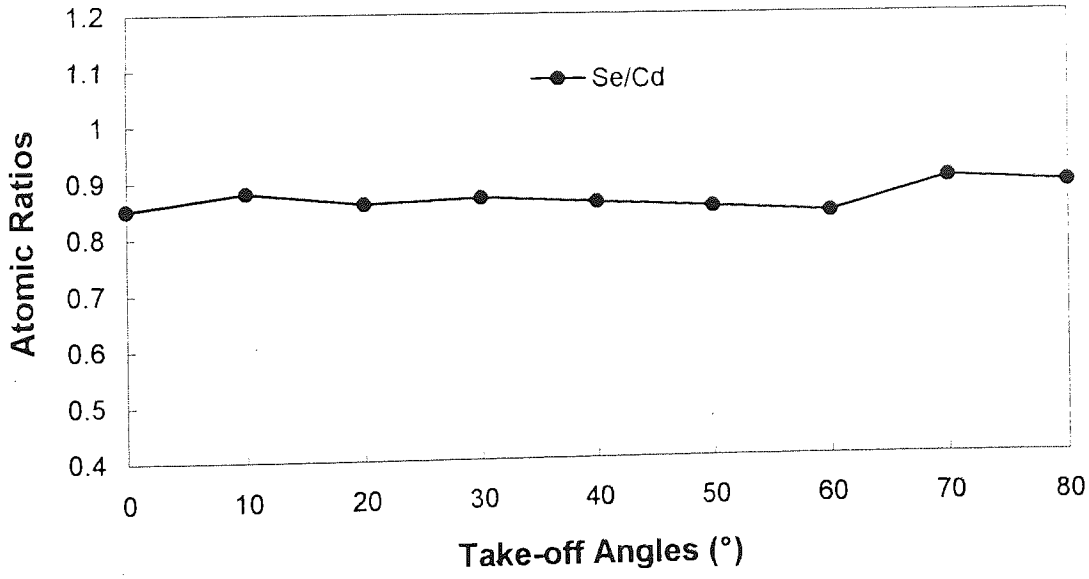

(b) ARXPS analysis of ion bombarded CdSe surfaces

Figure 4.31 Ion bombardment effects in CdSe surface observed by XPS

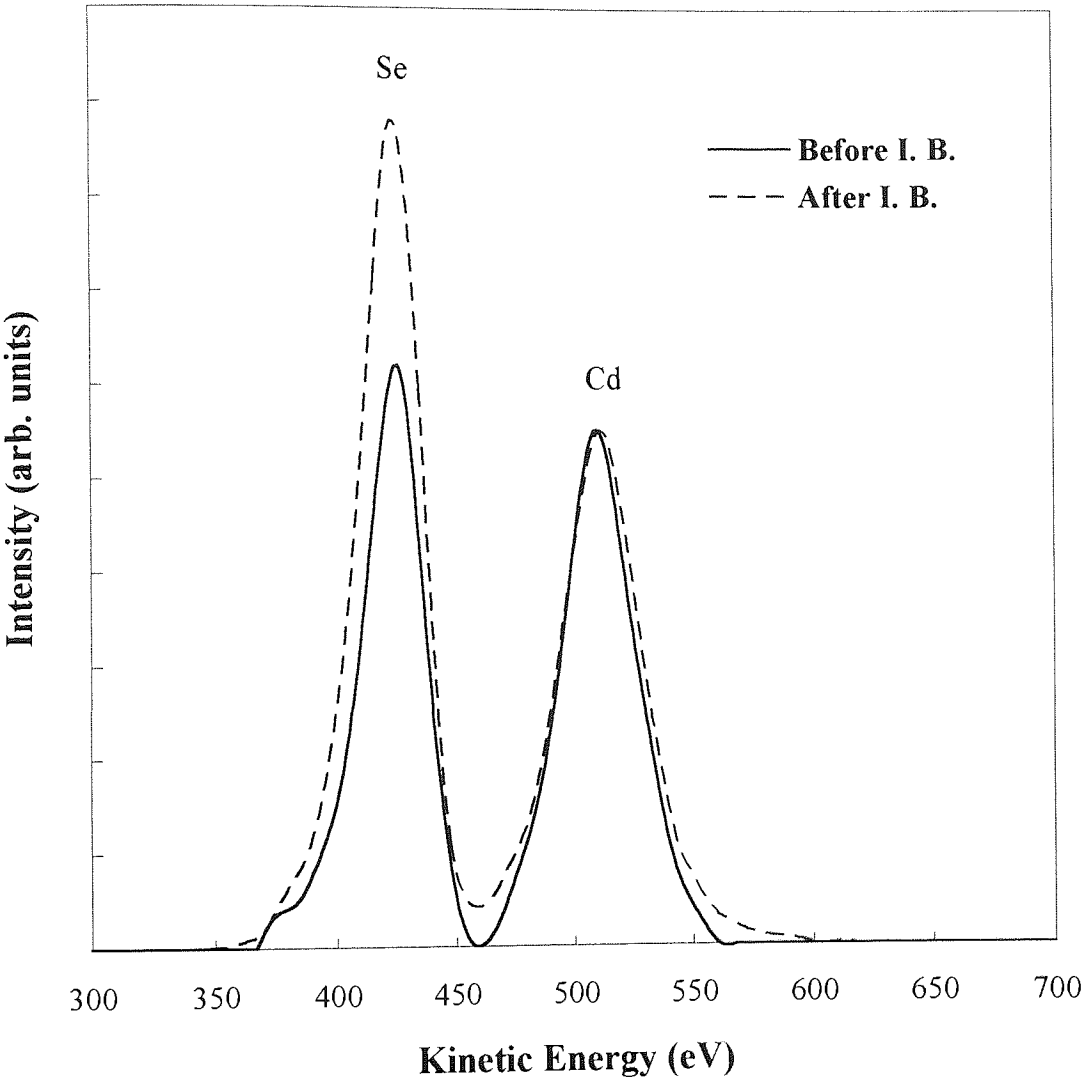

Figure 4.32 Ne ISS analysis of InSb surfaces before and after ion bombardment

decreased slightly to 0.95 at the very surface. This is probably because of the sublimation of small amount of the Se oxide formed during the air exposure, since Se oxides has very high vapour pressure [Ebina *et al.*, 1980].

The polished CdSe surface was bombarded by a 3keV argon ion beam for up to 50 minutes. The changes of the Se/Cd, O/Cd and C/Cd atomic ratios in the CdSe surface measured with XPS are shown in Figure 4.31a. The O signal disappeared after 1 minute sputtering, and the carbonaceous layer was completely removed after the first 4-5 minute of sputtering. The Se/Cd ratio decreased within the first 10 minute sputtering, then it approached a value of 0.87.

The results of ARXPS analysis of the bombarded CdSe surface are presented in Figure 4.31b. Although certain errors were involved in the measurements, ARXPS showed that the Se/Cd ratio at 80° was about 0.92, indicating that the selenium concentration may increase at the outermost atomic layers of the ion bombarded CdSe surface.

LEISS

The Ne^+ ISS spectrum obtained from the polished CdSe surface before Ar^+ bombardment is presented in Figure 4.32, indicated by the solid curve. The Cd and Se scattered peaks in the spectrum are found at kinetic energies of 510 and 426 eV, respectively. The Cd peak appears wider than Se one, this is obviously because Cd has more isotopes in nature than Se. The areal ratio of Se to Cd peak is about 0.92, so the Se/Cd atomic ratio calculated from Equation 2.30 is 0.94, indicating that the outermost layer of CdSe surface before ion bombardment was nearly stoichiometric.

After 50 minute Ar ion bombardment, the surface was re-examined with LEISS. The ISS spectrum taken from the bombarded CdSe surface is indicated by the dashed curve in Figure 4.32 and normalised to the Cd peak to show the ion bombardment effects. A significant increase in Se peak can be observed. Quantitative analysis indicates that the Se/Cd atomic ratio at the first atomic layer of the bombarded CdSe surface reaches 1.32. This means that ion bombardment results in the Se enrichment at the outermost atomic layer of the CdSe single crystal surface.

4.5.10. Concluding notes

Although chemical analysis is not the major concern in this project, it is still very important to gain knowledge on chemical bonding in the compound semiconductor systems to provide valuable information for theoretical studies.

Compared with pure Si and Ge samples, XPS analysis of the GeSi surface showed that there was no binding energy shift in Ge 3d and Si 2p peaks, indicating that GeSi is a perfect covalent compound. On the contrary, a big shift of 1.7eV in BE of Se 3d peaks observed in XPS from CdSe and pure Se surfaces suggested that CdSe is a more ionic system. The binding energy shift of Cd 4d in CdSe (about 0.5eV), however, was not as big as Se 3d, this may be due to the extra-atomic relaxation effects, similar to that in CdO (see Section 4.5.9).

For the six III-V compounds, the transition of bonding may be more clearly seen The binding energies of Ga 3d, In 4d, P 2p, As 3d and Sb $3d_{3/2}$ in different compound systems, are listed in Table 4.11. The BE shifts of Ga 3d in GaP, GaAs and GaSb vary from 1.3, 0.9 to 0.5eV, this implies that from Ga-P to Ga-Sb the ionic characteristics in the bonding are diminished. Similar conclusions may be reached for the In compounds. This is an important point to be taken into account in calculation of the surface binding energy in sputtering. The discussion on this topic is continued in Chapter 5.

Table 4.11 Binding energies of Group III and V elements in different states

(referred to C 1s at BE of 284.6eV)

	Oxide	P 2p	As 3d	Sb 3d3	Element
Oxide		134.1	44.8	539.6	
Element		130.0	41.8	537.4	
Ga 3d	20.4	129.3 19.5	41.1 19.1	537.3 18.7	18.2
In 3d5	445.1	128.5 444.3	40.6 444.1	536.9 444.0	443.9

In this summary of experimental work, it should be said that XPS has been applied successfully in quantitative analysis of the eight compound semiconductor samples. Based on the reference data obtained from the calibration work in this project, the surface structures of all the compound semiconductors and GeSi alloy prior to ion bombardment were revealed by the ARXPS technique, the surface composition beneath the contamination overlayer in all samples was found to be close to their stoichiometric value. This provided a good starting point for studying ion bombardment effects. For al samplesl studied, the compositional changes during the period of sputtering were clearly observed by XPS. The modifications on the compositional distribution have also been investigated by ARXPS and KRXPS.

In XPS analysis, the experimental errors come mainly from the two sources: (1) calibrations for elemental samples. Since it is impossible to obtain an absolutely pure surfaces by sputter cleaning, the intensities given in Table 4.2 generally contain relative errors in an order of 1 to 2%. For some elements, like Ga, the errors could be as large as 5%. Since the intensities are always underestimated, this effect may be reduced by taking relative atomic ratios. (2) In ARXPS experiments, mechanical precision in angular movement may introduce significant errors in high TOA measurement. According to Equation 2.20, the variation of photoelectron intensity due to the angular error of sample rotation can be estimated by:

$$\left|\frac{\Delta I}{I}\right| \propto \left|\frac{\sin\theta}{\cos^2\theta}\right| \cdot |\Delta\theta| \tag{4.6}$$

Assuming sample rotation can be controlled within an angular error of ±1°, the relative errors in measurements of photoelectrons at TOA from 0° to 80° can be may be estimated from Equation 4.6, which are listed in Table 4.12:

Table 4.12 Relative errors of photoelectron intensities at various TOAs (Δθ=0.5°)

TOA(°)	0	10	20	30	40	50	60	70	80
dI/I (±%)	0.01	0.2	0.3	0.6	1.0	1.6	3.0	7.0	28.5

It may be seen that at TOA of 80°, the relative errors of measured intensity due to angular adjustment can be as large as about 30%.

During ion bombardment, the crystalline structure in surface of a single crystal compound semiconductor may be destroyed [Malherbe and Barnard,1991] and cannot be restored without a high temperature annealing process (see Section 1.2.4), thus the crystallographic should not influence ARXPS analysis of the ion bombarded surfaces. However, the roughing effect due to ion bombardment may result in that the surfaces are no atomically flat and not ideal for ARXPS analysis. In addition, the photoelectrons refraction and reflection at surfaces at higher TOAs may also cause significant errors in ARXPS measurement [Fadley, 1976]. These may be the main reasons that for some samples, such as GaP, GaAs, GaSb, InSb and CdSe, ion bombardment modification on the compositional distribution were not obvious in ARXPS measurement. In the cases of GaAs and InSb, these difficulties have been overcome by using KRXPS. In studying ion bombarded GaAs and InSb surfaces, KRXPS clearly show that As and Sb segregation has occurred at the outermost layers. For the other samples, KRXPS technique, unfortunately, is not applicable since no adequate core level signals are available.

Thanks to the success of calibration work, LEISS has also been used successfully in quantitative analysis on most of sample surfaces. Combined with XPS analysis, the

changes of compositional distribution in the ion bombarded compound semiconductor surfaces have been observed clearly, this provides much valuable evidence for theoretical work.

In LEISS analysis, the errors in quantification may come from several aspects of LEISS experiments, but mainly from the calibration. Since LEISS experimental results are so sensitive to the conditions of the first-layer atoms at surface, the contamination from the residual gas species is important, such as O at Si sample surface. Most of the reference samples are amorphous, although the surfaces were well polished, the flatness may be still not as good as that of crystal surface. Differences in chemical states between elemental sample and compound, such as pure In and InP, may result in the differences in the ion survival probability, surface electrical conductivity (surface charging), atomic size (shadowing and blocking effects), ion-atom collision crossection *etc.*, these may be the major contribution to the experimental errors. To theoretically calculate the errors in LEISS is difficult, the repeat measurements showed that the total errors for most clean samples are in range from 5% to 10%.

Since no reference data of P was available, the calculated sensitivity factor for P may contain greater errors. Another factor influences the accuracy in quantifying InP and GaP data is that P in both sample is partially negatively charged, when positive He ions interact with P atoms, they are experienced bigger chance of neutralisation, thus the ion survival probability for He^+ ions scatterd at P atoms is smaller than that calculated from Equation 2.28 or 4.4. This leads to the underestimation of P/Ga and P/In ratios in LEISS analysis. Indeed, Barcz *at al.* [1980] did not observe compositional changes in GaP and InP surface after ion bombardment by LEISS.

In addition, for all the as-received compound surfaces, the contamination layers due to air exposure make LEISS technique impossible to be performed. Some cleaning procedures had to be used, this may cause a slight modification to the original surface composition, but these procedure were carried out so carefully that the modification are much less significant than those caused by ion bombardment.

Chapter 5 Ion Bombardment Effects in Compound Semiconductor Surfaces

5.1. Introduction

Based on the data obtained from XPS and LEISS experiments, ion bombardment effects in surfaces of the compound semiconductors and GeSi alloys are discussed extensively in this chapter. At the beginning, the projected ranges of 3keV Ar ions in GeSi, GaP, GaAs, GaSb, InP, InAs, InSb and CdSe are estimated by computer simulation using the TRIM code (see Section 1.4.2). This gives an indication of the depth to which surface modifications take place. Comparing this with sampling depth of LEISS and ARXPS provides a foundation for later discussions on ion bombardment effects. In the following two subsections, two different models are discussed. Sigmund's linear collision cascade theory and a model based on Gibbsian surface segregation and diffusion induced by ion bombardment. Some aspects of the theoretical models, including the scattering parameter, origin of sputtered particles, surface binding energy in Sigmund's theory, the surface free energy in crystalline solids, the function of ion bombardment in surface segregation, differences between surface segregation and diffusion, *etc.*, are also addressed. Finally, a hypothesis describing ion bombardment effects in compound semiconductor systems is proposed and the results from the XPS and LEISS observation of compositional changes in the ion bombarded semiconductor surfaces are interpreted in terms of this model.

5.2. Range of ion beam radiation and depth of XPS and LEISS measurement

Before evaluation of the XPS and LEISS results and discussion of ion bombardment effects in a solid surface, it is important to know the projected range of energetic ions which is related to the depth of ion beam damage and the detection depth of the surface analytical techniques used for the observation of the effects. The latter question is the easier to answer. The answer to the former question is not so straightforward, since there is no convenient experimental or analytical method to measure the penetration depth of the energetic ions in a solid and the distribution of recoils. A computer simulation using TRIM code has been utilised in this project for this purpose.

5.2.1. Ion projected range and recoil distributions in the compound surfaces

Using the TRIM code (see Section 1.4.2), the projected ranges of 3keV Ar ions at an incident angle of 51° in GeSi, GaP, GaAs, GaSb, InP, InAs, InSb and CdSe surfaces were calculated. These, together with nuclear and electronic stopping powers, are listed in Table 5.1. Two important features are immediately obvious from the table. First, nuclear stopping is the predominant mechanism for the energy loss of the 3keV Ar ions in these compound systems. Secondly, since the energy transfer from an incoming ion to lighter target atom is less than that to heavier atom, the ion projected range in low-mass target is longer than that in high-mass one. In another word, heavier mass target atoms have greater stopping power than the lighter ones to the incoming ions.

Table 5.1 Nuclear, electronic stopping powers, ion projected range and recoil depth in the eight compound semiconductor systems

A-B	GeSi	GaP	GaAs	GaSb	InP	InAs	InSb	CdSe
N. St. (eV/Å)	17.2	44.1	46.4	36.6	36.0	38.6	31.8	39.1
E. St. (eV/Å)	4.5	5.6	6.9	6.8	5.4	6.7	6.5	6.0
Ion range (Å)	48	33	26	28	33	26	28	26
Recoil depth (Å)	88	97	81	91	110	87	96	87

Ion bombardment damage in solid surfaces, however, depends not only on the behaviour of the ions, but also on that of recoils. In the low energy regime, since collisional cascades between recoils are the major events, surface damage may be influenced by recoils more than ions. This can be understood more easily from the depth distributions of the argon ions and recoils in the semiconductor systems as shown in Figure 5.1. These were obtained by simulating 10,000 Ar ions bombarding the semiconductor surfaces at an incident angle of 51°. The figures indicate two important facts: (1) the number of recoils is about 20 times greater than that of the incident ions, implying that the collision cascade, rather than the direct ion-atom interaction plays the more important role in modification of surface composition. (2) under the above conditions, ion beam induced damage is limited generally to a depth of about 100Å (except InP), and the maximum modification may take place in a range from 15 to 25Å. Here, we defined *recoil depth* as a depth, beyond which the number of the recoils is less than 5% of its maximum value. The recoil depth for the eight semiconductor compound systems have been given in Table 5.1. It may be seen that recoil depth is not entirely dependent on incident ion projected range, the reason is that ion projected range depends only on the stopping (nuclear and electronic) of the target materials to the ions; but the recoil depth also depends on that of the recoils.

5.2.2. Sampling depth of LEISS and XPS

As discussed in Chapter 2, the detection depth of LEISS using noble gas ions is generally limited to the first atomic layer no matter which material is studied. For XPS, however, the sampling depth can be changed, depending on kinetic energy and take-off angles of photoelectron detected, and the surface matrix of the target materials. All these factors have been included in Seah's formula [Seah and Dench, 1979], i. e., Equation 2.5. The average sampling depth at electron take-off angles of 0° and 80° used in these XPS measurement are given in Table 5.2. For GaAs and InSb, two different core level signals, that is, $2p_{3/2}$ and 3d lines for GaAs; and 3d and 4d lines for InSb, have been taken to allow the KRXPS technique to be applied. The advantages of this technique have been discussed in detail in previous chapters by comparison with ARXPS.

Table 5.2 Sampling depth (in Å) used in XPS analysis

TOA (°)	GeSi	GaP	GaAs*	GaSb	InP	InAs	InSb*	CdSe
0	68	68	67/29	75	75	73	79/65	72
80	12	12	12/5	13	13	13	14/11	13

* The first numbers are the sampling depth calculated from 3d lines for GaAs and 4d lines for InSb; the second ones are those from $2p_{3/2}$ for GaAs and $3d_{5/2}$ for InSb

Comparing Tables 5.1 and 5.2, it may be seen that the XPS measurements at 0° TOA sample almost the entire depth of the bombardment damaged region, whereas at 80° TOA the sampling depth of XPS is limited to the first 4-5 atomic layers.

It is also clear that although the surface sensitivity in XPS analysis can be enhanced by electron take-off angle, it is still not competitive with that of LEISS, this is the main reason that ARXPS results may not always agree with LEISS analysis, especially in studying a compound surface where there are no dramatic changes in compositional distribution in the first few atomic layers.

5.3. Linear collision cascade theory

5.3.1. Determination of the scattering parameter m for low energy sputtering

In Section 1.4.2, it has been mentioned that the nuclear stopping power developed by Ziegler and Biersack using a universal interatomic potential (so-called *ZBL nuclear stopping power*) has been proved to be more realistic than that derived from Thomas-Fermi inter-atomic potential (*T-F nuclear stopping power* for simplicity) in the description of atomic collisions in a solid, specially for low energy ion sputtering.

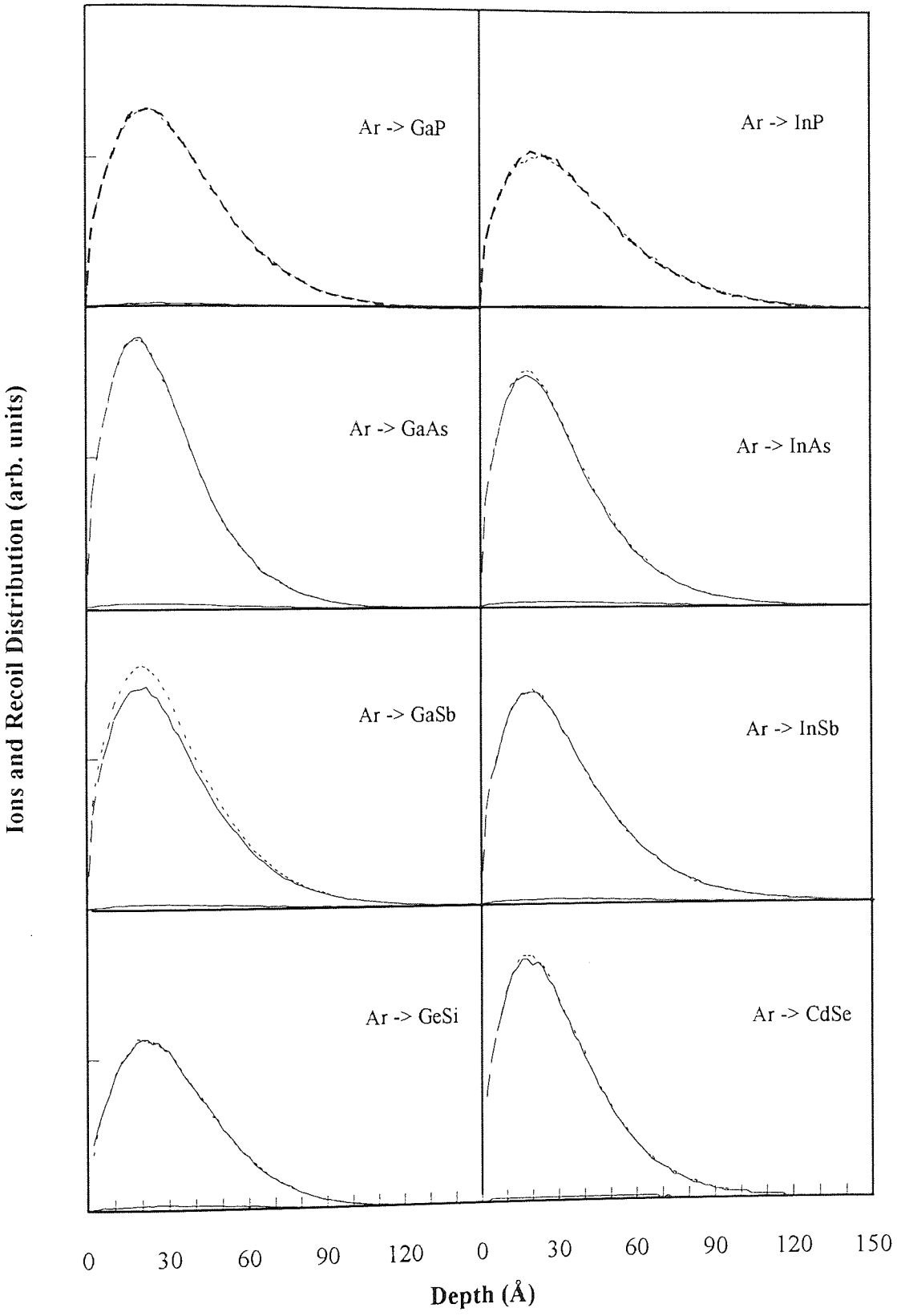

Figure 5.1 Ion and recoil distribution in 3keV Ar^+ ion bombarded compound semiconductor surfaces

However, because of the simplicity of the mathematics, the Thomas-Fermi model is still used in Sigmund's linear collision cascade model for theoretical analysis. An expedient to improve the accuracy of TF model is to monitor a physical parameter experimentally, such as the sputtering yield or the surface concentration, and to choose the scattering parameter m in Equation 1.23 or 1.44 to give the best fit between theoretical predictions and experimental results. For example, Malherbe *et al* [1986] found that the compositions of ion bombarded oxide surfaces may be predicted more accurately using Equation 1.44 if m=0.165 is selected. This indirect method of determining the scattering parameter m, however, is somewhat misleading since many other uncertainties in the models may also influence experimental results.

Since the scattering parameter m in TF model represents the magnitude of the nuclear stopping power, it may be more appropriate to choose m by directly comparing the TF nuclear power to ZBL one. To do this, it is convenient to use the concept of the reduced energy ε, which has been defined in Equation 1.69. From Equation 1.8 and 1.11, TF nuclear stopping power, i.e. Equation 1.12, can be simply rewritten as:

$$S_{TF} = \frac{1}{2(1-m)} \lambda_m \varepsilon^{1-2m} \qquad (5.1)$$

here λ_m varies with m from 0.5 (m=1.0) to 24 (m=0). The exact mathematical relationships between λ_m and m are unknown, but some values of λ_m from various authors determined by semi-empirical methods have been tabulated by Sigmund [1981], and these are listed in Table 5.3

Table 5.3 Values of λ_m and m [Sigmund, 1981]

m	1.0	0.5	0.333	0.192	0.055	0.0
λ_m	0.5	0.327	1.309	2.92	15.0	24.0

From the above data, a mathematical relationship between λ_m and m may be found easily by regression analysis, that is:

$$\lambda_m = 24.108 - 198.782m + 563.956m^2 - 520.72m^3 \qquad (0 \le m \le 0.4) \qquad (5.2)$$

A graphic illustration for λ_m-m relation is shown in Figure 5.2. Substituting from Equation 5.2 into Equation 5.1, the TF nuclear stopping power can be compared with the ZBL one which has already been described by Equation 1.68a. Figure 5.3 shows that the comparison between the ZBL nuclear stopping power and that of TF for m=0 to 0.3.

For the semiconductor samples bombarded by 3keV Ar ions, the screening radius and the reduced energy for the different elements calculated from Equation 1.66 and 1.69 are listed in Table 5.4. It may be seen that for different elements with different

reduced energy, a different scattering parameter m should be used. For example, for Si (ε =0.045) and P (ε=0.042), the reasonable values of m should be 0.20 and 0.19, respectively; For Ga, Ge, As and Se, m=0.16, will be adequate; but for Cd, In and Sb, m=0.14 should be chosen.

From the above analysis, it is clear that Equations 1.41 and 1.44 are not strictly valid for the prediction of surface composition for a system in which the elements have considerable differences in mass. From this point of view, the model proposed by Malherbe *et al.* [1986] for sputtering of oxides is not based on sound physical principles, since the mass differences between metal cation and oxygen anion in most oxides are significant, and the assumption that the scattering parameter m is the same for both metal cation and oxygen anion leads to confusion in the understanding of Sigmund's linear collision cascade theory, although the model has been used quite successfully in some cases.

Table 5.4 The screening radius and the reduced energy
for different combination of argon ion (Z_1=18, M_1=39.9) and the target atoms

Target Atom	Z_2	M_2 (amu)	a (Å)	E (keV)/ε	ε (E=3keV)
Si	14	28.1	0.124	68.0	0.045
P	15	31.0	0.123	73.0	0.042
Ga	31	69.7	0.113	114.3	0.026
Ge	32	72.4	0.113	116.2	0.026
As	33	74.9	0.112	119.6	0.025
Se	34	79.0	0.112	121.0	0.025
Cd	48	112.4	0.107	161.0	0.019
In	49	114.8	0.107	163.5	0.018
Sb	51	121.8	0.106	169.2	0.018

5.3.2. Correction to the nonstoichiometric sputtering model

If we take account of the difference in the power scattering parameter for the elements with different mass and still use Thomas-Fermi nuclear stopping power, that is Equation 1.12, to describe ion-atom interaction, Equation 1.40, the ratio of partial sputter yields derived from Sigmund linear collision cascade theory [Sigmund, 1981] should be written as:

$$\frac{Y_1}{Y_2} = \frac{x_1}{x_2} \cdot \frac{S_{21}(U_2)}{S_{12}(U_1)} = \frac{x_1}{x_2} \cdot f \cdot \left(\frac{M_2}{M_1}\right)^{m_1+m_2} \cdot \frac{U_2^{1-2m_2}}{U_1^{1-2m_1}} \qquad (5.3)$$

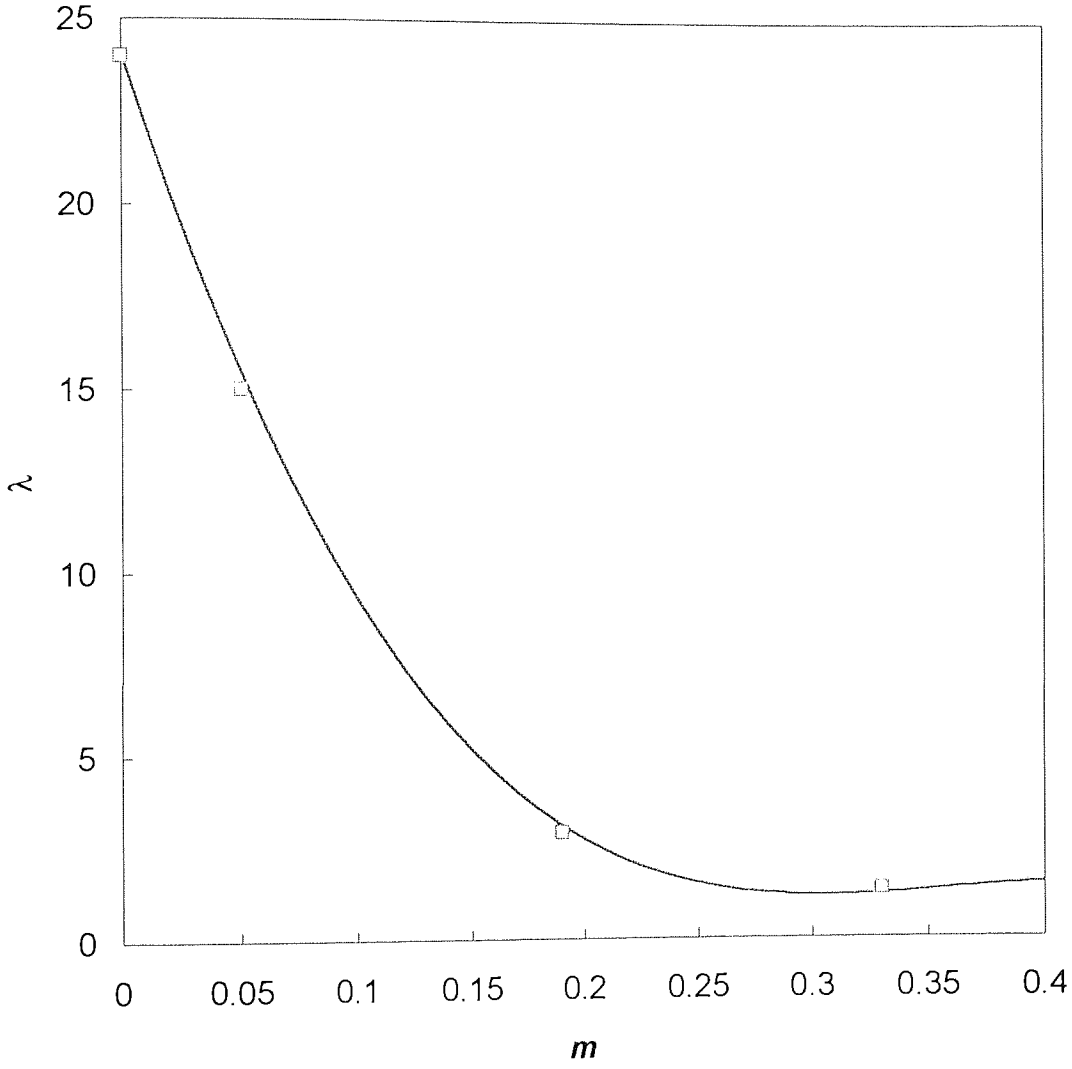

Figure 5.2 λ_m - m **curve**

$$\lambda_m = 24.108\text{-}198.782m\text{+}563.956m^2\text{-}520.72m^3$$

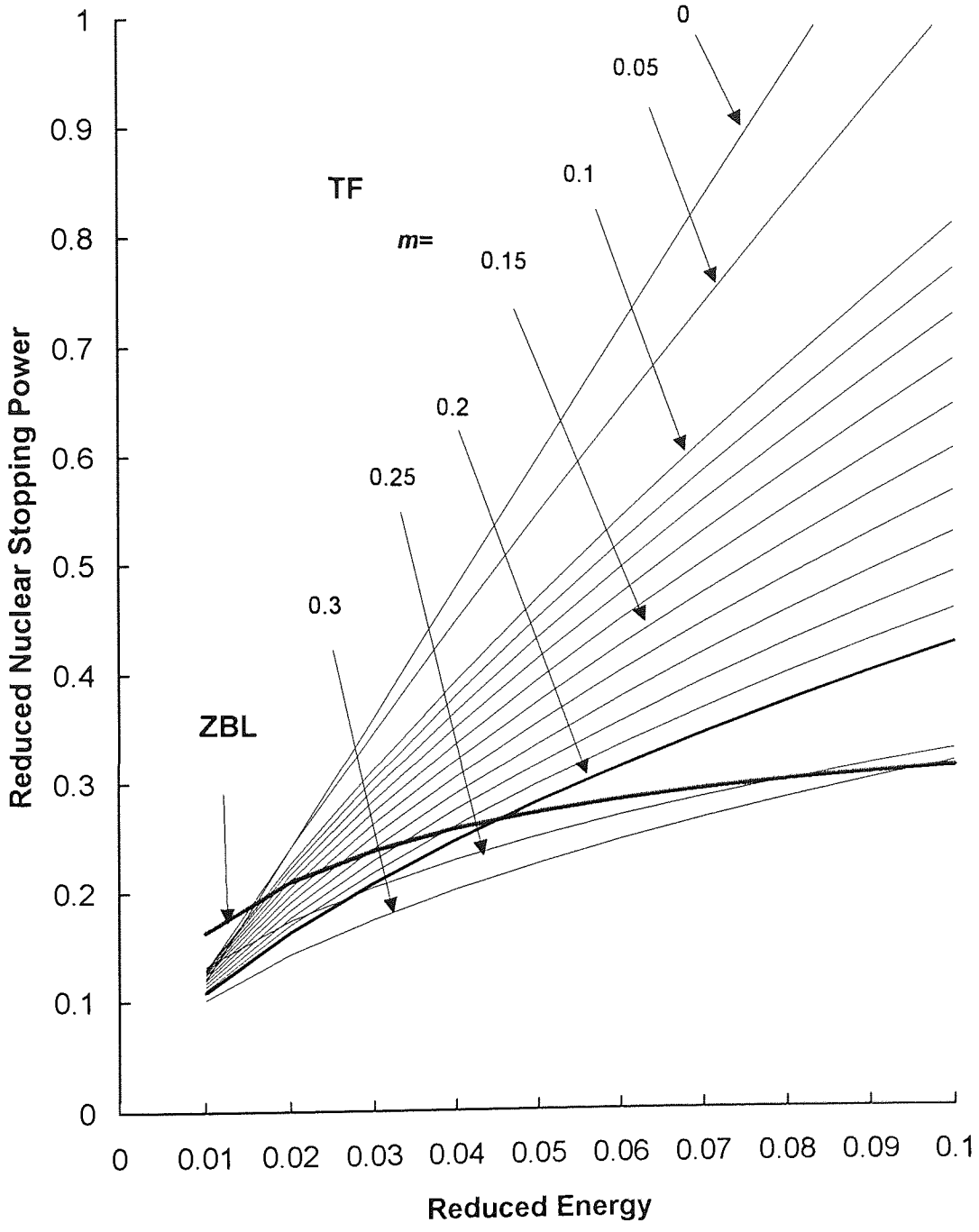

Figure 5.3 Comparison between ZBL and TF nuclear stopping power

here f is the correction factor which is expressed as:

$$f = \frac{1-m_1}{1-m_2} \cdot \frac{\lambda_{m_2}}{\lambda_{m_1}} \cdot (2Z_1Z_2e^2/a)^{2(m_2-m_1)} \cdot [\frac{4M_1M_2}{(M_1+M_2)^2}]^{-(m_2-m_1)} \qquad (5.4)$$

here the screen radius a is estimated from Equation 1.66. The surface atomic ratio for a binary system can be then calculated from:

$$\frac{(x_2/x_1)^s}{(x_2/x_1)^b} = f \cdot (\frac{M_2}{M_1})^{m_1+m_2} \cdot \frac{U_2^{1-2m_2}}{U_1^{1-2m_1}} \qquad (5.5)$$

For the elements with neglect mass differences, that is m_1 equals m_2, f is 1, and Equation 5.5 is reduced to Malherbe's model, e.g. Equation 1.44. But for those having considerable differences in mass, an error may be introduced by ignoring the factor f.

The values of the correction factor for the eight semiconductor compounds calculated from the Equation 5.4 have been listed in Table 5.5. The scattering parameter m are selected as 0.2 for Si, 0.19 for P, 0.16 for Ga, Ge, As and Se, and 0.14 for Cd, In and Sb. The corresponding λ_m values are calculated from Equation 5.2. From Table 5.5, it may be seen that for the lighter elements having the greater mass differences in a compound, for example GeSi alloy, ignoring the factor f may introduce significant errors.

Table 5.5 Correction factors for the eight compound semiconductor systems

	GeSi	GaP	GaAs	GaSb	InP	InAs	InSb	CdSe
f	0.92	0.94	1.0	0.98	0.96	1.02	1.0	1.02

5.3.3. Calculations of surface binding energies for compound semiconductors

The surface binding energy for different elements in compounds is another important factor in the Sigmund linear collision cascade theory in the determination of surface compositional changes. On this topic, it is convenient to consider three general extreme types of chemical bond formed between elements in a binary compound: *ionic*, *covalent* and *metallic bonds*. The different models for estimation to the surface binding energy were proposed to take account of the type of the compound. For example, the heat of sublimation was used simply for metallic alloys [Sigmund, 1969b] [Betz and Wehner, 1982]; but for ionic oxides and halides, the energies of ionisation, electron and ionic relaxation, and hole formation were considered [Kelly, 1987]. The compound semiconductors and GeSi alloys studied in this project, however, are generally categorised as covalent compounds, but with partially ionic character, so the bonds in this type of compound may be called partially ionic covalent bonds, or, more formally,

polar covalent bonds. This type of bonding structure has been analysed in detail using *linear combinations of atomic orbital* (LCAO) [Harrison, 1980], a more concise description was given by Pauling [1967].

In talking about the binding energy of a partial ionic covalent compound system, Pauling electronegativity is an important concept and is defined as a parameter that would allow the prediction of the approximate polarity of a covalent bond. To evaluate the electronegativity, Pauling [1967] assumed that when two different atoms A and B formed a covalent bond, if the electrons were shared evenly between A and B , the contributions of A and B to the bond A-B would be the same as those to a bond with like atoms, that is, A-A or B-B, the bond strength A-B would, therefore, merely be an average of the bonds A-A and B-B, which was called by Pauling a *normal covalent bond.* This is the *Pauling formalism* later used by Malherbe *et al.* [1986]. For convenience, Pauling expressed the estimation by the arithmetic mean rather than the geometric one, although the latter is obviously more accurate. In every actual binary compound consisting of unlike atoms, the strength of bond A-B appear to be greater than that of the corresponding normal covalent bond, Pauling ascribe this "excessive" bond strength to an extra ionic energy resulting from the difference of the atomic electronegativity. This is expressed as [Pauling 1967]:

$$\Delta = D(A-B) - \frac{1}{2}\{D(A-A) + D(B-B)\} \equiv (\varepsilon_A - \varepsilon_B)^2 \qquad (5.6)$$

where $D(A\text{-}A)$, $D(B\text{-}B)$ and $D(A\text{-}B)$ denote the energies of A-A, B-B, and A-B bonds, respectively; ε_A and ε_B are so-called *Pauling electronegativities* for atom A and B.

Malherbe *et al.* [1986] asserted that their models for calculation of binding energies of oxides, they are Equations 1.45 - 1.47, were developed essentially from Equation 5.6, unfortunately, there are two problems associated with it:

(1) According to Pauling's formalism, or Equation 5.6, $D(A\text{-}B)$ itself contains both covalent and ionic properties of the A-B bond. The appearance of the last term in Equations 1.45 and 1.46 is therefore misleading. This point can be seen clearly from the changes of bond strength of compound semiconductors listed in Table 5.6. The table shows that for Ga-P, Ga-As to Ga-Sb bonds, the strength changes from 2.39, to 2.18, to 1.99eV; which is about the same trend as the changes of differences in Pauling's electronegativity (0.5, 0.4, 0.3eV). Similar results may be found for indium compounds.

Even if the existence of this term were meaningful, its contribution to the binding energy should vary with the atomic concentration x and y, since the transitions between two bond types in a simple molecule, for example, from covalent to metallic bond or from covalent to ionic bond, can occur continuously. It can be seen that when x or y

approaches 0, Malherbe's model may give a wrong answer. When x=y=1, Equation 1.45 will not be reduced to Equation 5.6 as expected.

Table 5.6 Bond strength (eV) of diatoms at room temperature (25°C) [Lide, 1992a]

As-As	3.97	Ga-P	2.39	In-Sb	1.58
As-Ga	2.18	Ga-Sb	1.99	P-P	5.08
As-In	2.09	Ge-Ge	2.74	Sb-Sb	3.11
Cd-Cd	0.08	Ge-Si	3.13	Se-Se	3.46
Cd-Se	1.33	In-In	1.04	Si-Si	3.39
Ga-Ga	1.43	In-P	2.06		

(2) From the view point of quantum mechanics [Pauling, 1967], Equation 1.47 implies resonance between metallic state and ionic state, that is, a metallic bond with partially ionic properties. However, there is little evidence for a direct transition from the extreme ionic bond to the metallic bond in nature, this equation, or Malherbe's estimation of the binding energies of the metallic cations in metal oxides, is not physically meaningful. It was also not logical to consider the two atoms in one bond with different assumptions to the bond type, for example, in Equation 1.46, the bonding of oxygen anion in an oxide was treated as a covalent bond (with partial ionic properties), but in Equation 1.47, that of the metallic cation was considered as a metallic bond.

From the above discussion, the model proposed by Malherbe's *et al.* [1986] is not physically adequate in the calculation of surface binding energies for a compound system.

For an *AB* system, the binding energy of atom *A* in the solid can only come from two parts: interactions between like atoms, *A-A* and between unlike atoms, *A-B*. thus the average binding energy may be simply estimated using the pair-bond model proposed by William and Nason [1974]. This was originally used for calculation of the enthalpies of an ideal solution. Schematics of the pair bond model is illustrated in Figure 5.4. In their model, it is assumed that only the nearest neighbour take part in bonding. This approximation is generally reasonable for most simple solids with short-range interactions, since the interatomic potential function ϕ can be estimated from Lennard-Jones formulae[Tu *et al.* 1987]:

$$\Phi(r)=\left[\left(\frac{a_0}{r}\right)^{12}-2\left(\frac{a_0}{r}\right)^{6}\right] \tag{5.7}$$

where r represents the interatomic separation; ε_b is the minimum potential energy; a_0 the equilibrium distance ($r=a_0$, $\phi(r)= -\varepsilon_b$). When r equals $2a_0$, the potential energy changes by a factor of 32, the interaction energy beyond nearest neighbours may be ignored without introducing significant errors.

Following the William and Nason pair bond model and using the bond strengths of *A-A*, *B-B* and *A-B* bonds to replace the corresponding enthalpies in the model, a simple model for estimating the average surface binding energy in a certain layer may be developed, stepwise as follows:

$c_{A,B}$ are the concentrations of atoms *A* and *B* in one layer of *AB* system, $c_A + c_B = 1$.

$Z_{l,v}$ are the numbers of lateral and vertical bonds, respectively.

$D(A\text{-}A)$, $D(A\text{-}B)$ and $D(B\text{-}B)$ are the bond strengths of *A-A*, *A-B* and *B-B*.

For the nearest bonds in the layer:

$c_A Z_l$ is the number of lateral bonds associated with element *A* (similar for element *B*).

$\frac{1}{2} c_A c_A Z_l$ is the number of lateral *A-A* bonds, ½ included here is due to each *A-A* bond being counted twice (similar for *B*) .

$\frac{1}{2} c_A c_A Z_l D(A\text{-}A)$ the total bond energy due to *A-A* bonds.

$c_B c_A Z_l$ is the number of lateral *A-B* bonds.

$c_B c_A Z_l D(A\text{-}B)$ is the total energy due to *A-B* bonds.

For the vertical bonds:

$k c_A Z_v$ is the number of vertical bonds associated with element *A*, *k* is a constant, $k=\frac{1}{2}$ for first layer, in which no upper bonds exist; $k=1$ for any other layers below the first layer, in which both upper and lower bonds are including. Here the concentrations of the nearest neighbour layers (above and below) are assumed to be as the same as c_A.

$k c_A c_A Z_v$ is the number of vertical *A-A* bonds.

$k c_A c_A Z_v D(A\text{-}A)$ is the total energy of vertical *A-A* bonds.

$k c_B c_A Z_v D(A\text{-}B)$ is the total energy of vertical *A-B* bonds.

For a single atom *A*, the average binding energy may be calculated by continuing the summation of energy listed above, then divided by the number of *A* in the layer $c_A N$:

$$U_A = [\frac{1}{2} c_A^2 Z_l D(A-A) + \frac{1}{2} Z_l c_A c_B D(A-B) + c_A c_B k \cdot Z_v D(A-A) + c_A c_B k \cdot Z_k D(A-B)] / c_A N \quad (5.8)$$

where factor ½ in front of term 2 is used to assume that atoms *A* and *B* equally

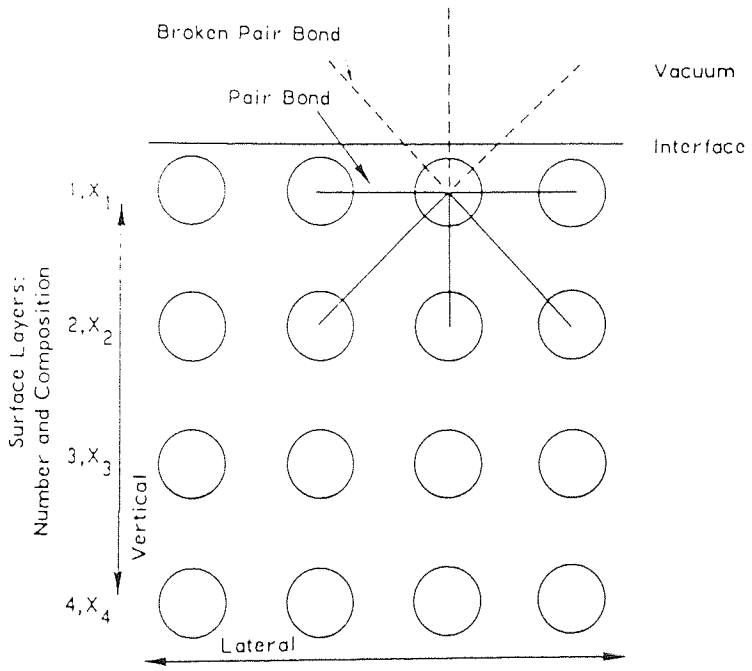

Figure 5.4 Schematic of pair-bond model

contribute to form an A-B bond. The above equation can be rewritten as:

$$U_A=[Z_l/2+kZ_v][c_AD(A\text{-}A)+c_BD(A\text{-}B)] \tag{5.9a}$$

Similarly, the average binding energy of atom B is:

$$U_B=[Z_l/2+kZ_v][c_BD(A\text{-}A)+c_AD(A\text{-}B)] \tag{5.9b}$$

The ratio of U_A/U_B is finally expressed as:

$$\frac{U_A}{U_B}=\frac{c_AD(A-A)+c_BD(A-B)}{c_AD(A-B)+c_BD(B-B)} \tag{5.10}$$

At solid surfaces, the calculation of atomic binding energy is complicated by the reduction of the co-ordination number and the surface relaxation [Tu, *et al.*, 1988], but, to zero order approximation, Equation 5.10 is still valid [Brongersma *et al*, 1978], it has been used in explaining phenomena of nonstoichiometric sputtering [Andersen, 1984]. Compared with Malherbe's model, the pair-bond model was established from a more solid physical base and consequently may be used with more confidence.

5.3.4. The origin of sputtered particles

In Chapter 1, the average depth from which sputtered atoms emerge, Δx_0, has been derived from Sigmund's linear collision cascade theory using the TF model and is expressed by Equation 1.31. As discussed in the above section, since TF model is generally not suitable for describing scattering at very low energy, Sigmund [1969b] improved the calculation of Δx_0 by using the Born-Mayer interatomic potential, which is actually equivalent to TF potential at m=0. Hence the depth of sputtered atoms emerging may be more accurately calculated from:

$$\Delta x_0=\frac{3}{4}\cdot\frac{1}{NC_0} \tag{5.11}$$

where $C_0=\frac{\pi}{2}\lambda_0 a_{BM}^2=1.81\text{Å}^2$ and λ_0=24 (see Table 5.3), the Born-Mayer screening radius a_{BM}=0.219Å and the number density N has been defined in Equation 1.15. It is very interesting to note that Δx_0 depends only on the density of the target.

From Equation 5.11, the average depth of sputtered atoms emerging from GeSi, GaP, GaAs, GaSb, InP, InAs, InSb and CdSe may be estimated, and these are given in Table 5.7. The figures in the table indicate that the sputtered atoms emerge from a depth of 1.5 to 3 monolayers, depending on the lattice constant and the orientation of crystals.

Table 5.7 Average depth Δx_0 for the eight binary systems*

	GeSi	GaP	GaAs	GaSb	InP	InAs	InSb	CdSe
d (g/cm^3)	3.83	4.13	5.32	5.62	4.79	5.66	5.78	5.66
M (amu)	50.4	50.4	72.3	95.7	72.9	94.9	118.3	95.7
N (atoms/Å^3)	0.126	0.136	0.122	0.097	0.109	0.099	0.081	0.098
Δx_0 (Å)	3.28	3.04	3.40	4.25	3.80	4.18	5.12	4.22

* the average density and atomic mass for GeSi are estimated by averaging those for pure Ge and Si; others taken from CRC Handbook (Lido, 1992d)

5.3.5. Imperfections and limitations of the model

In the physical sciences, it is rare to find a theoretical model which is absolutely perfect in the description of a phenomenon taking place in the real world, although the mathematics of the model might be rigorously developed. Most models have imperfections and limitations in use. To understand and to use a theoretical model properly it is essential to know its drawbacks and limitations. The major limitation of the Sigmund theory for low energy ion bombardment are due to the assumptions (see Section 1.3.1.2):

(1) the first assumption of *point particles* of the target atoms is not appropriate for estimating the depth of origin of sputtered atoms, since the real size of atoms are comparable to the calculated depths (see Table 5.7). This results in a slight overestimation of the depth from Sigmund theory. In fact, recent experiments [Oliva, *et al*, 1987] and computer simulation [Vicanek, *et al.*, 1989] have shown that most sputtered atoms (~80%) come from the first atomic layer, a small number (<20%) comes from the second layer and very few from the deeper region, and the average depth of sputtered atoms of 1.2 times monolayer is generally acceptable [Falcone *et al.*, 1987].

(2) In Sigmund' theory, it is assumed that the target is structureless and the atoms are distributed homogeneously. The first point is obvious not applicable for a crystal sample, however, since ion bombardment may destroy the crystalline structure, and the structure will not be restored without an annealing process (see Section 1.2.6), it may be reasonable to suppose that once bombardment takes place, the crystal structure will not affect the validity of the model; this has been proved by experiments [Malherbe, 1991]. The second point does not always hold for multicomponent systems in the radiated region in presence of the other

processes, such as, surface segregation, diffusion, *etc.*. This is particularly true after a short time of bombardment when preferential sputtering will have occurred.

(3) Collisions are not entirely binary and elastic even for low energy sputtering. Table 5.1 shows that the electronic stopping (inelastic) accounts for about 11 to 21% of total stopping. It will also be seen in the following subsections that inelastic ionisation process may be important for radiation induced elemental redistribution.

In addition, as discussed in the previous subsections, the calculation of surface binding energies and the selection of the scattering parameter are also crucial for accurate prediction of composition of an ion bombarded compound surface using Sigmund's model.

5.4. Radiation induced surface segregation and diffusion

5.4.1. Gibbsian surface segregation

A thermodynamic explanation of the phenomenon of surface segregation has already been given in Chapter 1, but a few points concerned with this topic are discussed below:

(1) Surface segregation and diffusion are two totally different physical phenomena, but they may occur simultaneously and are associated with each other, particularly in ion bombarded compound surfaces. Here, it is necessary to compare these two phenomena.

Surface segregation is different from diffusion in two general aspects: (1)acting range; (2)driven force. Surface segregation happens, normally, within the first two atomic layers and is driven by a force minimising surface free energy. Diffusion can occur in both surface and bulk in the solid and is mainly due to the existence of large atomic concentration gradients. Surface segregation is often accompanied by diffusion, since the rearrangement of atoms in the first two monolayers may result in a significant inhomogenous distribution of surface components, leading to the establishment of a concentration gradient.

(2) For a system with a free surface at equilibrium, the Gibbs-Duhem surface thermodynamic equation, that is, the differentiated Equation 1.55, can be written in a general form by including components of the surface stress σ_{ij} and strain tensors ε_{ij} [Zangwill, 1988] as:

$$Ad\gamma + SdT - VdP + Nd\mu + A\sum_{ij}(\gamma\delta_{ij} - \sigma_{ij})d\varepsilon_{ij} = 0 \qquad (5.12)$$

This is called the *Gibbs adsorption equation*, a fundamental result of surface thermodynamics. This may be the reason that the phenomenon of Gibbsian equilibrium surface segregation is also called Gibbsian Adsorption [Lam and Wiedersich, 1987] [Was, 1990]. Indeed, for a compound A_xB_{1-x}, if the composition at the surface is A_yB_{1-y}, and $y>x$, it means that there is a positive adsorption of A on the compound, according to the thermodynamics this adsorption must be accompanied by a decrease of the surface energy. Here, the entropy effects which make up for the difference between surface energy and surface free energy are ignored [Brongersma *et al*, 1978].

(3) The surface energy of pure elements can be expressed in terms of either surface tension or heat of vaporisation (sublimation). Surface tension, γ, is defined as the reversible work required to create a unit area of surface at constant temperature, volume and chemical potential [Overbury *et al*, 1975]. Heat of evaporation, H_V (or sublimation, H_S) is defined as the energy needed to transform one mole of liquid (or solid) into gas at 1 atm [Tu *et al.*, 1987]. Empirically, there is relation between γ and H_V [Kirscher, 1985]

$$\frac{\gamma \cdot a}{H_v} = 0.3 \sim 0.4 \qquad (a \text{ the area of a surface atom}) \qquad (5.13)$$

Although Equation 5.13 shows the correlation, strictly speaking, the surface energy changes may be more adequately calculated from the concept of surface tension rather than that of the heat of vaporisation (or sublimation), specially under non standard conditions, for example, in vacuum.

5.4.2. Surface tensions of solids

One of the major difficulties in applying the Langmuir-McLean equation, that is, Equation 1.56, to predict the surface compositional change due to surface segregation is the lack of reliable surface tension data for solids. A common way to directly measure surface tension of a solid is to increase the solid surface by adding more atoms or by stretching the existing surface. In this experiment, one may measure a combination of surface tension and surface stress, which are very difficult to distinguish. This difficulty does not exist in the case of liquid surfaces since the diffusion of atoms in liquids is so fast that the stress can be ignored. Therefore, surface tensions for pure elements at melting points can be measured more easily. Such results are shown in Figure 5.5 [Zangwill, 1988]. For solids, the assumption of linear temperature dependence has been frequently used in estimating surface tension:

$$\gamma_T = \gamma_0 - (\frac{d\gamma}{dT})_P T \qquad (5.14)$$

This equation derives from the expression of the Gibbs specific surface free energy,

$F(T)=U-ST$, since for a component system, $\gamma_T = F(T)$, $S=-(d\gamma/dT)$, $\gamma_0 = U(T=0)$. Overbury *et al.* [1975] showed that the for most elements the term $(d\gamma/dT)$ is changed by no more than 5% in a 100° temperature interval, which is not greater than the uncertainty of most surface tension experiments. The above assumption is universally accepted.

Since surface tensions at the melting point can be reasonable easily measured, with the assumption of linear temperature dependence, a more practical expression can be derived from Equation 5.14:

$$\gamma_t = \gamma_m + (t - t_m)\cdot\frac{d\gamma}{dt} \qquad (5.15)$$

where γ_m is the surface tension at the melting point t_m. The γ_m, $d\gamma/dt$, t_m, together with γ at room temperature (298K) and the area a of one bulk atom for the elements Si, P, Ga, Ge, As, Se, Cd, In and Sb are listed in Table 5.8.

The area a given in the table are usually estimated by the atomic mass M and density d of pure elements using the following equation [Fried *et al*, 1977]:

$$a = \left(\frac{M}{d\cdot N_A}\right)^{2/3} \qquad \text{where } N_A = 6.023\times10^{23} \qquad (5.16)$$

Equation 5.16 may be adequate for calculation of the surface free energy in surfaces of pure materials or most covalent compounds where no strong electron transfer between different elements occur, but for compounds, such as CdSe($\Delta\varepsilon$=0.7eV), GaP($\Delta\varepsilon$ =0.5eV) and InP ($\Delta\varepsilon$=0.4eV) [Pauling, 1967], large difference in Pauling's electronegativity between two elements implies significant electron transfer taking place when these compounds are formed. These systems appear to be more ionic, so it may be more appropriate to estimate the area a in these compounds using ionic radii of each component rather than from Equation 5.16. The ionic radii for Cd^{2+} and Se^{2-} in CdSe, Ga^{3+}, In^{3+} and P^{3-} in GaP and InP are 0.97, 1.98, 0.62, 0.81 [Materton *et al*, 1983] and 2.12Å [Lide, 1992], respectively, the corresponding values of a are calculated from $a = \pi r^2$ [Wynblatt and Ku, 1979] and given in parentheses in Table 5.8.

The surface tension of the solid surfaces will, in general, depend on the crystallographic orientation. This may be explained by considering interaction between atoms in a crystal system. Consider a bulk array of atoms with a pairwise potential ϕ. The potential energy represents the binding energy of an atom to all the other atoms in the solid. Then define: [Tu. *et al.*, 1987]

$$\gamma_0 = \sum_{k\neq l}\frac{\phi_{kl}}{2a} \qquad (5.17)$$

where a is the surface area. For a simple cubic crystal, each atom has six nearest

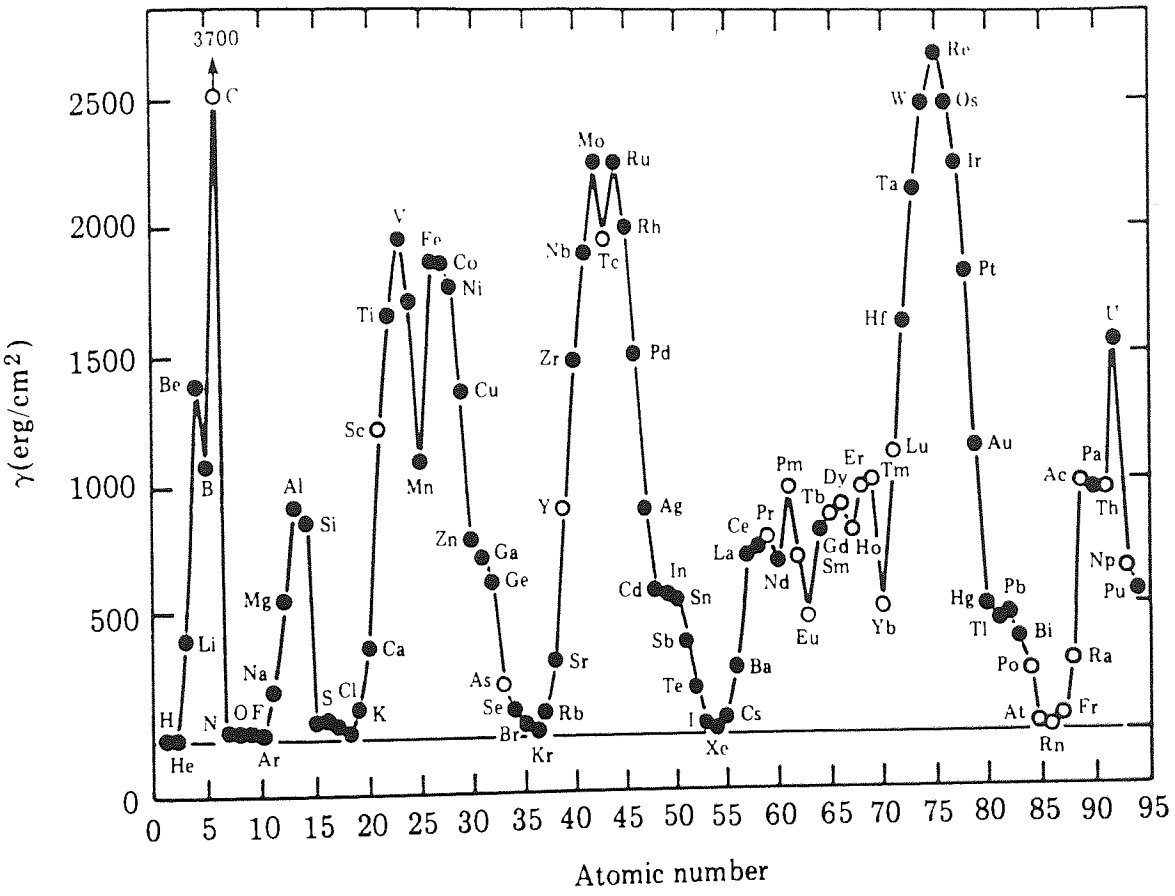

Figure 5.5 Variation of surface tensions for pure elements at melting point with atomic number (after Zangwill [1988])

Table 5.8 Surface tension and melting point of the elements*

Element	Si	P	Ga	Ge	As	Se	Cd	In	Sb
γ_m (J/m^2)	0.727	0.071	0.784	0.589	0.2	0.106	0.666	0.558	0.403
$-d\gamma/dT$ (10^{-3}J/m^2°C)	0.11	0.24	0.061	0.105	0.6	0.02	0.124	0.089	0.038
M.P. (°C)	1414	50	30	938	817	221	321	157	631
γ_{RT} (J/m^2)	0.880	0.076	0.784	0.685	0.675	0.11	0.703	0.569	0.426
a (10^{-20}m^2)	7.39	(14.1)	7.26 (1.21)	7.99	7.79	(12.3)	(2.96)	8.79 (2.06)	9.70

* Values for Si, P, Ga, Ge, Se taken from [Lide, 1992b]; those for Cd, In and Sb taken from [Overbury *et al.*, 1975]; For As, γ_m was taken from [Zangwill, 1988], $-d\gamma/dT$ was calculated from Equation 5.15 using $\gamma_{T=0k}$ =1.0J/M^2 [Gerkema and Miedem, 1983]

neighbours twelve second nearest neighbours, eight third-nearest neighbours, and so on. The energy required to remove an atom from the bulk is then

$$\phi_0 = 6\phi_1 + 12\phi_2 + 8\phi_3 + \ldots \equiv \gamma_0 \cdot a \tag{5.18}$$

For a simple cubic which is cleaved along (100) plane, the bond is broken for only a nearest neighbour, 4 second-nearest neighbours, 4 third-nearest neighbours and so on. Thus:

$$\phi = \phi_1 + 4\phi_2 + 4\phi_3 + \ldots \equiv \gamma_{100} \cdot a \tag{5.19}$$

The ratio R is:

$$R = \frac{\gamma_{100}}{\gamma_0} = \frac{\phi_1 + 4\phi_2 + 4\phi_3 + \ldots}{6\phi_1 + 12\phi_2 + 8\phi_3 + \ldots} \tag{5.20}$$

Using the Lennard-Jones potential, R for (100), (011) and (111) faces of a crystal can be calculated, they are 0.224, 0.235 and 0.212, respectively. The (111) surface is the lowest-energy surface of the principal surfaces. Therefore, for the crystal solid surfaces, the surface atomic ratio determined by Gibbsian equilibrium surface segregation should be expressed as:

$$\frac{(x_B / x_A)^s}{(x_B / x_A)^b} = e^{-R\cdot(\gamma_B \cdot a_B - \gamma_A \cdot a_A)} \tag{5.21}$$

5.4.3. The role of ion bombardment in surface segregation

Both surface segregation and diffusion occur frequently at elevated temperature.

However, for low energy ion beams with a current of the order of ~μA, the bombardment cannot produce sufficient heat in a semiconductor surface to produce thermal surface segregation and diffusion. This can be understood by considering estimates of surface temperature rise due to the power deposition of the ion beam. For simplicity, it is assumed that the heat generated by the ion beam is deposited only at the surface rather than through a finite bulk, the surface temperature rise can be calculated from: [Mack, 1988]

$$\Delta T_s(t) = 2 \cdot \frac{P}{A} \cdot \left(\frac{t}{\pi k d C_p} \right)^2 \tag{5.22}$$

where P is beam power, i.e., product of beam current and energy; A is bombarding area; k, d and C_p are thermal conductivity, density and the specific heat of the sample, respectively.

For silicon, k=1.3w/cm/°C, d=2.33g/cm^3; C_p=0.75J/g/°C. Under the bombardment of 3000eV Ar ion beam of current 1×10^{-6}A with a bombarding area of 0.8cm×0.6cm, the temperature rise after 50 minute bombardment in the silicon surface calculated from Equation 5.22 is only about 0.3°C. Hence the surface temperature rise is not an important factor in surface compositional changes in the compound semiconductors and GeSi alloy due to ion bombardment under the above conditions.

For solid surfaces of compounds at room temperature, the driving force caused by minimising surface free energy is, in fact, so small that the process of surface segregation may not occur, or may occur, but extremely slowly in the absence of an external influence. The main reason is the existence of strong binding forces between the surface atoms. During ion bombardment, the surface atoms may obtain sufficient energy from ions or recoils, to overcome the binding forces and become mobile within the solid, quite similar to atoms or molecules in liquids or in gas phases. This movement greatly speeds up the transfer process from one equilibrium state (initial surface compositional distribution) to another (redistribution due to surface segregation) greatly. On the other hand, according to the laws of thermodynamics, the collision will change the entropy S of a system, which has been expressed clearly by Lifshitz and Pitaevskii [1981] as:

$$\frac{ds}{dt} = -\int \ln f \cdot C(f) dV d\Gamma \tag{5.23}$$

here f is the atomic distribution function in phase space (v, Γ), $C(f)$ is defined in Equation 1.1. From this point of view, the ion bombardment may enhance thermodynamic segregation tendencies which were not allowed kinetically [Kirschner, 1985].

5.4.4. Radiation induced/enhanced diffusion

The effects of radiation induced diffusion on compositional distribution of the compound semiconductors and GeSi alloy may be evaluated by comparing the diffusion coefficient of each component in the compounds. The coefficient has been given by Equation 1.63. The pre-exponential factor D_0 and the activation energies Q_a for Ga, In, P, As and Sb self-diffusion in GaAs, GaSb, InP, InAs and InSb systems are listed in Table 5.9. Assuming that these values are valid at room temperature, and the relationship between the self-diffusivities and the activation energies still holds, the self-diffusion coefficients for Ga, In, P, As and Sb in GaAs, GaSb, InP, InAs and InSb systems at room temperature may be estimated, which are listed in the column 5 in Table 5.9. It may be seen that all the elements in the perfect compound systems have a very low diffusitivity, therefore, diffusion is unlikely to occur at room temperature without ion bombardment.

Table 5.9 Self-diffusivities and the active energies of Ga, In, P, As and Sb atom in GaAs, GaSb, InP, InAs and InSb [Lide, 1992c]

Diffusant	Materials	D_0 (m^2/sec)	Q_a (eV)	D_{RT} (m^2/sec)
Ga	GaAs	4×10^{-9}	2.6	2.73×10^{-54}
As		7×10^{-5}	3.2	1.80×10^{-60}
Ga	GaSb	3.2×10^{-1}	3.15	6.08×10^{-56}
Sb		3.4	3.45	3.97×10^{-60}
In	InP	10	3.85	1.31×10^{-66}
P		7×10^{6}	5.65	4.95×10^{-92}
In	InAs	60	4.0	1.95×10^{-68}
As		3×10^{3}	4.45	1.49×10^{-74}
In	InSb	5×10^{-6}	1.82	1.21×10^{-25}
Sb		5×10^{-6}	1.94	9.95×10^{-28}

However, as discussed in Section 1.3.3.5, the diffusion may be happened due to ion beam radiation, the difference in diffusivity for different elements may lead to changes in compositional distributions. This can be understood easily from computer simulations. Figure 5.6 illustrates the distributions of the vacancies in the 3keV Ar ion bombarded GeSi, GaP, GaAs, GaSb, InP, InAs, InSb and CdSe systems obtained from TRIM calculations. It shows that ion bombardment produces a vacancy-spike at a depth of about 20Å in the semiconductor surfaces. According to Wiederisch's model (see Section 1.3.3.4), compositional distribution in the radiated region of an alloy depends on

the gradient of total vacancies and preferential coupling between defect fluxes and the fluxes of certain alloying elements. This has been expressed by Equation 1.62. Using Equation 1.63, Equation 1.62 can be rewritten as:

$$\nabla x_A = k[e^{-\frac{H_{Av}-H_{Bv}}{kT}} - e^{-\frac{H_{Ai}-H_{Bi}}{kT}}]\cdot\nabla x_v = ke^{-\frac{H_{Av}-H_{Bv}}{kT}}[1-e^{-\frac{(H_{Ai}-H_{Av})-(H_{Bi}-H_{Bv})}{kT}}]\cdot\nabla x_v \qquad (5.24)$$

where coefficient k has a positive value associated with the diffusion coefficients and surface concentrations of element A and B in AB (see Section 1.3.3.4). H_{Av}, H_{Bv} and H_{Ai}, H_{Bi} stand or the migration energies of A or B atoms via vacancies and those of interstitial A and B.

According to Sullivan's analysis [1976], generally, $H_V >> H_i$. It is thus reasonable to assume H_{Ai}-$H_{Av} \approx -H_{Av}$ and H_{Bi}-$H_{Bv} \approx -H_{Bv}$, so the above equation can be re-written as:

$$\nabla x_A = k(e^{-\frac{H_{Av}-H_{Bv}}{kT}} - 1)\cdot\nabla x_v \qquad (5.25)$$

Hence Equation 5.25 implies that if the migration energy of A atoms via vacancies is lower than that of B atoms, or say $d_{Av} > d_{Bv}$ the concentration of element A may increase in the vacancy-rich region. The migration energy of atom via vacancies is generally unknown, however, it has been proved that a scaling relationship exists between the migration energy and the activation energy [Was, 1990]. Hence from the activation energy listed in Table 5.9, Equation 5.25 and Figure 5.6, it can be predicted that since Ga has lower activation energies than As and Sb elements in GaAs and GaSb, ion bombardment may result in higher Ga concentration in a region of 10-60Å in the surfaces of these two materials. Similar situations may be found for In in InP, InAs and InSb surfaces.

In addition, the diffusion may also be possibly enhanced by the ionisation process described by Bourgoin *et al.* [1978] during 3keV Ar ion bombardment. Indeed, the energy loss of keV Ar ions in the eight semiconductors by electron stopping shown in Table 5.1 is quite noticeable although it is not the dominant factor.

This process depends strongly on the ionisation probability, so the atomic redistribution in covalent systems caused by this mechanism is eventually determined by the difference in the first ionisation energy of different elements. The lower the 1st ionisation energy of the element is, the greater its ionisation probability is and the more enhanced mobility it experiences in diffusion. The 1st ionisation energies of Ga, In, P, As and Sb are given in Table 5.10 From this point of view, Ga and In having much lower ionisation energies than P, As and Sb should move even faster toward the vacancy spike region in the presence of ionisation enhanced mechanisms, resulting in Ga or In enriched at depths of about 20-40Å.

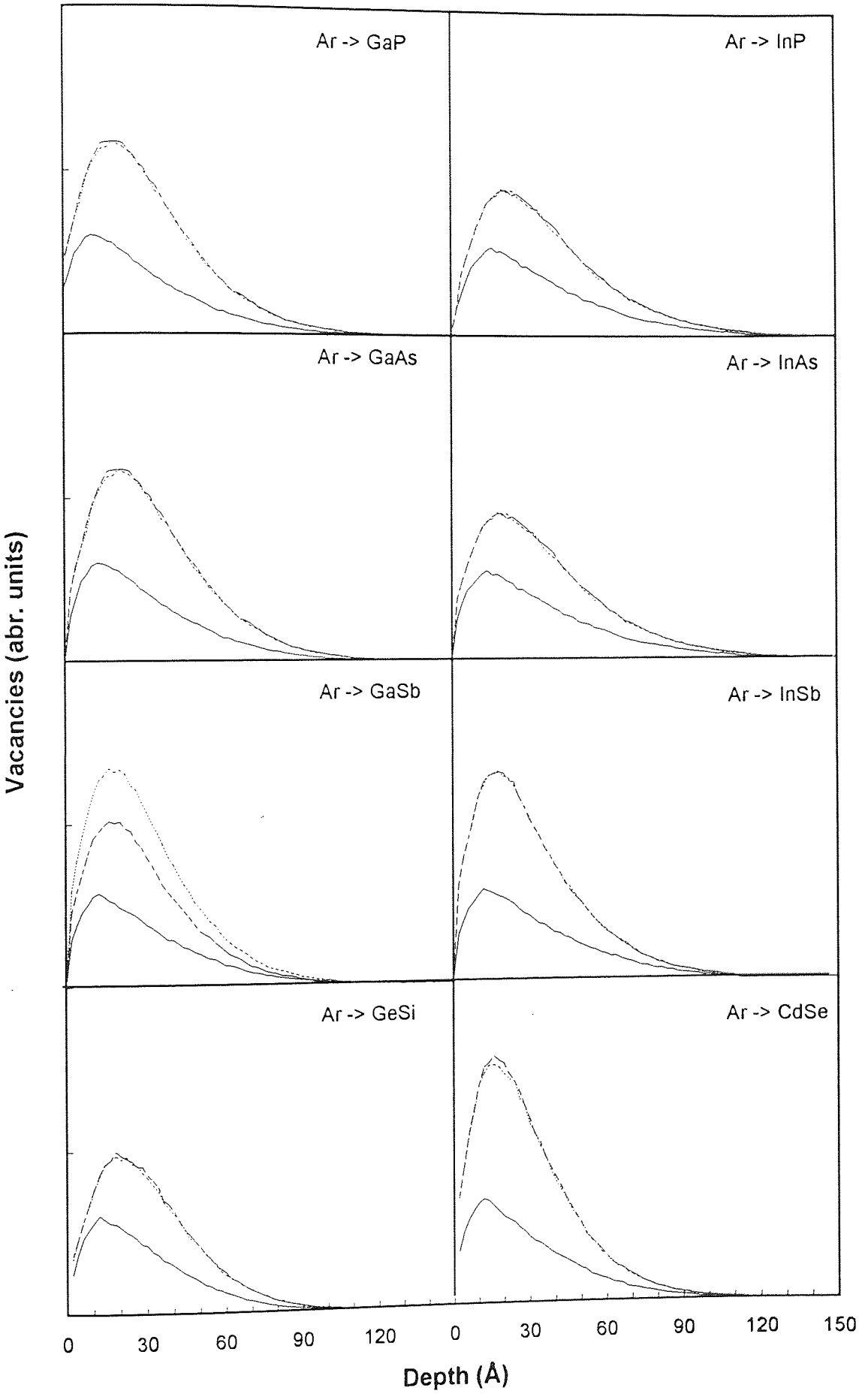

Figure 5.6 Vacancy distribution in compound semiconductor surfaces
(the solid lines: vacancies created by direct Ar^+ collision;
the dashed and the dotted lines: those created by recoils)

Table 5.10 The 1st ionisation energies of Ga, In, P, As and Sb

Element	Ga	In	P	As	Sb
I.E (eV)	5.99	5.79	10.49	9.81	8.64

Ion bombardment will generate not only vacancies in a crystal surface region but also interstitials, so the above discussions should principally include both vacancy related and interstitial-related diffusion mechanisms. According to the analyses done by Brinkman [1974], Dennis and Hale [1978] and Corbett *et al.* [1981], the central core region of collisions is generally rich in vacancy-related defects while the surrounding layer contains the interstitials which recoiled from the damaging collision (this type of structure is also called Brinkman zone, or BZ), the interstitial-related diffusion are ignored in talking about compositional changes in sub-surface of the ion bombarded compound semiconductors and GeSi alloy, specially in region of 20 to 40Å. In the immediate surface, interstitial migration processes may be important, but as analysed in the last two subsections, the compositional changes at the first one or two atomic layer is mainly driven by Gibbsian equilibrium segregation. It is also clear that ion bombardment will cause structural damages in the whole surface region of semiconductor crystals, the crystal structure will be destroyed and cannot be restored without an annealing process.

5.5. Ion bombardment effects in semiconductor surfaces

5.5.1. A hypothesis of ion bombardment effects

To summarise the above discussions, one may find that an accurate and quantitative theoretical explanation of the phenomenon of surface compositional changes due to ion bombardment is complicated, since at least three mechanisms, the nonstoichiometric sputtering described by Sigmund's linear collision cascade theory, Gibbsian equilibrium surface segregation and bombardment induced/enhanced diffusion, may be involved. However, according to the previous analysis, the three mechanisms may be dominant in the different surface regions, a qualitative or semi-quantitative description of compositional profile in the ion bombarded semiconductor surfaces may be made, this is illustrated by Figure 5.7. The surface compositional modification due to ion bombardment is generally divided into four surface regions at different depths:

Region I

This region actually indicates the surface layers which have been sputtered away after a period of sputtering time. The depth of this region depends on the erosion rate of

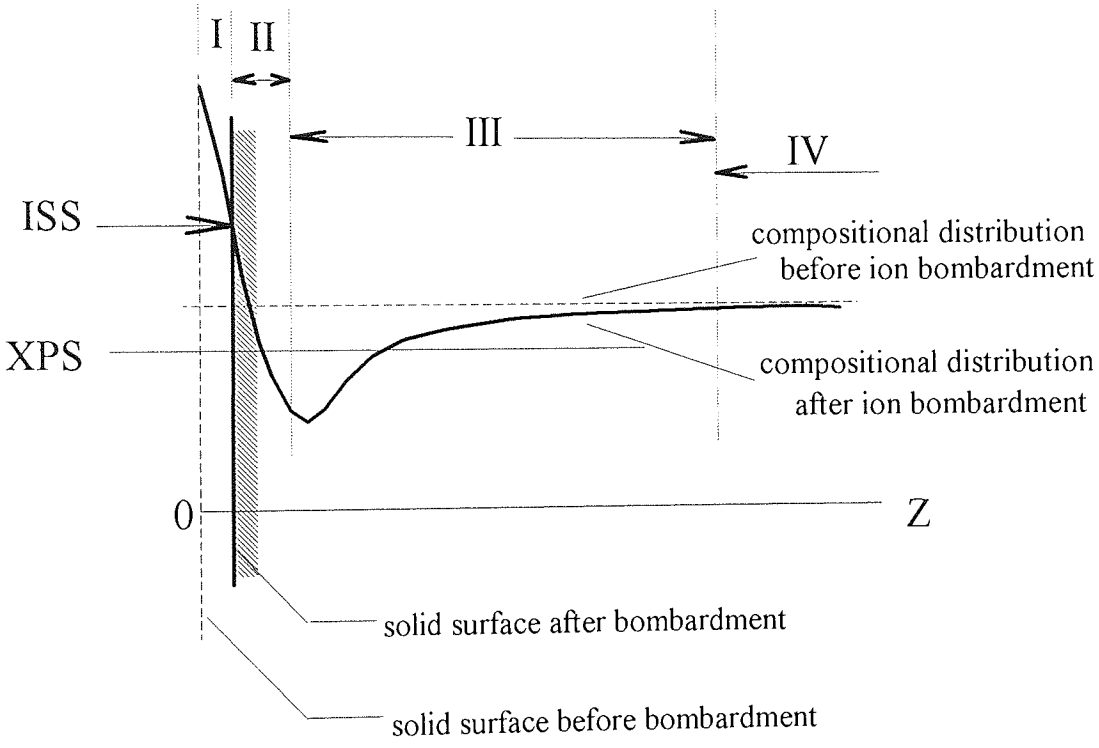

Figure 5.7 Schematic of compositional profile in an ion bombarded compound semiconductor surface

the ion beam to the target materials. Since for low energy sputtering, the surface compositional change predicted by the mechanism of nonstoichiometric sputtering effects derived from Sigmund linear collision cascade theory is based on the differences in partial sputtering yield of different elements, and the depth of origin of sputtered particles is limited to about 1.2 monolayers (see Sections 5.3.3 & 5.3.4), if this mechanism exists, it may affect the surface composition but only the first atomic layer.

Region II

This region includes the first few atomic layers in a bombarded compound surface. Gibbsian equilibrium surface segregation may cause the re-arrangement of atoms in the first two atomic layers. Supposing that atom *A* having lower surface energy segregates from the second layer to the first one driven by a force minimising the surface free energy during ion beam radiation, this will result in an enrichment of element *A* in the first atomic layer, by the law of mass conservation, a depletion of element *A* in the second atomic layer is expected. Once a concentration gradient in the immediate subsurface is formed, the segregation may also cause a diffusion of *A* atoms from the third, forth layer or even deeper levels towards the outermost surface region.

Region III

This includes the rest of the ion bombarded surface region beneath the segregation layers (Region II). The depth of this region is equal to the recoil depth (see Section 5.2.1). Although Gibbsian surface segregation may govern the compositional changes in the first few layers of this region interfacing Region II, computer simulation showed that 3keV Ar^+ bombardment in the semiconductor surfaces creates a vacancy spike at a depth of about 5 to 8 monolayer, according to Wiederisch's model (see Section 1.3.3.4) and the formation of such vacancy-rich regions may induce a flux of atoms, mainly from the bulk, migrating towards the vacancy spike. The differences in diffusion properties of each elements in the materials may change the compositional distribution in this depth range. This may be further enhanced by ionisation process described in Section 5.4.4.

Region IV

In this region, compositional distribution is not influenced by ion bombardment.

5.5.2. Comparisons between theoretical models and LEISS and XPS results

In the above theoretical analysis, it is suggested that both surface segregation and nonstoichiometric sputtering may cause the surface compositional changes in a binary

system during ion bombardment, particularly that at the first one or two atomic layers. To get a better understanding of ion bombardment effects in compound semiconductor surfaces, it is necessary to identify which mechanism is predominant in the compositional changes. According to the previous analysis, this can be done by comparing these two models with LEISS measurements on the surface compositional changes of GaP, InP, GaAs, InAs, GaSb, InSb and CdSe compound semiconductors and GeSi alloy. For this reason, the atomic ratios in surface $(x_B/x_A)^S$ (B represents Se, P, As, Sb and Si; A represents Cd, Ga, In and Ge) predicted by both Sigmund's linear collision cascade theory and Gibbsian surface segregation model, together with those measured from LEISS and normal XPS experiments, are tabulated in Table 5.11.

Table 5.11 Comparison between theoretical prediction and experimental observations on atomic ratios $(x_B / x_A)^s$ in the bombarded surfaces of CdSe, GaP, InP, GaAs, InAs, GaSb, InSb compound semiconductors and GeSi alloy

A-B	CdSe (111)	GaP (111)	InP (100)	GaAs (100)	InAs (100)	GaSb (111)	InSb (100)	GeSi (100)
Sigmund	2.14	1.03	1.01	1.47	1.38	1.58	1.55	0.64
Gibbs	1.47	0.94	1.06	1.27	0.72	2.74	1.63	0.56
LEISS	1.32	0.91	0.81	1.42	0.47	3.33	1.63	0.75
XPS	0.87	0.71	0.6	0.82	0.77	0.71	0.92	1.23

In the theoretical predictions, it is assumed that the atomic ratios in the bulk of the eight AB systems $(x_B/x_A)^b$ equals 1. The surface atomic ratios predicted by Sigmund theory are calculated from Equation 5.5. The surface binding energies were estimated using the pair-bond model, e.g. Equation 5.10. Some useful data in the calculation, such as the correction factors f and the bond strength of diatoms, were taken from Table 5.5 and Table 5.6, respectively. Those predicted by the Gibbsian equilibrium surface segregation are obtained using Equation 5.21 and the data provided in Table 5.8.

Nonstoichiometric sputtering model

From Table 5.11, it may be seen that the model derived from Sigmund theory appears to agree with the LEISS results measured from the bombarded GaP, InP, GaAs, InSb and GeSi surfaces quite well, but with noticeable derivations for CdSe and GaSb samples, and failed to predict that in InAs sample surface.

With the exception of InAs, the normal XPS results shown in the table appear to contradict the LEISS measurements. This is clearly due to the difference in the sampling

depth of the two surface analytical techniques which has been discussed in Section 5.2.2. The combination of XPS observation with LEISS results may provide very good evidence that ion bombardment will result in redistribution of surface composition, but the elements in the bombarded surfaces are re-distributed in such a way that the element enriched at the top layer of the surface may be depleted in the intermediate region. This fact cannot be explained by the nonstoichiometric sputtering model. According to the Sigmund linear collision cascade theory, if element B in AB system was removed preferentially, there would be a net flux of B atoms moving from the immediate subsurface or bulk to the surface, resulting in element B depletion in a region sampled by XPS, in another words, LEISS and XPS results should show the same trend in the surface compositional changes due to ion bombardment, this has not been proved by our experimental observations.

Gibbsian equilibrium surface segregation induced by ion bombardment

Compared with the nonstoichiometric sputtering model, Gibbsian equilibrium surface segregation model generally shows better agreement between theoretical prediction and LEISS results on all the eight semiconductor samples, this is illustrated more clearly by Figure 5.8. Beside that, a more important point is that the variations between LEISS and XPS experimental results may be interpreted by this model.

If A atoms segregates to the top layer of a system AB during ion bombardment, the partial sputtering yield for element A will increase, and more A atoms will be removed by sputtering. On the other hand, in order to maintain the surface free energy to the minimum, there must be a net movement of A atoms from the subsurface region, leading to the depletion of element A in the region, which is sampled by XPS. This is indeed the result observed in our experimental studies on most of compound semiconductor surfaces.

Although Figure 5.8 shows very good agreement between the predictions of this model and the LEISS observations, certain errors may be seen in the figure, which come not only from the LEISS experiments but also from the data cited from the references and used in the theoretical calculations. For example, the surface tensions for all elements generally contained errors of about 10%, resulting in the total errors of about 20% in the calculations. For As, the error from the estimated surface tension may be even greater. Errors may also be introduced by the approximation of the atomic sizes.

Ion bombardment induced/enhanced diffusion

Both the Gibssian surface segregation model and LEISS analysis showed that the In enriches at the ion bombarded InAs surface, XPS analysis on the surface, however, did

not show In depletion in the subsurface region, like those observed in the other seven sample surfaces, although the In concentration obtained from XPS is indeed lower than that measured by LEISS. This may be due to the effects of ion bombardment induced diffusion.

From Table 5.9, it may be seen that In atoms have greater diffusivity than As atoms in InAs, therefore, according to Wiederisch's model [Wagner, 1983], the In recoils will migrate much quicker than As atoms from the deeper region to the vacancy-rich region and occupy the empty lattice sites. The ionisation process may further speed up the In movement since In atoms have much lower ionisation energy than As atoms (see Table 5.10), consequently, the In concentration may be higher than As within the sampling depth of XPS.

The effects of ion bombardment induced/enhanced diffusion may be more definitely identified in InP and GaP samples. Within the experimental errors, LEISS measurements did not suggest the significant compositional changes at both sample surfaces, and theoretical prediction using both Sigmund's theory and Gibssian surface segregation model did not show that there is a strong driving force or any preferential sputtering effect changing the surface composition. Considerable P depletion, however, was observed in both samples by XPS analysis. Similar to InAs sample, this may be explained by the difference in diffusivity between In and P atoms (see Table 5.8) in InP and in their first ionisation energy, which suggest that In mat enrich in the intermediate surface region in ion bombarded InP surfaces. Due to the lack of information on diffusion properties of Ga and P in GaP, it is impossible to give definite theoretical explanations of the composition changes in the bombarded GaP surface. Referring to InP, it may be adequate to assume that Ga has greater diffusivity than P atoms in GaP sample. Ga atoms also have much lower ionisation energy (see Table 5.10), therefore, Ga should be enriched in the region detected by XPS during ion bombardment.

It should be pointed out that ion bombardment induced/enhanced diffusion may also affect the compositional redistribution in the other five semiconductor surfaces although the effect may not be seen as clearly as that in GaP, InP and InAs. However, since surface segregation takes place in the first few monolayers and the diffusion in the deeper regions, and the intensity of photoelectrons in XPS measurement decreases exponentially as the sampling depth, which the Gibssian surface segregation represents. XPS results may generally reflect the segregation effects more than that of the diffusion.

Based on the comparisons between theoretical analysis and experimental results, it is clear that the changes in compositional distribution in ion bombarded semiconductor surfaces are generally governed by Gibssian equilibrium surface segregation plus the

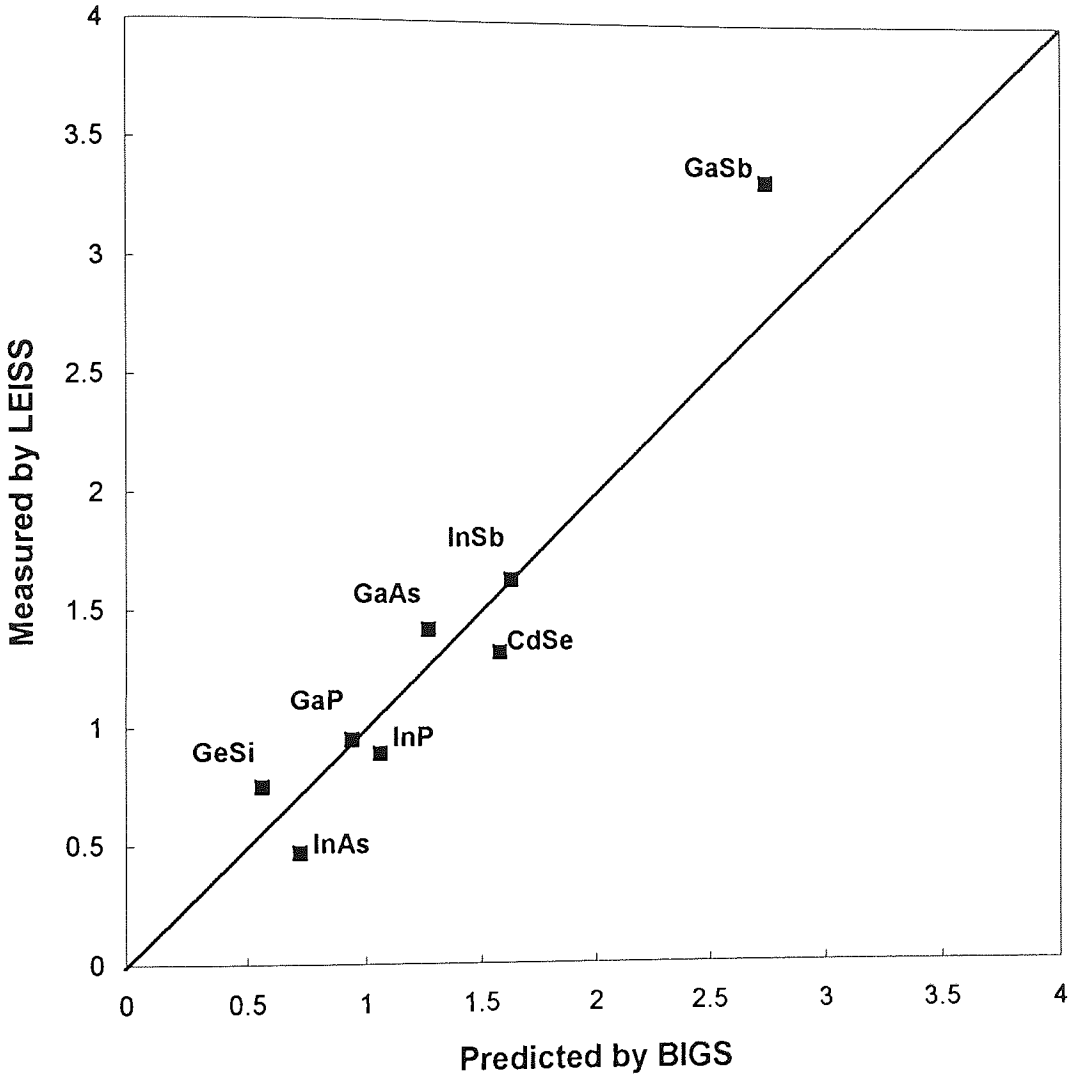

Figure 5.8 Comparison between predictions by bombardment induced Gibbsian surface segregation and measurements by LEISS

effects of diffusion induced/enhanced by ion beam bombardment. The current nonstoichiometric sputtering model derived from the Sigmund linear collision cascade theory does not adequately describe the ion bombardment effects in the semiconductor surfaces studied in this programme.

Chapter 6 Conclusions and Future Work

6.1. Introduction

Correct theoretical analysis needs more complete and convincing experimental evidence. On the other hand, interpretation of experimental observations requires a good understanding of theoretical models. The programme described in this thesis is essentially an experimental study, but efforts have also been made to identify, understand, improve and modify current theoretical models. In this final chapter, both experimental and theoretical work completed in this programme are summarised. Based on the work, the conclusions of the findings of this work on ion bombardment effects in compound semiconductor surfaces stated. Recommendations for future work in this field were outlined at the end of this chapter.

6.2. Conclusions

6.2.1. Experimental observation

Combining Low Energy Ion Scattering Spectroscopy and X-ray Photoelectron Spectroscopy has been successfully demonstrated as an effective vehicle for studying ion bombardment induced compositional changes in GeSi, GaP, GaAs, GaSb, InP, InAs, InSb and CdSe compound semiconductor surfaces. This complimentary approach provides more experimental evidence to elucidate the mechanisms responsible for the ion bombardment effects. To take full advantage of the use of these complimentary methods of analysis, accurate quantification is essential. Hence, pure elemental samples have been carefully prepared as standard references and examined under the same experimental conditions by means of both LEISS and XPS.

LEISS provides compositional information of the first atomic layer of a solid surface. It has proved an excellent technique for surface analysis, specially in studying the phenomenon of surface segregation. Although some fundamental aspects of this technique are still not well understood, quantitative compositional analysis of solid surfaces using this technique is possible under carefully controlled conditions if the reference data from the standard samples are available.

XPS gives results of integrated surface composition within a depth of about 5 to

over 30 atomic layers, depending on the kinetic energy of detected core level electrons, surface matrix and take-off angles. In investigation of ion bombardment effects on the surface compositional redistribution, normal XPS was, however, found to provide insufficient experimental evidence for theoretical analysis alone if not combined with other more surface specific analytical techniques. This may be the reason that although many XPS experiments in this field have been carried out, no clear physical picture has developed from these results.

In this study, the difference in sampling depth between XPS and LEISS was particularly emphasised. The interpretation of the segregation effects observed in this study are based on the difference in LEISS and XPS analyses due to this difference in sampling depth. With the exception of the phosphide samples, LEISS analysis shows that ion bombardment produces enrichment of a specific component at the outermost atomic layers of the compound semiconductor surfaces, whereas, the XPS results show that this same component is depleted in the immediate subsurface. In the cases of GaP and InP, LEISS did not show noticeable compositional change at the outermost layers, but XPS measurements indicated significant P depletion in the sub-surface region. The variance between LEISS and XPS measurements provides very clear evidence of the model of change of the compositional distribution in compound semiconductor surfaces due to ion bombardment. The model indicates that the change is due to thermodynamic processes, these are, bombardment induced Gibbsian segregation and/or diffusion. The results show that this is far more likely than the nonstoichiometric sputtering effect, which should show similar depletion in surface and sub-surface.

ARXPS was used extensively in investigating the initial surfaces of the compound semiconductors and GeSi alloy. The results confirmed that beyond the contamination overlayers all the samples of the compound semiconductors and GeSi alloy before ion bombardment were stoichiometric, this was a very good starting point for studying the ion bombardment effects. When used in investigating the ion bombarded surfaces, ARXPS results, however, were not sufficient to give clear indications of the compositional distribution in some sample surfaces. This was mainly due to roughing effects of ion bombardment modification on the surface structure, the bombarded sample surfaces were no longer ideally flat for use of this technique. In these cases, KRXPS has greater advantages and has been used successfully for showing As and Sb segregation in the bombarded GaAs and InSb, respectively.

6.2.2. Computer simulation

Although computer simulation techniques are still at an immature stage

for quantitatively predicting compositional changes in compound surfaces, they have been successfully used in this project to investigate some aspects on this topic which cannot be tackled with the current analytical methods and experimental techniques.

For 3keV Ar ion bombardment in GeSi, GaP, GaAs, GaSb, InP, InAs, InSb and CdSe surfaces, computer simulation using the TRIM code, indicated that nuclear stopping is the predominant mechanism for the energy transfer between energetic particles and target atoms. Collision cascades are major events for producing moving atoms, or recoils.

It was verified that the surface damage depth should be estimated using the recoil depth rather than the ion projected range. Compared with the sampling depth of normal XPS used in the experiments, it may be seen that almost the entire surface damage depth was detected by XPS technique.

6.2.3. Theoretical description

Sigmund linear collision cascade theory

By comparing the Thomas-Fermi nuclear stopping power with the Ziegler-Biersack-Littmark universal model, the range of the power scattering parameter *m* used in the Sigmund's theory has been well determined for 3keV Ar^+ collision with the semiconducting atoms from Si to Sb. Based on this, the nonstoichiometric sputtering model derived from the Sigmund theory has been improved by taking account of the differences in mass of different components.

The calculation of the surface binding energy in this model has been discussed in terms of the concept of Pauling's electronegativity. The Malherbe's model which has been used in this field was proved to lack a sound physical basis. The pair-bond model has been considered as a more appropriate one for estimation of the surface binding energy for compound semiconductors and GeSi alloy as well as other covalent systems.

The depths of origin of the sputtered particles from the Ar^+ bombarded semiconductor surfaces were estimated, the results indicated that the sputtered particles come from depth no more than two atomic monolayers, this leads to the conclusion that the nonstoichiometric sputtering model based on the partial sputtering yields calculated from Sigmund's theory is principally only suitable for prediction of composition in the first one or two atomic layer, in the absence of other mechanisms, predictions by this model may be close to LEISS measurements. This model, however, is essentially not applicable for anticipating the compositional changes in the deeper region of a

bombarded surface, that is the region sampled by XPS measurements, and cannot explain the variance between LEISS and XPS results.

Thermodynamic explanations to the ion bombardment effects

To gain a better understanding of the ion bombardment effects, Gibbsian equilibrium surface segregation induced by ion bombardment has been studied. The surface tensions of each element in the eight compound semiconductor samples at room temperature have been evaluated by carefully using the assumption of linear temperature dependence and by taking into account of the orientation effects solid crystal. The role of ion bombardment in Gibbsian surface segregation has been discussed.

Compared to the nonstoichiometric sputtering models, Gibbsian surface segregation gave a more satisfactory explanation to the ion bombardment effects. The compositions at the top layer of all the bombarded sample surfaces predicted by this model are in very good agreement with the LEISS measurements, but also the variance between LEISS results and XPS measurements can be explained.

During ion bombardment, the component with lower surface energy, say A atoms, will segregate to the top layer of the compound surface, the concentration of atoms A at this layer will increase, resulting in increase in the partial sputtering yield for atoms A, and more A atoms will be removed by sputtering. On the other hand, to maintain minimum surface free energy, there must be a net movement of A atoms from the immediate subsurface region, and A atoms will be depleted in this region, which is sampled by XPS. This is the reason that in most of cases LEISS results are contradicted by normal XPS measurements, as shown in Figure 5.8.

As indicated by computer simulation using TRIM code, 3keV Ar ion bombardment generates vacancy spikes at depths of about 8-10 monolayers in the compound semiconductor surfaces. According Wiedersich model, the formation of such vacancy-enriched regions may lead to a defect migration process, therefore, the compositional distribution in this region may be changed. For semiconductors, this diffusion may be further enhanced by ionisation processes. Since the diffusion processes generally take place in the region beyond the segregation affected region and the photoelectron intensity originating from this region is reduced exponentially with the depth, when both segregation and diffusion are present in the bombarded surface, the segregation effect is generally seen more easily than that of diffusion in XPS analysis. However, in the cases of GaP, InP and InAs, the diffusion effect became significant and was observed clearly in the XPS experiment.

The general description of the compositional profile illustrated in Figure 5.8 is, in

fact, quite similar to some published experimental results and theoretical analysis [Kelly and Oliva, 1986] [Shimizu, 1987]. What is new here is that by determining the dominant regions of all the possible mechanisms, compositional changes in the compound semiconductor surfaces observed in XPS and LEISS analyses have been discussed in detail based on theoretical analysis and computer simulation. From this work, it is clear that although linear collision cascades are the major events in ion bombardment of semiconductor surfaces, the changes in surface compositional distribution at first few atomic layers are governed mainly by bombardment induced Gibbsian surface segregation, which is theoretically similar to the model proposed by Kelly and Oliva [1986], but in the intermediate surface region, the surface compositional changes may be determined mainly by the defect migration processes described by Wiedersich model [Wagner *et al*, 183] and the bombardment induced/enhanced diffusion. Here, the author would like to end this subsection with the Sigmund's words [Sigmund, 1987]:

> *"By and large, we all had to realise, sooner or later, that bombardment induced composition changes may have very little to do with sputtering."*

This has been proved in this work.

6.3. Future work

The work on studying ion bombardment effects in compound semiconductor surfaces is far from complete, much effort should be made on both experimental and theoretical sides at least in the following aspects :

6.3.1. Experimental side

(1) More XPS and ISS investigation of ion bombardment effects in other compound semiconductors are required to further test the conclusions reached in this work.

(2) Experiments on the effects of the energy and fluence of the bombarding ions on the compositional changes in the semiconductors should be done to gain the complete understanding of the ion bombardment phenomena.

(3) Research on the effects of different bombarding ion species in the compositional changes in the compound semiconductor surfaces should be carried out.

(4) More complete complementary surface analytical techniques are required for obtaining the depth compositional profile in the bombarded compound surfaces.

(5) Proper algorithms are required to be developed for ARXPS analysis.

(6) For the phosphides, pure phosphorus samples must be obtained and calibrated for accurate quantification of XPS and LEISS data.

6.3.2. Theoretical work

(1) Further theoretical studies on Gibbsian segregation are required, particularly, the mathematical model for description of the relationship between the surface composition and the parameters of bombardment conditions need to be established.

(2) More proper mathematical models for describing the effects of ion bombardment induced/enhanced diffusion in compound semiconductor surfaces are needed to be developed.

References

Abstreiter G, "The future of electronics engineering", Physics World, **3**, 1992, 36-44

Adachi S, "Physical properties of III-V semiconductor compounds", John Wiley & Sons Inc., 1992, New York, U.S.A.

Alkajaersig K, Christensen H B, Gupta B K, Jensen H, "Ion bombardment of AlN films deposited in a reactive sputtering process with accurate control of the mass flow of the reactive gas", Surf. & Coat. Technol., **51**, 1992, 500-508

Andersen H H, "Computer simulations of atomic collisions in solids with special emphasis on sputtering", Nucl. Instr. and Meth. **B18**, 1987, 321-343.

Andersen H H in Chapter 6 of "Ion implantation and beam processing", eds Williams J S and Poate J M, Academic Press, 1984, London, 127-187

Andersen N and Sigmund P, "Energy dissipation by heavy ions in compound target", Matematisk-fysiske Meddelelser, **39(3)**, 1974, Copenhagen, Denmark, (English translation, British Lending Library)

Ansell R O, Dickinson T, Povey A F, Sherwood P M A, "X-ray photoelectron spectroscopic studies of electrode surface using a new controlled transfer technique", J. Electroanal. Chem., 1979, 79-89

Anwar M, Hogarth C A, Khan G A, Bulpett R, "X-ray photoelectron spectroscopic (XPS) investigations of etching and annealing effects on thin films of MoO_3", Spectrochimica Acta, **44**, 1989, 789-793

Appleton B R in Chapter 7 of "Ion implantation and beam processing", eds Williams J S and Poate J M, Academic Press, 1984, London, 210-211

Arkush R, Talianker M, Polak M, "AES study of aluminium and sulphur surface segregation in the Ni - 9%Al solid-solution", Scripta Metallurgica et Materialia, **24**, 1990, 297-300

Auciello O in chapter 1 of "Ion bombardment modification of surface: fundamentals and applications", eds Auciello O and Kelly R, Elsevier Science Publisher, 1984, Amsterdam

Barcz A, Croset M and Mercandalli L M, "Quantitatively in III-V compounds by low-energy ion scattering spectrometry", Surf. Sci., **95**, 1980, 511-526

Barnett R N, Landman U, Cleveland C L, "Surface segregation in simple metal alloys: an electronic theory", Phys. Rev. B, **28**, 1983, 6647-6658

Baretzky B, Moller W, Taglauer E, "Collision dominated preferential sputtering of tantalum oxide", Vacuum, **43**, 1992, 1207-1216

Barr T L, Natarajan B R, Eltoukhy A H, Greene J E, "Characterisation of InN, In_2O_3, and In oxy-nitride semiconducting thin films using XPS electron energy loss spectra", J. Vac. Sci. Technol., **16(2)**, 1979, 1-1

Baschenko O A and Nefedov V I, "Depth profiling of elements in surface layers of solids based on angular resolved X-ray photoelectron spectroscopy", J Electron Spectrosc. Related Phen., **53**, 1990, 1-18

Bertóti I, Kelly R, Mohai M and Tóth A, "Response of oxides to ion bombardment: the difference between inert and reactive ions", Nucl. Instr. and Meth., **B80/81**, 1993, 1219-1225

Betz G and Wehner G K in chapter 2 of "Sputtering by particle bombardment II", ed., Berish R, Springer-Verlag, 1983, Heidelberg

Biersack J P, "Computer simulations of sputtering", B27, Nucl. Instr. and Meth., **B27**, 1987b, 21-36

Biersack J P in chapter 1 of "Ion bombardment modification of insulators", eds Mazzoldi P and Arnold G W, Elsevier Science Publisher, 1987a, Amsterdam

Bondarenko G G, Kucheryavyi S I, "Surface segregation of lithium in aluminium-lithium alloys", Phys. and Chem. of Mater. Treatment,, **25**, 1991, 97-99

Bourgoin J C, Corbett J W, Frisch H L, "Ionisation enhanced diffusion", J. Chem. Phys., **59(8)**, 1973, 4042-4046

Bozack Michael J, Davis P R, "Production of high purity metal alloys by surface segregation", Mater. Sci. & Eng. A, **A150**, 1992, 255-261

Brejnak M, Modrak P , "Electronic theory of surface segregation in the coherent potential approximation: The surface segregation in CoNi, IrPt and RhPt", Surf. Sci.,

280, 1993, L285-L290

Briggs D, Riviére J C in Chapter 3 of "Practical surface analysis (second edition), volume 1: Auger and X-ray photoelectron spectroscopy", eds. Briggs D and Seah M P, John Wiley & Sons Ltd, 1990, Chichester, U. K.

Briggs D in Chapter 4 of "Handbook of X-ray and ultraviolet photoelectron spectroscopy", ed D Briggs, Heydonn & Son Ltd., 1977

Brinkman J A, "On the nature of radiation damage in metals", J. of Appl. Phys., **25**, 1954, 961-970

Brongersma H H, Sparnaay M J and Buck T M, "Surface segregation in Cu-Ni and Cu-Pt alloys; a comparison of low-energy ion-scattering results with theory", Surf. Sci., **71**, 1978, 657-678

Brown A, Gerrard N D, Humphrey P, Patterson A M, Vickerman J C, Williams I O, "Surface cleaning procedures for (100)-oriented GaAs and InP studied by SIMS", Chemitronics, **1**, 1986, 64-68

Bussing T D, Holloway P H, Wang Y X, Moulder J F and Hammond J S, "Composition depth profiles of oxidised silicon and sputtered GaAs from angle-resolved X-ray photoelectron spectroscopy", J. Vac. Sci. Technol., **B6(5)**, 1988, 1514-1518

Bussing T D and Holloway, "Deconvolution of concentration depth profiles from angle resolved X-ray photoelectron spectroscopy data", J. Vac. Sci. Technol., **A3(5)**, 1985, 1973-1981

Chiang J C, "Band-structure effects in AlSb-InAs-AlSb double barrier structures", Appl. Phys. Lett., **64(15)**, 1994, 1956-1958

Choudhury T, Saied S O, Sullivan J L and Abbot A M, "Reduction of oxides of iron, cobalt, titanium and niobium by low energy ion bombardment", J Phys. D: Appl. Phys., **22**, 1989, 1185-1195

Colligon J S, Kheyrandish H, Kaye S P, "Ion bombardment effects on SnO_2 and MoS_2 films", Vacuum, **43**, 1992, 135-139

Coratger R, Chahboun A, Sivel V, Ajustron F, Beauvillain J, "Scanning tunnelling microscopy of the damage induced by ion bombardment on a graphite surface", Ultramicroscopy, **Part A 42-44**, 1992, 653-659

Corbett J W, Karins J P, Tan T Y, "Ion-induced defects in semiconductors", Nucl. Inst. Meth., **182/183**, 1981, 457-476

Costa D, Carraretto A, Godowski P J, Marcus, P, "Evidence of arsenic segregation in iron", J. Mater. Sci. Lett., **12**, 1993, 135-137

Davidson M R, Hoflund G B, Outlaw R A, "Nondestructive depth profile study of oxygen-exposed large-gain silver using angle-resolved Auger electron spectroscopy and ion scattering spectroscopy", J. Vac. Sci. Technol. A, **9(3)**, 1991, 1344-1350

Dennis J R, Hale E B, "Crystalline to amorphous transformation in ion-implanted silicon: a composite model", J. Appl. Phys., **49**, 1978, 1119-

Dreysse H, Wille L T, Fontaine D, "Microscopic theory of surface segregation in binary alloys" Solid State Communications, **78(5)**, 1991, 355-358

Dudonis J, Pranevicius L, "Changes in surface composition induced by ion bombardment of multicomponent alloys", Surf. & Coat. Technol., **56**, 1993, 233-242

Dulkin, A E, Pyataev V Z, Sokolova N O, Moshkalyov S A, Smirnov A S and Frolov K S, "The study of GaAs reactive ion etching in Cl_2/Ar", Vacuum, **44(9)**, 1993, 913-917

Ebina A, Asano K, Suda Y, Takahaski, "Oxidation properties of II-VI compound surfaces studied by low-energy electron-loss spectroscopy and 21eV photoemission spectroscopy", J. Vac. Sci. Technol., **17**, 1980, 1074-1079

Eckstein W, "Quantitative predictions of sputtering phenomena", Surf. Interface Anal, **14**, 1989, 799-808

Epp J M, and Dillard J G, "Effect of ion bombardment on the chemical reactivity of Gallium Arsenide", Mater. Chem., **1**, 1989, 325-330

Es-Souni M, "Computer simulation of segregation kinetics in ternary alloys", Scripta Metallurgica, **23(6)**, 1989, 919-924

Evdokimov I N, Valizadeh r, Armour D G, Richardson N V and McConville C F, "Oscillatory evolution of an ion bombarded InSb(100) surface", Surf. Sci., **318**, 1994, 281-288

Fadley C S in Progress in Solid State Chemistry, **11(1)**, 1976, 265-343

Falcone G, Sigmund P, "Collisional sputtering yield corrections", Nucl. Instr. and Meth. inPhys. Res., **B18**, 1987, 398-401.

Fried V, Blukis U, Hameka H F, in Chapter 7 of "Physical chemistry", Macmillan Publishing Co., Inc., 1977, USA.

Gaarenstroom S W and Winograd N, "Initial and final state effects in the ESCA spectra of cadmium and silver oxides", J. Chem. Phys., **67**, 1977, 3500-3506.

Gallet D, Hollinger G, Santinelli C, Goldstein L, "*In situ* characterization of InP surfaces after low-energy hydrogen ion cleaning", J. Vac. Sci. Technol., **B10(4)**, 1993, 1267-1272.

Gerkema J, Miedema A R, "Adhesion between solid metals: observations of interfacial segregation effects in metal film lubrication experiments", Surf. Sci., **124**, 1983, 351-371.

Gillam E, "The penetration of positive ions of low energy into alloys and composition changes produced in them by sputtering", J. Phys. Chem. Sol., **7**, 55-67.

Giles R, *private communication.*

Giordano H, Alem O, Aufray B, "Kinetics of surface segregation in Cu(Sb) alloys: determination of the diffusion coefficients", Scripta Metallurgica et Materialia, **28**, 1993, 257-262.

Gorden J, "Nanoconstructive bombardment", Phys. World, **6**, 1990, 40-43.

Grove W R, "The electro-chemical polarity of gases", Phil. Trans., 1852, 87-101.

Hajcsar E E, Dawson P T and Smeltzer W W, "Surface segregation and preferential sputtering in Co-Ni alloys: computer simulation of Auger spectra", Surf. Interface Anal., **10**, 1987, 343-348.

Hammer G E and Shemenski R M, "Ion bombardment effects in the sputtering of single- and two-phase brass alloys; Cu:18-48%Zn", Surf. Interface Anal., **10**, 1987, 355-359.

Harrison W A, "Electronic structure and the properties of solids", W H Freeman and Company, 1980, San Francisco.

Hetzendorf G and Varga P, "Preferential sputtering and surface segregation in Au-Pd

alloys", Nucl. Instr. and Meth., **B18**, 1987, 501-503

Ho P S, Lewis J E and Chu W K, "Preferred sputtering on binary alloy surfaces of the Al-Pd-Si system", Surf. Sci., **85**, 1979, 19-28

Hofmann S and Erlewein, "A model of the kinetics and equilibrium of surface segregation in the monolayer regime", Surf. Sci., **77**, 1978, 591-602

Hofmann S and Sanz J M, "Quantitative XPS analysis of the surface layer of anodic oxides obtained during depth profiling by sputtering with 3keV Ar ions", Trace and Microprobe Techniques, **1(3)**, 1982-1983, 213-264

Holloway P H and Bussing T D, "Quantitative surface Analysis of layered materials", Surf. Interface Anal., **18**, 1992, 251-256

Ivanov S V, Kop'ev P S, Ledentsov N N, "Interplay of beryllium segregation and diffusion in heavily doped GaAs and AlGaAs grown by molecular beam epitaxy(thermodynamic analysis)", J. Cryst. Growth, **108**, 1991, 661-669

Iwasaki H, Mizokawa Y, Nishitani R, Nakamura S, " X-ray potoemision study of the initial oxidation of the cleaved (110) surfaces of GaAs, GaP and InSb", Surf. Sci., **86**, 1979, 811-818

Jones T S, Ding M Q, Richardson N V, McConville C F, "Effects of surface damage on surface plasmon excitations in doped InSb(100)", Appl. Surf. Sci., **45(1)**, 1990, 85-90

Kelly R, Miotello A, "Ion-beam mixing with chemical guidance II. Analysis for positive heats", Surf. Coatings Techn., **51**, 1992, 343-351

Kelly R, "Thermal sputtering as a gas-dynamic process", Nucl. Instr. and Meth., **B46,** 1990, 441-447

Kelly R, Miotello A, "Ion-beam mixing with chemical guidance II: analysis for positive heat of mixing", Surf. Coat. Technol., **51**, 1992, 343-351

Kelly R, "Bombardment-induced compositional change with alloys, oxides, oxysalts and halides: the role of segregation", Nucl. Instr. and Meth., **B39**, 1989, 43-56

Kelly R, "The surface binding energy in slow collisional sputtering, Nucl. Instr. and Meth.", **B18**, 1987a, 388-398

Kelly R in chapter 2 of "Ion bombardment modification of insulators", eds Mazzoldi P and Arnold G W, Elsevier Science Publisher, 1987b, Amsterdam

Kelly R and Oliva A, "The theory of preferential sputtering of alloys, including the role of Gibbsian segregation", NATO ASI Series E, **112**, 1986, 41-69

Kelly R in chapter 2 and chapter 3 of "Ion bombardment modification of surface: fundamentals and applications", eds Auciello, and Kelly R, Elsevier Science Publisher, 1984, Amsterdam

Kelly R, "On the problem of whether mass or chemical bonding is more important to bombardment-induced compositional changes in alloys and oxides", Surf. Sci., **100**, 1980, 85-107

Kelly R, "An attempt to understand preferential sputtering", Nucl. Instr. Meth., **149**, 1978, 553-558

Kerker G, Morán-López, Bennemann K H, "Electronic theory for segregation at surfaces of transition-metal alloys", Phys. Rev., **B15**, 1977, 638-642

Kirschner J, "Surface segregation and its implications for sputtering", Nucl. Instr. and Meth., **B7/8**, 1985, 742-749

Koshikawa T Goto K, "Surface compositional changes by segregation in sputtered alloys", Nucl. Instr. and Meth., **B18**, 1987, 504-508

Kumar K, Mookerjee A, Kumar V, "Surface segregation in random alloys", J. Phys., **F6**, 1976, 725-738

Jiang S L, Oliva A, Amoddeo A, Kelly R, "Composition profiles due to bombardment-induced segregation in Cu-Ni samples as deduced by Auger spectroscopy", Nucl. Instr. and Meth., **B45,** 1990, 646-650

Lam N Q and Wiedersich, "Bombardment-induced segregation and redistribution", Nucl. Instr. and Meth., **B18**, 1987, 471-485

Larsson M I, Hansson G V, Monte Carlo simulations of Ge segregation in strained Si and SiGe alloys, Surf. Sci., **291**, 1993, 117-128

Lazarescu V, Radovici O, Vass M, "Surface segregation induced by chemisorption at the alloy/solution interface", Appl. Surf. Sci., **55**, 1992, 297-301

Leerdam G C, Brongersma H H, "Shielding effects in oxides studied by low-energy ion scattering", Surf. Sci., **254**, 1991, 153-160

Ley L, Pollak R A, McFeely F R, Kowalczyk S P, Shirley D A, "Total valence-band densities of III-V and II-VI compounds from x-ray photoemission spectroscopy", Phys. Rev. B, **9**, 1974, 600-621

Li R S, Koshikawa T, "Ion radiation-enhanced diffusion and segregation in an $Au_{0.56}Cu_{0.44}$ alloy between -120°C and room temperature", Surf. Sci., **151**, 1985, 459-476

Liau Z L, Mayer J W, "Limits of composition achieved by ion implantation", J. Vac. Sci. Techn., **15**, 1629-1635

Liau Z L, Brown W L, Homer R, Poate J M, "Surface-layer composition changes in sputtered alloys and compounds", Appl. Phys. Lett., **30**, 1977, 626-628

Lide R D (ed), "CRC handbook of chemistry and physics (72nd edition)", CRC press, Boca Raton, USA, 1991, (a)9.105-9.113; (b)4.133-4.145; (c)12.77-12.91

Lifshitz E M, Pitaevskii L P, "Physical kinetics" (English translation from Russian), Pergamon Press Ltd, Oxford, UK, 1981, Chapter 1.

ch Linsmeier, "Auger electron spectroscopy", Vacuum, **45**, 1994, 673-690

Lucovsky G, Bauer R S, "Local atomic order in native III-V oxides", J. Vac. Sci. Technol., **17(5)**, 1980, 946-951

Mack M E in "Ion implantation science and technology (second edition)", ed Ziegler J F, Academic Press Inc., Boston, USA , 1988, 313-344

Magnat O S, Soukiassian P, Huttel Y, Huych Z., Gruzza B and Porte A, "Low-energy Ar ion bombardment-induced modification of surface atomic bond length on InP(100) wafer", Appl. Phys. Lett. **63(14)**, 1993, 1957-1959

Malherbe J B, "Ion angle dependence in the preferential sputtering of InP", Appl. Surf. Sci., **70-71**, 1993, 322-326

Malherbe J B, Barnad W O, Strydom I le R and Louw C W, "Preferential sputtering of GaAs", Surf. Interface Anal., **18**, 1992, 491-495

Malherbe J B and Barnard W O, "Preferential sputtering of InP: an AES investigation",

Surf. Sci., **255**, 1991, 309-320

Malherbe J B, Hofmann S and Sanz J M, "Preferential sputtering of oxides: a comparison of model predictions with experimental data", Appl. Surf. Sci., **27**, 1986, 355-365

Marchetti F, Dapor M, Girardi S, Cipparrone M, Tiscione P, "Auger quantitative analysis and preferential sputtering in brass alloys", Vacuum, **41**, 1990, 1706-1709

Marton D, Fine J, "Ion bombardment induced diffusion: A case study on a sputtered Ag/Ni layered system", Chem. Eng., **34**, 1990, 37-55

Masterton W L, Slowinski E J, Stamitski C L in Appendix 2 of "Chemical principles (alternate edition)", CBS College Publishing, 1983, New York, USA

Melendez O and Hoflund G B, Gillbert R E and Young V Y, "Factors which affect peak shapes and areas in ion scattering spectroscopy", Surf. Sci., **251/252**, 1991, 228-232

Miedema A R, "Surface segregation in alloys of transition metals", Metallkunde, **69**, 1978, 455-461

Miotello A, Kelly R, Laidani N, "Chemical and compositional changes induced by ion implantation in SiC and resulting hydrogen permeation properties", Surf. Coating Techn., **65**, 1994, 45-56

Miotello A, Kelly R, "Ion-beam mixing with chemical guidance IV. Thermodynamic effects without invoking thermal spikes", Surf. Sci., **314,** 1994b, 275-288

Miote A, Kelly R, "Ion-beam mixing with chemical guidance part III: phase formation as a kinetic rather than thermodynamics phenomenon", Thin Sol. Films, **241**, 1994a, 192-197

Mitchell D F, Sproule G I, Graham M J, "Sputter reduction of oxides by ion bombardment during Auger depth profile analysis", Surf. Interface Anal., **15(8)**, 1990, 487-497

Mizutani T, "Preferential sputtering of oxygen from SiO_2 by low-energy ion beam and neutral beam bombardment", Japanese J. of Appl. Phys., **30(4A)**, 1991, L628-L631

Modak S, Khanra B C, "Surface segregation in small bimetallic particles", Solid State Communications, **84**, 1992, 663-667

Modak S, Gangopadhyay S, "Surface segregation of Pt-Ni alloys, Solid State

Communications", **78(5)**, 1991, 429-432

Muscat J P, "Surface segregation in binary alloys: a simple theoretical model", J. Phys., **C15**, 1982, 867-879

Niehus H, Heiland W and Taglauer E, "Low-energy ion scattering at surfaces", Surf. Sci. Reports, **17**, 1993, 213-304

Niehus H in "Practical surface analysis (second edition), volume 2: ion and neutral spectroscopy", eds. Briggs D and Seah M P, John Wiley & Sons Ltd, 1992, Chichester, UK

O'Connor D J, Kang H J, Pigram P, Roberts R H, He S, "Surface segregation of NiZr", Appl. Surf. Sci., **70-71**, 1993,114-117

Oechsner H, Schoof H, Stumpe E, " Sputtering of Ta_2O_5 by Ar^+ ions at energies bellow 1keV", Surf. Sci., **76**, 1978, 343-354

Ohtani N, Mokler S M, Xie M H, Zhang J, Joyce B A, "RHEED investigation of Ge surface segregation during gas source MBE of $Si/Si_{1-x}Ge_x$ heterostructures", Surf. Sci., **284**, 1993, 305-314

Oliva A, Kelly R, Falcone G, "Comments on collisional sputtering theory", Nucl. Instr. and Meth., **B19/20**, 1987, 101-108

Oostra D J and Vries A E, "Chemical sputtering by ions electrons and photons", Nucl. Instr. and Meth., **B18**, 1987, 618-624

Orrman-Rossiter K G, Al-Baysti A H and Armour D G, "Low energy ion-scattering analysis of the GaAs(100) surface", Surf. Sci., **225**, 1990, 341-354

Overbury S H, Bertrand P A, Somorjai G A, "The surface composition of binary systems: Prediction of surface phase diagrams of solid solutions", Chem. Rev., **75(5)**, 1975, 547-560

Pauling L, "The chemical bond", Cornell University Press, 1967, New York

du Plessis J and Taglaur E, "Surface concentration modification of PtPd alloys by noble gas ion sputtering", Surf. and Interf. Anal., **22**, 1994, 556-560

Pugacheva T S, Kovalev S P, Il'icheva I E, Kalinovski A P, "Thermal peaks and their

contribution to sputtering during low-energy ion bombardment of solids", Phys. Chem. and Mech. of Surf., **8**, 1992, 194-207

Reniers F, Jardinier-Offergeld M, Bouillon F, "Auger electron spectroscopy study of the surface segregation in silver-palladium alloys", Surf. Interface Anal., **17**, 1991, 343-351

Robbins M O, Falicov L M, "Electronic theory of ordering and segregation in binary alloys: application to simple metals", Phys. Rev., **B25**, 1982, 2343-2357

Schoeb A M, Raeker T J, Yang L, Wu X, King T S, DePristo A E, "Driving force for surface segregation in bimetallic catalysts", Surf. Sci., **278**, 1992, L125-L130

Seah M P, Briggs D, in Chapter 1 of "Practical surface analysis (second edition), volume 1: Auger and X-ray photoelectron spectroscopy", eds. Briggs D and Seah M P, John Wiley & Sons Ltd, 1990, Chichester, U. K.

Seah M P in "Practical surface analysis (second edition), volume 1: Auger and X-ray photoelectron spectroscopy", eds. Briggs D and Seah M P, John Wiley & Sons Ltd, 1990, Chichester, U. K.

Seah M P and Dench W A, "Quantitative electron spectroscopy of surfaces: a standard data base for electron inelastic mean free paths in solids", Surf. Interface Anal., **1**, 1979, 2-11

Senhaji A, Treglia G, Eugene J , Khoutami A, Legrand B, "Alloy surfaces and surface alloys: From equilibrium to kinetics", Surf. Sci., **287-288** , 1993, 371-376

Seto S, Ohwaki K, Koguchi T, Irisawa T, "Acceleration of diffusion bonding of dissimilar metals by ion bombardment", J. of Japan Weld. Soc., **10**, 1992, 38-43

Sherwood P M A in Appendix 3 of "Practical surface analysis (second edition), volume 1: Auger and X-ray photoelectron spectroscopy", eds. Briggs D and Seah M P, John Wiley & Sons Ltd, 1990, Chichester, U. K.

Shirley D A, "High resolution X-ray photoemission spectrum of valence band of gold", Phys. Rev., **B5**, 1972, 4709-4714

Shimizu H, Ono M, Koyama N, Ishida Y, "Sputter-enhanced diffusion phenomena in Cu/Ni alloys at elevated temperatures", J. Appl. Phys., **53**, 1982, 3044-3052

Shimizu H, Ono M, Nakayama K, "Quantitative Auger analysis of copper-nickel alloy surfaces", Surf. Sci., **36**, 1973, 817-821

Shimizu R, "Preferential sputtering", Nucl. Instr. and Meth., **B18**, 1987, 486-495

Siegbahn K, Nordling C, Fahlman A, Nordberg R, Hamrin K, Hedman J, Johansson G, Bergmark T, Karlsson S E, Lindgren I, Lindberg B, "Atomic, molecular and solid state structure studies by means of electron spectroscopy", Almqvist and Wiksells, 1967, Uppsala

Sigmund P, "Preferential sputtering from isotopic mixtures and alloys of near-neighbour elements", Nucl. Instr. and Meth., **B18**, 1987b, 375-387

Sigmund P, "Mechanisms and theory of physical sputtering by particle impact", Nucl. Instr. and Meth., **B27**, 1987a, 1-20

Sigmund P in chapter 2 of "Sputtering by particle bombardment I", ed Behrisch R, Springer-Verlag, 1981, Heidelberg,

Sigmund P, "Collision theory of displacement damage, ion ranges and sputtering", Rev. Roum. Phys., **17(7)**, 1972, 823-870, (English translation, British Lending Library)

Sigmund P, "Theory of sputtering I: sputtering yield of amorphous and polycrystalline targets", Phys. Rev., **184(3)**, 1969b, 384-416

Sigmund P, On the number of atoms displaced by implanted ions or energetic recoils atoms", Appl. Phys. Lett., **14**, 1969a, 114-117

Singer I L, Murday J S and Cooper L R, "Surface composition changes in GaAs due to low-energy ion bombardment", Surf. Sci., **108**, 1981, 7-24

Smith G C, "Quantitative surface microanalysis by auger and X-ray photoelectron spectroscopy", Materials, Characterization, **25**, 1990, 37-71

Smith G C and Livesey A K, "Maximum entropy: a new approach to non-destructive deconvolution of depth profiles from angle-dependent XPS", Surf. Interface Anal., **19**, 1992, 175-180

Spicer W E, Chye P W, Garner C M, Lindau I, Pianetta P, "The surface electronic structure of III-V compounds and the mechanism of Fermi level pinning by oxygen (passivation) and metals (Schottky barriers)", Surf. Sci., **86**, 1979, 763-788

Sproul W D, Rudnik P J, Legg K O, Munz W D, Petrov I, Greene J E, "Reactive sputtering in the ABSTM system", Surf. & Coat. Technol., **56**, 1993, 179-182

Storp S and Holm R, "ESCA investigations of ion beam effects on surfaces", J. Elec. Spect. Relat. Phen., **16**, 1979, 183-193

Sullivan J L, Saied S O, Bertoti I, "Effect of ion and neutral sputtering on single crystal TiO_2", Vacuum, **42**, 1991, 1203-1208

Sullivan J L, "The diffusion of compensating impurities in single crystal cadmium sulphide", J. Electrochem. Soc., **123(8)**, 1976, 1251-1253

Swartzfager D G, Ziemecki S B, Kelly M J, "Differential sputtering and surface segregation: the role of enhanced diffusion", J. Vac. Sci. Technol., **19**, 1981, 185-191

Tan L, Yuen W T, Harris J J, Phillips C C, Stradling R A, "Magneto-transport and magneto-optics in narrow-gap III-V compounds based on InSb", Physics B: Condensed Matter, **184**, 1993, 184-191

Teraoka Y, "Chemisorption-induced surface segregation and order-disorder transition", Surf. Sci., **244**, 1991, 135-148

Thomas J H and Hofmann, "Ion bombardment induced changes in silicon dioxide surface composition studied by X-ray photoelectron spectroscopy", J. Vac. Sci. Technol., **A3(5)**, 1985, 1921-1928

Tu H N, Mayer J W and Feldman L C, "Electronic thin film science for electrical engineers and materials scientists", Macmillan Publishing Company", 1987, New York

Tyler B J, Castner D G and Ratner B D, "Regularization: a stable and accurate method for generating depth profiles from angle-dependent XPS data", Surf. Interface Anal., **14**, 1989, 443-450

Universitat K K G, "Hydrocarbon-based etching of InP", Appl. Surf. Sci., **65-66**, 1993, 614-618

Valeri S, Lolli M, Ottaviani G, "GaAs and InP surface behaviour under ion bombardment, alkali deposition and oxygen exposure", Vacuum, **41**, 1990, 643-646

Vam L P, Gautier M, Duraud J P, Gillet F, Jollet F, "XPS, EELS and LEED study of

monocrystalline Al_2O_3 (0001) surfaces: Modifications induced by heat treatment or ion bombardment", Surf. Interface Anal., **16**, 1990, 214-215

Vicanek M, Rodriguez J J and Sigmund P, "Depth of origin and angular spectrum of sputtered atoms", Nucl. Instr. and Meth., **B36**, 1989, 124-136

Voges D, Taglauer E, Dosch H, Peisl J, "Surface segregation on Fe3Al(110) near the order-disorder transition temperature", Surf. Sci., **269**, 1992, 1142-1146

Wagner C D, "NIST X-ray photoelectron spectroscopy database (version 1.0)", National Institute of Standards and Technology, 1989, Gaithersburg, USA

Wagner W, Rehn L E, Wiedersich and Naundorf V, "Radiation-induced segregation in Ni-Cu alloys", Phys. Rev. B, **28(12),** 1983, 6780-6794

Ward R J, Wood B J, "A comparison of experimental and theoretically derived sensitivity factors for XPS", Surf. and Interface Anal., **18**, 679-684

Was G S, "Ion beam modification of metals: compositional and microstructural changes", Progr. in Surf. Sci., **32**, 1990, 211-332

Watts J F, "X-ray photoelectron spectroscopy", Vacuum, **45**, 1994, 653-671

Weast R C, Lide D R, Astle M J, Beyer W H (eds), "CRC handbook of chemistry and physics (70th edition)", CRC Press, Inc., 1992, Boca Raton, Florida, F-187

Weigand P, Hofer W, Varga P, "Investigation of $Pt_{25}N_{75}$(111): preferential sputtering and surface segregation", Surf. Sci., **287-288**, 1993, 350-354

Webb R P, in Appendix 3 of "Practical surface analysis (second edition), volume 2: ion and neutral spectroscopy", eds. Briggs D and Seah M P, John Wiley & Sons Ltd, 1992, Chichester, UK

Williams F L and Nason D, "Binary alloy surface compositions from bulk alloy thermodynamic data", Surf. Sci., **45**, 1974, 377-408

Wilson I H, Zheng N J, Knippping U, Tsong I S T, "Effect of isolated atomic collision cascades on SiO_2/Si", Phys. Rev., **B38**, 1988, 8444-8450

Wilson I H in "Ion bombardment modification of surface: fundamentals and applications", eds Auciello, and Kelly R, Elsevier Science Publisher, 1984, Amsterdam

Wilson I H, "The topography of sputtered semiconductors", Rad. Effects., **18**, 1973, 95-103

Winter H F, "Physical sputtering: a discussion of experiment and theory", Rad. Effects on solid surf., **170th meeting of American Chemical Society**, 25-26 Aug. 1975, Chicago, 1-29

Winter H F, "Mass effect in the physical sputtering of multicomponent materials", J. Vac. Sci. Techno., **20**, 1982, 493-497

Wittmaack K in "Practical surface analysis (second edition), volume 2: ion and neutral spectroscopy", eds. Briggs D and Seah M P, John Wiley & Sons Ltd, 1992, Chichester, UK

Wyk G N, Plessis J and Taglaur E, "Sputtering and radiation-enhanced segregation in amorphous Cu-Ti alloys", Surf. Sci., **254**, 1991, 73-80

Wyublatt P, Ku R C, "Surface energy and solute strain energy effects in surface segregation", Surf. Sci., **65**, 1977, 511-531

Yamawaki M, Yamaguchi K, Tanaka S, Liu X, Qian J P, "Surface segregation of a low-Z element and its impact on interaction with hydrogen", J. Nucl. Mater., **196-198**, 1992. 592-595.

Zalm P C, "Quantitative sputtering", Surf. Interface Anal., **11**, 1988, 1-24

Zangwill A, "Physics at surfaces", Cambridge University Press, 1988, Cambridge, U. K.

Zhang J P, Hemment P L F, Bussmann U, Robinson A K, Castle J E, Liu H D, Watts, J F, Newstead S M, Powell A P, Whall T E, Parker E H C, "The study of $Si_{0.5}Ge_{0.5}$ alloy implanted by high dose oxygen", Nucl. Instr. and Meth. in Phys. Res., **B55**, 1991, 691-696

Ziegler J F in "Ion implantation science and technology (second edition)", ed Ziegler J F, Academic Press Inc., Boston, USA , 1988, 3-61

Publications

1. **A study of contaminant overlayer on Ge(100) surface using kinetic resolved XPS**

   W. Yu, John L. Sullivan and Sayah O Saied, Vacuum, **45(5)**, 1994, 597-601.

2. **Ion bombardment effects in GeSi(100) surfaces studied by XPS and ISS**

   W. Yu, John L. Sullivan and Sayah O Saied, Surf. Sci., **307-309**, 1994, 691-697.

3. **ARXPS and LEISS characterisations for chemically etched and ion-bombarded GaAs(100) surfaces**

   John L. Sullivan, W. Yu and Sayah O Saied, Surf. Interf. Anal., **22**, 1994, 515-519.

4. **A study of the compositional changes in chemically eteched, Ar ion bombaded and reactive ion etched GaAs(100) surfaces by means of ARXPS and LEISS**

   John L. Sullivan, W. Yu and Sayah O Saied, Appl. Surf. Sci., 90**(3)**, 1995, 309-319.

5. **XPS and ISS studies of ion bombarded GaSb, InSb and CdSe surfaces**

   W. Yu, John L. Sullivan and Sayah O Saied, Surf. Sci., 1995, in press.

Pergamon

Vacuum/volume 45/number 5/pages 597 to 601/1994

0042–207X/94$7.00+.00

study of contaminant overlayer on Ge(100) rface using kinetic resolved XPS

Wei, John L Sullivan* and Sayah O Said, *Department of Electronic Engineering and Applied Physics, on University, Aston Triangle, Birmingham B4 7ET, UK*

ved for publication 7 April 1993

ELSEVIER

surface science

Surface Science 307–309 (1994) 691–697

Ion bombardment effects in GeSi(100) surfaces studied by XPS and ISS

W. Yu, J.L. Sullivan *, S.O. Saied

Department of Electronic Engineering and Applied Physics, Aston University, Birmingham B4 7ET, UK

(Received 20 August 1993)

SURFACE AND INTERFACE ANALYSIS, VOL. 22, 515–519 (1994)

ARXPS and LEISS Characterizations for Chemically Etched and Ion-bombarded GaAs(100) Surfaces

J. L. Sullivan,* W. Yu and S. O. Saied
Department of Electronic Engineering and Applied Physics, Aston University, Birmingham B4 7ET, UK

NH
SEVIER

Applied Surface Science 90 (1995) 309–319

applied
surface science

A study of the compositional changes in chemically etched, Ar ion bombarded and reactive ion etched GaAs(100) surfaces by means of ARXPS and LEISS

J.L. Sullivan *, W. Yu, S.O. Saied

Department of Electronic Engineering and Applied Physics, Aston University, Birmingham B4 7ET, UK

Received 13 February 1995; accepted for publication 27 June 1995

XPS and LEISS studies of ion bombarded GaSb, InSb and CdSe surfaces

W. Yu[1], J. L. Sullivan[2] and S. O. Saied

Department of Electronic Engineering and Applied Physics, Aston University, Birmingham, B4 7ET, UK

(accepted for publication by Surface Science on 30th September, 1995)